STABILIZATION OF SECONDARY STRUCTURE OF SYNTHETIC ALZHEIMER ß-AMYLOID PROTEIN ANALOGS IN THE PRESENCE OF ALUMINUM (III) IONS

A

Thesis

Presented to the Faculty

of the University of Alaska Fairbanks

in Partial Fulfillment of the Requirements

for the Degree of

DOCTOR OF PHILOSOPHY

By

Sandip Bipin Vyas, B. Sc. (Honours), M. Sc.

Fairbanks, Alaska

December 1995

STABILIZATION OF SECONDARY STRUCTURE OF SYNTHETIC ALZHEIMER ß-AMYLOID PROTEIN ANALOGS IN THE PRESENCE OF ALUMINUM (III) IONS

By

Sandip Bipin Vyas

Recommended:

Advisory Committee Chair

Head, Department of Chemistry and Biochemistry

Approved:

Dean, College of Natural Sciences

Dean of the Graduate School

Nov 28, 1995

Date

Abstract

The gradual accretion of fibrillar protein deposits in a tissue or organ is a hallmark of all amyloidogenic diseases. These deposits accumulate as senile plaques and cerebrovascular deposits in the brain and are characteristics of Alzheimer's disease. A majority of the brain amyloid deposits consist of a 40 amino acid protein, the Alzheimer ß-protein, AßP, which in a soluble form is ubiquitous in biological tissues. In order to provide a more detailed understanding of the structural transformations of soluble AßP, sequence analogs derived from ß1-40, and having His → Arg, and L-Asp → D-Asp substitutions were synthesized.

The kinetic variations of ß1-40 and ß6-25 were studied using amide circular dichroism spectroscopy by monitoring ellipticity changes of the peptide

backbone. In both peptides, the gradual loss of secondary structure was a multiphasic process which was also dependent on concentration. The circular dichroism titrations with metal ions revealed the involvement of at least two ions in the conformational transitions of ß1-40 and ß6-25. The association of Al(III) with L-Asp → D-Asp derived analogs caused surprising conformational changes in ß6-25, which were distinct from ß1-40. Microheterogeneous products corresponding to Al(III)-bound peptide species were resolvable on the reversed-phase surface. The association of aluminum was investigated by low field ^{27}Al nuclear magnetic resonance spectroscopy. The signal corresponding to Al(III)-bound peptide species revealed that at least four Al(III) ions were bound to ß1-40 and ß6-25 between pH 5 and 6. Moreover, ß1-40 effectively competed with EDTA to bind with Al(III).

This study also describes a strategy which resolved the band broadening in reversed-phase high-performance liquid chromatography of ß1-40 and derived analogs. Chromatographic parameters related to interactive contact area of ß1-40 and derived analogs were determined on reversed-phase matrix. The peptides were bound to the reversed-phase surface in their monomeric form. Slow partition kinetics appear to contribute to significant band broadening, which suggests a secondary retention effect – indicating a conformational change due to unfolding on the stationary phase surface.

Dedication

To
my sister Minu, and
CV

in knowing whom, I discovered
that they are the salt-bridges of
my ionic life...

Table of Contents

List of Figures

List of Tables

List of Abbreviations

AD	Alzheimer's disease
APP	Alzheimer precursor protein
AßP	Alzheimer ß-protein
CD	circular dichroism spectroscopy
CNBr	cyanogen bromide
CV	cerebrovascular
DCC	dicyclohexylcarbodiimide
DCM	dichloromethane
Dhbt	2-hydroxy-4-oxodihydrobenzotriazole
DITC	diisothiocyanate
DMF	dimethylformamide
EDT	1,2-ethanedithiol
EMS	ethylmethylsulfide
Fmoc	9-fluorenylmethoxycarbonyl
HCHWA-D	hereditary cerebral hemorrhage with amyloidosis-Dutch
HFIP	hexafluoroisopropanol
HOBt	1-hydroxybenzotriazole
HPLC	high performance liquid chromatography
Mbh	4,4'-dimethoxybenzhydrl
Mtr	4-methoxy-2,3,6-trimethylbenzenesulfonyl
NMM	N-methylmorpholine
NMR	nuclear magnetic resonance spectroscopy
Opfp	pentafluorophenyl
Pepsyn KA	polyamide-kieselguhr
PIP	piperidine
PITC	phenylisothiocyanate
PS-PEG	polystyrene-polyethylene glycol

PVDF	polyvinylidene difluoride
RP-HPLC	reversed-phase high performance liquid chromatography
SEC	size exclusion chromatography
SP	senile plaque
SPPS	solid-phase peptide synthesis
tboc	tert-butyloxycarbonyl, tert-benzyloxycarbonyl
*t*Bu	tert-butyl
TFA	trifluoroacetic acid
TFE	trifluoroethanol
TLC	thin layer chromatography

Acknowledgements

It is often a daunting chore to make the acknowledgments and summary astute, bright and candid, without being deceitful, monotonous, or zesty. Since, like all other dissertations, these are often the most read sections, I will endeavor to keep these as interesting, elevating and stimulating as the rest of this work. Many, from the past and present, have contributed significantly toward preserving the tottering sanity which is mandatory in accomplishing such lofty ventures during one's lifetime, and it would be invidious not to name them here.

At the outset, I will always be thankful to Dr. Duarte deFreitas at Loyola University for developing my interest in protein biochemistry and helping me get to UAF, and to Prof. Larry Duffy for taking me under his wing. In his inimitable style, Dr. Duffy always kept me moving. During the unanticipated setbacks, if it

was not for his "It's a learning experience," graduate life would indeed have been agonizing. His immutable freedom to all students in the laboratory fuels the fire which is necessary to develop as conscientious workers. And yes, he also taught me that the results are not wrong, only the interpretations are. For all that he has done for me at UAF and beyond, I thank him. Also, I sincerely appreciate the timely and gentle goading from my graduate advisory committee which resulted in focussing my efforts.

I commend the Department of Chemistry, the then Biochemistry and Molecular Biology program, James R. Crook Fellowship of the UA Foundation and the Alzheimer's Disease and Related Disorders Association for providing continued financial support throughout my gradual term at UAF, and the Graduate School for providing supplemental travel monies for all my annual southerly migrations to present the ongoing work in our laboratory. Many thanks to Drs. Sathy Naidu and Gerry Plumley from the IMS for giving me extracurricular opportunities during a couple of long summers. I thank Tracy Garrison for initiating the CD work in our laboratory. The CD work could not have been complete without the prompt arrangements made by Dr. John Sutherland of Brookhaven National Laboratory, and the excellent technical assistance from Dr. Krzysztof Polewski during the long hours spent at Port U9B of the NSLS.

Sheila Chapin, Marlys Schneider, and St. Laura Morisky nurtured and humored me all along, Beth Laursen let me keep my desk, and Norma Mosso let me be - for this I will always be thankful to them. Linnea Delatour and Joan

Roderick were always there when I needed their company and I cherish them. Andreé Porchét is to be especially remembered for the priority given to all my amino acid analyses, for baking many nutritious cakes, and for being so much help in the laboratory. Others who helped me make mundane official matters enjoyable were Jean James, Sally Ray and Nancy Connolly from the IAB. I also thank Dwight Ittner and Carol Haas for their prompt help with interlibrary loans, and Richard Veazey of IMPACT for his timely intervention in the preparation of the presentation slides. I now remain indebted to Dr. Katharyn Spiegel and Char Raby of Parke Davis' DomLab for keeping me awake during the hours which were spent polishing this document.

I express special appreciation to my laboratory colleagues, Xiaohong Zhao and Sherri Trask, for providing me with inspiration to finish sooner, and See-Tarn Woon for making me laugh. I also appreciate the efforts of the City of Fairbanks and the Alaska State Troopers for tolerating me on the roadways and letting me live to enjoy them. All my ABR soccer teammates can now take a breather in that they will not have me outrun them; o yes, I am definitely slower after the mastoid bone fragmentation. Carol and Mason, thank you for providing me with all the music during the conception of the first draft of this dissertation, but I must mention that, I was driving down the road feeling bad, that fateful day. I thank Jack Townsend for being a true Maverick during the Two-Way Fun Tests, and Allen Doyle for sparing me the painful exertions of training for running races. Chuck "Horse" Morgan, Paul and Maureen Canarsky and Bhaskar Neogi kept

all the fun and frolic and frosties coming, both on and off the badminton courts; thank you comrades. Mars Chambers and Neil Barten will be remembered for bringing in a refreshing change in our basement headquarters along with Steve Lewis, Mike Petrula and Eva Saulitis. It's a pity Neil, that I will not be waking you up in the wee hours of the long winter nights.

Many others who have been friends, philosophers, or guides include - Tracer Martinson, who kept laboratory life endurable by her friendly banter in the hallowed hallways of AHRB, R. Michael McKay for his keen intellect in adding two and two, and the youthful Aynsley McKay for proof reading a majority of this manuscript. John Loquvam taught me how to vanquish those sitting ducks on a 12% grade and the acumen involved in silently slipping past unsuspecting bicyclists. To Steve Butler and Gina Interrante, I say, Listen up! The Windy City is just too flat for me. With Brent Golden, I agree *Montani sempre liberi.* The collective brain power of the highly erudite group of Mosa Mohammed, Alex Lai, Soren Alimchandani and the Satyals will be remembered for the numerous, stimulating and sometimes vapid conversations. The Gillis' with their sweethearts Anders and Christina, and the Wyllie Echeverrias with Vickie, Beckie and Tessie, always provided me the ideal family atmosphere which is necessary at these latitudes. Genezaret Barron spent innumerable cold nights with me to shoot the *Aurora Borealis,* using monochrome films; Paco, no one will snuff you away from my memory. The endearing kinships arising from these rendezvous have survived beyond the compilation of this work.

Much of the impetus to finish this work came from my parents, Mummie and Pappa. He equipped us with toy construction sets, while building macrostructures himself, showed me the importance of the structure of beams, girders and columns in their function, and let me find the question of all questions without telling me in as many words. To Mummie, thanks for letting me know that to understand the physical world outside, one has to go deep inside oneself first, and that, sometimes, letting things happen has its own charm. To Jagdip, my giant little brother, I can only wish that I can be as strong as you are, both, emotionally and physically. To, Laurie Wonnell, thanks for being a confidante and a pal in the strangest of places; to Anna Yeakley, I say, it was nice of you to let me see the path leading to the other end of this Universe; you consolidate my faith in human society. Deborah Koons stood by me with tissue restorers while I was slaying the demons and helped me stand during the "tripod daze," and Christa Morrow helped me get strong shoulders for the same; thank you both for letting me fulfil the prerequisites to shrug this world.

And finally, thank you Amy Lloyd, for keeping the laboratory filled with all the excitement that I could handle.

Chapter 1

Introduction

The deposition of fibrillar proteinaceous matter in brains and other tissues in the body is a characteristic of many amyloidogenic diseases such as multiple myeloma (Glenner et al., 1970), scrapie (Prusiner et al., 1983), Down's syndrome (Masters et al., 1985), type II diabetes (Nishi et al., 1990), leukoaraiosis (Tabaton et al., 1991) and Alzheimer's disease (Katzman and Saitoh, 1991). The process of amyloid deposition is yet unclear, but it is believed that amyloid deposits lead to dysfunction and death for the tissue or organ. In Alzheimer's disease, the progressive neurodegeneration is correlated with the accumulation of senile plaques (SPs), the occurrence of cerebrovascular (CV) deposits, and neurofibrillary tangle (NFT) formation in the brain.

Irrespective of the origin, amyloid deposits are stained with Congo red giving a characteristic green birefringence under polarized light, and exhibit an X-ray diffraction pattern typical of ß-pleated sheets. The CV and SP deposits have been found to be made up primarily of the Alzheimer ß-protein, AßP, a 39-43 amino acid protein having frayed amino and carboxyl termini (Masters et al., 1985; Roher et al., 1993). The formation of amyloid deposits is one of the foci of this study.

Certain metals, like aluminum, iron and zinc have been proposed as risk factors in many neurodegenerative ailments (Frederickson, 1989; Connor et al., 1992), and may therefore have a neurotoxic effect. The involvement of metal ions such as aluminum was discovered in various pathological disorders including Parkinsonism with dementia (Hirano et al., 1961) and AD (Crapper et al., 1973). The overall aluminum levels in undiseased human brain have been found to increase with age (Katzman et al., 1978), and in AD brains, higher levels of many elements including aluminum are found (Thomson et al., 1988). The aluminum salts in AD brains were found to be closely associated with the NFTs (Perl and Brody, 1980; Candy et al., 1986; 1992;), albeit its presence in SPs is still controversial (Landsberg et al., 1992). The association of aluminum with AßP, and its significance in amyloid deposition is another theme of this thesis. A brief review of the studies in the field of amyloid research is now given. This will be followed by a discussion of the factors involved in the structural stability of the AßP, and finally, the goals of this study.

1.1. The Generation of Amyloid

The term, amyloid, was coined in the mid 19th century by Rudolph Virchow to describe the stainable carbohydrate deposits in the liver. Some years later, Friedreich and Kekule found these deposits to be made of protein, not starch (Hind, 1986). The nomenclature, however, prevailed, and is currently used to identify *all* forms of fibrillar and relatively insoluble protein deposits. Glenner et al. (1970) were successful in solubilizing and purifying amyloid deposits from people having systemic amyloidosis, an inherited condition which is characterized by a widespread deposition of amyloid throughout the body. A subsequent analysis of these deposits revealed them to be fragments of immunoglobulin light chain (Glenner et al., 1970). Other amyloid deposits which are tissue or organ specific are found in localized amyloidosis, and can arise from genetic or non-genetic factors (Glenner, 1980). Like most age-related diseases, the slow manifestation of symptoms in amyloidosis is analogous to a gradual deposition of amyloid.

Although it has not been satisfactorily proven in the pathogenesis of AD, the amyloid can be generated by two major possible routes (Fig. 1.1). As proposed by the enzymatic theory, cleavage of a precursor protein due to modifications by enzyme, and/or cleavage by modified enzyme takes place, releasing peptides which aggregate to give the amyloid deposits. Alternately, it can be theorized that conformational changes occur in the released peptide fragments imparting resistance to further proteolysis and a subsequent

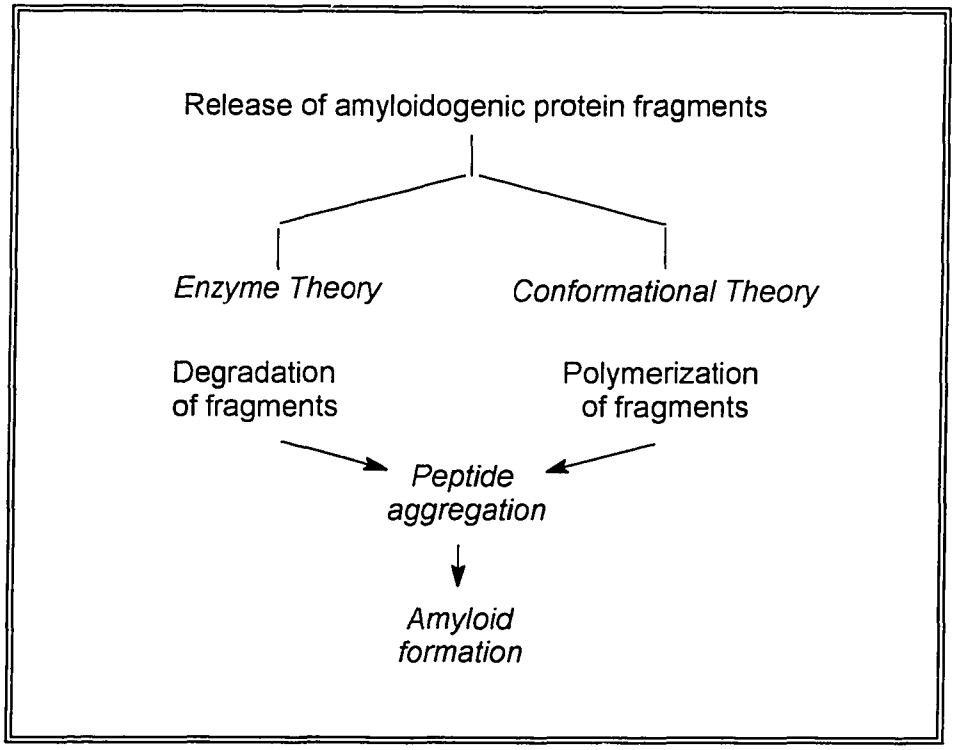

Fig. 1.1 Possible mechanisms for the generation of amyloid.

aggregation. In fact, a conformational change is associated with cerebral amyloidosis in scrapie, a prion-related disease (Prusiner, 1991). The final event during amyloidogenesis in all instances is, however, dysfunction and concomitant death for the tissues and organs involved. When localized sites in the brain have a predilection for amyloid deposition, the result is a progressive loss of cognitive functions due to the inevitable death of associated neurons.

1.1.1. Identification of Amyloid

The difficulties in purifying the insoluble amyloid deposits led to elucidation of their morphology long before characterization of the protein. Divry (1952) employed Congo red to specifically stain the amyloid deposits and identify them under polarized light. In 1959, Cohen and Calkins used electron microscopy and observed that the amyloid deposits from different origins possessed identical fibrillar morphology. Cooper (1974) observed that the amyloid deposits stained by the dye Congo red exhibited a distinctive birefringence pattern, red under non-polarized light and green under polarized light.

Glenner (1980) used X-ray diffraction and found that amyloid deposits exhibited reflections characteristic of repeating ß-sheet motifs. A similar morphology is found in *Bombyx mori* silk, which was schematically described by

Marsh et al. (1955) as a stacked cross-ß assembly even before the advent of high resolution structural techniques. The direction of the sheets is perpendicular to, *i.e.*, across, the direction of the fibril formed (Fig. 1.2) which gives rise to macroscopic fibrillar structures. Amyloid deposits have also been identified by certain tinctorial properties of fluorophores like thioflavine S and thioflavine T (Vassar and Culling, 1959). Although the mode of interaction is not fully understood, these stains have been used as suitable probes for all amyloids, including AßP. The observed birefringence could be due to a structured binding of the dye molecule to the repeating cross-ß motif of amyloid proteins. The binding could arise due to the ionic interactions between the negatively charged sulfate groups of Congo red and the positively charged amino acids, histidine, arginine and lysine (Klunk et al., 1989) present in AßP. Caging of the dye between the stacked cross-ß sheets could also take place, as has been suggested by Cooper (1974), and Glenner (1980).

1.2. The Alzheimer's ß-Protein

The most characteristic histopathological feature of Alzheimer's disease is the localized amyloid deposits in the brain as senile plaques, as well as neurofibrillary tangles. Amyloid deposits are also seen in brains of aged

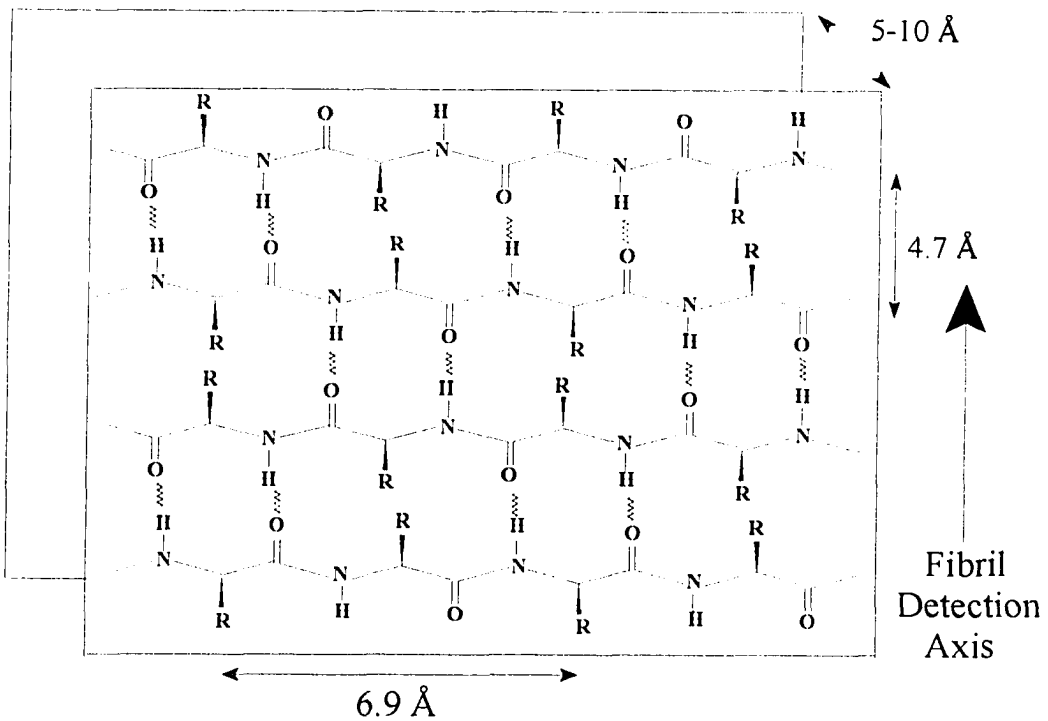

Fig. 1.2 Schematic representation of cross-ß sheet formation. This is the most popular model for all amyloid-forming proteins. Based on X-ray diffraction, the interstrand distance along the fibril meridian is 4.7 Å and, depending on the peptide, the intersheet distance varies between 5-10 Å.

primates - monkeys, dogs, and polar bears (Selkoe, 1989). The partial amino acid sequence of leptomeningeal amyloid in AD was first reported by Glenner and Wong (1984a) which corresponded to a 4.2 kDa protein, the Alzheimer ß-Protein, AßP. The amyloid deposits found in the aged and AD brain are found primarily in the entorhinal cortex and hippocampal regions (Whitehouse et al., 1982; Pearson et al., 1985). The AßP deposits in senile plaques are associated with the walls of blood vessels (neuritic plaques), and amyloid deposition also takes place in the cerebrovascular region (Wisniewski and Terry, 1973). The primary structure of AßP purified from neuritic plaques and vascular amyloid indicate peptides varying between 42-43 and 39-40 amino acids respectively (Masters et al., 1985; Selkoe et al., 1986; Prelli et al., 1988; Miller et al., 1993; Roher et al., 1993).

There has been extensive unresolved discussions on whether the formation of senile plaques or neurofibrillary tangles is the primary change in AD (Wisniewski et al., 1994). There are reasons to believe that amyloid deposition precedes the neuropathological phenomena (Giaccone et al., 1989; Mann, 1989; Motte et al., 1989). Supporting this belief was the discovery of a 40 residue soluble AßP variant, ß1-40, which was produced constitutively by normal cells (Seubert et al., 1992; Shoji et al., 1992). The longer variant of AßP, ß1-42, has also been identified in human cerebrospinal fluid (Vigo-Pelfrey et al., 1993). Moreover, the AßP first deposited in pre-amyloid deposits (Wisniewski et al., 1994) is not stainable with either Congo red or thioflavine S (Tagliavani et al.,

1988) which indicates that the morphology of AßP varies with the deposits. Given the possibilities that soluble variants of AßP circulate freely in their biological environment, it appears that under appropriate conditions, AßP would eventually lead to amyloid formation.

In Alzheimer's disease, the mechanisms of amyloid formation have been at the forefront of most current research. The identification of soluble forms of AßP has made it necessary to know the pathway(s) by which they are generated. Synthetic peptides homologous to AßP have been shown to form amyloid fibrils *in vitro* (Castano et al., 1986; Kirschner et al., 1987). It is clear that these peptides do not spontaneously form aggregates but only under conditions which are conducive to form fibrils. The aggregation of these peptides was demonstrated to be related to their concentration, pH of the solutions, the presence of salt, and metal ion concentrations (Castano et al., 1986; Kirschner et al., 1987; Barrow et al., 1992; Burdick et al., 1992; Hilbich et al., 1992). Once formed, the well-defined morphology of these aggregates can exert its toxic influence in their vicinity.

The amyloid deposits contain components of a complementary cascade which could usher the events leading to annihilation of the neuronal milieu in elderly or AD brains. The best hypothesis about the origin of neuritic plaques contends that their origin is free from any neuritic involvement (Yamaguchi et al., 1988; Armstrong et al., 1991). In fact, many researchers have found that AßP exerts neurotoxic effects based on its aggregated state (Whitson et al., 1989;

Yankner et al., 1990; Pike et al., 1993). The opposing view is that selective amyloid deposition does not co-exist with neurofibrillary abnormalities (Davies, 1994). Altered neurites may initiate the aggregation of monomeric AßP to form amyloid (Price, 1986). There are instances when AßP enhances the survival of neurons (Whitson et al., 1989, 1990). Thus, the amyloid deposits might be a tombstone heralding some secondary event(s) in an aging or AD brain. Regardless, AßP is intimately involved with neuronal degeneration. The extensive characterization of the primary structure of AßP variants has allowed researchers to isolate and identify the cDNA for the parent protein of AßP.

1.2.1. The Alzheimer Precursor Protein

The proteins found in the amyloid deposits of AD, like all other amyloidogenic proteins, are formed by degradation of a much larger precursor protein (Glenner, 1988; Selkoe, 1989; Crowther, 1991). Kang et al. (1987) have shown that the AßP is a by-product of processing a large integral membrane glycoprotein, the Alzheimer precursor protein, APP. The human APP exists as three major isoforms ranging from 695 to 770 amino acids (Fig. 1.3) which are expressed throughout the body (Palmert et al., 1989), but whose biological function is still unclear. APP isoforms, arising due to alternatively spliced pre-mRNA (Kang, 1987; Lemaire, 1989), possess 56 and 75 amino acid

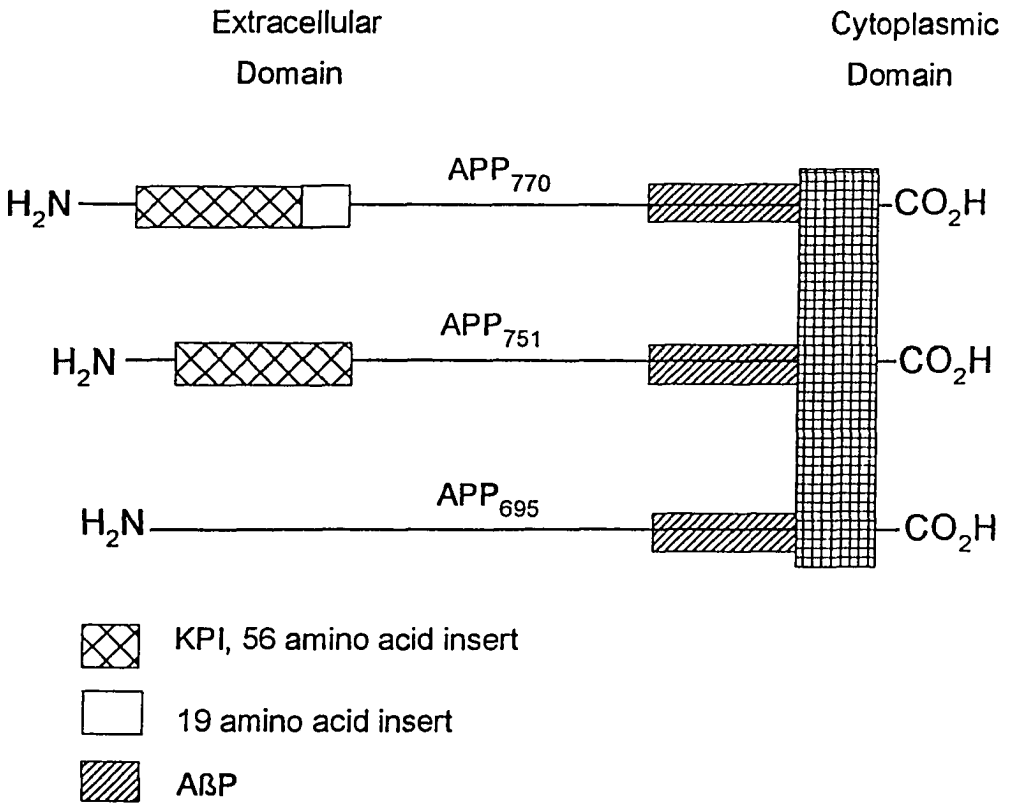

Fig. 1.3 The schematic of the full-length Alzheimer Precursor Protein, APP, isoforms APP_{695}, APP_{751} and APP_{770}. The longer APPs include the Kunitz protease inhibitor (KPI) region and a 19 amino acid insert near the amino terminus in the extracellular domain. The lengths of the respective regions are not to scale.

Kunitz-protease inhibitors (KPI) inserts to form, respectively, APP_{751} and APP_{770}.

The processing of APP is now extensively characterized and recent metabolic data suggest that soluble forms of AßP are released from various cells and tissues (Gandy et al., 1994). One processing pathway results in the cleavage of APP between Gln^{611}–Lys^{612} or Lys^{612}–Leu^{613}; which is in the AßP region (Palmert et al., 1989; Esch et al., 1990; Seubert et al., 1993). When this occurs, a large soluble extracellular protein, protease nexin II, is released; since there is no intact AßP sequence in the released protein, there is no amyloid deposition by this mode of processing (Hardy and Higgins, 1992). However, cleavage by a "secretase," one of the several enzymes responsible for the processing of the APPs (Sisodia et al., 1990; Pasternack et al., 1992), generates amyloidogenic peptides. The amino acid sequence of the AßP region of APP showing the proteolytic sites is given in Fig. 1.4.

Other evidence for cleavage of APPs is consistent with action occurring within the lysosomal/endosomal system (Golde et al., 1992; Haass et al., 1992). The lysosomal processing of APP leads to potentially amyloidogenic fragments, which could be further metabolized to produce AßP variants (Shoji et al., 1992). There may be other factors which are equally important in forming amyloid deposits from the soluble AßP variants; these contributions could arise from processing of soluble AßP into aggregated forms (Knauer et al., 1992), and/or the association of AßP with other molecules (Wisniewski and Frangione, 1992).

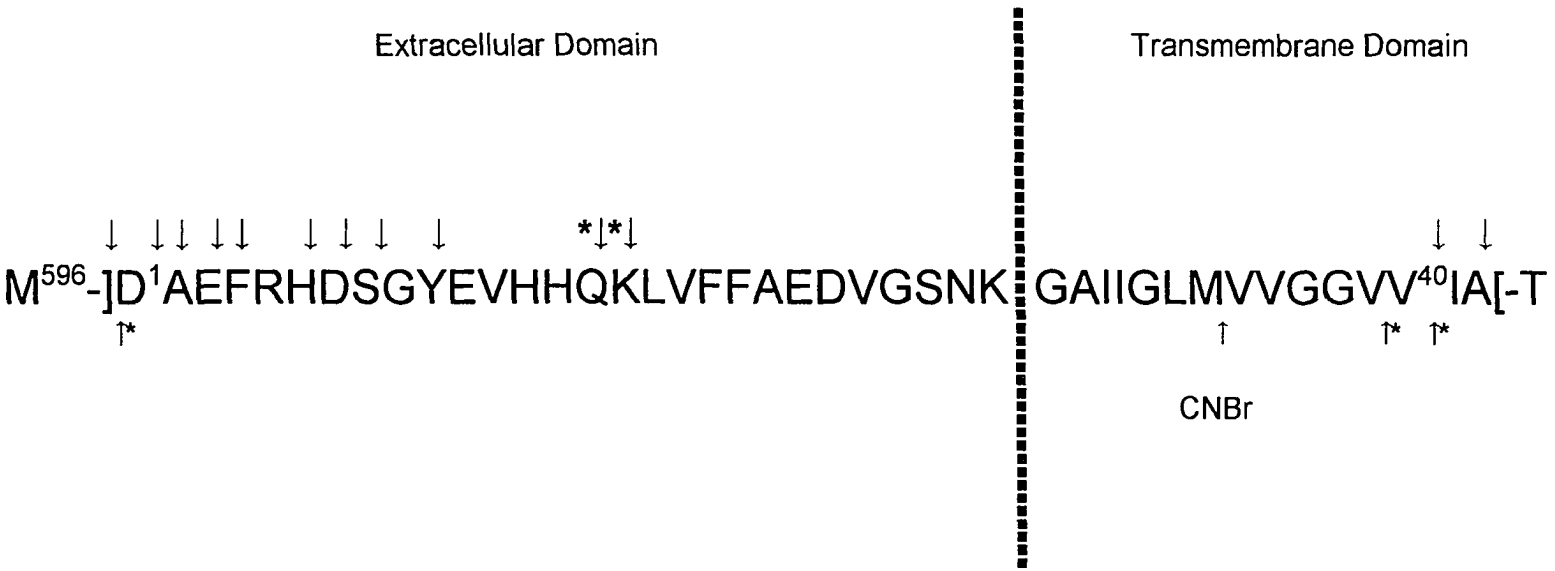

Fig. 1.4 Primary sequence of human Alzheimer ß-protein, AßP, indicating the proteolytic sites. The non-amyloidogenic sites of the AßP region of APP (-] [-) which generate large soluble by-products are indicated above the sequence by *↓. The cleavage sites that form the neuritic plaque amyloid peptides are given above the sequence by ↓, and those forming the cerebrovascular amyloid peptides are shown below the sequence by ↑*. The CNBr cleavage site in AßP is indicated by ↑.

1.3. Intrinsic Factors for AßP Deposition

There have been several studies on the sequence similarities between the senile plaque core protein and the cerebrovascular amyloid (Glenner and Wong, 1984a; Masters et al., 1985; Selkoe, 1986; Selkoe et al., 1987). The heterogeneity in the amino and carboxyl termini of the isolated AßP variants would indicate differences in degradative pathways of the APP, or multiple proteolytic attacks on the amyloid protein (Miller et al., 1993). However, results from electron microscopy of purified brain amyloid (Glenner, 1980) mutually agree with synthetic peptides homologous to the AßP sequence (Kirschner et al., 1987). The amyloid fibrils are observed to be rigid unbranched structures which self-associate and form twisted helices with a periodicity akin to the cross-ß fibrils of *Bombyx mori* silk protein. The morphology of the CV and SP amyloid deposits and the fibrils formed by synthetic peptides indicate that there must be considerable inherent contribution from the peptide molecule. These intrinsic factors arise due to the amino acids constituting the protein(s), their positions along the peptide backbone, and the side chain contributions.

1.3.1. Putative Salt-bridges in AßP

Kirschner et al. (1987) have proposed a salt-bridge between charged residues His^{13} and Asp^{23} as a mode for intersheet stabilization in synthetic ß1-28

(Fig. 1.5), which exhibits fibrillar morphology similar to AßP. The formation of ion-pairs resulting in increased ß-pleated sheet content has also been suggested on the basis of pH studies on synthetic AßP fragments ß1-28, ß1-39 and ß1-43 (Barrow and Zagorski, 1991; Fraser et al., 1991; Burdick et al., 1992). These observations are in agreement with the morphology of native SP amyloid isolated from post-mortem brain tissue (Masters et al., 1985). The pH dependence of AßP and enhanced ß-pleated sheet structure in solution would suggest a strong contribution from the amino terminal region, which contains all the ionizable residues, to form stable oriented fibrils.

Fraser and colleagues (1991b, 1992; Inouye et al., 1993) maintain the importance of electrostatic interactions between His and Asp/Glu residues as the primary driving force for the fibril formation of ß1-40 and its derived analogs. Their reversible fibril assembly/disassembly was pH-dependent which was consistent with observations of Masters et al. (1985) that oligomers of AßP occurred only when the histidine residues were ionized.

1.3.2. Mutations in AßP of Different Origins

When compared to human AßP, there are three amino acid substitutions in the rodent AßP sequence, Arg^{5}→Gly, Tyr^{10}→Phe and His^{13}→Arg which are present in the extracellular amino-terminal region. The human AßP readily forms

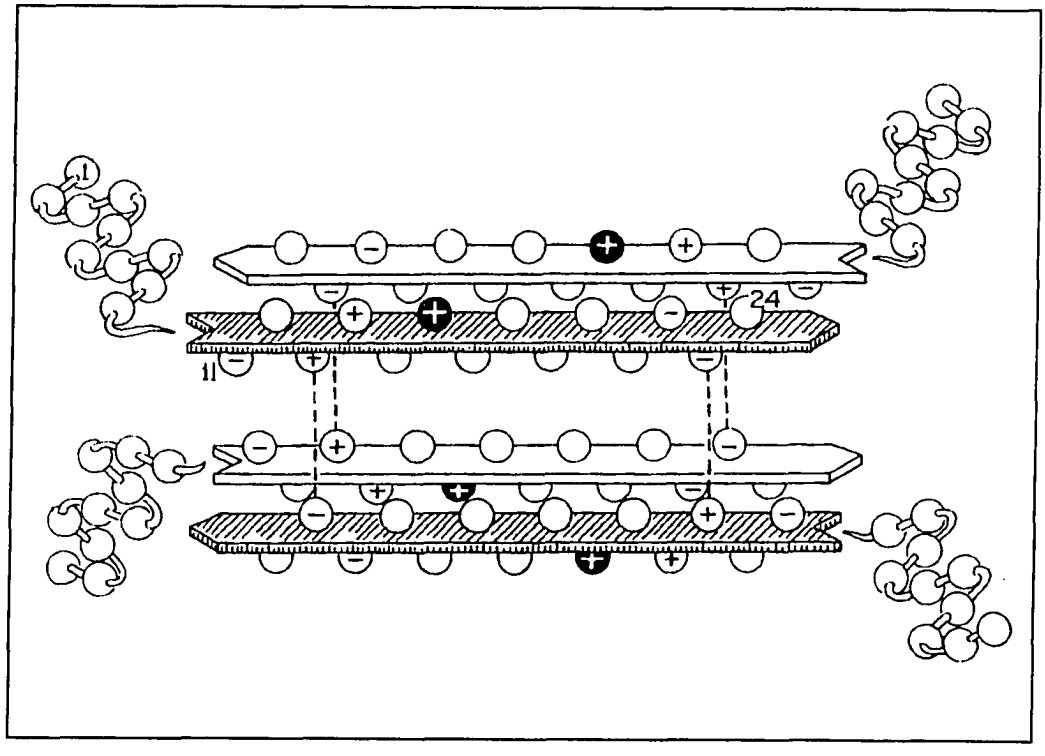

Fig. 1.5 The hypothetical aggregation model for ß1-40 based on putative intersheet electrostatic interaction between His^{13}-Asp^{23}. The antiparallel ß-strands are shown with a meridian spacing of 4.7 Å. The lysine residues, Lys^{16} (darkened circles), in the sheets face outside. Only the first 24 residues have been indicated here for clarity.

a cross-ß structure, revealed by the X-ray diffraction study (Kirschner et al., 1987), but the rodent AßP forms ß-pleated sheets only under certain conditions (Otvos et al., 1993). The differences in primary sequence for the rodent AßP could account for its inability to form fibrillar deposits (Fraser et al., 1992; Otvos et al., 1993). On the other hand, the synthetic peptide corresponding to the Dutch variant of familial AD, *hereditary cerebral hemorrhage with amyloidosis, Dutch type* (HCHWA-D) with a single Gln^{22}→Glu change greatly accelerates fibril formation (Wisniewski et al., 1991; Fraser et al., 1992; Fabian et al., 1993), indicating its greater propensity to form ß-pleated sheets. It is intriguing to note that the fibrils formed by the Dutch mutant have the potential to act as templates speeding fibril formation by non-mutant peptides (Frangione et al., 1993).

1.3.3. Hydrophobicity and Solubility

The two major fragments of the human AßP consist of ß1-39 in the cerebrovascular amyloid (Glenner and Wong, 1984a) and ß1-42 in the extracellular senile plaque deposits (Masters et al., 1985). Hilbich et al. (1992) have observed that substitutions of hydrophobic amino acids at the carboxyl terminus reduces the amyloidogenicity of peptides homologous to AßP. Synthetic peptide homologs of AßP with very different solubilities were also observed by Burdick et al. (1992). The hydropathic analyses of the primary

sequence of AßP, based on Kyte-Doolittle and Fauchere-Pliska scales for hydrophilicity, are given in Fig. 1.6 (panel A). There are two regions with discrete hydrophobicity, the carboxyl end having maximum hydrophobicity, while the amino terminus is distinctly more hydrophilic. The hydrophobic carboxyl terminal is also the end terminus which has higher propensity for ß-sheet formation according to Chou-Fasman analysis (panel B).

The intrinsic insolubility of AßP, arising due to the amino acid content and sequence of the peptide, was investigated by Halverson and coworkers (1990). By using the amide I band absorption, they found that the strong intermolecular interactions in the highly hydrophobic region comprising residues 34-42 may be responsible for the inherent insolubility of this fragment. Their spectroscopic data also indicated that ß26-33 and ß34-42 fragments possessed ordered ß-sheet structure in the solid state. For the ß34-42 peptide, which contains at least 45% branched residues, the antiparallel ß-sheet character in the solid state, and the unusual resistance to solvolysis, were only overcome by strong amide-chelating solvents like LiBr/THF (Halverson, 1992). The carboxyl terminal domain was therefore proposed as a major determinant of the aggregation of the AßP which could nucleate ß-pleated sheets in amyloid fibrils. The reduction in solubility can be attributed to the increase in hydrophobicity for the larger fragments. There are reports that the Leu^{17}–Val^{21} region provides the hydrophobic cluster for packing of the synthetic amyloid fibrils (Fraser et al., 1992; Inouye et al., 1993). The van der Waals interaction between amino acid

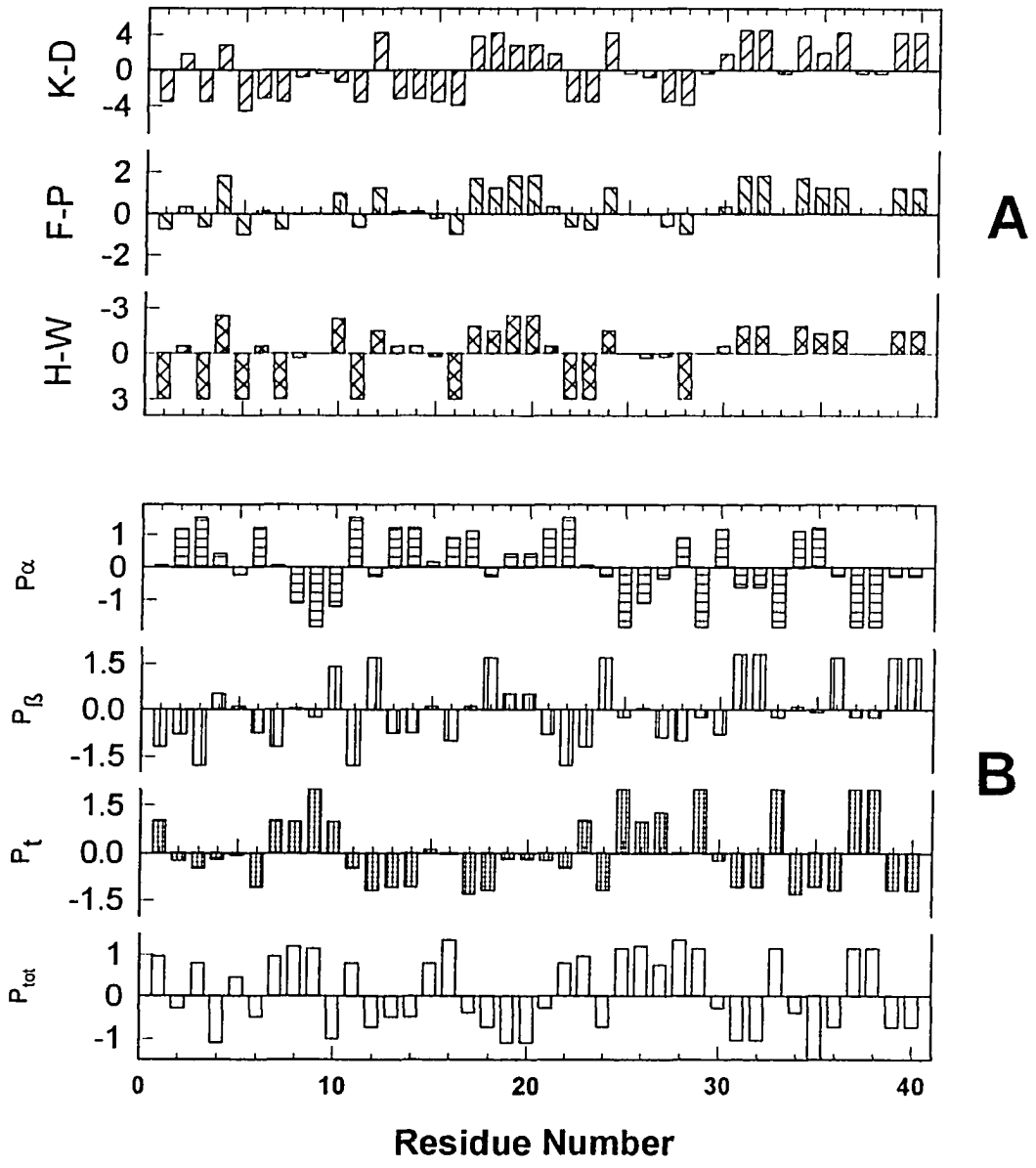

Fig. 1.6 Primary sequence analyses of secondary structure and hydrophilicity of ß1-40. Panel A gives the hydrophilicity profiles for ß1-40 using Kyte-Doolittle (top), Fauchere-Pliska (middle), and Hopp-Woods (bottom) algorithms. Panel B shows the distribution of propensities for α-helical (P_α), ß-sheet (P_β), ß-turn (P_t) and the total (P_{tot}) amino acid sequence.

side chains become increasingly important during stacking of the ß-pleated sheets, and with a concurrent solvent-exclusion can pack the sheets tightly which would result in stable fibrils.

1.3.4. Membrane Anchoring Site

There is mounting evidence that intact AßP variants are membrane-associated in fractions isolated from the cerebral cortex, cerebral microvessels, and leptomeningeal vessels (Wisniewski and Terry, 1973; Matsumoto and Fujiwara, 1991; Haass et al., 1992), platelets, and in bacilovirus-infected insect cell lines (Gardella et al., 1992; Ghiso et al., 1992; Gandy et al., 1992; Ramabhadran et al., 1993). The AßP sequence possesses a cell-adhesion site (Chen and Yankner, 1991). The Hopp-Woods designation, a measure of hydrophilicity (Fig. 1.6, panel A), locates a potential cell-adhesion site near the amino terminus of AßP. Ghiso et al. (1992) demonstrated that the –RHDS– sequence of the 109 amino acid carboxyl terminus (amino acids 5 to 8 in the AßP nomenclature) of APP, which includes the AßP, promotes cell-substratum adhesion. This larger fragment which contains the putative transmembrane and cytosolic regions of the APP, spontaneously forms amyloid fibrils. The cell-attachment region could anchor the AßP domain thereby inducing the proteolysis of APP, eventually leading to fibrillar aggregates.

1.3.5. Secondary Structure of AßP Variants

The presence of soluble forms of AßP variants emphasizes the dual nature possessed by the amino acid sequence in these proteins. It has been theorized earlier that inhibition to proteolysis of proteins liberated from the processing of APP can take place due to a change in conformation. In fact, a conformational change in the amyloid forming scrapie protein, PrP^{Sc}, is known to be responsible for its aggregation (Prusiner, 1991). In spite of being a debatable issue, the conformational state of AßP might be a key determinant in neurotoxicity (Kosik and Coleman, 1992). However, due to the existence of AßP in various conformational states which are modulated by its environment, one could speculate on the inconsistency between neurotoxicity reports from different laboratories. Based on the Chou-Fasman analysis (Chou and Fasman, 1977; 1978) of its primary sequence (Fig. 1.6, panel B), AßP has inherent propensities of forming α-helical and ß-pleated sheet structures.

There has been a proliferation of spectroscopic investigations on the secondary and tertiary structures of synthetic peptides homologous to the native AßP sequence. Using electron microscopy and X-ray diffraction, Kirschner and colleagues (1987) found that aggregates formed by the amino terminal domain comprising residues ß1-28 resembled the *in vivo* amyloid of senile plaque cores. Solid state Fourier transform infrared (FTIR) spectroscopic studies on the hydrophobic carboxyl region, comprising ß34-42, showed that it is made entirely of antiparallel ß-pleated sheets (Halverson et al., 1990; Halverson, 1992).

The circular dichroism (CD) spectroscopy done by several groups has shown that the amino terminus of AßP, ß1-28, forms α-helical structure which can be modulated by the solution environment (Hollosi et al., 1989; Barrow and Zagorski, 1992; Burdick et al., 1992). The CD findings on the longer synthetic variant, ß1-42, between pH 4 and 7 revealed that a secondary structure transition was accelerated at pH 5.5, suggesting that the Val^{40}–Ala^{42} segment was critical for the ß-sheet stability in solution (Barrow et al., 1992). The HCHWA-D sequence having a point mutation, $Glu^{22} \rightarrow Gln$, has the highest predicted ß-sheet content of any amyloid sequence (Fabian et al., 1993). Hollosi et al. (1989) used the smaller fragments, ß1-12 and ß11-25, and showed that these peptides, respectively, exhibited a random coil and antiparallel ß-pleated sheet structures in aqueous solutions. Employing high resolution nuclear magnetic resonance (NMR) spectroscopy, a short α-helical stretch between Ala^2-His^6 and a longer α-helical segment between Tyr^{10}/Glu^{11}-Ser^{26} was identified (Barrow and Zagorski, 1991; Sorimachi and Craik, 1994). In the rodent AßP, having $Arg^5 \rightarrow Gly$, $Tyr^{10} \rightarrow Phe$ and $His^{13} \rightarrow Arg$ substitutions, Otvos et al. (1993) found that a double conformational transition region located between residues 9-19 in the extracellular domain. A commercial preparation of synthetic ß1-40 has been reported to form calcium-ion channels when incorporated into phosphatidyl-serine liposomes (Arispe et al., 1993).

Solid state dispersive infrared spectroscopy and CD were used to demonstrate the requirements for *in vitro* filament formation in synthetic amyloid

peptides (Hilbich et al., 1991). These workers found that all the information leading to aggregation is stored in the ß-sheet forming sequence of the 12-43 segment. Their results showed that the 10-42 fragment formed the core ß-sheet portion of filaments during aggregation; however, they also believe that residues 29-42 primarily forms an α-helix. With the aid of isotope-induced shifts in the amide I band, Halverson and coworkers (1991) found that the valine residues at positions 36, 39 and 40 are in the ß-pleated sheet region of the ß34-42 aggregate, whereas Leu^{34}, Ile^{41}, and the Gly^{37}–Gly^{38} sequence were not part of an idealized cross-ß sheet due to a cis-amide linkage.

1.3.6. Post-translational Modifications in AßP

The occurrence of D-amino acids in proteins as a post-translational modification is an important stereochemical event. Bada (1985) pointed out that in some cases, D-enantiomers arise spontaneously from racemization reactions related to the aging phenomenon. Altered forms of aspartic acid, *viz.*, L-iso-Asp and D-Asp, were first detected in the protein partially purified and isolated from SPs (Shapira et al., 1988). The effects of racemization of Asp^1, Asp^7 and Ser^8 in AßP from the brain parenchyma may be to impart stability and proteolytic resistance in neuritic plaques (Roher et al., 1993). These isomerizations can cause structural alterations in the polypeptide backbone leading to functional

changes in the AßP. In fact, the D-Asp levels in the brain proteins from rats are enhanced due to a high aluminum diet (Anderson et al., 1990).

Other modes of modifications in AßP involve oxidation of methionine residue at position 35 (Prelli et al., 1988), which inhibits cleavage by cyanogen bromide, or certain proteases. Deamidation and phosphorylation which occur in many proteins with time, could also influence fibril formation in AßP. Such modifications can have deleterious consequences on structure-function relationships of the proteins.

1.4. Extrinsic Factors

The molecular organization and morphology of macromolecular assemblies seen in AßP deposits are also governed by the environment. Some of the extrinsic factors which modulate the peptide conformation include pH, temperature, metal ions and presence of other peptides and proteases. The association of aluminum with brain amyloid has gained much publicity with a specific focus on its neurotoxic role in Alzheimer disease. The compositions of CV and SP core amyloid deposits show considerable heterogeneity in both the amino and carboxyl termini lending credence to the hypothesis of multiple proteolysis (Glenner and Wong, 1984a; Masters et al., 1985). The role of these fragments in aggregation or stability of the deposit has not been studied.

1.4.1. The Role of Aluminum

Metals are known to be good chelators of Asp-, His-, Glu- and Cys-amino acids. Metal ions also form complexes with the polypeptide backbone, in part due to the stabilization of the intermediate carbanion formed by the loss of α-H; and this interaction increases the racemization rate by several orders of magnitude (Buckingham et al., 1967). Elevated levels of D-asp in the brain proteins of rats have been observed when solutions of $AlCl_3$ were fed orally over a period of ten weeks (Anderson et al., 1990).

There are elevated levels of aluminum and other metals in the brain tissues of AD patients (McDermott et al., 1978, 1979; Markesbury et al., 1981; Thompson et al., 1988). High levels of aluminum have been found in the autopsied Alzheimer brain NFTs (Perl and Brody, 1980) and SPs (Candy et al., 1986; Crapper et al., 1973). In the case of SPs, high levels of aluminosilicate were seen by some workers (Candy et al., 1986), while this observation is strongly contested by others (Landsberg et al., 1992). The fact that Al^{3+} has a high affinity for PO_4^{3-} was proposed in the appearance of NFTs which include phosphorylated proteins (Perl, 1985).

Arispe et al. (1993) have found that Al^{3+} blocks calcium-ion channels which are formed by ß1-40. The amino terminus of AßP consists of aspartate, glutamate, and histidine residues, which are known to complex trivalent cations (Chalet et al., 1984). Aluminum ions have a potential to form interchain and intrachain peptide complexes and could increase the structural stability of the

peptides by forming macromolecules using water-metal bridges (Hollósi et al., 1994). It can be recalled that the intersheet distance of 4.7 Å in ß1-40 and derived analogs (Fig. 1.5) could be stabilized by accommodating such bridges. More recently, several workers have demonstrated that Al^{3+} interacts with ß1-40 in solution (Exley et al., 1993), while other reports include aggregation caused by Al^{3+}, Fe^{3+} and Zn^{2+} (Mantyh et al., 1993; Kawahara et al., 1994).

1.5.2. The Presence of Other Peptides and Proteins

The proteolytic cleavages occurring in APP takes place within the putative transmembrane sequence of AßP which lead to the formation of amyloid deposits. While only 25-30% of the mass has been characterized, the protein content of amyloid deposits outnumber all other CV and SP proteins by a mole ratio of 40:1 (Miller et al., 1993). The amyloid deposits include peptides having frayed amino and carboxyl termini of AßP (Roher et al., 1993). The AßP has also been shown to be overexpressed in some, but not all, AD brains (Seubert et al., 1992; Cai et al., 1993). Other exogenous molecules which are good candidates for fibrillogenesis, and are ultrastructurally related with the amyloid fibrils include lipids, amyloid P component (Hind, 1986), and glycosaminoglycans (Snow et al., 1988). It is therefore important to understand the role of these peptides and proteins in the aggregation of AßP.

The fibril formation in synthetic peptides homologous to ß1-40 is inhibited when incubated with human cerebrospinal fluid (Wisniewski et al., 1993). Apolipoprotein isoforms E and J have been shown to bind to soluble AßP (Strittmater et al., 1993). The penchant for fibril formation is greatly enhanced in soluble synthetic AßP derived analogs by the presence of apo E3 and E4 (Sanan et al., 1994). Since amyloid generation takes place over years, any increase in the nucleating agents would also result in considerable acceleration of the aggregation rate (Hofrichter et al., 1974). In fact, supersaturated solutions of AßP variants, ß1-39 and ß1-40 are stable for days, whereas an equimolar solution of ß1-42 leads to precipitation of the peptide (Jarrett et al., 1993). This indicates that nucleation-dependent mechanisms might be important in the aggregation of soluble AßP (Jarrett and Lansbury, 1993). Moreover, the derived analogs, ß26-39 and ß26-40, precipitate from solution upon the addition of more hydrophobic fragments, ß26-42 and ß26-43 (Jarrett et al., 1993).

1.5. Objectives

The collation of preliminary and published data gives rise to an emerging scene which includes parts played by the increased production of soluble AßP and AßP variants and their precursors, mutation and racemization,

and external factors like pH, metal ions and solution environment. However, there are some important links missing from the picture. The foremost is the conversion of soluble AßP, which in its native physiological form has a mixture of secondary structures, to the predominantly stacked ß-pleated sheet structure of the insoluble amyloid deposits. In the aged and diseased stage, this conformational change could be triggered by a host of endogenous and exogenous factors as described above.

This thesis sought to discover and identify the importance of the structural domains of AßP responsible for the intractable nature of the amyloid deposits. Since many amyloidogenic proteins having little or no sequence homology, but very similar morphology, it was hoped that tracing the pathway(s) followed by AßP might also provide better direction for understanding amyloidosis in other cellular dysfunctions. The role of secondary structure in the aggregation of AßP was studied by using synthetic ß1-40 and derived analogs. Also, the role of aluminum in the conformational stability of the polypeptide backbone was investigated.

Chapter 2 describes the syntheses and purification of ß1-40 and derived analogs which were used for evaluating secondary structural characteristics. These analogs were investigated to provide clues for secondary structural changes by studying their chromatographic behavior. The reversed-phase high-performance liquid chromatography (RP-HPLC) studies are highlighted in chapter 3. The kinetics of secondary structure change in aqueous solutions of

ß1-40 and derived analogs were performed using circular dichroic (CD) spectroscopy and are elucidated in chapter 4. The association of aluminum with ß1-40 and ß6-25 was studied using ^{27}Al nuclear magnetic resonance (NMR) spectroscopy. The characterization of Al(III)-complexed peptide species, and chromatographically-pure Al(III)-bound ß1-40 and ß6-25 peptides based on their unique ^{27}Al NMR resonances is covered in chapter 5.

Chapter 2

Materials and Methods

Introduction

In order to understand the function of AßP, it is important to work with a protein which is amenable to structural investigations. To elucidate the process of aggregation in AßP, it is also necessary to study the protein as its structural domains, preferably in solution. To obtain an array of overlapping peptides in a soluble form, the investigations in this work utilized peptides containing D-amino acids, and substitutions of amino acids which are not present in the native AßP sequence. The natural sources of AßP variants, *viz.*, the cerebrospinal fluid (Seubert et al., 1992), and the post-mortem AD brains (Glenner and Wong, 1984) yield only minuscule amounts of AßP, for instance,

only 100 pg of AßP per neuritic plaque core can be isolated (Miller et al., 1993). The manipulation of biological systems by genetic engineering to produce AßP has been limited in the face of its structural novelty; however partial success has been achieved with bacterial cell lines to generate a larger cytosolic fragment of APP to yield 325 µg/mL of protein (Gardella et al., 1992; Ghiso et al., 1992). Chemical synthesis, on the other hand, has proved to be a valuable approach to manufacture a large number of AßP variants in substantial quantities (Hendrix and Lansbury, 1992). A stepwise coupling of amino acids on a non-compressible support, usually a resin, offers a viable chemical approach for obtaining large amounts of peptides which are easily purified with a minimum of difficulty (Merrifield, 1963). The total synthesis of ß1-40 and derived analogs using a stepwise solid-phase peptide synthesis (SPPS) approach utilized here have provided a practical tool to simultaneously manufacture peptide analogs in substantial amounts for the study of their structure-function relationships.

Any pretension to the ease of chemical synthesis of AßP and derived analogs and the subsequent purification of the product is vehemently denied. The chemistry cannot be taken for granted, because experience has shown that subtle synthetic problems lurk even in the simplest of amino acid sequence (Kent, 1988). These problems are exacerbated by the difficult amino acid sequence of AßP at the carboxyl terminus; some of which have been overcome by using exotic fragment-condensation to generate AßP sequence analogs (Hendrix and Lansbury, 1992; Halverson, 1992). Most synthetic difficulties in

AßP also involve large resin loadings - the propensity to form aggregates during synthesis has been repeatedly stressed by peptide chemists (Kent, 1988). The aggregation is intensified by the carboxyl terminal of AßP which forms antiparallel ß-pleated sheets during synthesis (Halverson, 1992), and therefore requires extensive measures to keep the growing peptide chain solvated during the assembly of amino acids. The stepwise synthesis of ß1-42 has also suggested difficulties during purification due to its insolubility (Burdick et al., 1992) as compared to ß1-40.

Keeping these factors in mind, SPPS was employed in this study to generate fragments of AßP, *viz.*, ß1-40 and derived analogs. Low resin loadings, and multiple couplings in conjunction with solvating agents were used during the stepwise assembly of the peptides; this approach eliminated the purported aggregation during stepwise assembly. Also, elimination of the two ß-branched amino acids in the generally difficult –VGGVV(*IA*)– sequence of ß1-42 alleviated the aggravation of inefficient couplings during assembly of ß1-40. Forbearance coupled with low resin-loading usually terminated in yields satisfactory for the structural investigations of pure ß1-40 and derived analogs; however, the assembly of forty amino acids starting with an initial hydrophobic sequence, and the coupling of the His–Arg and Arg–Arg sequence in the derived analogs warranted considerations unique to ß1-40. A brief overview of the protocols employed in the stepwise synthesis of peptides, and their actual use in the synthesis of AßP and derived analogs is therefore in order.

2.1. Problems and Strategies in Solid Phase Peptide Synthesis of ß1-40

The introduction of solid phase method for chemical syntheses of peptides by Bruce Merrifield (1963) has greatly improved the ability to generate large quantities of peptides; an improvement over solution methods where the primary obstacle was the poor solubility of protected intermediates (Wieland, 1978). Also, unnatural and/or unusual amino acids can be easily incorporated in the growing peptide chain, which is useful for structure-function studies in proteins and peptides. The severity of reaction conditions during solid-phase peptide synthesis, *viz.*, large excesses of reagents, extended reaction times, and elevated temperatures mandates side chain protection in the amino acids (Atherton and Sheppard, 1987). The Merrifield technique employs *tert*-butyloxycarbonyl (tboc) protection for the α-amino group, and the amino acids are assembled sequentially from the carboxyl to the amino terminus on a non-collapsible solid support, usually a clay or resin. The lability of the resin-peptide bond depends on the chemical nature of the linking group of the support to the first amino acid. However, the use of repetitive acidolysis causes cleavage of the peptide from the resin during assembly (Fankhauser et al., 1973), and partial acetylation (Kent et al., 1979) leading to undesired side products. Also, the removal of tboc protective group requires use of the very corrosive hydrofluoric acid, mandating special handling and equipment. Moreover, some of the side-chain protecting groups are not completely removed by strong acids.

The orthogonal approach of side-chain protection and coupling by the use of 9-fluorenylmethoxycarbonyl (fmoc) amino acids provides a safer and more efficient alternative to the Merrifield chemistry of peptide synthesis. The protected side chains are easily cleaved by a relatively safe, trifluoroacetic acid (TFA), to which appropriate scavengers are added. The orthogonal strategy of fmoc-chemistry involves a simultaneous protection of the growing peptide chain at the amino end by the fmoc-group and the use of protected amino acid esters (Udenfriend and Meienhofer, 1979-1985). During cleavage from the resin, a concurrent deprotection of the amino acids gives the crude peptide which is subsequently purified by preparative and analytical chromatography.

2.1.1. Solvation of Solid-Phase

The most important and fundamental consideration during SPPS is the macroscopic insolubility of the solid support (Sarin et al., 1980), and the solvation of the resin-peptide (Kent, 1985). The ability of a resin to swell is directly related to the net increase in free energy from solvation of the linear peptide chain. However, with a sequence of nonpolar amino acids and side chain protecting groups the peptide is prevented from dilution by solvent, eventually leading to decrease in the free energy of peptide within the resin matrix and shrinking of the resin (Sarin et al., 1980). The resultant collapse of

the peptide-resin leads to truncated sequences; this problem of keeping the peptide-resin solvated during assembly is exacerbated in peptides forming ß-pleated sheets (Kent, 1985), like AßP. Use of polar solvents, like dimethylformamide (DMF) helps in alleviating this condition by simultaneously solvating the nonpolar groups and also swelling the resin (Sarin et al., 1980; Atherton and Sheppard, 1985). The use of higher substitutions which lead to higher overall peptide yields results in peptide-resins whose solvation has changed substantially during the course of synthesis (Sarin et al., 1980). For the purpose of syntheses of ß1-40 and derived analogs it was therefore simpler to use loadings which gave less than 1 g peptide per gram of resin.

2.1.2. Side-Chain Protection in Fmoc-Amino Acids

Most of the amino acids of the AßP contain functional side chains, *e.g.*, acidic carboxyl groups (aspartic, glutamic acids); basic residues (lysine, histidine, arginine); and hydroxyamino acids (serine, tyrosine). The various side-chain protecting groups for these amino acids are summarized in Table 2.1, and their use during coupling of these amino acids is highlighted below:

(a) Aspartic and Glutamic acids: The side chains of aspartate and glutamate residues are in excellent position to form the respective succinimide and pyrrolidone carbonyl derivatives (Fig. 2.1). These reactions can be avoided by

using sterically hindered esters which minimize the ring-forming interactions. *t*-butyl (*t*Bu) esters of aspartic and glutamic acids were used for the ease during acidic cleavage,.

(b) Histidine: The imidazole (im) of histidine gets partially acylated during coupling reactions and the acyl-im can promote acyl transfer side reactions. Imidazole ring is in itself a powerful catalyst of chiral α-carbons and facilitates self racemization of the carboxyl-activated histidine. Alkyl derivatives can be located on the π- or the τ-nitrogen atom of the im, and the acid-labile *t*-benzyl-oxycarbonyl (*t*Boc) compound (Fig. 2.2) is considered appropriate for fmoc-histidine. The im-boc derivative exhibits substantial stability toward deprotection and acylation steps during the peptide chain growth (Atherton et al., 1987).

(c) Arginine: The exceptionally high basicity of the guanidine group of arginine mandates special attention during stepwise synthesis. The side-chain monoacyl derivatives (benzyloxycarbonyl, butyloxycarbonyl) when assigned to the ω-nitrogen offer limited protection and are susceptible for lactam formation (see Fig. 2.3). Diacyl derivatives could be better in preventing unwanted secondary peptide chain growth (Atherton and Sheppard, 1987). The 4-methoxy-2,3,6-trimethylbenzenesulfonyl derivative (Mtr) however has been found to be a useful protective group for guanidine, and also acid-labile (Atherton et al., 1983). However, complications arise during deprotection when *His-Arg* and *Arg-His* sequence is encountered due to partial conversion of arginine to ornithine. The deprotection of Arg(Mtr) is dealt separately in a later section.

(d) *Lysine*: The protection offered by benzyloxycarbonyl group to the lysine side chain is considered adequate. The pentafluorophenyl (OPfp) ester of boc-Lys couples reliably and the boc functionality is acid-labile, requiring no special techniques (Atherton et al., 1981).

(e) *Tyrosine*: The *t*-butyl group protects the phenolic side chain of tyrosine rather well and is easily liberated during treatment with trifluoroacetic acid solutions (Stewart and Young, 1984).

(f) *Methionine*: Unprotected methionines oxidize to methionine sulfoxide when cleaving with trifluoroacetic acid (Stewart and Young, 1984). While this is reversed by the use of *N*-methylmercaptoacetamide (Houghton and Li, 1979), avoiding oxidation by using ethylmethylsulphide (EMS) during cleavage of peptide from the resin support is equally satisfactory.

2.1.3. Activation of Fmoc-Amino Acid Esters

Merrifield chemistry uses *t*-boc amino acids which are activated and coupled as preformed symmetrical anhydrides in methylene chloride (Kent, 1988). Unfortunately, the fmoc-amino acids are not so readily soluble in methylene chloride and are sterically hindered to form anhydrides. This minor inconvenience is overcome by using activated esters of the respective fmoc-amino acids. Efficient couplings have been shown for pentafluorophenyl

(OPfp) esters (Kisfaludy and Schon, 1983) in the presence of 1-hydroxy-benzotriazole (HOBt) as catalyst (Atherton et al, 1988). While the OPfp esters are suitable for most of the amino acids, the analogous 2-hydroxy-4-oxodihydrobenzotriazole (Dhbt) esters prove necessary for serine and threonine since their OPfp esters are relatively insoluble in DMF. The generic OPfp and Dhbt esters of the fmoc amino acids are shown in Fig. 2.4. However, caution has to be exercised when using Dhbt ester of fmoc-serine since under appropriate reaction conditions, undesirable azidobenzoate is formed (Fig. 2.4) which leads to truncation of the peptide chain (Atherton et al., 1988).

2.2. General Procedures for Synthesis and Purification of ß1-40 and Derived Analogs

At the time this thesis was begun, there was a necessity to come up with a satisfactory stepwise SPPS protocol for ß1-40, as large quantities of this peptide and its constituent fragments were desirable using the minimum steps. Since the stability of the synthetic peptide(s) was also evaluated over time, large amounts of peptides readily obtained by the stepwise protocol were needed. Initially, the stepwise syntheses of ß1-28, ß1-40 and ß6-25 were performed on a Milligen/BioSearch semi-manual peptide synthesizer.

Table 2.1

Summary of Fmoc-Amino Acids' Protecting and Blocking Groups During SPPS

Amino Acid	**Protecting Group[1]**
Asp, Glu	OtBu
Asn, Gln	Mbh, Trt
Ser, Tyr	*t*Bu, ODhbt
His	Fmoc, Trt
Lys	Boc
Arg	Mtr, Pmc

[1] Abbreviations:

Fmoc	9-fluorenylmethoxycarbonyl-
OtBu, *t*Bu	*tert*-butyl-
Mbh	4,4-dimethoxybenzhydryl-
Trt	trityl-
ODhbt	3,4-dihydro-4-oxo-benzotriazin-3-yl-
Boc	*t*-butoxycarbonyl-
Mtr	4-methoxy-2,3,5-trimethylbenzenesulfonyl-
Pmc	2,2,5,5,7-pentamethylchroman-6-sulfonyl-

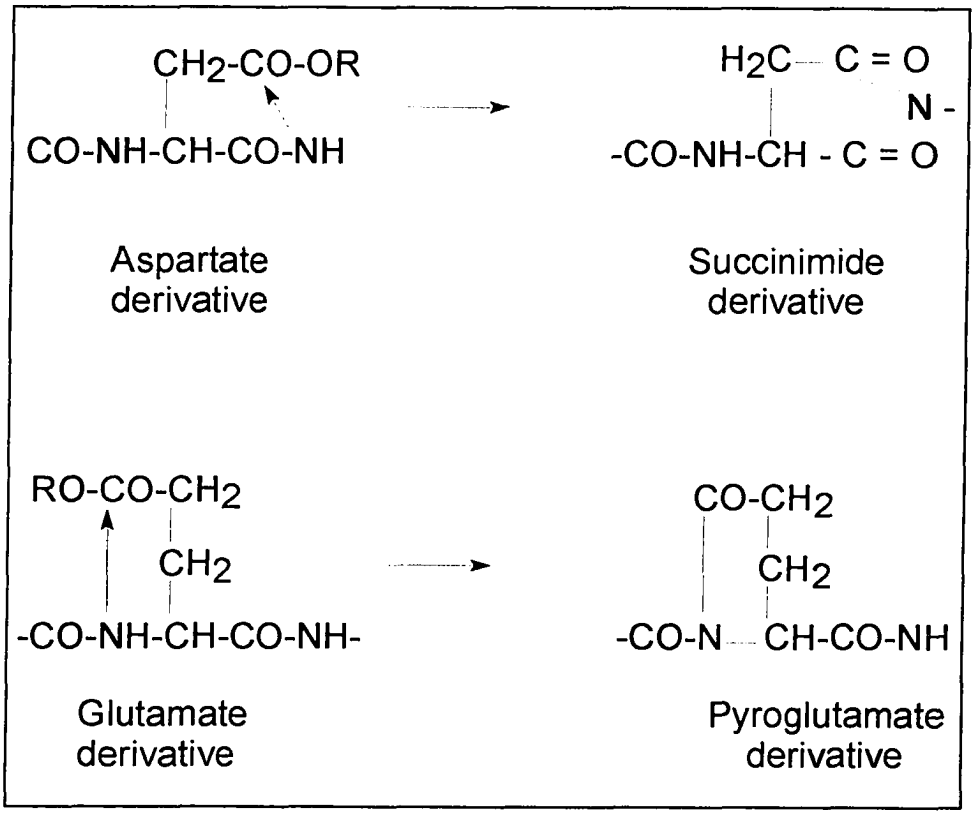

Fig. 2.1 Side-chain esters in aspartate and glutamate residues form cyclized derivatives. Sterically hindered esters, R = *t*-butyl or cyclohexyl, minimize these interactions.

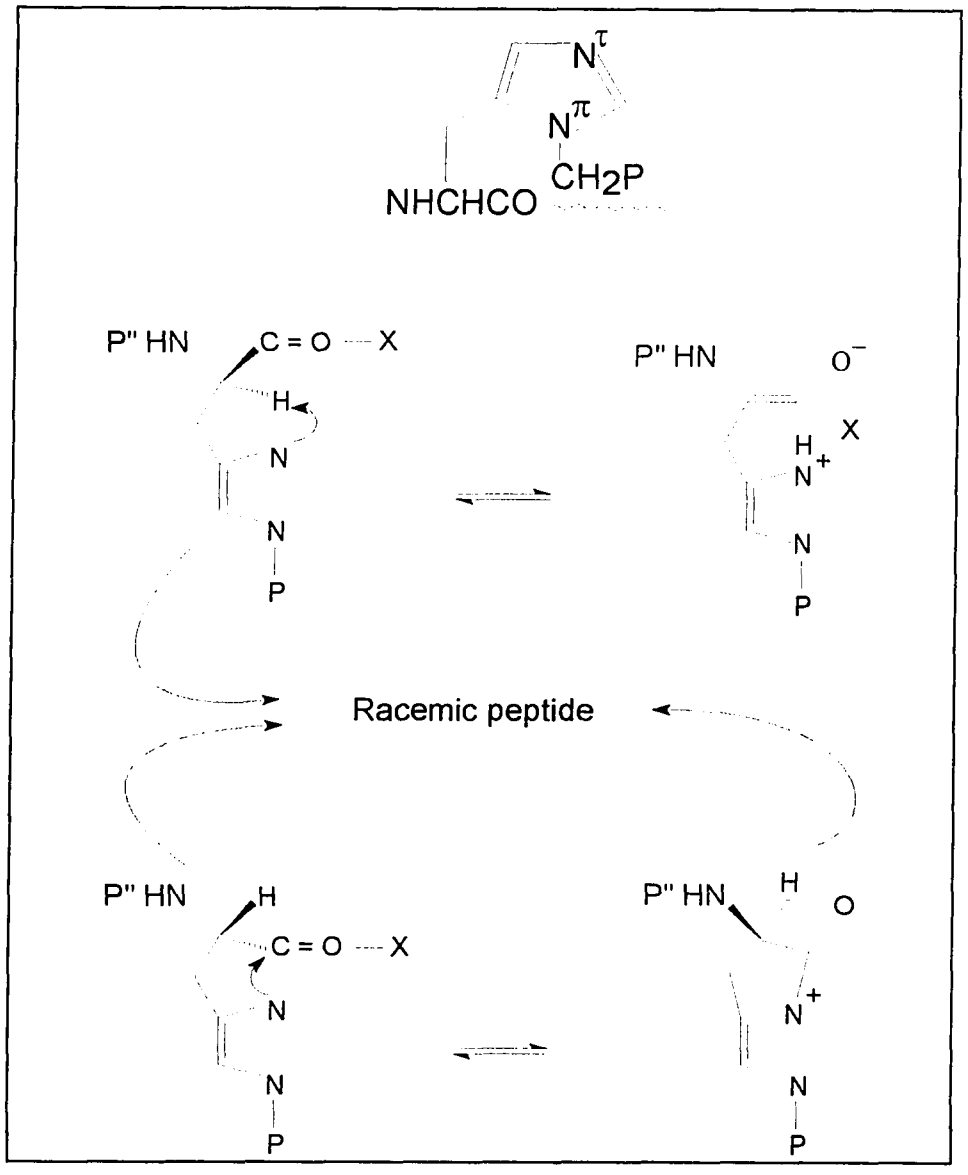

Fig. 2.2 Self-racemization in histidyl residues - differentiation of π- and τ-derivatized histidine residues. The intrinsic activity of the two side-chain nitrogens is similar, and both mechanisms can be made inoperable by placing electron-withdrawing groups (P = Trt, or Fmoc). The α-amino protecting group, P", is Fmoc.

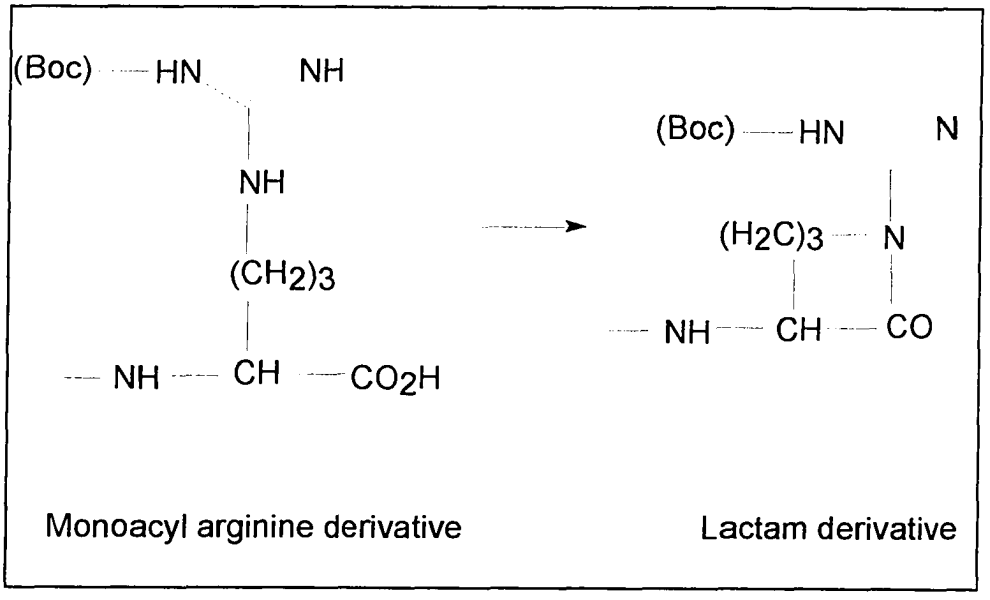

Fig. 2.3 Cyclization in the arginyl guanidine group; lactam formation from activated carboxyl. The ring formation is accelerated by a base.

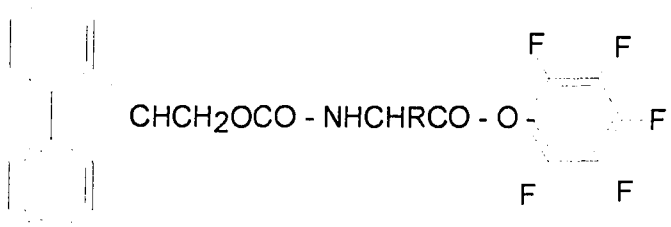

Pentafluorophenyl ester of Fmoc-amino acid

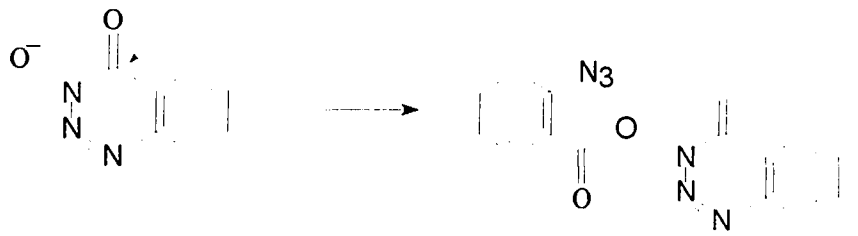

3,4-dihydro-1-hydroxy-3-oxo-benzotriazin-3-yl ester

azidobenzoate ester

Fig. 2.4 Pentafluorophenyl (OPfp) and 3,4-dihydro-4-oxobenzotriazin-3-yl (ODhbt) esters of fmoc-amino acids. Formation of azidobenzoate takes place on activation of the triazine of ODhbt by carbodiimide, which is in turn attacked at the ring carbonyl of the second molecule. Formation of the azidobenzoate species leads to chain termination when Fmoc-Ser-ODhbt is used during SPPS.

For the assembly of ß1-40 and its fragments, 100% dry dimethylformamide (DMF) provided a good solvation and coupling medium for the polyamide-kieselguhr resin-peptide. Additionally, the use of 10% anhydrous trifluoroethanol (TFE) or hexafluoroisopropanol (HFIP) in dry DMF during multiple couplings was found to be extremely efficient for the stepwise assembly of the 40 to 29 segments of ß1-40 and ß8-40. Also, the resins used had low subsitutions, 0.07-0.1 mEq which resulted in lower overall yields of peptides but did not result in truncated sequences or secondary peptides. By using higher syntheses temperatures, coupling efficiency was greatly improved. Typical temperatures between 40° and 42°C were obtained and this was deemed effective in increasing the coupling of the activated fmoc-amino acid esters.

2.2.1. Stepwise Synthesis of Protected Peptides

The ß1-40 and derived analogs were assembled either by (i) peptide elongation on Pepsyn KA-Axx-Fmoc resins, or (ii) preparing the Pepsyn KA resin with the starting amino acid, *i.e.*, Fmoc-Axx, where Axx represents the amino acid. Before assembling the peptides, quantitative amino acid analysis was performed to determine the level of resin substitution. Typically, < 0.1 mmol/g (0.07-0.09 mmol/g) resin equivalent was used. This alleviated the purported aggregation on the resin for the larger fragments. ß1-40 has a very hydrophobic

carboxyl end, *viz.*, residues 29-40 (Fig. 1.5) for which the standard coupling schemes cannot be satisfactorily applied. The special coupling techniques used for the 40 to 29 segment included (*a*) triple couplings, (*b*) increased temperatures, and (*c*) either 10% TFE or HFIP solution in DMF. During coupling of the protected fmoc-amino acid , the OPfp esters were activated to anhydrides in DMF using HOBt. The cleavage of the fmoc group during the coupling step was performed by the use of a relatively mild base, 20% piperidine (PIP), while the resin-peptide linkages were cleaved by TFA having appropriate scavengers.

The general methodology for stepwise Fmoc-SPPS is schematically shown in Fig. 2.5. The starting resin (1.0 g) was allowed to swell at room temperature for 15 min in dry DMF. The finer resin particles were decanted before the swollen resin was loaded in 10 cm glass columns available from Millipore, Marlborough, MA. The first synthetic cycle involved washing the resin with 100% dichloromethane (DCM) for 10 min. The fmoc-amino acid attached to the resin was deprotected using PIP. The next fmoc-amino acid was coupled as its activated ester and the deprotection-coupling cycles repeated for the desired peptide sequence. The progress of the coupling steps was qualitatively monitored by the absorbance of the deprotected fmoc group at 365 nm after each coupling cycle.

The activation and coupling criteria for the amino acids used for the semi-manual syntheses of ß1-40 and derived analogs were as follows:

(i) Fmoc-Val, Fmoc-Ile, Fmoc-Leu and Fmoc-Tyr(tBu): Dissolve a 4-fold excess of the amino acid in 10 mL of dry DMF, activate using equimolar 1-hydroxybenzotriazole (HOBt), vortex, let stand for 15-30 min, inject through a 0.5 μM filter into loop, couple for 120 min, 10% TFE or HFIP in DMF used as solvating agent, temperature of solvents maintained between 40° and 45°C;

(ii) Fmoc-Gly and Fmoc-Ala: Same as in **(i)**, except that coupling times were reduced to 60 min after Gly^{25}, 10% TFE or HFIP in DMF, temperature of solvents maintained between 40° and 45°C;

(iii) Fmoc-His(Fmoc), Fmoc-Lys(tBoc), Fmoc-Asp(tBu), Fmoc-Glu(tBu), Fmoc-Asn and Fmoc-Gln: Same as in **(i)**, however coupling was performed for 90 min at room temperature;

(iv) Fmoc-Arg(Mtr): Same as in **(i)**, except for the monosubstituted Arg^{13} and Arg^{14} analogs where coupling was extended for 180 min and assembly was done at room temperature;

(v) Fmoc-Ser(ODhbt): Fmoc-Ser(ODhbt) was chromatographed for purity before coupling; same as in **(i)**, however the activated ester solution was kept cold at 5°C. The occurrence of substantial syntheses-impurities terminating at Ser^{8} and Ser^{26} was randomly observed. These failed sequences were later traced to certain Fmoc-Ser(ODhbt) batches used during syntheses. Chromatographically-pure Fmoc-Ser(ODhbt) esters were used to avoid this minor inconvenience in the subsequent preparations of ß1-40 and derived analogs;

(vi) Fmoc-D-Asp(tBu): Same as in **(i)**, except the coupling times were 150 min for the tri-D-substituted analog of ß1-40.

Analogous methodology was used for obtaining the derived analogs ß1-28, ß6-25, ß22-35, ß15-28 and the `synthesis-impurities' ß8-40 and ß26-40. In the case of ß1-40, D-Asp was substituted at positions 1, 7 and 23 to give the respective [D-Asp^{1,7,23}]ß1-40, [D-Asp^{7,23}]ß1-40, [D-Asp^{1,23}]ß1-40, [D-Asp^{1,7}]ß1-40 and the mono-substituted D-analogs of ß1-40. ß6-25 was also synthesized with D-Asp substitutions at 7 and 23. The complete array of peptides synthesized for this study is given in Table 2.2.

2.2.2. Cleavage and Deprotection Methods

Certain amino acids are susceptible to interfering reactions during cleavage of the side-chain protecting groups using TFA. Of particular concern was the Mtr group protecting Arg residues. Moreover, the low-resin loading employed required optimization of the yield of pure peptides. This was done by systematically employing a battery of cleavage mixtures containing scavengers, *viz.*, phenol, thioanisole, 1,2-ethanedithiol (EDT), EMS, in order to standardize the most effective protocol for each peptide analog. The general scheme used was a variation from published procedures and is represented in Fig. 2.6. The following cleaving cocktails containing the scavenging agents were used:

(i) Reagent Z: 90% TFA, 5% phenol, 5% H_2O,

(ii) Reagent E: 70% TFA, 25% EDT, 5% H_2O,

(iii) Reagent R: 87% TFA, 6.5% thioanisole, 4% EDT, 2.5% anisole,

(iv) Reagent K: 83.5% TFA, 5% phenol, 5% thioanisole, 4% EDT, 2.5% anisole. With Met containing peptides, 1 part EMS was added to 99 parts of cleaving mixture. All reagents were freshly prepared on a v/v basis, sonicated for 10 sec and kept under nitrogen in the dark during use. The comparison of the cleavage and deprotection protocol for ß1-40 and ß6-25 is given in Table 2.3.

The resin-bound peptide was dried *in vacuo* to remove all traces of DMF or DCM. Cleaving reagent was then added; the proportion was usually 5 mL for each 100 mg and an additional 1 mL for each 10 mg of resin-peptide. An atmosphere of nitrogen or helium was always maintained in the reaction flask. The reaction flask was covered with aluminum foil to shield the mixture from light. All cleavage reactions were carried at room temperature.

Aliquots (100 µL) were drawn every hour in polypropylene tubes after 2 h, filtered and were vacuum centrifuged. This resultant crude product was treated with 500 µL cold diethyl ether at 4°C three times to remove all traces of residual organics. The presence of the expected peptide was established by Vis/UV spectroscopy and on the basis of extinction coefficients of Tyr, ϵ_{275} = 1400 $M^{-1}cm^{-1}$ and ϵ_{258} = 195 $M^{-1}cm^{-1}$ for all peptides. Additionally, thin layer chromatography (TLC) was performed to verify the extracted components.

Silica gel 60 (2.5 X 7 cm plates) was used and the developing solvent was $CHCl_3$:MeOH:HAc::80:15:5. Visual identification was done after placing the TLC plate in another chamber containing 4N HBr in glacial HAc for 15 min, spraying with ninhydrin, and heating.

The bulk of the reaction mixture was ready for further treatment when no differences between the consecutive aliquots were observed. After filtering and washing the bulk resin with two aliquots of 2 mL of cleaving reagent, the filtrate was concentrated on a rotary evaporator. The crude product was washed with cold diethyl ether to remove all traces of cleaving reagent and blocking groups. The bulk product was dissolved in 2% HAc and these peptide solutions were filtered through Millipore Millex 0.5 μM filters, followed by desalting on Biogel P-6 columns. Additional desalting was done on 0.5 cm disposable C_{18} columns by applying 0.2 mg/mL solutions. Peptides were usually recovered (90-97%) by running 40% to 50% MeCN containing 0.2% TFA. The eluting peptide fractions were lyophilized using a Labconco freeze dry Lyph Lock 4.5 system, and the amorphous residues were stored under helium or nitrogen at -70°C.

Custom peptide syntheses of ß22-35 and the 20-mer cytoplasmic carboxyl terminal (ßC-pep) of the full length APP_{695} was done by Cambridge Research Biochemicals, MA, USA. For long term storage, the peptide-resins were stored after drying to constant weight at -70°C in polystyrene tubes or glass vials under an inert atmosphere. These were taken up for cleavage and

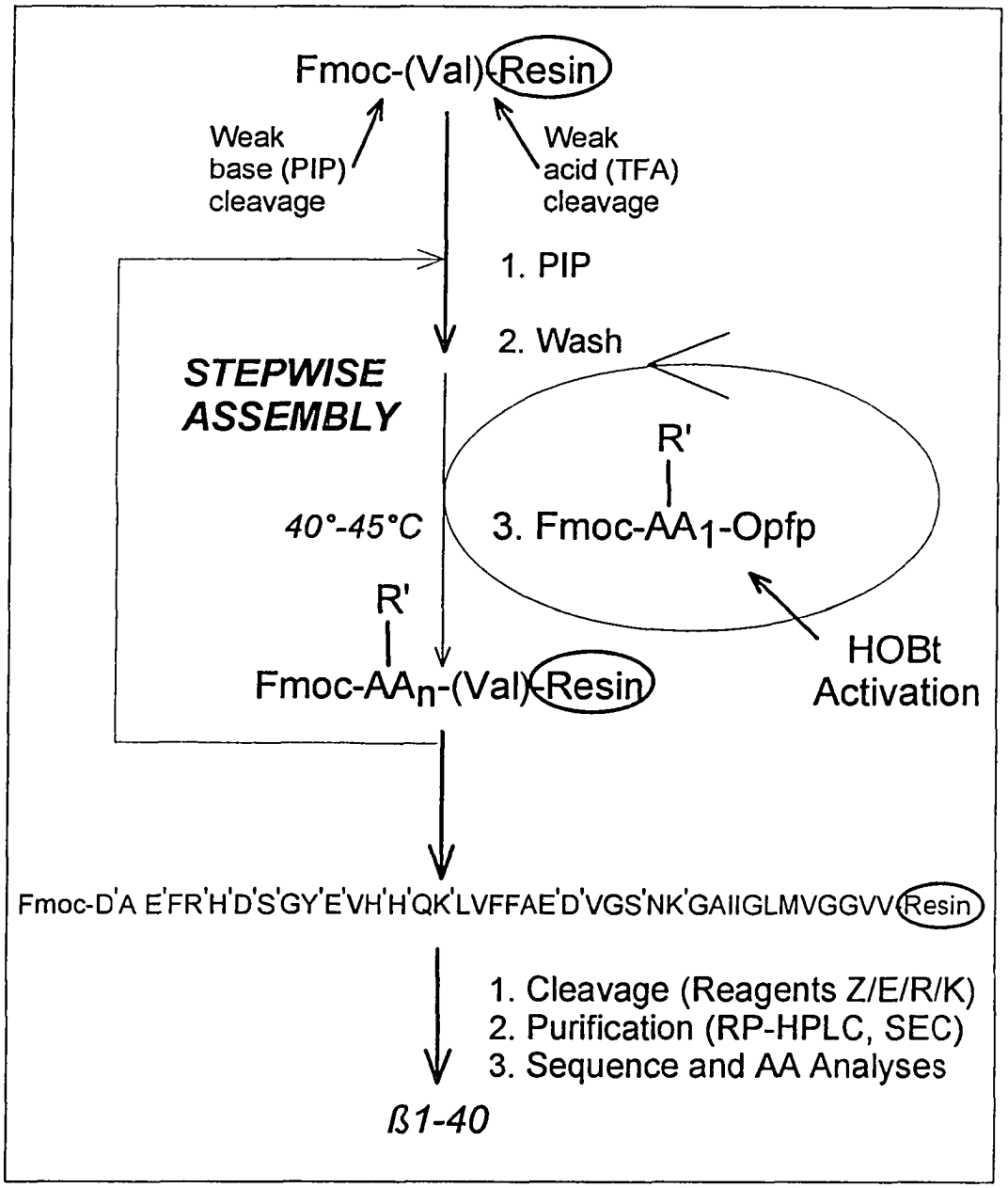

Fig. 2.5 General scheme for the total synthesis of ß1-40 and derived analogs by SPPS. The side-chain protected amino acids are denoted by " ' " defined in Table 2.1. The starting resin for ß1-40 synthesis was either (i) Pepsyn-KA-Val-Fmoc (purchased pre-linked, or prepared by coupling the Fmoc-AA to resin), or (ii) PS-PEG-Val-Fmoc.

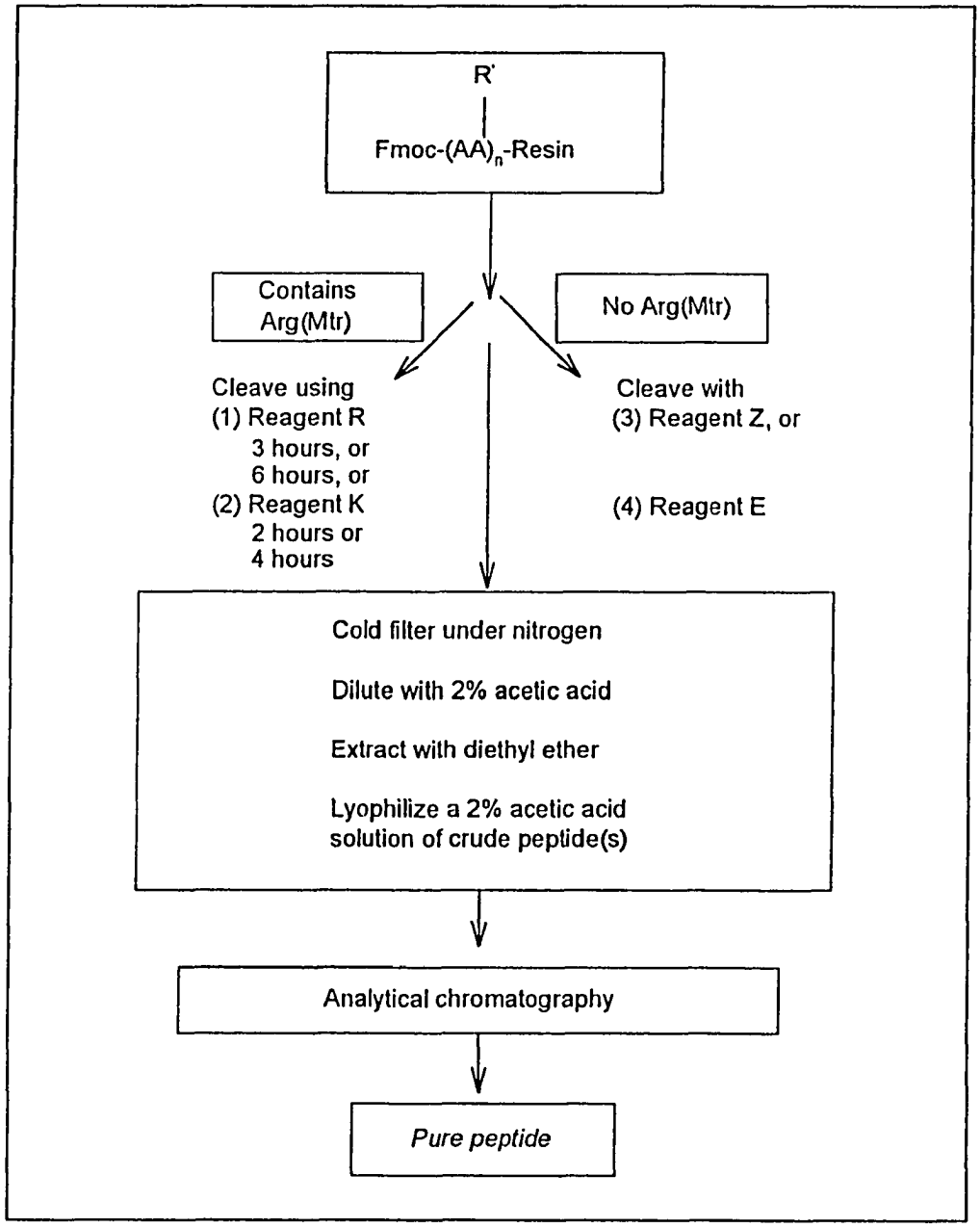

Fig. 2.6 Cleavage, deprotection and isolation schemes for the AßP fragments.

Table 2.2[a]

AßP Analogs Synthesized for Chromatographic and Spectroscopic Studies

Number	Peptide	Primary sequence
1	**ß1-40**	*D*[1]-A-E-F-R-H-*D*[7]-S-G-Y-E-V-*H*[13]-*H*[14]-Q-K-L-V-F-F-A-E-*D*[23]-V-G-S-N-K-G-A-I-I-G-L-M-V-G-G-V-V
2	[Arg[13]]ß1-40	D-A-E-F-R-H-D-S-G-Y-E-V-**R**[13]-H-Q-K-L-V-F-F-A-E-D-V-G-S-N-K-G-A-I-I-G-L-M-V-G-G-V-V
3	[Arg[14]]ß1-40	D-A-E-F-R-H-D-S-G-Y-E-V-H-**R**[14]-Q-K-L-V-F-F-A-E-D-V-G-S-N-K-G-A-I-I-G-L-M-V-G-G-V-V
3A	[Arg[13,14]]ß1-40	D-A-E-F-R-H-D-S-G-Y-E-V-**R**[13]-**R**[14]-Q-K-L-V-F-F-A-E-D-V-G-S-N-K-G-A-I-I-G-L-M-V-G-G-V-V
4	[Arg[13],D-Asp[23]]ß1-40	D-A-E-F-R-H-D-S-G-Y-E-V-**R**[13]-H-Q-K-L-V-F-F-A-E-D-D[23]-V-G-S-N-K-G-A-I-I-G-L-M-V-G-G-V-V
5	[Arg[14],D-Asp[23]]ß1-40	D-A-E-F-R-H-D-S-G-Y-E-V-H-**R**[14]-Q-K-L-V-F-F-A-E-D-**D**[23]-V-G-S-N-K-G-A-I-I-G-L-M-V-G-G-V-V
6	[D-Asp[1]]ß1-40	D-**D**[1]-A-E-F-R-H-D-S-G-Y-E-V-H-H-Q-K-L-V-F-F-A-E-D-V-G-S-N-K-G-A-I-I-G-L-M-V-G-G-V-V
7	[D-Asp[7,23]]ß1-40	D-A-E-F-R-H-D-**D**[7]-S-G-Y-E-V-H-H-Q-K-L-V-F-F-A-E-D-**D**[23]-V-G-S-N-K-G-A-I-I-G-L-M-V-G-G-V-V
8	[D-Asp[1,7,23]]ß1-40	D-**D**[1]-A-E-F-R-H-D-**D**[7]-S-G-Y-E-V-H-H-Q-K-L-V-F-F-A-E-D-**D**[23]-V-G-S-N-K-G-A-I-I-G-L-M-V-G-G-V-V

[a] continued on next page

Table 2.2 (contd.)

Number	Peptide	Primary sequence
9	**ß1-28**	D-A-E-F-R-H-D-S-G-Y-E-V-*H*^{13}-*H*^{14}-Q-K-L-V-F-F-A-E-D-V-G-S-N-K
10	[Arg^{13}]ß1-28	D-A-E-F-R-H-D-S-G-Y-E-V-**R**^{13}-H-Q-K-L-V-F-F-A-E-D-V-G-S-N-K
11	[Arg^{14}]ß1-28	D-A-E-F-R-H-D-S-G-Y-E-V-H-**R**^{14}-Q-K-L-V-F-F-A-E-D-V-G-S-N-K
12	[Arg^{13,14}]ß1-28	D-A-E-F-R-H-D-S-G-Y-E-V-**R**^{13}-**R**^{14}-Q-K-L-V-F-F-A-E-D-V-G-S-N-K
13	ß6-25	H-*D*^{7}-S-G-Y-E-V-*H*^{13}-*H*^{14}-Q-K-L-V-F-F-A-E-*D*^{23}-V-G
14	[Arg^{13}]ß6-25	H-D-S-G-Y-E-V-**R**^{13}-H-Q-K-L-V-F-F-A-E-D-V-G
15	[Arg^{14}]ß6-25	H-D-S-G-Y-E-V-H-**R**^{14}-Q-K-L-V-F-F-A-E-D-V-G
16	[Arg^{13,14}]ß6-25	H-D-S-G-Y-E-V-**R**^{13}-**R**^{14}-Q-K-L-V-F-F-A-E-D-V-G
17	[Arg^{13,14},d-Asp^{23}]ß6-25	H-D-S-G-Y-E-V-**R**^{13}-**R**^{14}-Q-K-L-V-F-F-A-E-D-**D**^{23}-V-G
18	[d-Asp^{23}]ß6-25	H-D-S-G-Y-E-V-H-H-Q-K-L-V-F-F-A-E-D-**D**^{23}-V-G
19	[d-Asp^{7,23}]ß6-25	H-D-**D**^{7}-S-G-Y-E-V-H-H-Q-K-L-V-F-F-A-E-D-**D**^{23}-V-G
20	**ß8-40**	S-G-Y-E-V-H-H-Q-K-L-V-F-F-A-E-D-V-G-S-N-K-G-A-I-I-G-L-M-V-G-G-V-V
21	**ß26-40**	S-N-K-G-A-I-I-G-L-M-V-G-G-V-V

The peptides are designated by the numbers given in bold; these numbers are referred in the succeeding tables and figures.
The bold face peptide labels indicate the native sequence analogs of ß1-40 for which the primary sequence is indicated by the single letter code of amino acids; the italics indicate the amino acid substitutions in the derived analogs.
The amino acids given in bold in the derived analogs indicate the substitutions.

purification as and when needed. Impure fractions arising due to inappropriate storage of purified peptides were eliminated due to their better stability at -70°C, and especially if the peptide was left on the solid phase.

2.2.3. Evaluation of the Stepwise Solid-Phase Syntheses

Purification using reverse-phase chromatography

All deprotected peptides were chromatographed on reversed-phase (RP) columns before characterization by Edman degradation and quantitative amino acid analyses. Two high-performance liquid chromatography (HPLC) systems were employed for purification: *(i)* an initial semi-preparative system, and *(ii)* analytical system. A SpectraPhysics Model 570 pump, and an Extended Range 8100XR Liquid Chromatograph replete with a thermostated column chamber were used and semi-preparative chromatography was performed on two semi-preparative C_{18} columns: a Vydac 10 X 300 mm, 50-100 μM, 300 Å, and an Altex 8 X 150 mm C_{18}. The following gradients were employed for purifying the crude peptides: (a) a linear AB gradient from 0-100% B in 30 min at a flow rate of 10 mL/min; Solvent A: 0.1% TFA in 15% MeCN; Solvent B: 0.1% TFA in 75% MeCN, or (b) isocratically with 40% MeCN containing 0.1% TFA at elevated column temperatures appropriate to the peptide. All solvents were degassed by sonication for 30-40 min or sparged with helium during chromatography.

Peptides (8-10 mg) were introduced as aqueous solutions (2 mL) for each semi-preparative run and the eluting peptide fractions were recovered, pooled, and lyophilized to yield fluffy amorphous powders. These fluffy products were dissolved in 2-10% acetic acid (HAc), the solutions were vigourously vortexed, filtered using Millipore Millex 0.22 μM filters and the filtrate was subjected to analytical chromatography.

Analytical reversed-phase high performance liquid chromatography (RP-HPLC) was performed using dual Waters Model 510 pumps operated via a Baseline 810 chromatographic workstation. A Waters U6K injector with a 200 μL loop, and two Waters 441 detectors operating at 214 and 254 nm completed the dedicated peptide purification setup. The following columns were employed for analytical purifications: Vydac 4.6 X 150 mm, 5 µ, 300 Å C_{18}, 4.6 X 300 mm, 5 µ, 300 Å C_4 and C_8, and Beckman Ultrasphere ODS 5 µ, 300 Å C_{18}. The flow rate for all analytical chromatography was 1.0 mL/min using linear AB gradients at room temperature. Mixtures of solvents A (0.1% TFA in 0-20% MeCN), and B (0.1% TFA in 60-100% MeCN) were composed as per the peptide chromatographed. Linear gradients were used for the more hydrophilic peptides, whereas ß26-40 was purified isocratically. For each analytical separation, typical loadings contained between 0.1-0.3 mg peptide as aqueous solutions containing 10 µL MeCN. The appropriate fractions were pooled, lyophilized immediately and the pure peptide verified for sequence and amino acid analyses.

The summary of yields for the ß1-40 and ß6-25 analogs is given in Table 2.3. The yields of pure peptides, as determined by quantitiative amino acid analyses, varied between 50-80% (based on the resin) from all the syntheses. The analytical RP-HPLC profiles for ß1-40 using the cleaving protocols given in Table 2.3 are depicted in Fig. 2.7. The `apparent' increase in the amount of impurities with inappropriate cleavage was determined to be due to the higher extinction coefficients of the organic protecting groups, and are therefore not a true representation of synthesis or deprotection efficiency. The increase in the pure peptide content indicates the actual efficiency of each cleavage/scavenger mixture as seen from the summary in Table 2.3. The generation of microheterogeneity from a typical truncated sequence during synthesis ofß1-40 is illustrated in Fig. 2.8. A more detailed evaluation of these synthesis-fragments is undertaken in chapter 3.

A clear picture of improper deprotection and interfering side reactions during cleavage of ß6-25 and the [Arg^{13}]ß6-25 derived analog is illustrated by the RP-HPLC profiles given in Fig. 2.9. The Mtr group released during deprotection of Arg had reacted with thioanisole giving a seemingly large impure fraction. The actual content of the incompletely deprotected [Arg^{13}]ß6-25 was 6 mole% based on quantitative amino acid analysis. These results are summarized in Table 2.3.

Further characterization of the peptides in solutions was done by size exclusion chromatography (SEC). A Millipore FPLC with a Waters 425 tunable UV Detector operating at 214 nm was used to perform SEC on Protein Pak

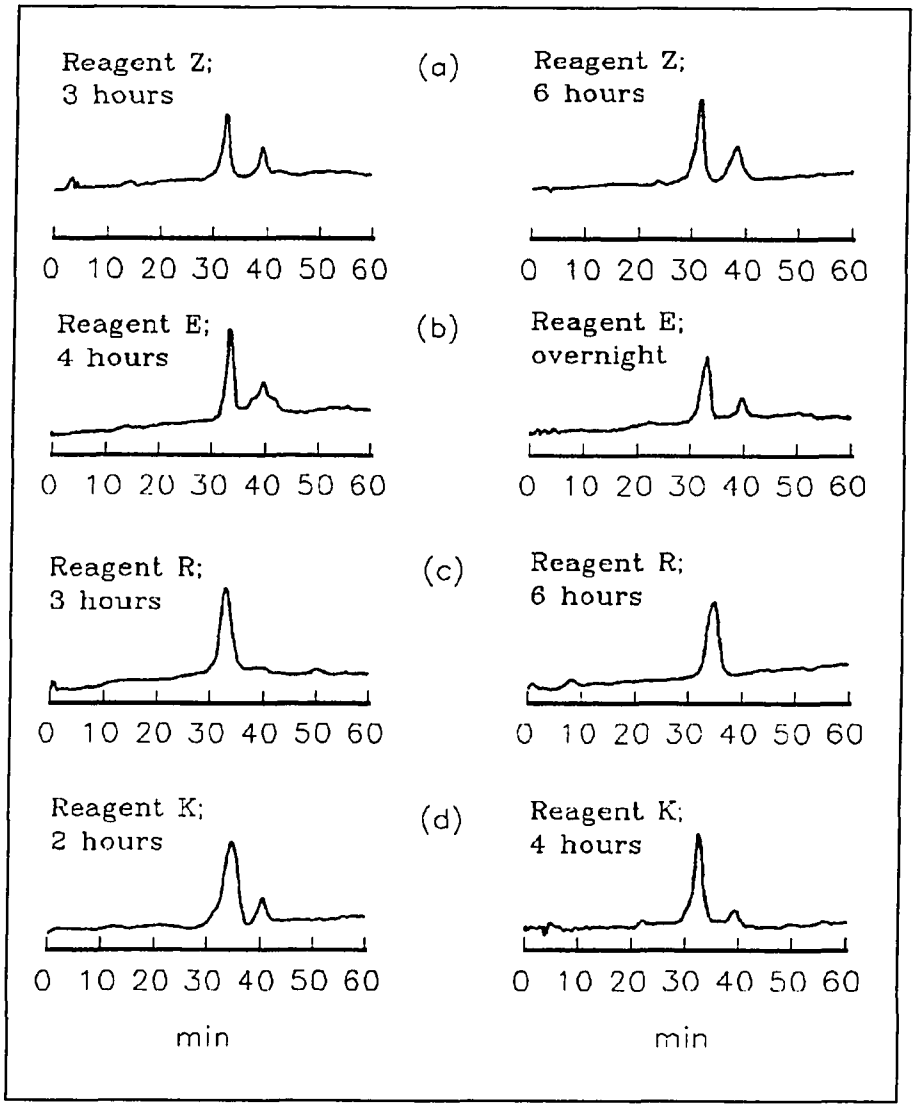

Fig. 2.7 Analytical RP-HPLC elution profiles of crude ß1-40 as a time-dependent function of cleaving mixtures. (**a**) Reagent Z, (**b**) Reagent E, (**c**) Reagent R, and (**d**) Reagent K. The chromatography was performed on a 4.6 X 300 mm Beckman Ultrasphere C_{18} column operated at ambient temperatures. A linear gradient from 0-100%B in 60 min was used at a flow rate of 1.0 mL/min using solvent A as 0.1% TFA and solvent B as 0.1% TFA in 80% MeCN. The column was equilibrated in solvent A for 10 minutes prior to start of the gradient.

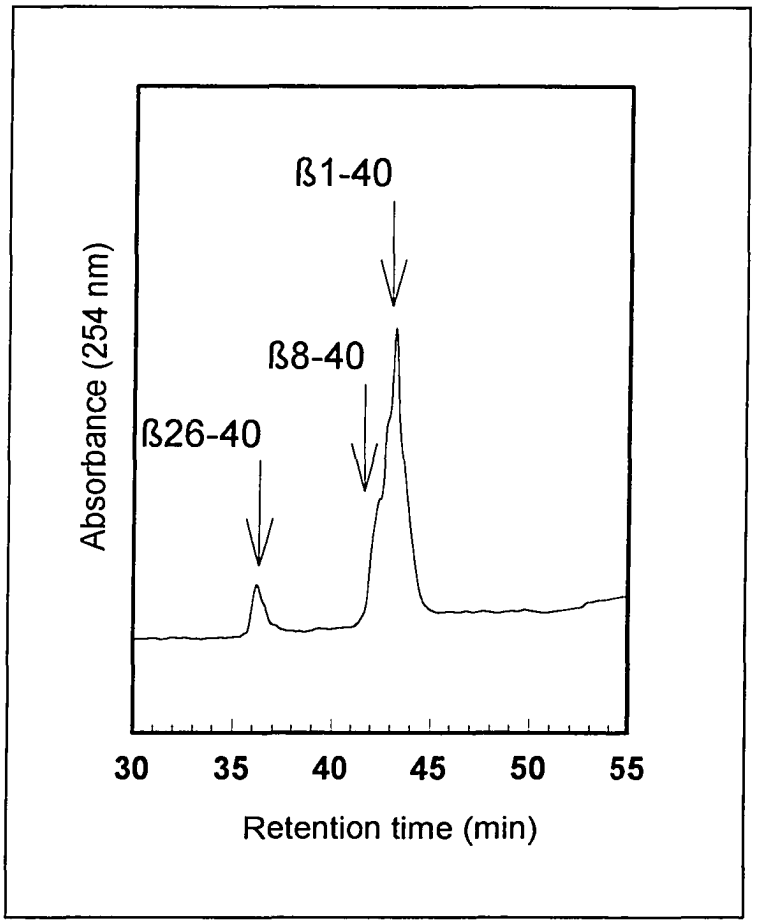

Fig. 2.8 Analytical RP-HPLC profile of a representative impure synthesis of ß1-40 showing the elution of ß26-40 and ß8-40 synthesis-fragments. Chromatographic conditions as given in Fig. 2.7. The identity of the fractions indicated by arrows were determined by quantitative amino acid analysis and Edman sequencing.

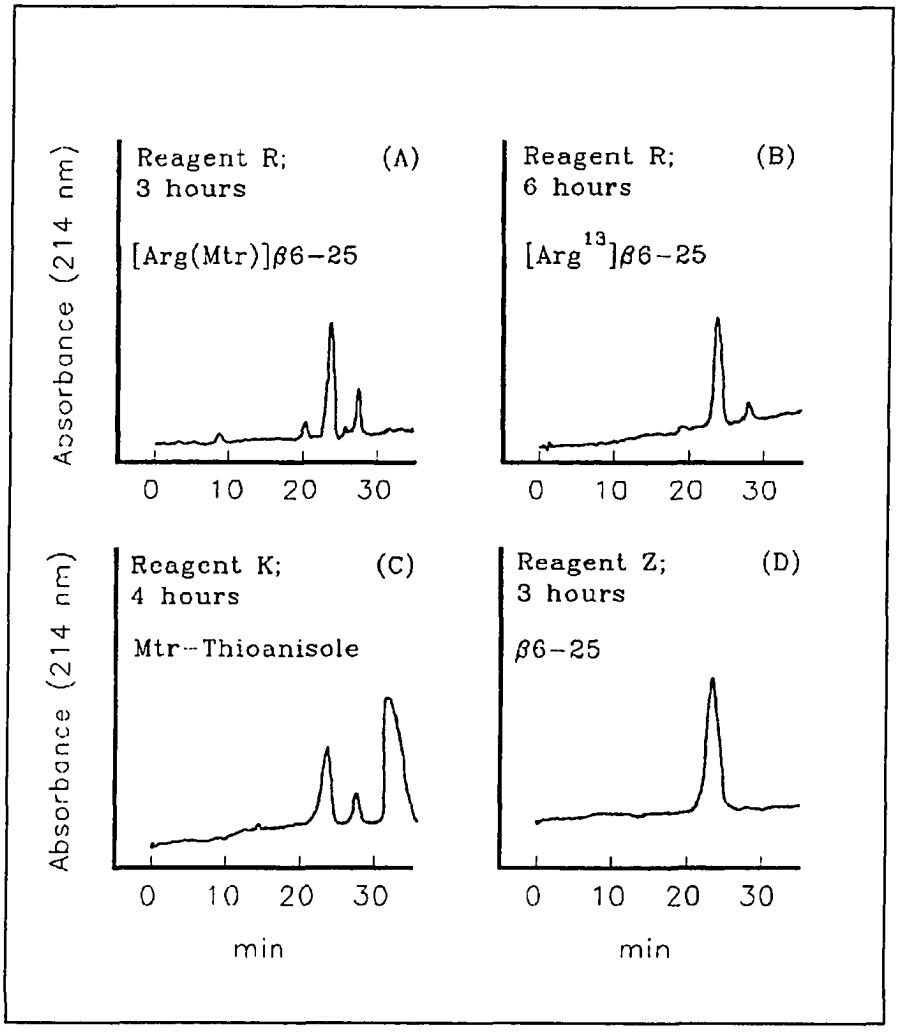

Fig. 2.9 Analytical RP-HPLC elution profiles for crude ß6-25, [Arg^{13}]ß6-25, and [Arg(Mtr)]ß6-25. Chromatographic conditions as given in Fig. 2.7. The peak eluting just before 30 min is the incompletely deprotected [Arg(Mtr)]ß6-25 seen in panels (A)-(C), while the broad hydrophobic component in (C) is Mtr/thioanisole. The pure [Arg^{13}]ß6-25 derived analog elutes near 25 min, as seen in (D).

Table 2.3

Comparison of Methods of Deprotection and Cleavage for all Synthetic Analogs

Method	ß1-40 mg[1] (%)[2]	[Arg[13]] ß1-40 mg[1](%)[2]	[Arg(Mtr)] ß1-40 (%)[2]	ß6-25 mg[1] (%)[2]	[Arg[13]] ß6-25 mg[1] (%)[2]	[Arg(Mtr)] ß6-25 (%)[2]
Reagent R						
3 hours	45 (69.2)	40 (61.2)	18.8	34 (85.0)	28 (70.8)	13.3
6 hours	9 (81.0)	46 (70.5)	8.0	34 (86.2)	28 (80.8)	6.0
Reagent K						
2 hours	48 (72.5)	43 (65.1)	21.7	35 (84.5)	29 (83.4)	12.3
4 hours	50 (77.7)	44 (68.9)	13.2	37 (92.8)	32 (91.0)	5.1
Reagent E						
4 hours	36 (58.7)	20 (31.3)	41.1	37 (91.1)	22 (62.6)	25.6
overnight	40 (61.2)	23 (33.3)	36.2	32 (85.4)	18 (58.5)	20.0
Reagent Z						
4 hours	35 (48.8)	15 (23.3)	65.5	36 (90.6)	16 (45.5)	40.4
overnight	38 (51.5)	17 (28.9)	55.3	36 (91.8)	17 (48.2)	38.6

1 The recovery of crude peptides were based on 200-250 mg of resin-peptide. The resin substitutions 0.084 mEq for ß1-40, and 0.09 mEq for ß6-25.

2 The percentages were based on calculations from analytical RP-HPLC of the crude peptides. The amounts of peptides were based on the extinction coefficients for all the indicated peptides at 214 nm, and quantitative amino acid analyses.

TSK300SW gel 10 X 300 mm and Sephadex-G250 10 X 450mm columns. The peptides were chromatographed using 0.1% TFA in 50% acetonitrile (MeCN) containing 100 mM KCl at a flow rate of 0.25 mL/min. The molecular weight markers used as calibration standards were BSA (64 kDa), myoglobin (16 kDa), cytochrome *c* (12 kDa), aprotinin (6 kDa), ß-chain of insulin (3.5 kDa) and bacitracin (1.4 kDa).

Amino acid sequence analyses during synthesis

Progressive verification of the assembled amino acids was done by subjecting the resin-peptide to gas-phase sequencing on a Model 6600 ProSequencer from MilliGen equipped with on-line PTH identification unit. The resin-peptide was washed with DMF, dried *in vacuo*, and a polyvinylidene difluoride (PVDF) membrane sandwich was prepared. The resin-peptide-PVDF sandwich was sealed on all sides with a spatula to entrap the resin-peptide. Two peptide bearing resin beads were sufficient for sequence analysis with an equivalent PTH derivative in pmol range (Matsudaira, 1987).

Sequence analyses was only qualitative at this stage and was used to verify the assembly of fmoc amino acid esters on the resin. The resin-peptides routinely tested were those containing the hydrophobic carboxyl terminal, especially, the 29 to 40 segment, and the D-Asp containing peptides. High noise levels were usually developed during later cycles for the sandwiched resin sequencing and assignments were difficult. Substitution of

1.5% diidopropylethylene amine (w/w) for the coupling base gave reasonable background (Farnsworth et al., 1991). Proper assignment of the two serine residues present in the longer peptides was accomplished by lowering the cartridge temperature to 45°C (Scott et al., 1988).

Post-synthesis sequence analyses

The sequence of the assembled peptide was verified on chromatographically-pure peptides after the RP-HPLC purification. The peptides were covalently attached on PVDF membranes impregnated with diisothiocyanate (DITC) obtained from Millipore. Attachment buffer was 5% N-methylmorpholine (NMM) in 70% methanol containing 0.1% cyclohexylamine. The membrane was warmed to 55°C on a heating block for 5-10 min and this procedure repeated to load at least 100 pmol peptide on the membrane. Membranes prepared in such manner gave good repetitive yields. Only peptides with the desired sequence were used for structural analyses.

Cleavage by Trypsin and CNBr

The problems with high background were worsened during the later stages of sequencing and poor repetitive yields were obtained beyond the fifteenth sequencing cycle. Internal amino acid sequence was performed in such cases to avoid ambigious sequence assignments. This technique was used for all the D-Asp and the Arg^{13} and/or Arg^{14} substituted peptides. These peptides

were covalently bound on arylamine (AA) membranes to verify each of their sequence.

Similar methodology was utilized for the tryptic and cyanogen bromide (CNBr) digests of peptides. It was necessary to remove interfering buffers and this was performed by analytical chromatography of the digested peptides on a Deltapak 3.9 X 150 mm C_{18} reverse phase column. The eluting peptide fractions were directly loaded on Immobilon-AA or DITC membranes for sequence determination. Chromatographically-pure peptides were dissolved in 2% acetic acid solution and 50 µg aliquots were dried in polystyrene tubes. The resulting films were suspended in 50 µL 100 mM citrate buffer (pH 7). After sonication for 1 min, trypsin digestion was performed for 12 h and 37°C. The reaction was terminated by freeze-drying. These tryptic digests were resolved by RP-HPLC, using a linear AB gradient consisting of A: 0.1% TFA in 20% MeCN and B: 0.1% TFA in 80% MeCN developing over 60 min, at a flow rate of 1 mL/min. Detection of the eluting components was done at 214 nm. The eluting components were subjected to Edman sequencing after lyophilization of pooled fractions.

For the CNBr cleavage, the peptides were incubated overnight at room temperature in 50 µL formic acid containing 10 µM CNBr (Scott et al., 1988). The conversion of methionine to methionine sulfoxide was prohibited by addition of mercaptoethanol. This mixture was chromatographed directly on Vydac C_4 reverse phase column under conditions identical to the tryptic digests. The

eluting components were subject to sequencing after lyophilization of the pooled fractions for their identification.

Amino Acid Analysis

(a) Determination of resin substitution

Quantitative amino acid analyses were performed on all resins to verify the amount of resin substitution. Two resin beads (50 µg) were hydrolysed under vacuum with 50 µL of constant boiling 6N HCl and 0.1% phenol for 12 h at 105°C. Norleucine was used as an internal standard. At the end of hydrolysis, the sample was diluted in 100 µL Li-N sample buffer (Beckman Instruments, Palo Alto) and analyzed on a Beckman 6300 Amino Acid Analyzer which uses post-column derivatization and ninhydrin reagent. Detection was at 570 nm for primary amines and 440 nm for secondary amines.

(b) Determining amino acid composition

Qualitative amino acid analyses for all synthetic peptides were initiated following analytical chromatography. In the case of peptide fractions, and tryptic digests, amino acid analyses on the solid obtained after repeated freeze-thawing and degassing of the pooled eluants under vacuum. Hydrolysis was performed using constant boiling 6N HCl containing 0.1% phenol in a sealed tube at 110°C for 24 h. The hydrolysate was diluted with 200 µL of Li-N sample buffer and analyzed at 440 and 570 nm. Norleucine was used as an internal standard and

in the case of D-Asp containing peptides, the corresponding analyses was compared with the unsubstituted peptide as control. There was extensive degradation of serine residues for all these peptides.

(c) Quantitative amino acid analyses

The results of quantitative amino acid analyses are summarized in Table 2.4. All values were normalized in the form of ratios with respect to nor-Leu which was used as the internal standard.

Additionally, a spectrophotometric analysis method was employed to determine the relative concentration of Tyr and Phe in peptide solutions using ϵ_{275} = 1400 $M^{-1}cm^{-1}$ and ϵ_{258} = 195 $M^{-1}cm^{-1}$ respectively (Mihalyi, 1969). The presence of a single tyrosine, without any interfering tryptophan (Chrastil, 1986) in most of these peptides greatly facilitated the quantitative analyses.

2.2.4. Peptide Concentration Determination

Besides the quantitative amino acid analyses outline in the earlier section, concentrations of peptides were determined by Vis/UV spectroscopy using a Hewlett-Packard 8452A Single Channel Photo Diode Array Spectrometer. Since elution was monitored at 214 and 254 nm during chromatography, extinction coefficients were determined at these wavelengths.

Table 2.4

Amino Acid Analyses of Purified AßP Analogs [a]

Amino Acid	$(1)_{1*}$	$(2)_{1*}$	$(4)_{1*}$[b]	$(6)_{1*}$[b]	$(7)_{1*}$[b]	$(9)_{1*}$	$(12)_{1*}$	$(13)_{1*}$	$(17)_{1*}$[b]	$(19)_{1*}$[b]	$(20)_{1*}$	$(21)_{1*}$
D	3.69(4)[2]	3.72	2.65	*2.58*	*1.88*	3.84(4)[2]	3.77	1.84(2)[2]	*0.97*	*0.55*	1.74(2)[2]	0.24(0)[2]
E	3.81(4)	3.69	3.75	3.58	3.75	3.72(4)	3.445	1.79(2)	1.82	1.75	2.91(3)	0.33(0)
S	1.11(2)	1.21	0.88	0.99	1.11	0.85(2)	1.025	0.49(1)	0.65	0.63	1.04(2)	0.35(1)
G	5.88(6)	5.73	5.81	5.55	5.67	1.87(2)	1.83	1.78(2)	1.91	1.83	5.73(6)	3.84(4)
H[c]	2.66(3)	*1.67*	*1.73*	2.76	2.54	2.57(3)	0.83	2.75(3)	*0.83*	2.64	1.67(2)	0.35(0)
R[c]	1.01(1)	*1.88*	*1.83*	0.89	0.91	0.92(1)	2.68	0.07(0)	*1.79*	0.09	0.14(0)	0.14(0)
A	2.67(3)	2.54	2.73	2.81	2.67	1.87(2)	1.85	0.93(1)	0.94	0.89	1.84(2)	0.94(1)
Y	0.99(1)	0.97	0.91	0.89	0.94	0.97(1)	0.97	0.90(1)	0.89	0.88	0.95(1)	0.05(0)
V	5.84(6)	5.72	5.75	5.55	5.67	2.77(3)	2.78	2.74(3)	2.72	2.84	5.88(6)	2.74(3)
M	0.45(1)	0.54	0.55	0.51	0.53	0.21(0)	0.18	0.33(0)	0.34	0.25	0.44(1)	0.40(1)
I	1.67(2)	1.67	1.65	1.67	1.60	0.05(0)	0.01	0.00(0)	0.01	0.02	1.75(2)	1.81(2)
L	1.74(2)	1.77	1.77	1.72	1.75	0.87(1)	0.88	0.90(1)	0.81	0.83	1.67(2)	0.83(1)
F	2.54(3)	2.45	2.67	2.37	2.38	2.51(3)	2.45	1.54(2)	1.80	1.75	1.76(2)	0.66(1)
K	1.89(2)	1.85	1.78	1.91	1.75	1.75(2)	1.85	0.95(1)	0.95	0.89	1.75(2)	1.11(1)

[a] signifies the mean of five quantifications within 0.5 standard deviation.
[b] gives the values for two determinations for these [D-Asp] analogues.
[c] denotes that these were His→Arg substitutions, and the amino acid content for these peptides were calculated accordingly.
[1*] The numbers correspond to peptides given in Table 2.2.
[2] Values in parentheses are the expected amino acid content of pure peptides.
The *underlined italics* denote either a [D-Asp] or His→Arg substitution.

The absorbance was converted to relative concentration using extinction coefficients determined for pure and unscavenged peptides. The following ϵ_{214}, ϵ_{254} were determined: ß1-40 = 13400, 11300 $M^{-1}cm^{-1}$, ß6-25 = 7900, 6800 $M^{-1}cm^{-1}$, ß1-28 = 9600, 9900 $M^{-1}cm^{-1}$, ß8-40 = 10800, 9900 $M^{-1}cm^{-1}$ respectively.

The Bradford assay (Bradford, 1976) was generally quite reliable for the peptides in solutions in mutually supporting data from quantitative amino acid analyses. However, with ß26-40, aged peptide solutions (〉 72 h), and for basic solutions, accuracy was hampered due to insolubility, and slight gelling of solutions, respectively. Peptide concentrations were measured using bicinchoninic acid (Smith et al., 1985). When resolubilization procedures required use of guanidine hydrochloride, a modified Bradford protocol was also employed (Gotham et al., 1988).

2.3. Spectroscopic Methods for Structural Studies

The secondary structure adopted by AßP is greatly influenced by the *intrinsic* and *extrinsic* factors which were highlighted in chapter 1. In order to study the conformations of ß1-40 and its derived analogs in aqueous solutions, these peptides were studied using circular dichroism (CD) spectroscopy. CD was also used to evaluate changes in conformation taking place over time, and

under the influence of external factors, like ligands which could bind to and/or affect the orientation of the peptide backbone. Additionally, the effect of aqueous aluminum in peptide solutions was investigated using ^{27}Al nuclear magnetic resonance (NMR) spectroscopy. NMR was also used to verify the association of aluminum in peptides which were incubated with aluminum over a period of time.

2.3.1. Circular Dichroic Spectroscopy

Circular dichroism spectra were recorded on a Jasco J-720 Spectropolarimeter using a slit width of 2 mm at 1 nm interval between 190 and 260 nm. A cylindrical cell with sample path length of 0.05 mm was used for all peptide solutions measured on the J-720. An atmosphere of ultrapure nitrogen was maintained in the sample chamber at a flow rate of 5 L/min during all measurements. The analog time constant was 1 sec, and the scan rate was set at 1 nm/sec. Repetitive scans were used to improve the signal-to-noise ratio, and an average of four scans were routinely performed. With low peptide concentrations, sixteen scans were averaged. No smoothing functions were applied on any measured CD data. The raw ellipticity was transformed into molar ellipticity and calculations performed on the unsmoothed data. A cubic-spline algorithm was used to plot CD spectra for all observed data.

Far ultraviolet CD (far UV/CD) spectra were measured using the vacuum UV/CD spectrometer at the Port U9B of the Brookhaven National Laboratory's National Synchrotron Light Source (NSLS) (Sutherland et al., 1992). Simultaneous determination of absorbance and CD was possible with this CD spectrometer. CD spectra were recorded after routine calibrations of the spectrometer using an aqueous solution of (+)-10-camphorsulphonic acid (CSA). This was a necessary step to verify the integrity of the light source after every *'injection'* of the UV ring. The ratio of CD for CSA at 192.5 to 290.5 nm > -2.00 was considered to be satisfactory in keeping with published values (Chen and Yang, 1977). The path lengths used for observations were kept low, typically 0.015-0.050 mm using mylar spacer between quartz windows in the Gray cells (Gray et al., 1984). The low path lengths facilitated obtaining good CD spectra between 260 and 178 nm, since high concentrations of peptide solutions could be used, and the `background' absorbance was reduced to ≈ 1.5 in the spectral region. The boil-off from liquid nitrogen was used to purge the monochromator at least for 15 min before opening the spectrometer window to the lamp-source. In buffered solutions the signal to noise ratio was poor and data were not collected below 195 nm.

Typically, CD was measured with an analog time constant of 4 sec, and a scan rate of 1 nm/min. The CD spectra given are given as an average of four observations unless specifically stated. For particularly noisy samples, the analog time constant was increased to 16 sec with a subsequent sacrifice in the

number of averaged scans. All CD spectra were corrected for the contributing solvent by digital subtraction. Smoothing operations were performed on all measured CD taken at NSLS for secondary structure analysis using Varselec.

2.3.2. Nuclear Magnetic Resonance Spectroscopy

^{27}Al NMR spectra were obtained at ambient temperature on JEOL FX90Q Spectrometer with a tunable broad band probe operating at 23.30 MHz. Pulse recycle times used were 0.5 s, the 90° pulse length was 55 μsec, and the time between two pulses was sufficient to allow the magnetization to equilibrium (Bottero et al., 1980). The free induction decays (FIDs) were accumulated in 1K, and Fourier transform (FT) performed on 16K by the zero-filling technique. The following sets of accumulation conditions: *(a)* slow accumulation using a 1 KHz window to observe the reference signal, whereby linewidths were measured with an accuracy of *ca.* 0.5 Hz, and *(b)* fast accumulation with a 3.5 to 10 KHz window for observing all other ^{27}Al species (Akitt and Milic, 1984). However, using condition (b), the accuracy in linewidth measurements was sacrificed. No weighting function was applied to the FIDs and depending on Al(III) concentrations, 1000 to 50000 transients were routinely collected.

Data were collected from samples held in a Wilmad 513-PP coaxial 10mm tube with $AlCl_3$ in H_2O as the internal standard. The NMR tubes used in this study had no ^{27}Al signal detectable by FX90Q. D_2O (10% v/v) was always

used in the inner tube for field-frequency lock. This ensured the lock integrity by avoiding formation of air bubbles when probe temperature increaesd. Accumulation times were varied from minutes for concentrated ([Al(III)] > 70 mM) and acidified solutions to 2 h for the dilute ([Al(III)] = 1 mM) solutions. The chemical shifts reported in this study are in relation to the hexaaquo ion, $[Al(H_2O)_6]^{3+}$, as reference using the following convention: negative shifts are reported for upfield resonances while those downfield are positive.

In order to find the amount of aluminium bound to different species, experiments were performed by using reference samples of the ion $[Al(OH)_4]^-$ at 10^{-1}, 5×10^{-2}, and 2×10^{-2} M placed in the annulus of the coaxial 10 mm tube. The peak of $[Al(OH)_4]^-$ signal was located at 80 ppm from the $[Al(H_2O)_6]^{3+}$ as reference. A simple integration of the peaks was performed to calculate the amount of aluminium bound in each detectable species. Alternately, the content of Al^{3+}-bound species was correlated by its relative intensity ratio to the reference signal. Anhydrous $AlCl_3$, $AlBr_3$ and AlI_3 were used without any purification. All solutions were made on a w/v basis using $AlCl_3$, $AlBr_3$ or AlI_3 in an inert atmosphere of nitrogen.

Using the standard inversion recovery sequence, the T_1 determined for a signal having a linewidth of 85 Hz in an acidified Al(III) solution was 4.1 ms. This value is in close agreement with the value of T_2 = 3.7 ms obtained from the relation, $T_2 = 1/(\pi \Delta \tau)$, where $\Delta \tau$ is linewidth, and is consistent with the line broadening due to a fast exchange situation. The pH values for each sample

were measured both before and after recording the spectra using a 5 mm Beckman Futura Plus S110A micro-electrode directly inserted into the NMR sample tube. The spectrum was considered for data only if the pH values agreed to within 0.1 pH units.

2.4. Strategies in Peptide Sequencing

D-amino acids

The D-Asp containing peptide analogs were found to be resistant to Edman sequencing at the substituted positions although their chromatographic behavior was similar to the L-Asp containing peptides. It was generally observed that the L-Asp containing peptides eluted earlier than the corresponding D-Asp analogs on RP-HPLC.

When the amino acid compositions of the D-Asp containing peptides was found to be as expected, and had identical chromatographic behavior as the L-Asp peptide, either the tryptic or staphylococcal protease digests of these peptides were subjected to Edman degradation verify the amino acid sequence. This strategy was deemed satisfactory since D-Asp was used during the stepwise synthesis of these structural analogues. The syntheses of ß1-40 and ß6-25 with D-Asp amino acids were always identified on their protease digests. A more detailed investigation on the chromatographic behavior of the D-Asp substituted peptides is given in chapter 3.

Metal-bound peptides

Al(III) incubations were studied chromatographically and spectroscopically as one of the extrinsic factors influencing secondary structure of ß1-40. Tryptic and CNBr digests of the Al(III)-incubated peptides were chromatographed on Vydac C_4 4.2 X 250 mm, and subjected to Edman degradation. Before CNBr treatment, peptides were treated with 2-mercaptoethanol (50 µL + 10-20 µg peptide, under helium for 12 hours) to reduce methionine sulfoxide. The site of Al(III) association was confirmed by the peptide mapping of the Al(III)-incubated digests with the corresponding control peptides. A similar strategy has been previously demonstrated using ß6-25 which was treated with platinum(II)terpyridine complex (Vyas and Duffy, 1989). The presence of Al(III) in the incubated peptide fractions was also verified independently by ^{27}Al NMR spectroscopy.

2.5. Materials

The resins for solid-phase peptide synthesis, polyamide-kieselguhr (Pepsyn KA), polystyrene-polyethylene glycol (PS-PEG), and the fmoc-amino acid esters were purchased from Millipore, Marlborough, MA. Additionally, 1-hydroxybenzotriazole (HOBt), dimethylformamide (DMF), piperidine (PIP),

MeCN (HPLC grade) was from Fisher Scientific, and trifluoroacetic acid (TFA) was supplied by Pierce Chemical Company, Rockford, IL. HPLC grade trifluoroethanol (TFE) and hexafluoroisopropanol (HFIP) were purchased from Sigma Chemicals, St. Louis, MO.

The sequencing chemicals, cyclohexylamine, phenylisothiocyanate (PITC), TFA, methanol (MeOH), n-heptane, ethyl acetate, were supplied by Milligen/BioSearch; N-methylmorpholine (NMM) was from Pierce. Reagents for Bradford assay and bicinchoninic acid (BCA) assay were purchased from Pierce Chemical Company, IL. All chemicals for quantitative amino acid analyses were supplied by Beckman Instruments, Palo Alto, CA. MOPS, HEPES, Tris-HCl were purchased from Aldrich Chemicals. Anhydrous Al(III) salts, anisole, thioanisole, ethanedithiol, ethylmethylsulfide, GnHCl, and GnSCN were purchased from Fluka Chemicals. Water was collected via a MilliQ system.

Chapter 3

High Performance Liquid Chromatography Studies of AßP and Derived Analogs

Introduction

Chromatographic matrices are adopted universally as effective supports for purification of peptides and proteins from a variety of sources. The ever increasing use of solid phase peptide synthesis and isolating small quantities of bioactive peptides from complex synthetic and proteolytic mixtures require efficient isolation protocols. Several investigations have been carried out on synthetic peptides corresponding to full length AßP variants, *viz.*, ß1-43, ß1-42, ß1-40 and ß1-39 (Fraser et al., 1991b; Hilbich et al., 1991; Barrow et al., 1992; Burdick et al., 1992; Jarret et al., 1993) and on the derived analogs ß1-28, ß26-40, ß34-42, and ß6-25 of the CV and SP core protein (Hollosi et al., 1989;

Halverson et al., 1990; Fraser et al., 1991b; Barrow et al., 1992; Burdick et al., 1992; Inouye et al., 1993; Jarret et al., 1993; Otvos et al., 1993; Sorimachi and Craik, 1994).

Synthetic peptides sharing sequences with AßP have been used extensively to prepare fibrils with morphology similar to the native amyloid. The biophysical studies on the AßP variants and derived analogs have shown the importance of two distinct regions to the stability of this protein: (i) the carboxyl terminal comprising ß26-42, which includes factors to initiate the purported formation of aggregates due to hydrophobic interactions (Halverson et al., 1990, 1991; Jarrett et al., 1993), and (ii) the amino terminal region comprising ß1-28, due to ion-pair formation between ionizable amino acids (Kirschner et al., 1987; Fraser et al., 1992; Inouye et al., 1993). Therefore, the conformational characteristics of the complete AßP could be dependent on the relationship between these two regions.

The prolific studies on the conformational stability of AßP in the AD brain has prompted many investigators to use a variety of techniques to investigate the underlying molecular basis. Some techniques which provide information on the structural organization of purified peptides include, but are not limited to, CD, EM, NMR, FTIR, and light scattering. As a matter of convenience, most preliminary steps in rapid selective separation of pure AßP peptides utilize reversed-phase high performance liquid chromatography (RP-HPLC). There have been reports that synthetic peptide analogs of AßP and the native AßP

elute as a broad peak during chromatographic purification (Hilbich et al., 1992; Burdick et al., 1992; Otvos et al., 1993; Roher et al.,1993). The inherent relationship which exists between the chromatographic behavior of the AßP peptides and their primary, secondary or tertiary structures has, however, not attracted much attention.

The use of RP-HPLC requires sorption/desorption of the peptide from a rigid, microparticulate *n*-alkyl bonded stationary phase by using variations in the polarity of a mobile phase. Separation of peptides and proteins generally utilize gradient elution using aqueous organic cosolvents; and, under optimized chromatographic conditions, quantitative recoveries can be made. However, with certain peptides and protein mixtures, low recoveries are coupled with poor resolution and peak capacities (Hearn and Grego, 1984). The chromatographic behavior of biomolecules have led to extensive investigations of the molecular basis for the mechanism of observed retention. Recent advances in sorbent technology have led to unique evaluations of the physico-chemical interactions of proteins and peptides with chemical matrices which are not amenable by other approaches (Aguilar et al., 1987). Indeed, the use of RP-HPLC has provided insights into the secondary and quaternary structure of tropomysin (Stone et al., 1975), myosin light chain kinase (Hearn and Aguilar, 1987), the kinetics of unfolding of proteins (Benedek et al., 1984; Lau et al., 1984), the process of assembling amphipathic α-helices (Zhou et al., 1990), and the relative stability and interactive behavior of neuropeptide Y analogs (Aguilar et al., 1993). It is

obvious from these studies that the spatial organization dictated by specific amino acids determines the chromatographic interaction of these biomolecules.

The premise of understanding chromatographic behavior of peptides and proteins lies in predicting their retention times based on amino acid composition, using the hydrophobicity coefficients of individual amino acids (Guo et al., 1986). This approach assumes the movement of the peptide as a rigid moiety on its passage through the chromatographic matrix based on the criteria of the linear solvent strength and the general plate height theory. The retention time of such a solute generally agrees with the prediction based on theoretical and mechanistic descriptions (Glajch et al., 1986). However, it has been reported that significant discrepancies occur when secondary equilibria between the solute and sorbent are established (Hearn et al., 1985). In fact, many chromatographic studies present evidence of band broadening and denaturation in polypeptides which result from initiation of secondary conformational changes at the stationary-phase surface (Hearn and Grego, 1984; Lau et al., 1984; Lu et al., 1986; Hearn and Aguilar, 1987). These RP-HPLC observations of retention and band broadening behavior of peptides have provided criteria for optimization of separation methods (Hearn and Aguilar, 1986). It is now understood that the disagreement between the predictions and the observed retention times and bandwidths in peptides and proteins is usually the influence of amino acid sequence, not the composition (Hearn and Aguilar, 1987). Nonetheless, an intimate relationship exists between the primary, secondary and tertiary

structures of a biomolecule and its chromatographic properties (Hearn and Aguilar, 1987).

Spectroscopic techniques like CD, NMR and FTIR provide details on the equilibrium conformation(s) of AßP and analogs within the spectroscopic time scale. Based on CD and solution NMR evidence, it has been suggested that the amino terminal possesses a putative α-helical character (Hollosi et al., 1989; Sorimachi and Craik, 1994); the carboxy end is mainly ß-pleated sheets according to ss-NMR and FTIR studies (Halverson et al., 1990). However, in the presence of a hydrophobic reversed-phase matrix, some of these conformations can be locked in a "near equilibrium" state (Glajch et al., 1986). Hence, the correlation of conformational behavior in terms of the hydrophobic effect and ionic interactions involved in the conformational transitions in these regions would lead to an important aspect in the structure/function studies of the AßP.

The interactive behavior and relative stability of ß1-40 and derived analogs with chromatographic matrices is presented in this chapter. Chromatographic parameters which include hydrophobic contact area were determined to evaluate the influence of the hydrophobic matrix in stabilizing the secondary structural components. These are of particular relevance, since the toxicity of ß1-40 is related to stable tertiary and quaternary structure of AßP (Yankner et al., 1990; Pike et al., 1993). Since the higher order structures of AßP are extremely sturdy due to intrinsic forces, destabilizing these would provide clues to the formation of the soluble form of AßP.

3.1. Reversed-Phase High Performance Liquid Chromatography of ß1-40 and Derived Analogs

From its introduction a decade ago, rapid separation procedures using reversed-phase high performance liquid chromatography have seen a vast growth. The selectivity in these separations is based on sorption/desorption between the solutes and stationary phase using a mobile phase to elute the desired component (Hearn, 1983). There are four major factors influencing the eluting characteristics of such organic moieties as peptides and proteins on reversed-phase matrices:

(a) Peptide composition. The overall hydrophobicity of the polypeptide arises from the relative hydrophilic/hydrophobic ratio of its constituent amino acids. The key factor in preparative and analytical separation using RP-HPLC is essentially based on the relative hydrophobic contact between solutes, in this case peptides, and the sorbent, in this case non-polar stationary phase (Hearn and Grego, 1984). Conformational constraints notwithstanding, the retention of peptides generally follows their predicted value based on the contributions from their amino acids (Guo et al., 1986). This is however only valid with small peptides up to 15 residues, after which the predictions do not hold (Wilson et al., 1981; Mant et al., 1988; Zhou et al., 1990).

(b) Primary structure dependency. Several groups have reported that peptides with identical compositions but different amino acid sequences have widely differing retention times which deviate from the predicted retention times and/or

elution characteristics (Guo et al., 1986; Hearn and Aguilar, 1987). Since the hydrophobic contribution from the amino acids essentially remains unchanged, the deviations can be explained by the sequence-dependent effects which consist of *near-neighbor* and *conformational* effects. The near-neighbor effect can be defined as solely sequence-dependent, and the conformational effect is one which is due to the peptide favoring a unique conformation or having specific interaction with the hydrophobic matrix (Zhou et al., 1990). Thus, the peptide having a preferential conformation which interacts with the stationary phase experiences an apparent change in the hydrophobic interaction (Benedek et al., 1984; Lau et al., 1984; Zhou et al., 1990).

(c) Peptide size. Chromatographers have noted that peptides larger than 20-mer elute earlier than their predicted times based on hydrophobicity (Wilson et al., 1981; Wehr et al., 1982; Mant et al., 1988). Such non-ideal behavior is the result of certain amino-acids being effectively removed from interaction with the hydrophobic stationary phase due to stabilized secondary and tertiary structures in these large peptides. However, for more ideal peptides, the retention times are linear functions of the length of peptides on a given reversed-phase support (Mant et al., 1988; Mant et al., 1989; Zhou et al., 1990).

(d) Residence time and mobile phase. The elution behavior of a peptide may be further influenced by its time of residence on the column and the organic modifier used (Hearn, 1983; Hearn and Grego, 1984). Such a phenomenon has been shown for α-chymotrypsinogen, lysozyme and soybean trypsin inhibitor

(Benedek et al., 1984), where denaturation processes in RP-HPLC result in band broadening (Hearn and Grego, 1984; Hearn and Aguilar, 1987). Indeed, the native and synthetic AßP variants exhibit broad elution profiles during chromatographic purification (Hilbich et al., 1991; Burdick et al., 1992; Miller et al., 1993; Roher et al., 1993).

It is the contention in this study that ß1-40 and derived analogs provide a good model to study the effects of conformation on their retention behavior. The nature of interaction of ß1-40 and derived analogs with the hydrophobic stationary phase was evaluated in terms of induced conformational effects within the chromatographic parameters. This was done with the following objectives: (i) to locate a preferred conformation in the peptides, (ii) to demonstrate the relevance of this conformation in the interactive behavior of the peptide on the stationary phase, (iii) to evaluate factors which cause band broadening in these peptides, and (iv) to gain insight into the dominant hydrophobic effect which stabilizes peptide structures in solution. Thus, the interaction(s) of these peptides with other hydrophobic surfaces would also provide clues to proteins which share similar sequence and structure.

3.1.1. Experimental Chromatographic Behavior of ß1-40 and Derived Analogs

Determination of the oligomeric form of peptides during RP-HPLC and SEC

Aqueous solutions of ß1-40, ß1-28, ß6-25, ß8-40, ß15-28, ß26-40 and ß22-35 peptides were prepared and the concentrations determined by quantitative amino acid analyses and/or BCA assay. The His → Arg and L-Asp → D-Asp substituted ß1-40, ß1-28 and ß6-25 analogs were also used to study the effects of substitutions on the chromatographic properties. In case the peptide was not soluble in water, a solution of 2-10% MeCN in water (v/v) was used. Linear gradient elution was performed for each peptide solution using 0.1% TFA (v/v) in MilliQ water (solvent A) and 0-100% of 0.1% TFA in MeCN (v/v) (solvent B). The solvents were degassed either by sonication or sparging with helium. The retention times of the peptides were determined following their introduction on 4.6 X 150 mm Vydac C_{18} and C_8 columns. The gradient was employed over 60 min at a flow rate of 0.8 mL/min at room temperature. The gradient conditions from 0-100% B in 60 min, schematically given in Fig. 3.1*(a)*, will hereinafter be termed as the *normal* gradient. The chromatographic conditions given in panels *b-f* are discussed in section 3.3.1.

The elution profiles of individually loaded peptides are shown in panel A of Fig. 3.2. The homogeneity of these peptides can be easily ascertained from the peak profiles. Of the peptides shown, the ßC-pep, which is the carboxy terminal of the full length APP, does not share sequence homology with the rest

of the peptide fragments. It should be mentioned that ßC-pep is a highly charged cytosolic domain of APP, is very hydrophilic, and does not possess the putative cell-adhesion –RHDS– sequence (Ghiso et al., 1992). When the retention times were plotted against theoretical molecular weights as indicated in panel B of Fig. 3.2, a log linear relationship with a correlation coefficient = 0.91 was obtained. This would indicate that the ß1-40 and derived analogs were being bound as monomers on the reversed-phase column. An exponential relationship between molecular weight and retention times had been demonstrated by Zhou et al. (1990) and Lau et al. (1984) for a series of amphipathic peptide analogs having the same sequence but different lengths.

The effect of change in the *n*-alkyl chain length on retention time is illustrated in Fig. 3.3. The ß1-40 and derived analogs were chromatographed under identical conditions to the study done above. It was clear that these peptides exhibited similar behavior on C_8 matrix (correlation coefficient = 0.92) as that observed on the C_{18} matrix. This figure also compares the retention behavior of the Arg^{13} and Arg^{14} substituted ß1-40 and ß6-25 derived analogs. The retention times for these analogs are slightly longer on C_{18} than C_8, however they follow log linear relationships with respect to molecular weight. Such analogous characteristics indicate that these peptides have similar interactions with the stationary-phase surface, based on the hydrophobicity of C_8 and C_{18} and the length of the peptide chain. The complicating features related to ß22-35 are treated under a separate heading later in this section.

Fig. 3.4 illustrates the influence of mobile phase on retention times for ß1-40 and derived analogs. When TFE was substituted for MeCN (v/v) in mobile phase B, a positive change was seen in the slope of the plot of retention times and molecular weights (correlation coefficient = 0.72). From the chromatographic behavior between MeCN and TFE, it was evident that these peptides experienced variable interactions with the reversed-phase surface which were dependent on the sequence. Since the peptides ß1-40, ß8-40, ß1-28, ß6-25 and ß15-28 share the common Gln^{15}–Gly^{25} sequence, it would seem that this common epitope was affected by TFE in the mobile phase.

The propensity of the Asp^{1}–Val^{12} sequence at the amino terminal of ß1-40 to form α-helices in TFE based cosolvents, and the central Glu^{11}–Gly^{25} segment to maintain ß-pleated sheet structure in aqueous solutions has already been reported (Hollosi et al., 1989; Sorimachi and Craik, 1994). TFE is considered to be a non-interactive solvent and benign in chromatographic circles (Lau et al., 1984). However, TFE destabilizes the tertiary and quaternary interactions in coils producing single stranded α-helices, or more generally promotes intramolecular hydrogen bonding (Urry et al., 1971). Taken together, it would seem that TFE was more effective in inducing conformational changes in ß1-40 and derived analogs on the stationary phase support than was MeCN. Nevertheless, the log linear correlation of retention times with molecular weights suggested that these peptides were bound in their monomeric form on the reversed-phase support.

The disruption of tertiary and quaternary interactions in proteins, or the nonspecific peptide aggregation in a nonpolar environment of reversed-phase chromatography is not surprising since hydrophobic interactions are the major stabiilizing forces. Nonetheless, it was necessary to ascertain the monomeric nature of these peptide solutes during chromatography. This was accomplished by loading peptide solutions on a size exclusion column TSK 300SW using the following solvent systems: system 1 was 0.1% TFA in 150 mM KCl as solvent A, and solvent B was solvent A with 50% MeCN; system 2 was 0.1% TFA in 150 mM KCl as solvent A, and solvent B was solvent A containing 50% TFE. The inclusion of KCl in the solvents reduces the ionic interactions between the column matrix and peptides (Mant et al., 1987). After chromatography of the individual peptides, the retention times were plotted against their theoretical monomeric molecular weights as depicted in Fig. 3.5. A log linear relation of their molecular weights and retention times was observed which indicated that these peptides were bound to the column matrix in their monomeric forms. If ß1-40 and derived analogs interact as monomers in the absence of the hydrophobic reversed-phase matrix, then it is assumed that they interact in their monomeric form when in contact with it. This observation also suggested that the ß1-40 and derived analogs of same length (*e.g.*, the His $\rightarrow$ Arg substituted, and the D-Asp containing peptides) exhibited identical sizes since they had identical retention times during SEC.

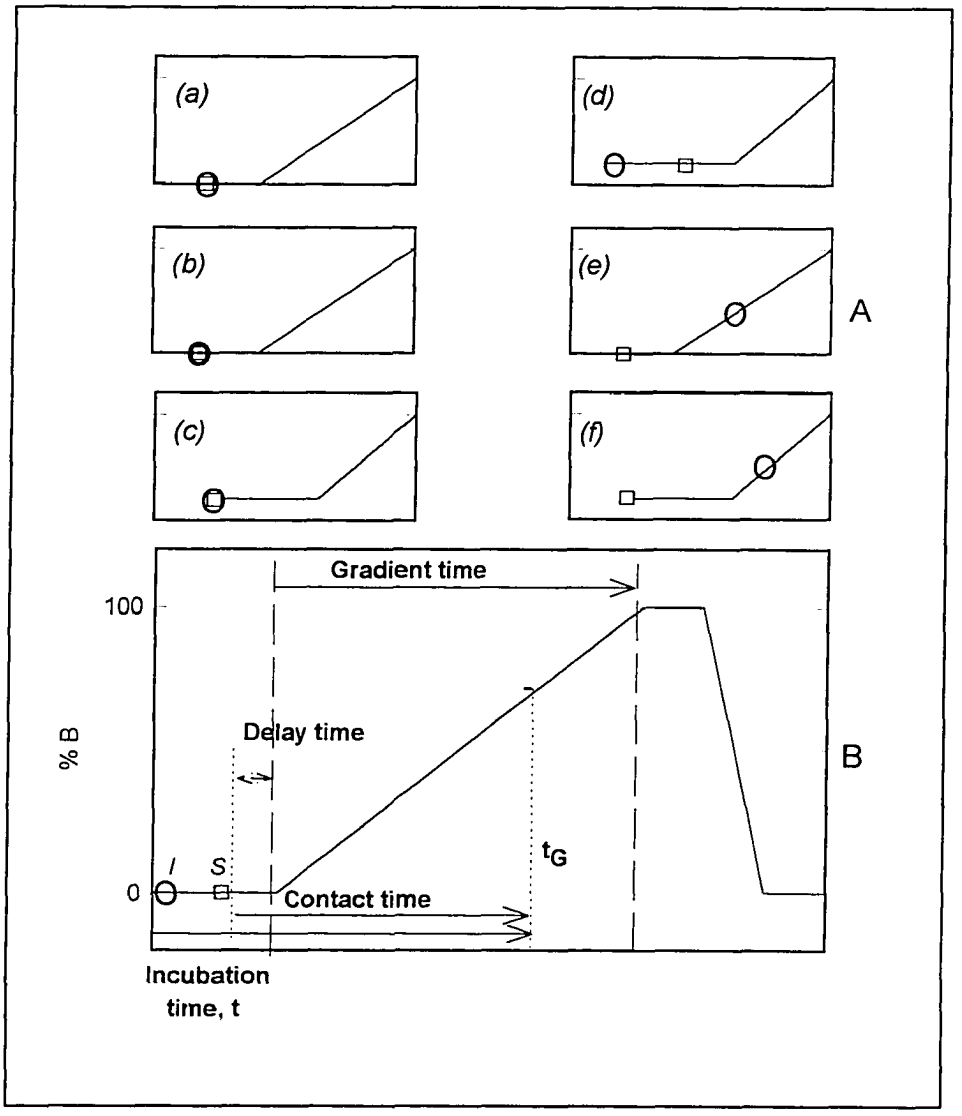

Fig. 3.1 RP-HPLC strategy for on-column incubation experiments. Panel **A** gives the six kinetic experiments by changing the incubation, contact, delay, and gradient times. Panel **B** schematically defines the injection of peptide (circle), *I*, start of gradient (square), *S*, and the gradient time.

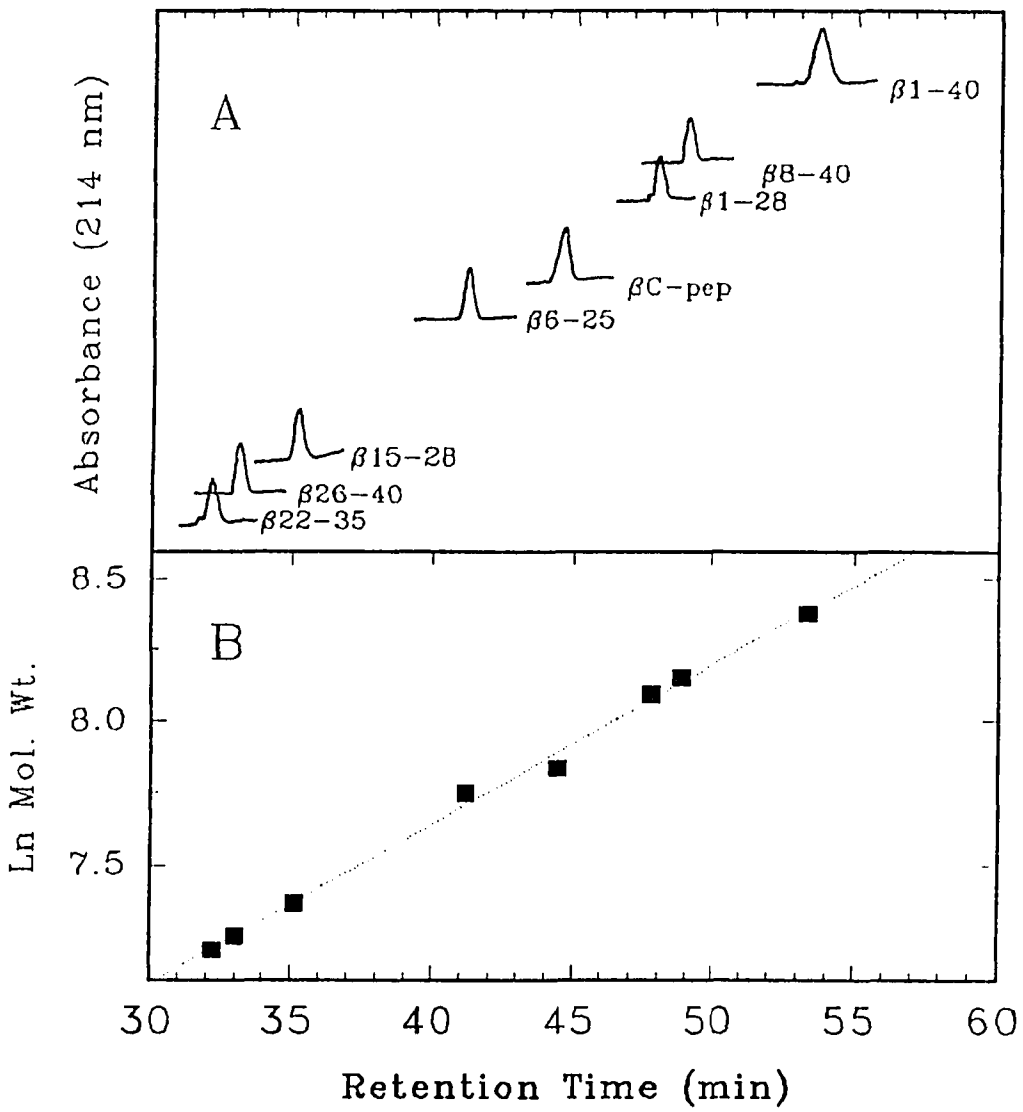

Fig. 3.2 HPLC of ß1-40 and derived analogs on reversed-phase surface octadecyl matrix. Panel A gives the elution profiles of singly loaded peptide solutions. Column: 4.6 X 150 mm Vydac C_{18} operated at room temperature; solvent A was 0.1% TFA, solvent B was 0.1% TFA in MeCN; linear gradient from 0 - 100% B in 60 min at a flow rate of 0.8 mL/min. Panel B represents the retention time relationship in terms of ln molecular weight.

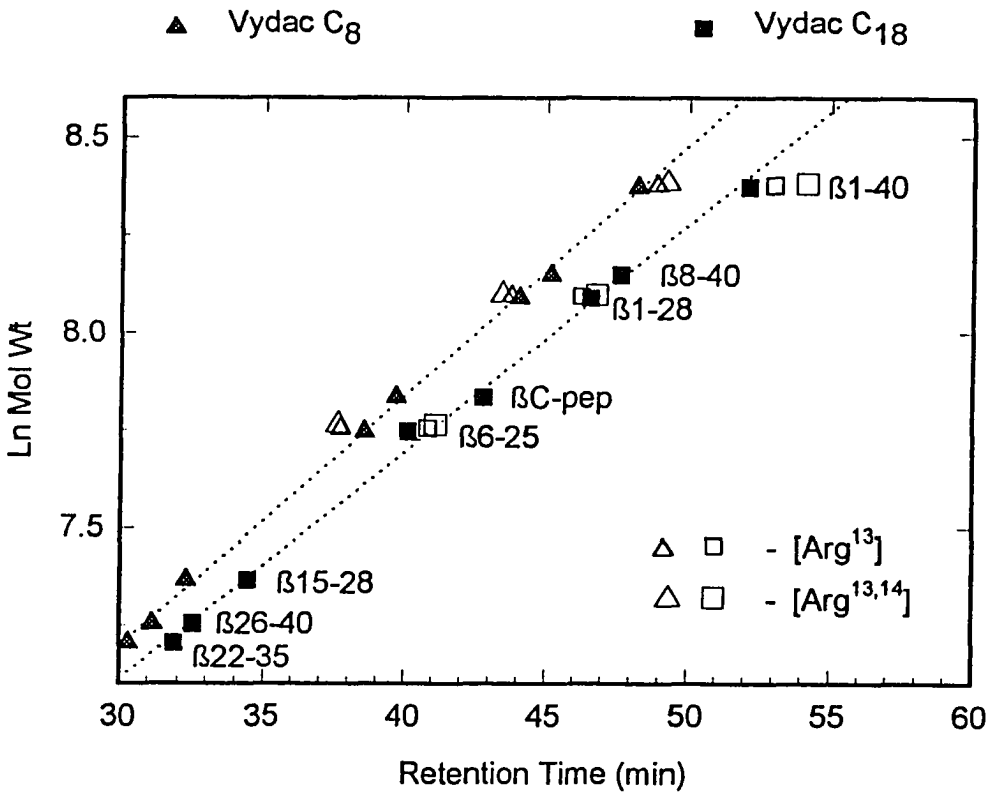

Fig. 3.3 Comparison of RP-HPLC behavior of singly loaded peptides between C_8 and C_{18} matrices. Gradient conditions were as given in Fig. 3.2 with a flow rate of 1.0 mL/min; columns operated at room temperature. The hollow symbols represent retention times for the [Arg^{13}] and [$Arg^{13,14}$] analogs of ß6-25 and ß1-40 on the respective columns.

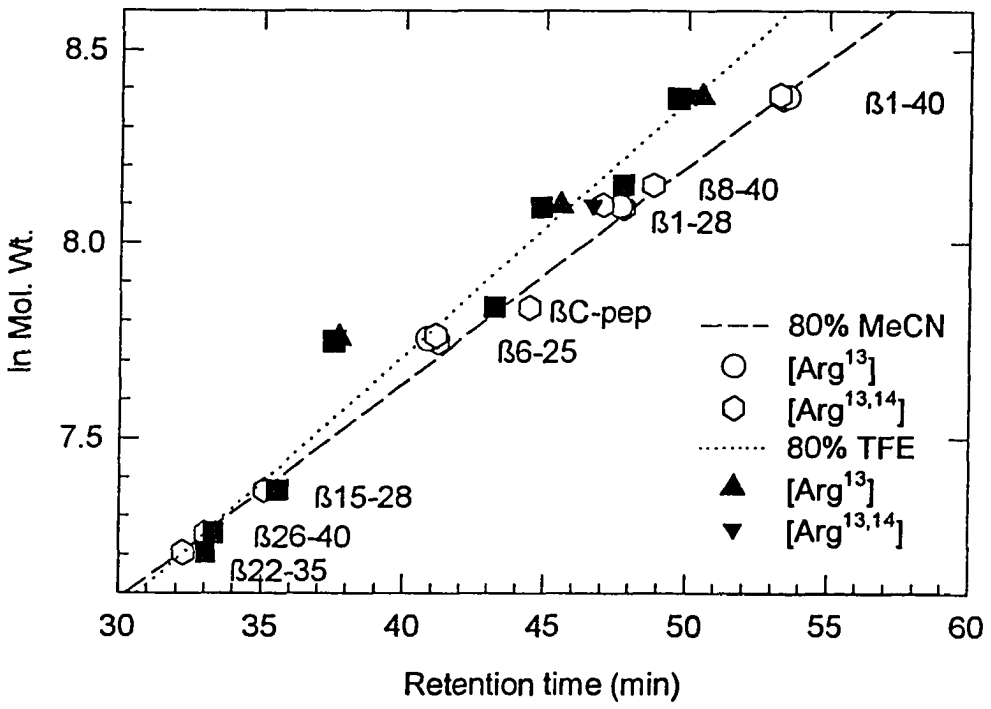

Fig. 3.4 Comparison of RP-HPLC behavior as a function of mobile phase; MeCN and TFE. The retention data using 0.1% TFA in 80% MeCN as solvent B is given by the linear regression through data (hollow symbols); the retention data on substituting 80% TFE for MeCN in B is given by the solid symbols. The retention times for the His · Arg substituted analogs are also indicated. Column: Vydac C_{18}, operated at ambient temperature; flow rate was 1.0 mL/min; *normal* gradient conditions. All data are the mean of three chromatographic runs.

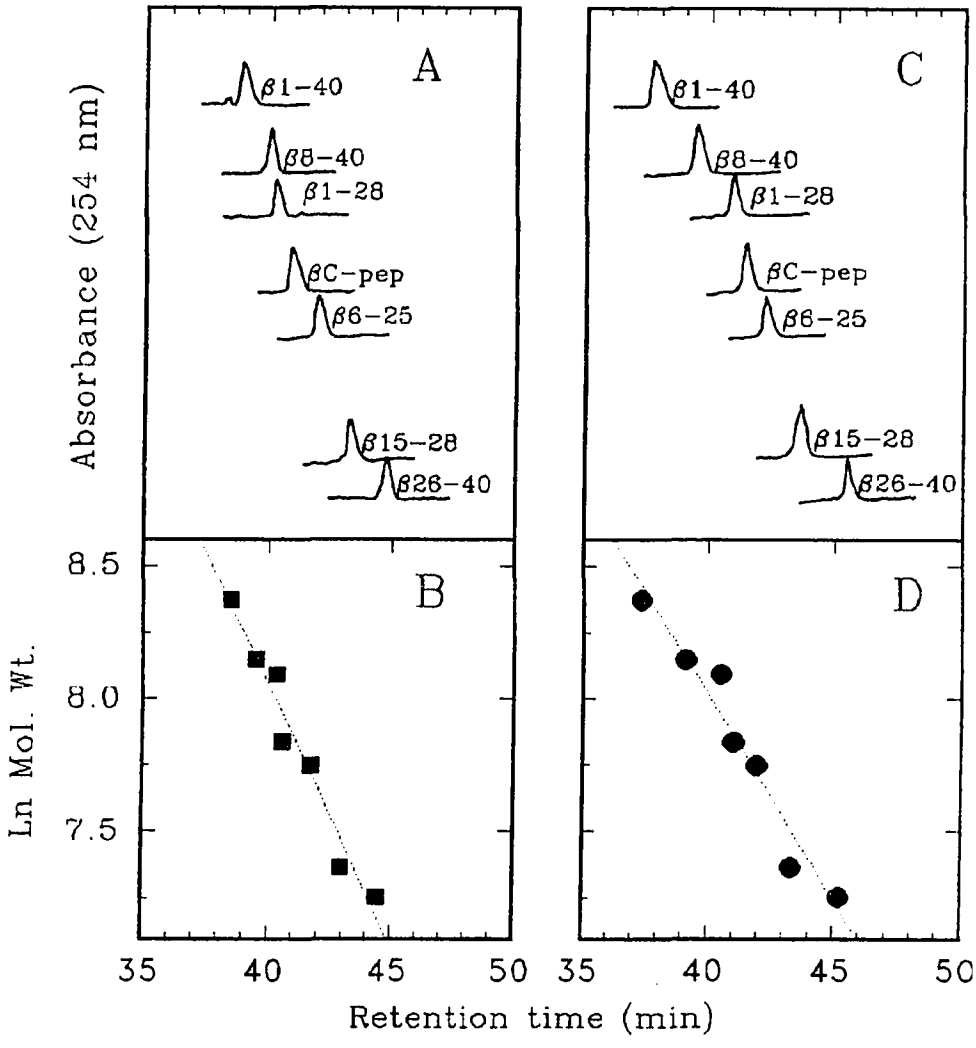

Fig. 3.5 Verification of monomeric nature of ß1-40 and derived analogs in solution by SEC. Column: Protein Pak TSK 300SW operated at room temperature; solvent A was 0.1% TFA in 150 mM KCl, solvent B was 0.1% TFA in 150 mm KCl containing either 50% MeCN or TFE; flow rate was 0.25 ml/min. Panel A gives elution profiles using MeCN in mobile phase; retention data in terms of molecular weight is plotted in B; panels C and D gives corresponding study using TFE in mobile phase. Data for ß22-35 oligomers are not included.

Equilibrating oligomers of ß22-35 during chromatography

ß22-35 in solution exhibited atypical elution behavior as illustrated in Fig. 3.6. When a freshly prepared solution containing 10 µg ß22-35 was chromatographed on the C_{18} matrix using identical gradient conditions as the previous study, four distinct components having identical peak areas were resolved. The nature of the eluting components was examined after collecting the individual fractions, concentrating *in vacuo* and reloading on the column. The elution profiles of these solutions are shown in panel A of Fig. 3.7. All components for any given re-loading had the same mass as determined by peak areas, suggesting that equilibration of these eluting components took place in solution and that the components were resolved on the reversed-phase support. In another examination, the fractions were collected, lyophilized, the residue dissolved and loaded on the column. These solutions also exhibited identical elution profiles in terms of retention times and peak areas to the profiles obtained for the concentrated fractions. Such chromatographic behavior indicated that ß22-35 formed equilibrating oligomers in solution.

To verify if the phenomenon observed with ß22-35 was indeed equilibration of oligomers in the denaturing conditions of the reversed-phase surface, size-exclusion chromatography was performed under conditions identical to the previous study. A typical elution profile of ß22-35 solution is shown in panel B of Fig. 3.7. A broad peak corresponding to a 12 KDa component was eluted under SEC conditions which suggested that in the

absence of a reversed-phase support, ß22-35 existed as an octamer in aqueous solution.

The chromatographic profiles on the hydrophobic matrix therefore indicated the denaturation of an octamer. When the retention times were plotted against the theoretical molecular weights for $(ß22\text{-}35)_n$, for n = 1, 2, 4, and 8, these followed log linear relationship (Fig. 3.6) with a correlation coefficient = 0.72. The most stable form of ß22-35 in freshly prepared aqueous solution therefore seemed to be the octamer which equilibrated into its monomer, dimer and tetramer on passage through the reversed-phase column:

$$(ß22\text{-}35)_8 \overset{(RP)}{\rightleftharpoons}_{(solution)} (ß22\text{-}35) \leftrightarrow (ß22\text{-}35)_2 \leftrightarrow (ß22\text{-}35)_4$$

The observed chromatographic behavior indicates that there must be more than just sequence-dependent effects experienced by ß22-35 on the reversed-phase support, and that the hydrophobic stationary phase support is capable of disrupting intermolecular hydrophobic interactions. A similar effect has also been reported for soyabean trypsin inhibitor during chromatographic purification (Hearn et al., 1985). The net effect of the reversed-phase matrix on these independent and dynamic interconversions of ß22-35 was the formation of stable oligomers in an otherwise denaturing condition, which gave rise to long-lived metastable forms on the chromatographic time scale. These oligomeric forms can therefore be analyzed in the same way as an equilibrium process with an apparent concentration of the different forms treated as equilibrium concentrations (Hearn et al., 1985).

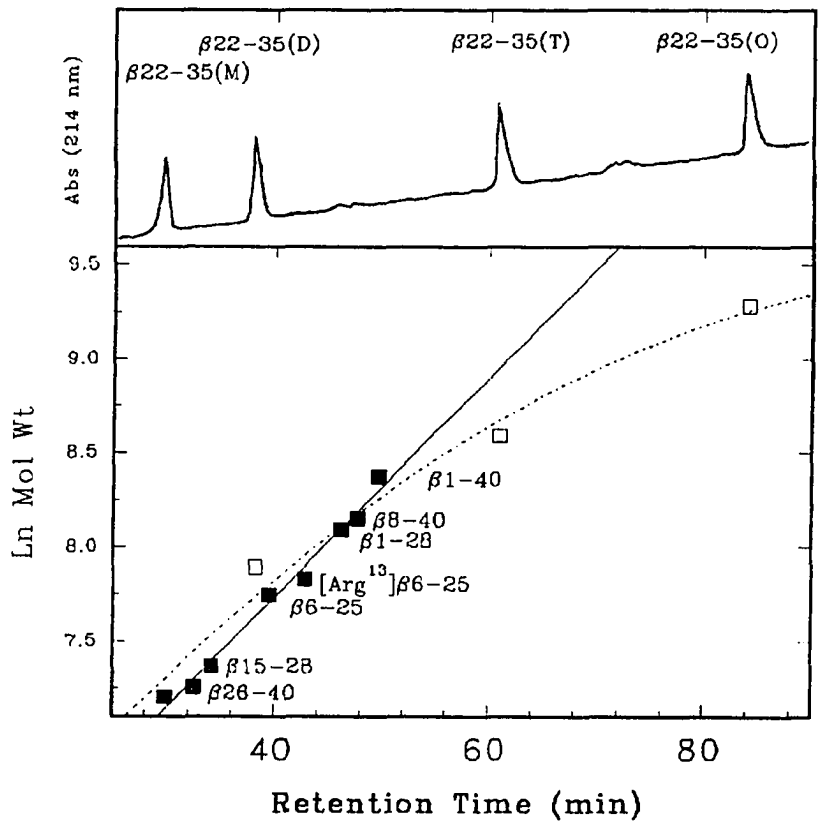

Fig. 3.6 Characterizing oligomerization of ß22-35 in solution. The separation of the respective oligomers of ß22-35 on Vydac C_{18} in the top panel; the comparison of log linear plot of theoretical molecular weights of ß22-35 versus retention time (□) with ß1-40 and sequence analogs. The log linear relationship for ß22-35 is shown by the dashed line. Chromatographic conditions as per Fig. 3.2 for 60 min, then 100% B till 90 min.

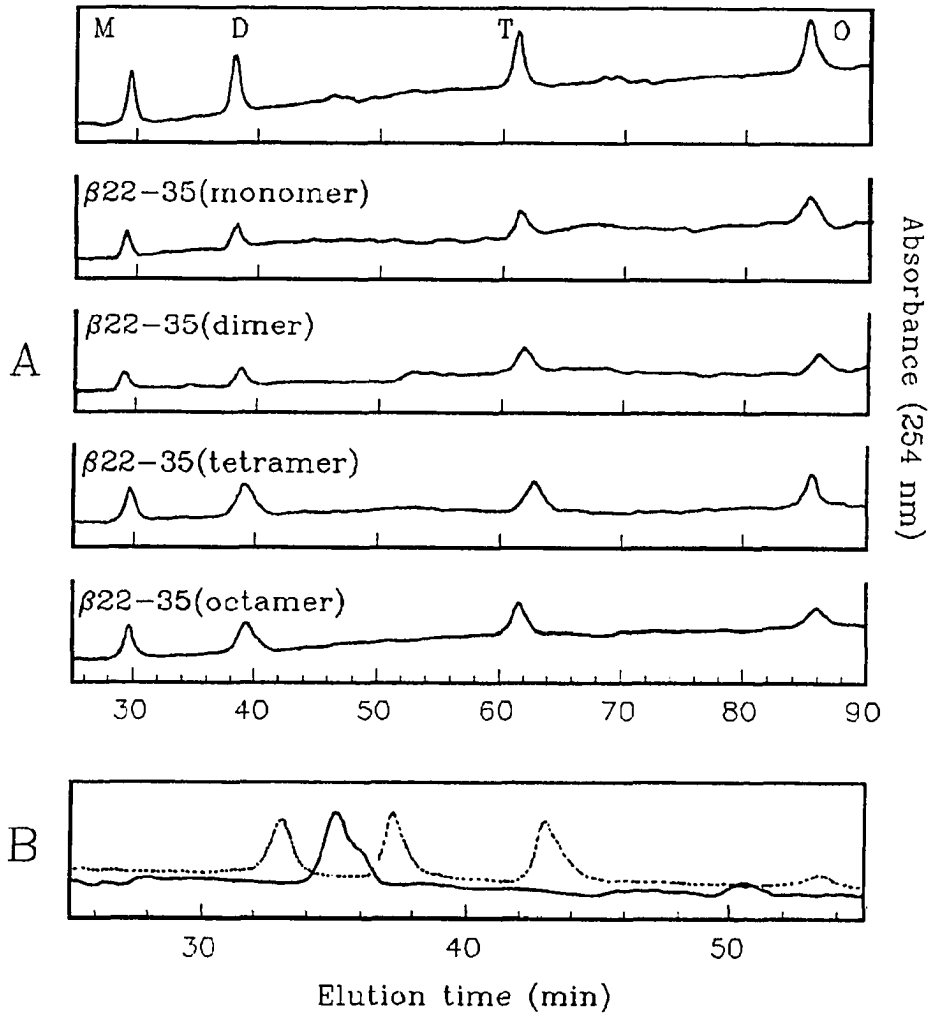

Fig. 3.7 Elution profiles of ß22-35 oligomers on reversed-phase and size exclusion chromatography. The eluting fractions from Fig. 3.6 were collected individually, lyophilized, dissolved in 2% HAc and loaded on the Vydac C_{18}. Panel A shows from top to bottom the RP-HPLC of monomer, dimer, tetramer, and octamer respectively. Panel B shows the SEC profile of a lyophilized ß22-35 fraction corresponding to the monomer eluting at 30 min. The dashed curve represents molecular weight markers: myoglobin (17 KDa), aprotinin (6 KDa), and insulin B-chain (3.5 KDa).

3.2. Evaluation of Chromatographic Behavior of ß1-40 and Derived Analogs During RP-HPLC

As noted before, the chromatographic purification of synthetic and native AßP preparations on reversed phase supports yield the pure peptides as broad peaks (Burdick et al., 1992; Miller et al., 1993; Otvos et al., 1993; Roher et al., 1993). Several investigations on AßP and its derived analogs have suggested the propensity of the carboxy terminal corresponding to residues 34-42 to form stable antiparallel ß-pleated sheet structure (Halverson et al., 1990; Lansbury, 1992), and the amino terminal residues 1-28 adopts α-helical structure in these peptides (Barrow and Zagorski, 1992; Sorimachi and Craik, 1994) due to the flexibility of the backbone (Hollosi et al., 1989). Secondary structural content of these peptides can also be modulated due to amino acid substitutions, and the presence of membrane mimicking solvents (Barrow et al., 1992; Laczkó-Hollósi et al., 1992; Otvos et al., 1993) These studies show that the organization of ß1-40 and derived analogs include domains in which the orientations of the peptide backbone are predicated by the amino acid sequence.

It can be therefore hypothesized that the polypeptide on introduction to the stationary phase support is adsorbed in a specific orientation, along with other orientations which are equally likely. Chromatographic parameters related to the physico-chemical properties of a solute can then be derived using the linear solvent strength model, which under normal reversed-phase gradient

elution predicts a linear relationship between the median capacity factor, log k^*, and the median organic mole fraction, ψ^* (Stadalius et al., 1976):

$$\log k^* = \log k_0 - S \cdot \psi^* \quad (1)$$

According to the solvophobic theory applied to polypeptides (Hearn, 1983), the magnitude of the chromatographic contact area projected by the peptide (solute) and the predilection which it has for the chromatographic ligands (sorbent) is given by log k_0 and the slope, S. The application of equation 1 implies that the retention behavior does not involve aberrant properties on the part of the solute, like differential migration processes due to a medley of competing secondary effects. The slope will also be affected for the adsorption/ desorption processes which involve participation of different classes of interactive sites on the heterogenous sorbent (Hearn and Aguilar, 1987). Thus, in the case of closely eluting peptides having constitutionally dissimilar contact area dependencies, the manipulation of secondary solution equilibria should result in change in interactive behavior.

Determination of chromatographic parameters as a function of organic solvent concentration

In order to examine the consequence of amino acid substitutions within the peptides on interaction with the hydrophobic stationary phase gradient

elution data were accumulated for ß1-40 analogs. The following set of peptides as given in Table 2.1, were studied: (i) ß1-40, and derived analogs having His → Arg substitutions at positions 13 and 14, L-Asp → D-Asp substitutions at positions 1, 7, and 23, (ii) ß1-28, and derived analogs having His → Arg substitutions at positions 13 and 14, (iii) ß6-25, and derived analogs having L-Asp → D-Asp substitutions at positions 7 and 23. Additionally, ß1-40 and ß6-25 having both His → Arg and L-Asp → D-Asp substitutions were also examined.

The peptides were individually chromatographed on the Vydac C_{18} column at a flow rate of 1.0 mL/min as per conditions described by Fig. 3.1*(a)*. The column was operated at temperatures between 25 and 65°C at linear gradient times between 30-90 min. Elution profiles were generated, and the retention data was analyzed by adopting the Pek'N-ese protocol (Hearn and Aguilar, 1987) for the chromatographic parameters highlighted in Appendix B. The inherent errors using areas of eluting components having asymmetric peak profiles were ± 12% compared to the absolute mass recoveries over the same mass range. However, these errors were ± 5% when a strict elution time window at the peak maxima was applied. Data collection was in triplicate, and linear regression analysis using ANOVA was performed to get the S and log k_0 given by equation 1 (typical correlation coefficients were between 0.90-0.97).

Fig. 3.8 gives the plots of log k^* versus ψ^* obtained at 22°C which represents the elution data as per equation 1. From the observed data, it is obvious that there is considerable resolution between *all* the substituted analogs

of ß1-40 (panel A), ß1-28 (panel B) and ß6-25 (panel C). The His → Arg substituted peptides generally tended to elute later than the unsubstituted peptides while shorter retention times were observed for the peptides having D-Asp substitutions at positions 7 and 23. These results show that there is a significant change in the interactive behavior of these peptides associated with amino acid substitutions. The most significantly longer retentions were for peptides having dual substitutions of Arg and D-Asp. The later elution of the Arg and D-Asp substituted peptides is therefore more representative of increase in the hydrophobic character. To elucidate the role of secondary structure in the chromatographic behavior of these derived analogs, the data were analyzed with respect to temperature.

Dependence of S and log k_0 on temperature

The implications of the chromatographic parameters, S and log k_0, are that these are related to the magnitude of the hydrophobic contact area between the solute (peptide) and the sorbent (column), and a measure of free energy changes associated with the adsorption process in the absence of the mobile phase (Horvath et al., 1976). When these parameters are obtained from the study of closely related peptides in a range of chromatographic conditions, a quantitative elucidation of differences in peptide orientation and affinity for the sorbent can be made (Aguilar et al., 1993). The solution conformation of peptides is dependent on temperature, a parameter which was easy to modify

in this chromatographic study. However, a comparatively rigid molecule not easily perturbed by the imposed chromatographic conditions was needed as control. Angiotensin III, which is a partially-folded heptapeptide, having minor secondary structure (Matsoukas et al., 1991), and N-acetylphenylalanine methyl ester (N-AcF), which does not possess any secondary structure, were used as controls for this study.

Fig. 3.9 illustrates the dependence of the slope parameter, *S*, and log k_0 for ß1-40 and derived analogs as a function of temperature. There were obvious inferences from the observed *S* values of the peptides compared to the controls: (i) *S* values for the longer peptides, ß1-40 and ß8-40 were higher than all the other peptides, which suggested the chromatographic contact area was higher in these peptides, (ii) *S* increased with temperature, which suggested that there was an increase in the interactive region, (iii) *S* did not change appreciably after 60°C, indicating that the change in the chromatographic contact area was complete. The increase in log k_0 followed similar trend to *S* below 40°C. The absence of the first 7 residues in ß8-40 significantly altered its interactive behavior compared to ß1-40. At temperatures higher than 40°C, log k_0 decreased for the longer peptides which would suggest that the increase in the chromatographic area was accompanied by a decrease in the interactive behavior of these peptides for the sorbent. The chromatographic contact area for ß6-25 increased in temperature as seen from the *S* values.

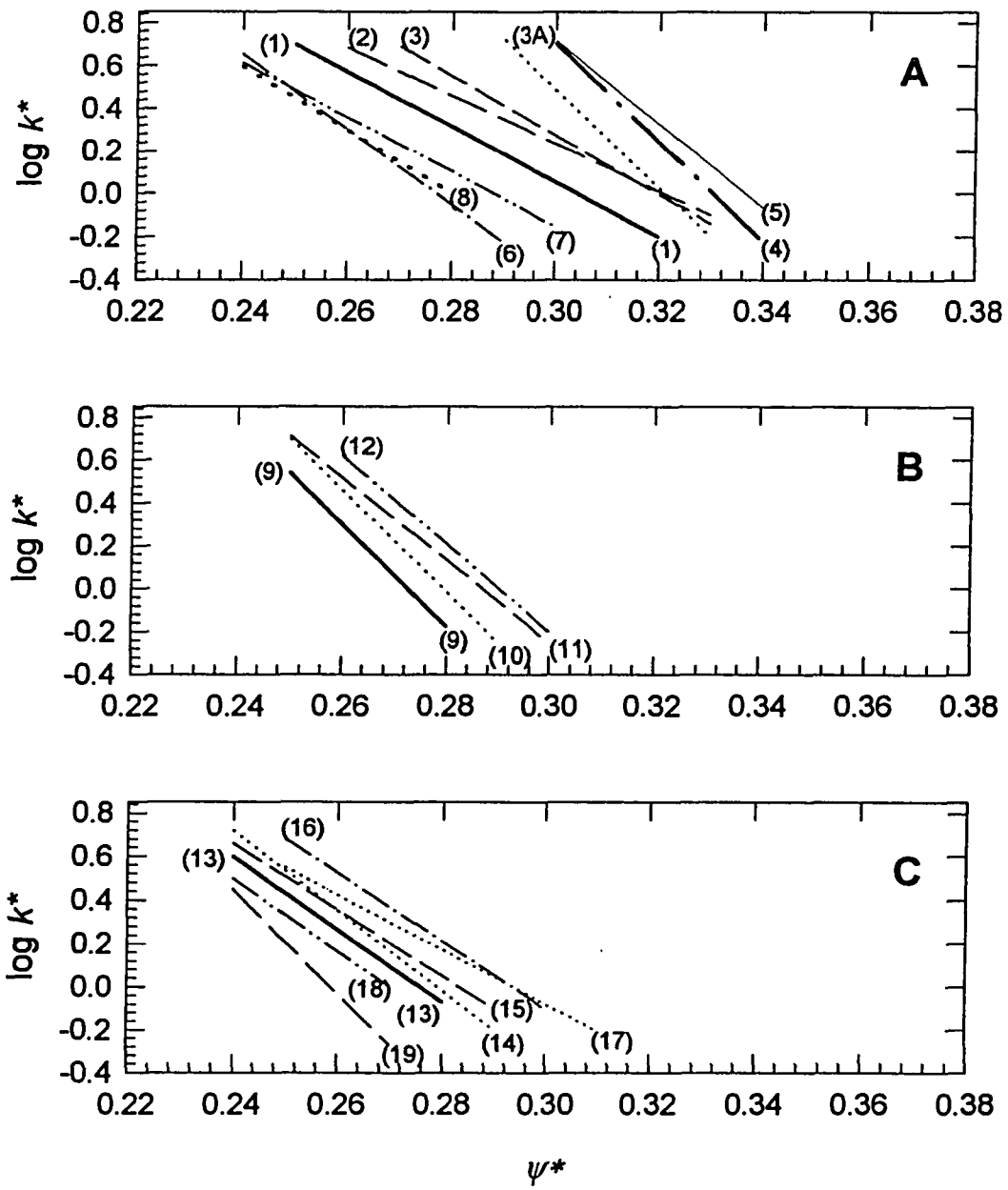

Fig. 3.8 Plots of log k^* versus ψ^* for ß1-40 and derived analogs on C_{18} at 22°C. The lines represent the best fit analysis to data points (excluded for clarity). Panel **A**: plots for ß1-40 (1), [Arg^{13}]ß1-40 [Arg^{14}]ß1-40 (3), [Arg^{13,14}]ß1-40 (3A), [D-Asp^{1}]ß1-40 (6), [D-Asp^{7,23}]ß1-40 (7), [D-Asp^{1,7,23}]ß1-40 (8), [Arg^{14},D-Asp^{23}]ß1-40 (5); panel **B**: plots for ß1-28 and its [Arg] derived analogs; panel C: ß6-25 (13), [Arg^{13}]ß6-25 (14), [Arg^{14}]ß6-25 (15), [Arg^{13,14}]ß6-25 (16).

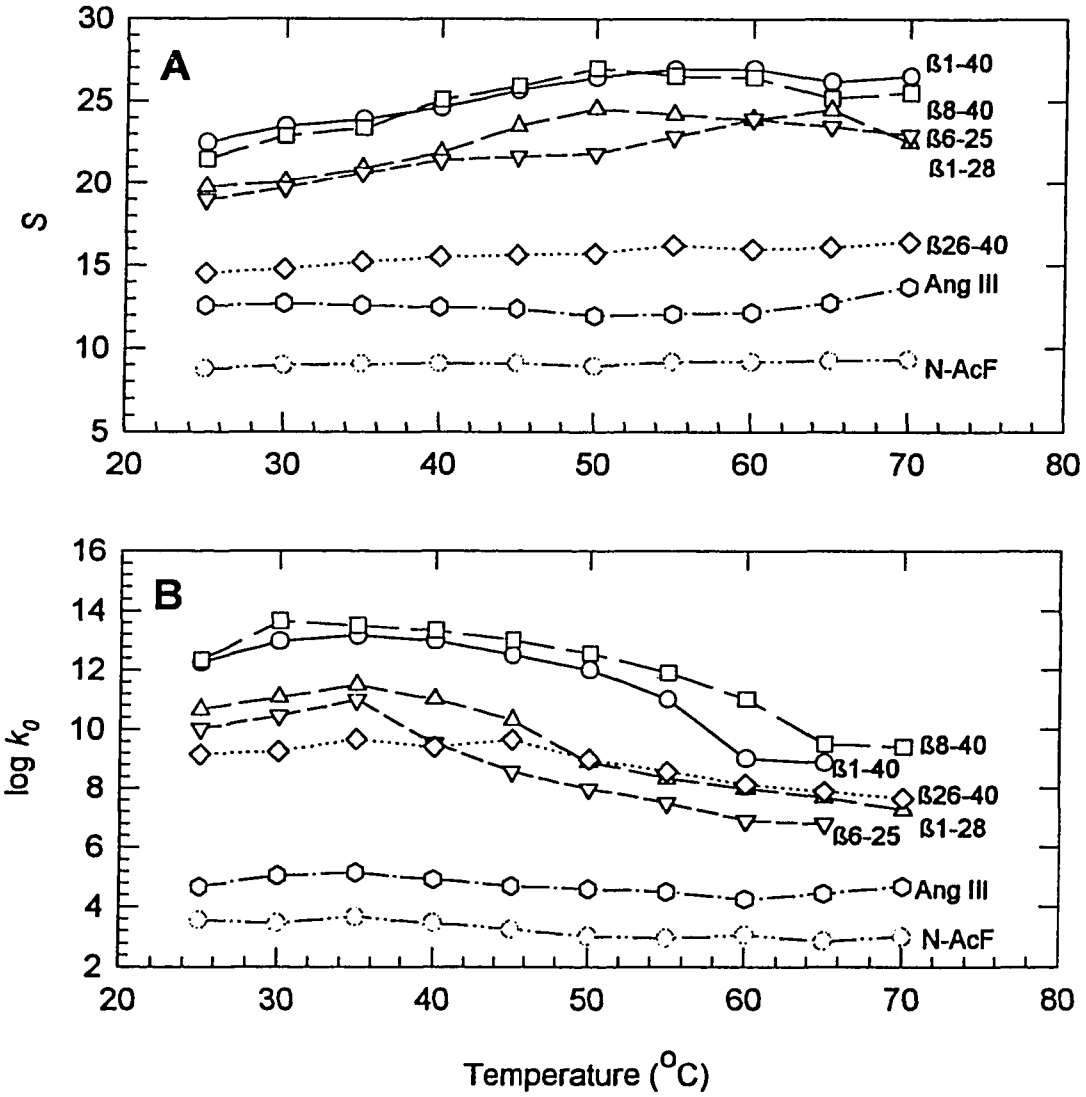

Fig. 3.9 Plots of S (A) and log k_0 (B) versus temperature for ß1-40 and derived analogs, angiotensin III and N-acetylphenylalanine methyl ester eluted from Vydac C_{18}.

However, the log k_0 decreased simultaneously. This suggested that when the first 5 residues at the amino and the 15 residues at the carboxyl terminus residues were removed, there was a significant reduction in the affinity for the stationary phase surface. This was further affirmed with the chromatographic behavior of ß26-40. There was no significant reduction in the log k_0, although with an increase in temperature the S value showed an increase. It would, therefore, appear that the carboxyl terminal region shows consistency in terms of increase in the chromatographic contact area, whereas increasing the peptide chain at the amino terminal results in altered interactions with the reversed-phase surface.

3.3. Evaluation of Band Broadening of ß1-40 by Gradient Elution RP-HPLC

The pivotal dependence of relative retention times and bandwidths of polypeptide solutes involves the mole fraction of the organic modifier, ψ, in the mobile phase. It is, however, generally assumed that solute mixtures can be resolved in a nicely designed gradient system on a given column with the same relative bandwidth. Many chromatographers have noted in practice that this requirement, although important for optimized resolution, is rarely achieved for

polypeptides and proteins (Hearn and Grego, 1984; Hearn et al., 1985; Stadalius et al., 1985; Hearn and Aguilar, 1986). The small diffusion coefficients of (macromolecular) peptide solutes in aqueous-organic cosolvent mobile phases result in the observed plate number, *N*, to be significantly smaller and consequently, the plate height number, *h*, to be significantly larger than the *N* values obtained for low molecular weight organic compounds (Snyder, 1980). The combined effect of these manifestations results in very steep slopes, $S > 10$, for the linearized plot of capacity factor, *k'* versus the organic mole fraction and generally results in increased bandwidths. Moreover, specific solvation or buffer interaction of the silanophilic properties of the heterogeneous *n*-alkyl bonded stationary phase surface and conformational phenomena of these peptide solutes bestow band broadening on the eluting component.

In this section, the bandwidth dependency of ß1-40 is presented as a function of different gradient elutions, column temperature, and the chromatographic residence times. Since the chain length of the *n*-alkyl ligand and the hydrocarbon ligand density influence the chromatographic behavior (Hearn, 1983), all examinations were done on the same 4.6 X 150 mm Vydac C_{18} column. This study furthers the knowledge of the RP-HPLC of ß1-40 and derived analogs so that optimum resolving conditions can be employed, peak shape can be controlled, and an understanding of the secondary equilibria established by the peptide at the reversed-phase surface can be achieved.

3.3.1. Changes in Band Shape as a Function of Organic Modifier Concentration

To obtain detailed data on the rate constants associated with the adsorption/desorption kinetics or conformational interconversion of different forms of ß1-40 on reversed-phase chromatography, a deliberate scouting of elution protocols was done. The column was thermostatically controlled between 20°C and 45°C. The dedicated RP-HPLC setup was modified to increase the gradient steepness parameter, and to increase the chromatographic residence time. Also, the injector was placed nearer to the column using a 10 cm stainless steel tubing so as to reduce the temperature effects on the peptide in the injection loop. The mobile phase A consisted of varying amounts of the organic modifier (MeCN or TFE) from 0% to 20% v/v in 0.1% TFA, as demanded by the experiment. The gradient reaching the column was adjusted for the delay time which was 3.7 min (using a 2 mL sample loop) for the setup. The gradient-setup was such that the column was always returned to its initial condition after the completion of each run. The gradient conditions are schematically represented in Fig. 3.1.

For this study, the following terminology was adopted from Benedek et al. (1984). The *gradient time* was defined as the time necessary to convert the solvent in the column from 100% A to 100% B (Fig. 3.1). The *start of gradient* was defined when % B increased from its initial composition after the peptide was introduced on the matrix (*S*, Fig. 3.1). The *contact time* was defined as the

difference between the time of injection and the time of elution of the component as detected (not adjusted for time of its passage from column to detector as the length of tubing was unchanged throughout the study). The contact time was adjusted for the component by verifying the retention for unretained sodium nitrate (= 1.8 min). The *incubation time, t*, was the time from injection to the start of the gradient at the column. This is schematically illustrated in Fig. 3.1 composite, panel B. The residence time of the peptide in the mobile phase was considered to be a constant for all elutions. For want of a better term, the *native* peptide in this study denotes the pure synthetic peptide having a *preferred* conformation, and is used to differentiate from its conformation during residence on the hydrophobic stationary phase. It is true that both conformers have identical sequences and amino acid compositions, but different interactions with the hydrophobic matrix (*i.e.*, chemically similar but conformationally distinct).

The peptide content was determined by BCA and quantitative amino acid analyses. All elution data were analyzed as per the protocol outlined earlier in section 3.2. The following experimental conditions, given in Fig. 3.1, were imposed in order to initiate the band broadening studies:

Fig. 3.1*(a)* shows the normal gradient protocol with the injection being concurrent with start of the gradient. As per criteria in panel *(b)*, ß1-40 was injected and allowed to incubate for a specific time between 10 and 60 min on the column after which the gradient was initiated and the elution of the peptide was monitored. Panel *(c)* indicates the inclusion of the organic modifier (MeCN

or TFE) in solvent A at the start of the gradient. The incubation experiment with solvent A containing the organic modifier is indicated in panel *(d)*. These examinations were done in duplicate. The peak areas for the *native* peptide were determined for the given incubation times and compared with those of area for zero time from panel *(c)*, and linear regression was performed using ANOVA. The implications of the gradient and on-column incubation schemes given by panels *(e)* and *(f)* will be discussed in later sections.

Fig. 3.10 summarizes the changes in bandwidths as a function of incubation times and the nature of solvent A using a constant gradient time. The peptide eluted approximately at the same organic modifier content, which was between 40 and 45% MeCN or TFE in these experiments. It is evident that as the peptide was incubated on the column for longer periods of time, the band of the eluting peptide was broadened considerably; the bandwidths for the incubation experiment for 0, 10, 30, 60 and 120 mins with solvent A containing no organic modifier were respectively 0.8 mL, 4.0 mL, 7.2 mL, 9.6 mL and 11.2 mL. The flow rate dependency of bandwidths is given in the composite in panel B. It is evident that the peak shape was not particularly influenced by the flow rate for a given gradient time. The band broadening appeared to occur significantly after the on- column incubation time was more than 10 minutes. For longer incubation times, there was only a little change in the peak shape. The mass recovery from these incubations was approximately 35%.

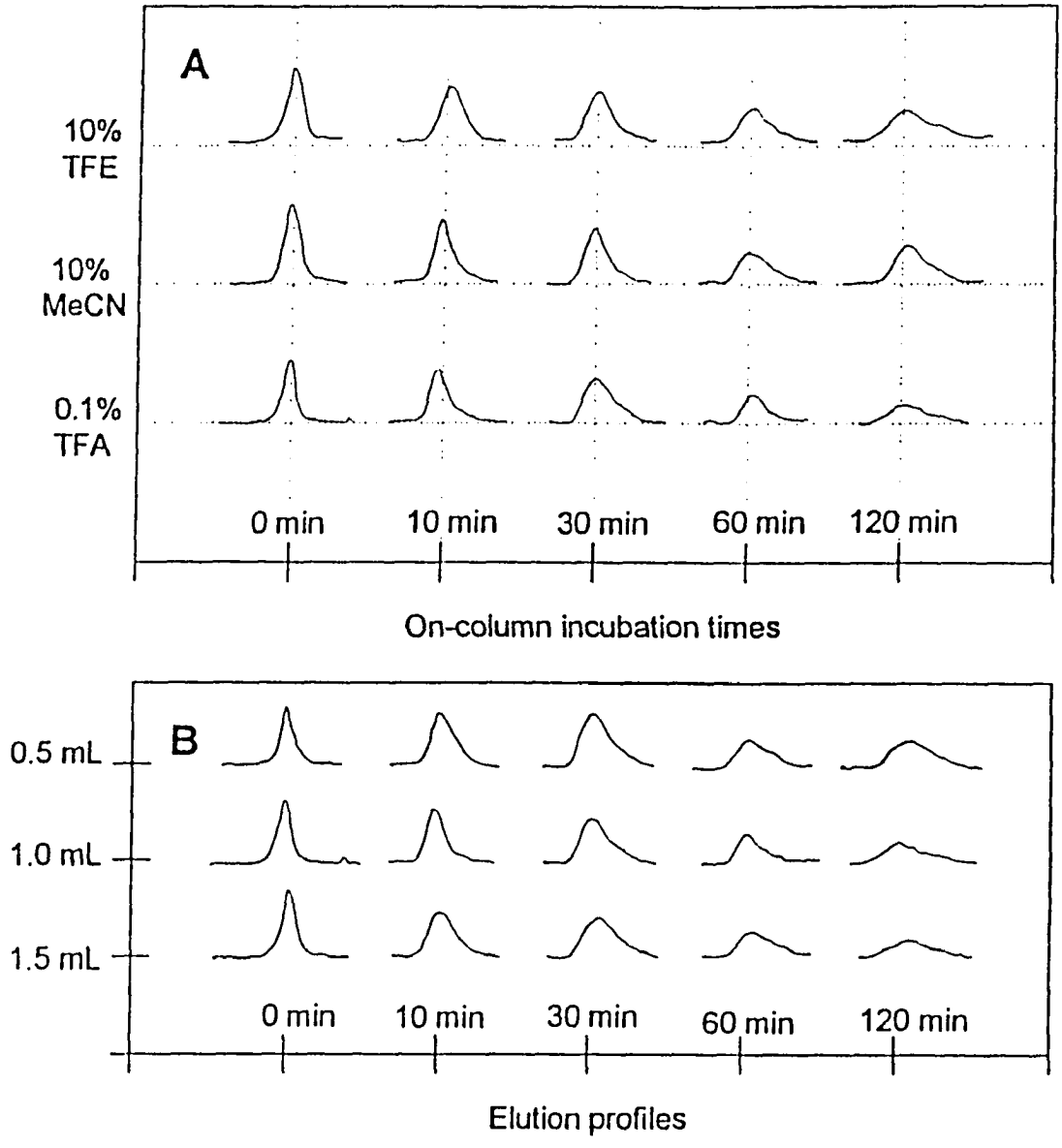

Fig. 3.10 Elution profiles of ß1-40 as a function of on-column incubation and organic modifier. Panel A gives the chromatographic profiles on the reversed-phase column, Vydac C_{18} as per gradient conditions as per Fig. 3.1*(a)* - *(d)*. Panel B gives the elution profiles for the flow rate dependency of ß1-40 using solvent A as 0.1% TFA in 10% MeCN with a gradient from 0-100% B in 60 min.

3.3.2. Rate Constants of Bandwidth Increase for ß1-40 During RP-HPLC

According to the linear solvent strength theory, the retention time and bandwidth from gradient elution data correlate well with changes in the same parameters derived from isocratic elution after adjustments of the experimental variables. However, the experimental gradient elution data for ß1-40 indicated that several mechanisms could influence its chromatographic behavior. To determine the rate of band broadening during the imposed chromatographic conditions, the elution volumes were compared. The elution volumes for the test conditions were normalized to the elution volume for ß1-40 obtained under *normal* gradient condition. The mass recoveries from all chromatographic conditions were high and ranged between 60 to 85 per cent based on peptide assay and quantitative amino acid analyses.

For zero incubation time, the amount of *native* peak eluted is given by

$$V_n = Ne^{-k^* tG} \qquad (1)$$

where

V_n = elution volume of *native* peak in *normal* gradient conditions,

N = amount of peptide applied to the column,

t_G = time from injection until elution (elution time), and

k^* = average rate constant for the various conditions involved in the gradient.

In a normal chromatographic run, given by the schematic in Fig. 3.1*(a)*, where the gradient is started when peptide is applied to the column, k^*t_G is constant. However, for the on-column incubation experiments, given by Fig. 3.1*(b)* where the gradient is started after the appropriate incubation time, t, an additional first-order kinetic expression can be written as

$$V_i = N_i \, e^{-kt} \tag{2}$$

where

V_i = elution volume in experimental condition,

N_i = amount of injected material,

k = rate constant, and

t = on-column incubation time.

The normalized elution volume, V, which reflects the band broadening, is then given as the quotient of elution volumes obtained using equations 1 and 2, which is

$$V = a \, e^{-kt} e^{-k^* tG} \tag{3}$$

which after rearrangement, simplifies to

$$\ln V = (\ln a - k^* t_G) - k \cdot t \tag{4}$$

Equation 4 is of the form $y = mx + c$, with the term in parentheses being a constant for a given setup. Assuming that the injected material was kept constant, a plot of ln *V versus t* will yield *k*, the rate constant for band broadening of ß1-40 on the reversed-phase matrix for a given gradient and temperature condition. The amount of peptide injected was kept between 20 to 30 µg for each chromatographic run, with the injection size varying between 10 to 20 µL depending on the concentration. There is, however, the discrepancy in determining the exact value of k^*, since any deviations in chromatographic behavior occurring prior to incubation time and zero time will affect the elution volume of *native* peak, and will reflect in the k^* term. Nevertheless, the rate constant for the band broadening on the stationary phase can still be determined as *k*.

Fig. 3.11 gives the band broadening data as a function of on-column incubation times at various column temperatures. The kinetic plots according to equation 4 are linear at the temperatures studied (20° to 45°C) within the range of incubation times from 0 to 60 min, as would be expected for a first-order phenomenon. Each data point represents the mean of three observations. Using least-squares analysis, the first-order rate constant for the bandwidth kinetics at each temperature and for each solvent system was determined for ß1-40. These are summarized in Table 3.1. The rate constants for band broadening based on elution volumes were reproducible within ±5%.

It is noteworthy that as the MeCN concentration was increased, the rate of broadening was decreased. Also, at low column temperatures the *native* ß1-40 content was low, which is reflected in the increased slope in Fig. 3.11. From Table 3.1, it is also apparent that to achieve similar elution volumes when no organic modifier is present in solvent A, the column temperature must be increased. From the observed data, the half-life of the band broadening rate for ß1-40 was calculated to be *ca.* 25 min. Similar study with ß8-40 yielded the half-life of bandwidth increase to be *ca.* 17 min. Earlier in this chapter, it was observed that the chromatographic contact area of ß1-40 was not significantly changed after 60°C. In light of the data shown above, this would indicate that below 60°C, the bandwidth behavior of ß1-40 under given chromatographic conditions appears to be consistent with a first order kinetic model for gradient elution derived from approximations from the theoretical treatment from linear solvent strength concepts. Nevertheless, this model should be able to distinguish and differentiate different band broadening phenomena. These facets can be inspected from comparisons between peak capacity and separation variables or from experimental and theoretical bandwidths.

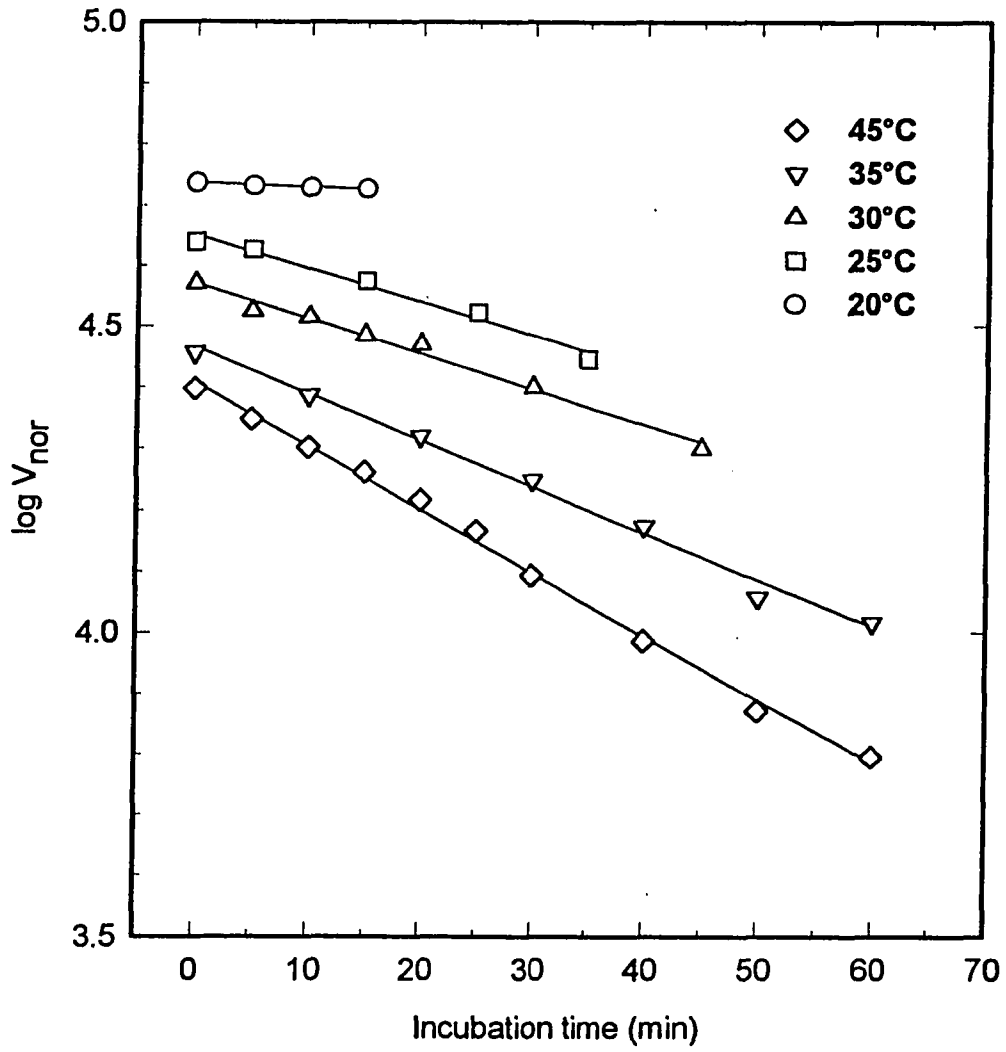

Fig. 3.11 First-order kinetic plots of rate constant of band broadening of ß1-40 on varying column temperatures as function of on-column incubation time, *t*. The data points are the log of mean of at least two elution volumes normalized on the elution volume of ß1-40 obtained under *normal* gradient conditions. The lines are the fits for best-curve analysis for the observed data as per equation 4.

Table 3.1

Rate Constants for Observed Band Broadening for ß1-40 on Octadecyl Surface

Incubation solvent	k (10^{-5} sec^{-1}) at column temperature (°C)			
	20	25	30	45
0.1% TFA (pH 2.5)	67	61	45	19
0.1% TFA in 4% MeCN	48	42	29	05
0.1% TFA in 8% MeCN	32	21	15	n.d.
0.1% TFA in 12% MeCN	12	10	4	n.d.
0.1% TFA in 20% MeCN	02	03	n.d.	---

n.d. not determined

3.3.3. Bandwidth Relationships

The band broadening phenomena can be further discerned through analysis of experimental and calculated peak capacity data. The average resolution of eluants has been defined in terms of peak capacity (*PC*) by Stadalius et al. (1985), in terms of the number of peaks that can be accommodated in a chromatogram having time t_G with a uniform resolution for all peaks by

$$PC = t_G \cdot F / 4\sigma_v \qquad (5)$$

where σ_v is the bandwidth measured in volume units within 1 standard deviation. The influence of flow rate on the peak capacity for a constant gradient time of 60 min is shown in Fig. 3.12. The *PC* increased to a maximum at a particular flow rate for each peptide and subsequently decreased. The observed *PC* for each group of peptides was essentially the same. These results further stressed the inescapable conclusion that the *PC* for each peptide was far from optimal at both low and high flow rates. It was also very clear that the peak capacity for each peptide was distinct.

These results strongly suggest that the band broadening process within the reversed-phase matrix cannot be strictly described by kinetic models for solutes behaving as rigid moieties during its passage through the column. Indeed, even though the peptides were bound as monomers on the stationary phase surface as demonstrated in earlier sections, the combined effect of the

length of the peptide and the amino acid sequence is considerable. The influence of flow rates on peak capacities has also been observed in other polypeptides of varying sizes; in thyrotropin-releasing hormone, bradykinin, neurotensin and somatostatin by Stadalius et al. (1984), in bovine trypsin by Hearn et al. (1985), in luteinizing hormone-releasing hormone and growth hormone releasing factor by Hearn and Aguilar (1986) and in myosin related peptides by Hearn and Aguilar (1987). It therefore reflects on the similarities, or dissimilarities, of the retention phenomena for a series of peptide analogs when they are introduced on a hydrophobic surface. It can therefore be considered that the *PC versus F* plots can be used to derive conditions not only for resolutions of peptides *per se*, but also to delineate the retention and kinetic behavior with mechanisms of interactions between the solute and the stationary phase surface.

3.3.4. Resolving a Typical Mixture of Synthesis-fragments

The difference in rates of band broadening was used to separate a mixture of synthesis-fragments, ß26-40 and ß8-40, during chromatographic purification of ß1-40. The retention times for ß1-40 and ß8-40 (Fig. 3.2) as well as the peak capacities were close (Fig. 3.12) for satisfactory resolution of the peptide mixture. The implications of the residence time of the peptides in the

band broadening is that if the mechanism is fast compared to the phase equilibration of peptides on the column matrix, the gradients given by Fig. 3.1*(e)* or *(f)* must lead to identical elution profiles for ß1-40 and ß8-40. Two parameters are simultaneously varied in these examinations, the mobile phase into which the peptide is injected and the contact time with the stationary phase surface.

Fig. 3.13 illustrates the elution profiles of a mixture of ß1-40 and ß8-40 from a typical analytical run obtained under normal gradient conditions (panel A), and when the injection was done *after* the start of the gradient as per conditions in Fig. 3.1 *(e)* or *(f)*. It was difficult to judge the homogeneity of the peptides from the elution profile as illustrated in panel A; however, a closer scrutiny of the eluting fractions was undertaken. The characterization of the fractions based on amino acid and sequence analyses is given in Table 3.2. It was discerned that the major peak actually consisted of ß8-40 and ß1-40. There was considerable resolution of the major peak when the peptide mixture was subjected to the experimental gradient as depicted by the profile in panel B. The different band broadening rates for ß1-40 and ß8-40 (section 3.3.2) were therefore successfully used for resolving a mixture of these peptides.

3.3.5. Effects of Extrinsic Factors

The overall process of polypeptide retention under reversed-phase conditions can be given as a cumulative effect of three separate events, viz., protein solvation in the bulk mobile phase, hydrocarbon ligand solvation by the bulk mobile phase components and interaction of the solvated solute with the solvated reversed-phase surface. For a thorough understanding of peptide retention behavior during RP-HPLC, it is not sufficient to demonstrate the effect of various intrinsic factors like nearest neighbor or peptide chain length on interactive behavior under various chromatographic conditions; it is also necessary to evaluate how the solvation of the peptide influences its residence on the stationary phase surface.

The observed change in elution characteristics of ß1-40 and derived analogs on reversed-phase chromatography was shown to manifest as a major change in chromatographic performance. Most often, these changes lead to loss of recovered peptide, which in this study was comparatively high, ranging between 15 and 40% of the injected mass. However, in some cases, a complete retention of the solute has been reported with increase in the ionic strength of the mobile phase, for *e.g.*, α-chymotrypsinogen (Cohen et al., 1984). The band broadening phenomenon has also been associated with microheterogeneity and aggregation (Kerlavage et al., 1983; Hearn and Grego, 1984). In the following section, the retention of ß1-40 and derived analogs was followed after individually introducing them on the reversed-phase matrix and the elution

profiles of peptide mixtures were plotted to study the effects of induced microheterogeneity.

Ionic Strength Effects on Retention Times and Recovery of Peptides

The popular use of TFA in reversed-phase chromatography is due to its high volatility - advantageous during recovery of peptide via lyophilization, and its extreme effectiveness in suppressing non-specific interactions of the peptide solute with the stationary phase support (Mant and Hodges, 1987). RP-HPLC studies of ß1-40 and derived analogs were performed on *n*-alkyl bonded silica with a low-pH water-acetonitrile eluant, where the acidic side chains of Glu and Asp are expected to be partially ionized. *In lieu* of non-ideal behavior, the interaction with the stationary phase support would be primarily from the carboxy terminal residues 29 to 40, all of which are hydrophobic. To scrutinize the role of the column matrix with respect to non-specific interactions with the solute, the mobile phase was loaded with increasing amounts of salt and the mass of peptide recovered was measured from the C_4 and C_{18} matrices.

Fig. 3.14 summarizes the change in retention times as a function of increasing ionic strength of the mobile phase when compared with normal gradient. It is evident that there was no significant variation in the retention of ß26-40 and ß22-35(M), however, the slight increase in retention of ß1-40, ß8-40, ß1-28, ß6-25 and ß15-28 on both, the C_4 and C_{18} columns implied an increase in their hydrophobic interaction. More striking is the dramatic effect the change

in elution volumes had on the recovery of the same molar quantity of the peptides as illustrated in panel C. There was at least a 33% reduction for ß1-28, with equimolar recovery of ß1-40 accompanied by a 50% reduction in the elution volume. These results indicate that the bandwidths were considerably narrower when increasing ionic strength to μ = 0.200 than those obtained under *normal* chromatographic conditions.

Exogenous Peptides

Investigation of the interaction of ß26-40 and ß8-40 with ß1-40 was undertaken with the express aim to explore the interaction of these carboxyl terminal variants in the presence of the hydrophobic stationary phase and in solution. A mixture of these peptides was allowed to incubate in solution for a given length of time, and this incubated mixture was loaded on the column and elution performed using normal gradient.

Incubation in Solution: ß1-40 with ß26-40 and ß8-40

Incubations of ß1-40 with ß26-40, and with ß8-40 at ambient temperatures were loaded as their solutions on the Vydac C_{18} column under normal gradient conditions. The elution profiles for solutions having a 9:1 mole ratio of ß1-40 and ß26-40, and a 1:1 mole ratio with ß8-40 which were incubated for 48 h are shown in Fig. 3.15. When comparing the profiles with pure peptides (profile **c**), it is evident that extraneous chromatographic peaks were generated.

The elution profiles obtained on reinjection of the individual components are shown in Fig. 3.16. Reinjection of **a(1)** yielded only a single component with retention time and peak profile for ß26-40, while **a(2)** emerged as a mixture of ß26-40 and ß1-40 within the chromatographic parameters. The reinjections of **a(3)** and **a(4)** yielded pure ß1-40, whereas the reinjection of **a(5)** indicated a component for which the peak identification did not match for either ß26-40 or ß1-40. Similar results were obtained for the reinjection of incubated ß1-40 and ß8-40 (**Fig.** 3.15, panel B). These chromatograms demonstrate that the microheterogeneity increased at the expense of the pure peptides. Subsequently, all the components were characterized by sequence and quantitative amino acid analyses which are summarized in Table 3.3.

Based on these analyses, it was of interest to note that the extraneous peptide components could be identified as a distinct mixture of pure peptides, hetero-oligomers. In conjunction with the chromatograms, these analyses indicate that the pure peptides were independently converted to oligomeric peptides which were meta-stable within the chromatographic environment. This was a very important finding, since this chromatographic strategy was employed to stabilize these hetero-oligomers and study their formation over time.

Kinetic Studies: ß26-40 with ß1-40 and ß8-40

The generation of the major microheterogeneous product formed on incubation of the relatively hydrophobic carboxy terminal peptide, ß26-40, with ß1-40 and ß8-40 was followed over time. Addition of ß26-40 solution to ß1-40 in a 1:99 to 1:9 mole ratio, based on quantitative amino acid analyses, was studied for 168 h. These mixtures were sonicated briefly immediately after preparation and the incubations were performed at ambient temperatures. At the end of the test period, periodic aliquots were drawn, centrifuged, and the supernatant was loaded directly on the column.

The mass of the eluting hetero-oligomeric component was measured was normalized on the peak areas for pure peptides for the same mole ratio. The kinetic data are given in Fig. 3.17. In order to verify that the observed elution behavior concurred with the process of oligomerization of ß1-40 and ß26-40, the data given in Fig. 3.17 were fitted into an integrated equation for irreversible association kinetic model of the form $M_1 + M_2 \rightarrow O_{12}$, where M signifies the monomer and O the oligomer:

$$\ln [O_{12}] = \ln [O_{12}]_0 - k_1 \cdot t \qquad (9)$$

where

$[O_{12}]_0$ is the oligomer concentration at zero time,

$[O_{12}]$ is the oligomer concentration at any time t, and

k_1 is the rate constant for oligomer formation in solution.

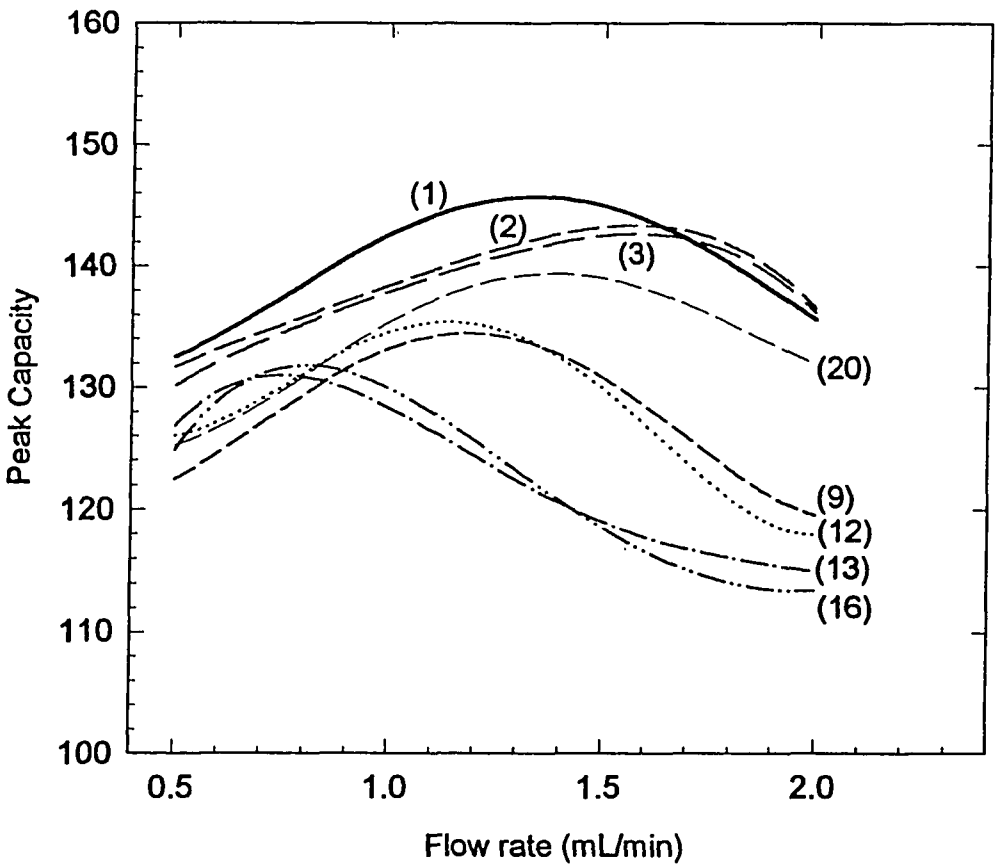

Fig. 3.12 Plot of peak capacity as a function of flow rate for ß1-40 and derived analogs at a constant gradient time of 60 min. The flow rates employed were 0.5, 0.8, 1.0, 1.25, 1.50 and 2.0 mL/min; data points have been excluded for clarity. The numbers in brackets denote ß1-40 and derived analogs according to the designation given in Table 2.3: ß1-40 (1), [Arg^{13}]ß1-40 (2), [Arg^{14}]ß1-40 (3), ß1-28 (9), [Arg^{13}]ß1-28 (12), ß-26 (13), [$Arg^{13,14}$]ß6-26 (16), and ß8-40 (20).

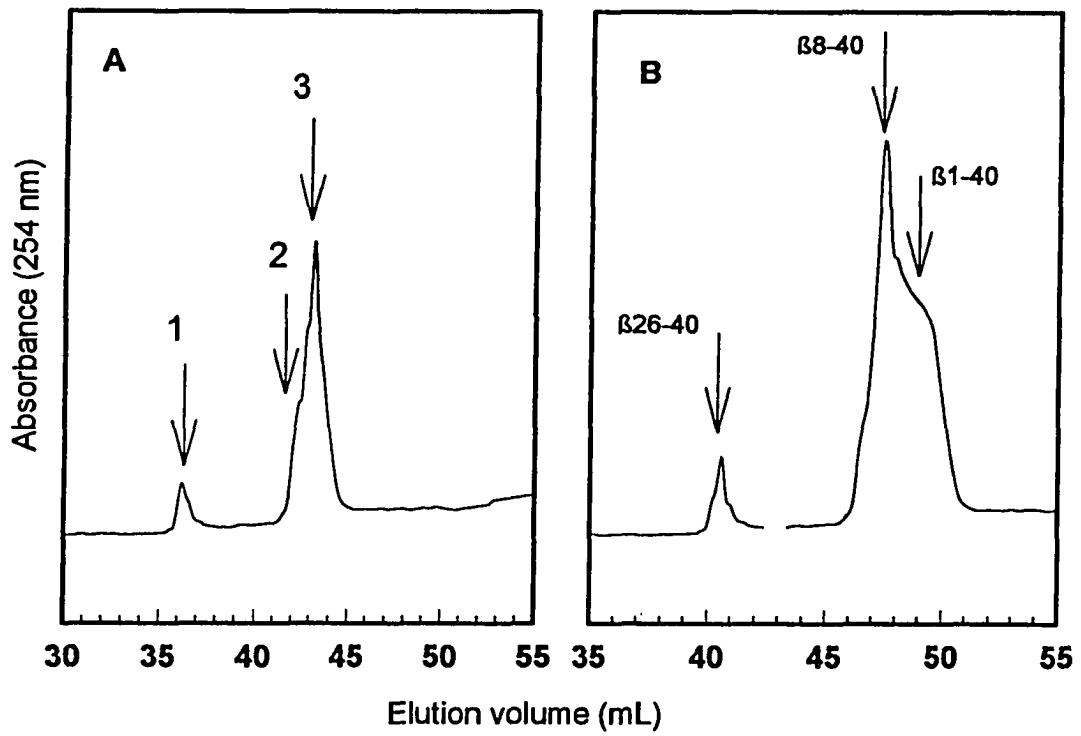

Fig. 3.13 Resolution of synthesis-fragments ß26-40 and ß8-40 from a typical ß1-40 synthesis. The elution profile in panel A was generated at room temperature using Vydac C_{18} operated under *normal* gradient conditions at room temperature and a flow rate of 1 mL/min. Panel B shows the resolution of the broad more hydrophobic fraction during gradient elution using solvent A as 0.1% TFA in 17.5% MeCN and 0.1% TFA in 100% MeCN as solvent B; the column was operated at 30°C, using a flow rate of 1.5 mL/min. The gradient was established as follows: 0% B for 5 min and then 0-100%B in 30 min. The peptide solution was injected exactly 15 min after the start of the run as per conditions given in Fig. 3.1*(f)*. The numbers denote the fractions which were characterized by sequencing and amino acid analysis.

Table 3.2

Sequence and Amino Acid Analysis of "Impure" ß1-40 Synthesis

Fraction	Predicted sequence	Composition and sequence observed
1	ß26-40	NKGAIIGLXVGGVV
2	ß8-40	XGYXVHHQKLVFFAEDVG...
3	ß1-40	DAEFRHDSGYEVHHQKLVFFAEDVG...

X denotes poor identification during sequencing and less than 20 mole% of that residue on quantitative amino acid analyses.
The underlined italics denote the repetitive yield was less than 55 mole % for that cycle. When a known sequence was obtained for more than six residues with a good repetitive yields, sequencing was not taken further, and this is denoted by "...".

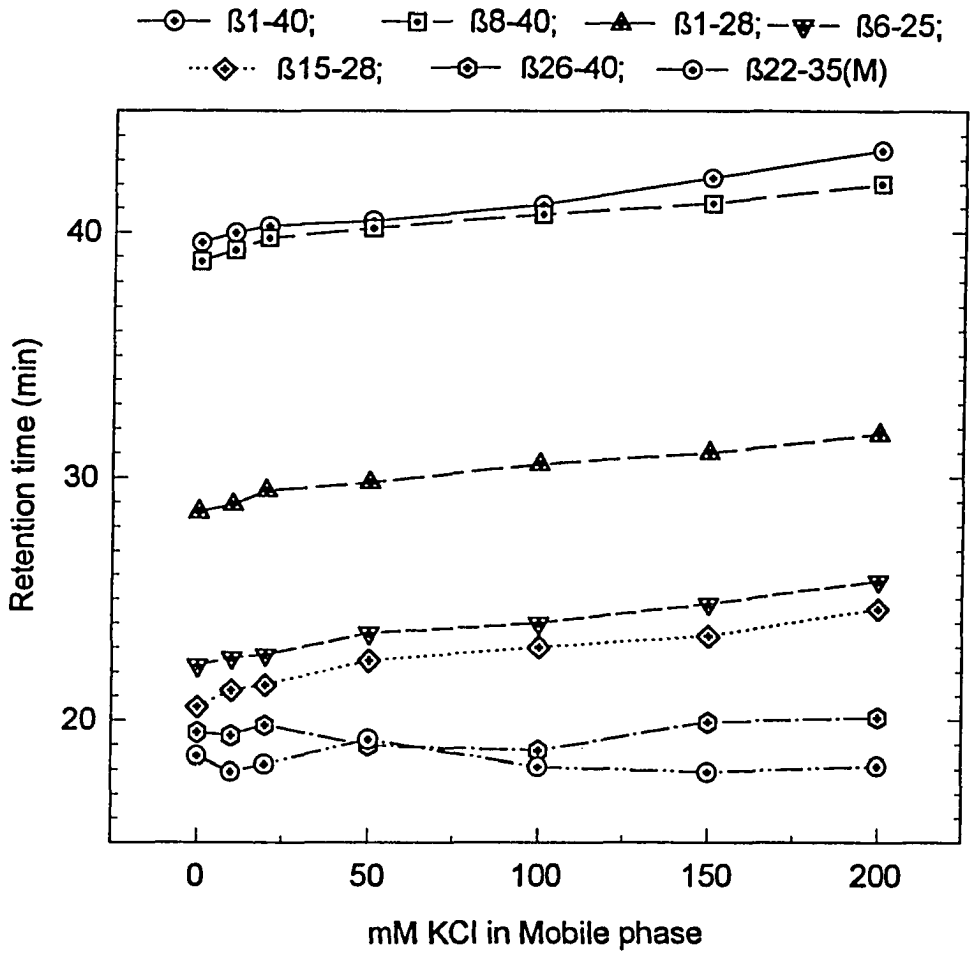

Fig. 3.14 Plot of elution behavior as a function of mobile phase ionic strength, μ, for ß1-40 and derived analogs on reversed-phase column C_8. The data points represent retention times using normal gradient with ionic strength variations from, μ = 10 to 200 mmol/L KCl in solvents A and B containing 0.1% TFA in 20% MeCN, and 0.1% TFA in 80% MeCN respectively. The flow rate of 0.8 mL/min.

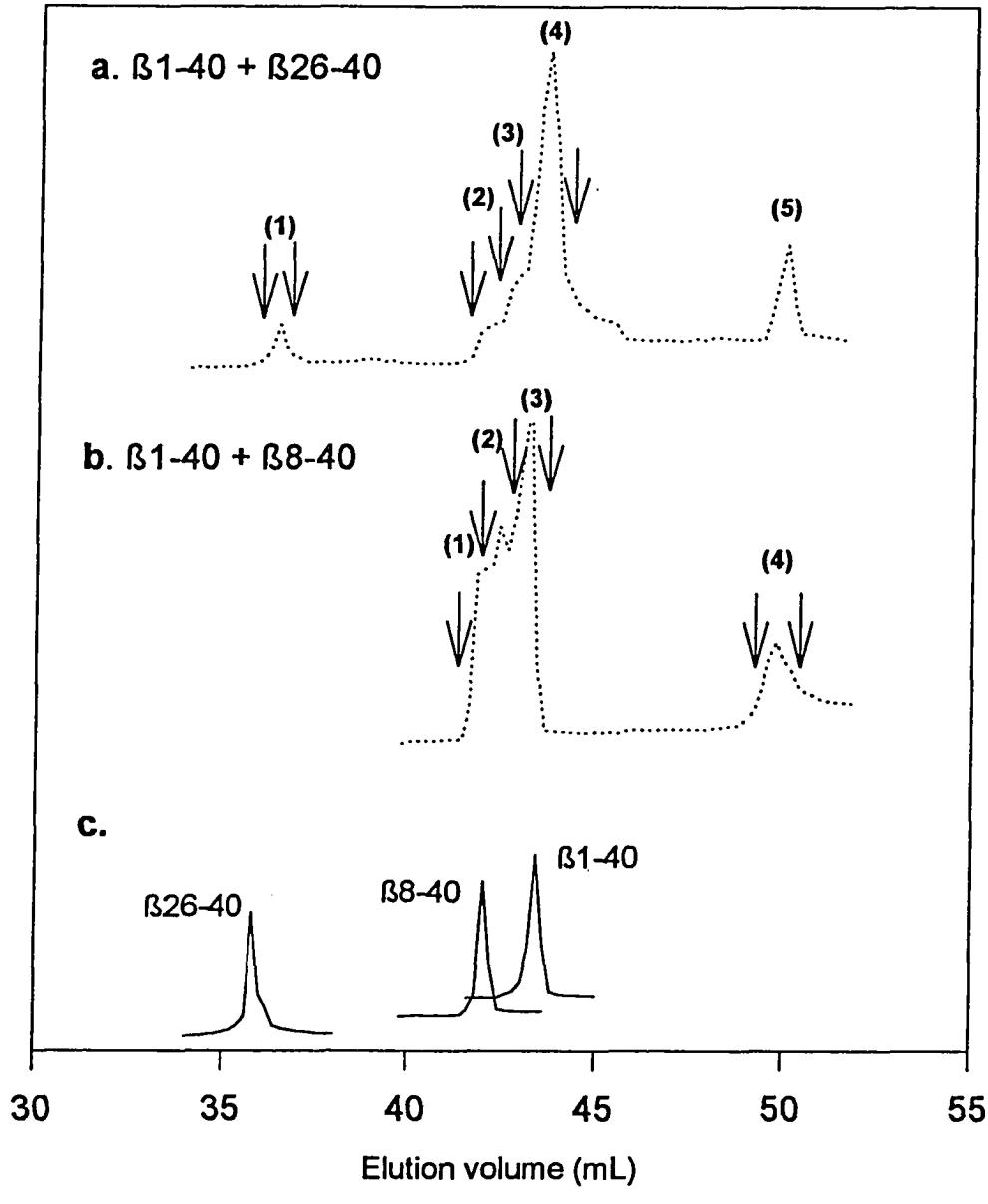

Fig. 3.15 RP-HPLC behavior of incubating equimolar ß1-40 with ß26-40, and with ß8-40 in-solution on Vydac C_{18}. The elution profiles for the ß1-40 incubation with ß26-40 (a), with ß8-40 (b), and the pure peptides (c) were obtained using normal gradient conditions. The arrows indicate the corresponding fractions were analyzed by quantitative amino acid and Edman sequencing of the numbered components (Table 3.3). The concentration of ß1-40 was maintained at 200 µM and solutions were stood at room temperature with intermittent sonication.

Table 3.3

Sequence and Amino acid Analyses of ß1-40 Incubations with ß8-40 and ß26-40

Fraction	Predicted sequence	Composition and sequence observed
a(1)	ß26-40	*N*KGAIIGLXVGGVV
a(2)	ß8-40	XGYEV*H*HQ...
a(3)	none	(i) *D*AEFRHDSGY... (ii) GYXVXXQKLVFF...
a(4)	ß1-40	*D*AEF*RH*DSGY...
a(5)	none	(i) *D*AEF*R*HDSGY... (ii) XX*G*AIIGLXVGGVV
b(1)	ß8-40	*G*YEV*HH*QQKLVFF...
b(2)	none	*D*AEFRHDXGY...
b(3)	ß1-40	*D*AEFR*H*D...
b(4)	none	(i) XGYEVHHQ... (ii) DAEFR*H*DXGY...

X denotes poor identification during sequencing and less than 20 mole% of that residue on quantitative amino acid analyses.
The underlined italics denote the repetitive yield was less than 75 mole % for that cycle. When satisfactory repetitive yields were obtained for six or more cycles for a know sequence, sequencing was not taken further and is denoted by "...".

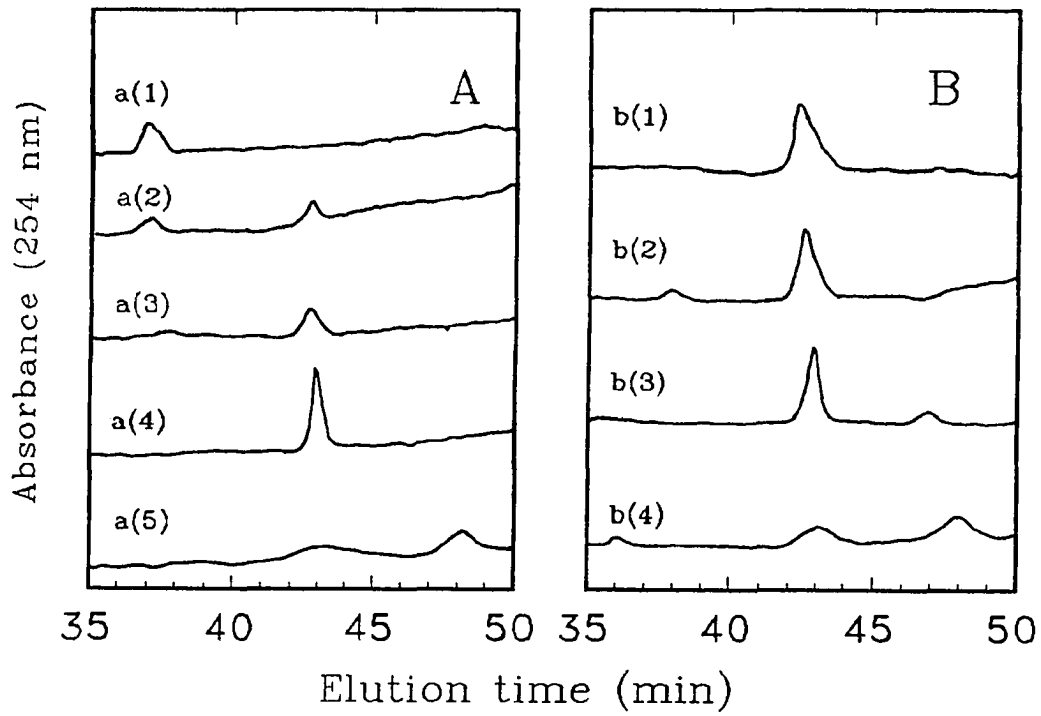

Fig. 3.16 RP-HPLC profiles of the pooled fractions of ß1-40 incubation with ß26-40 and ß8-40. The numbers on the chromatograms indicate the pooled fractions from the ß1-40 and ß26-40 (panel A) and ß1-40 and ß8-40 (panel B) incubations given in Fig. 3.15

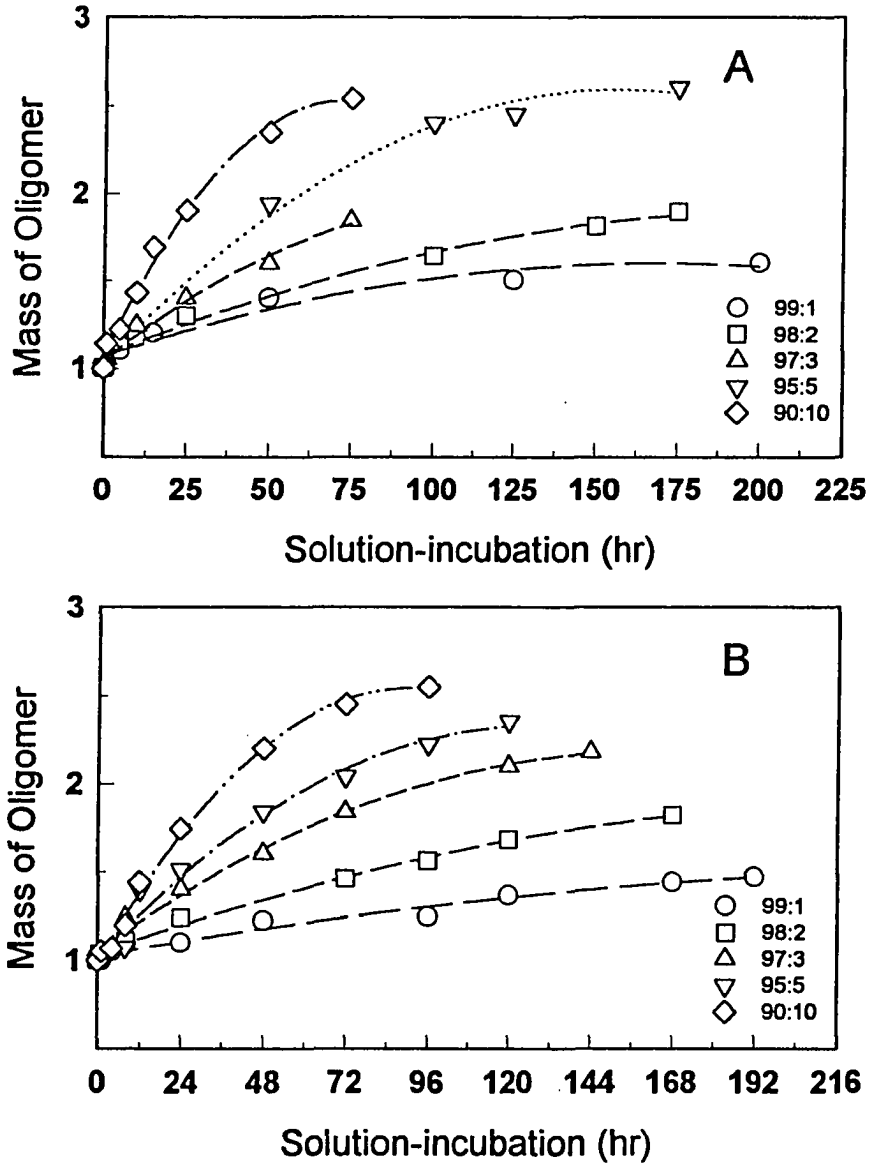

Fig. 3.17 Kinetic profiles for solution-incubation of ß26-40 with ß8-40 (A) and ß1-40 (B) over 168 hours expressed as normalized mass of the heterogenous product. The mass were determined by on the basis of peak areas obtained for pure peptides injected at the same mole ratio. The lines are fits to data according to equation 9. Each data point represents the mean mass from three chromatograms.

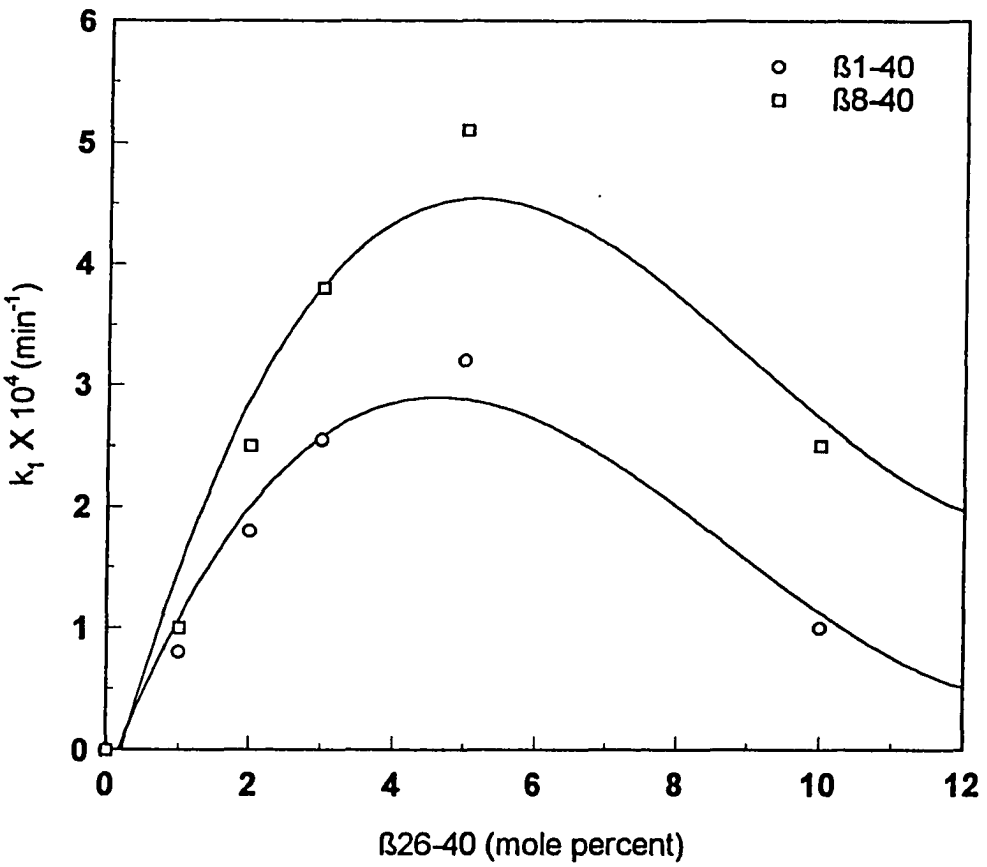

Fig. 3.18 The rate constant dependence of RP-HPLC-determined association of ß26-40 with ß1-40 and ß8-40. The data points represent the rate constant of oligomer formation on incubating ß26-40 with ß1-40 and ß8-40 derived from the mathematical fits to chromatographic mass given in Fig. 3.17.

The rate constants for this oligomerization were found for mole ratios between 0:100 and 1:9 ß26-40:ß1-40 and are shown as a function of ß26-40 in Fig. 3.18. It was difficult to increase the concentration of ß26-40 in aqueous solution beyond 10 mole% because of its insolubility. When the rate constants were plotted as the function of mole fraction of ß26-40, a bell-shaped behavior was found with the inflexion at 5 mole% of ß26-40.

3.4. Discussion

As is customary with all solutes undergoing slow dynamic interconversion under regulated chromatographic conditions, the arduous path of a polypeptide is replete with phenomena not experienced by rigid molecules. The intent of this study was to delineate the secondary structural components of ß1-40 by studying its interactive behavior on reversed-phase matrices. In this study, 0.1% TFA in MeCN gradient system popularly used in the RP-HPLC of peptides and proteins caused ß1-40 and derived analogs to interact in their monomeric form with the *n*-alkyl bonded surfaces. The retention times followed a log linear relationship in the presence of TFE, as with MeCN, which strongly suggested that the peptides were monomeric helices in the presence of TFE. In the absence of a solid hydrophobic surface, the amino terminal sequence

Asp^{1}–Val^{12} sequence has a higher propensity for α-helix formation in TFE solutions (Hollosi et al., 1989; Barrow and Zagorski, 1991; Sorimachi and Craik, 1994); however, in MeCN, the AßP variants exist predominantly as ß-pleated sheets (Fabian et al., 1993; Otvos et al., 1993), *i.e.*, although ß1-40 can adopt an α-helical structure in helix inducing solvents, the helical structure is destabilized in the presence of MeCN. Perhaps, the hydrophobic stationary phase sorbent induces helix formation in these peptides, and more so on the simultaneous substitutions of His → Arg at positions 13, 14 and L-Asp → D-Asp at 1, 7, 23 respectively. Studies correlating structural effects of model peptides forming amphipathic α-helices on hydrophobic surfaces have also been made by other chromatographers (Zhou et al., 1990; Blondelle and Houghten, 1992; Aguilar et al., 1993). This would explain the observed chromatographic behavior of ß1-40 and derived analogs on the reversed-phase surfaces.

However, the denaturant conditions of reversed-phase liquid chromatography did not prevent the secondary equilibria which were established by these peptides. The magnitude of the chromatographic area of ß1-40 and the His → Arg and L-Asp → D-Asp derived analogs was dependent on the organic modifier, which suggested that the interactive behavior with the stationary phase surface was sensitive to the position of substitution. Obviously, the His → Arg and L-Asp → D-Asp substitutions in ß1-40, ß1-28 and ß6-25 significantly increased the chromatographic contact region. However, the increased contact area was severely affected by temperature, and the thermal transitions were

associated with a resultant decrease in the predisposition of the peptide for the hydrocarbonaceous ligands. The phenomenon of competing equilibria is however not unique to ß1-40, but has been observed in many proteins and model peptides of various lengths (Hearn and Grego, 1984; Hearn et al., 1985; Hearn and Aguilar, 1986a; 1986b; 1987). The consensus among chromatographers is that changes in interaction of polypeptides with the stationary phase during RP-HPLC results in changes in chromatographic parameters of these solutes, leading to retention time changes and band broadening (Benedek et al., 1984; Hearn and Grego, 1984; Hearn and Aguilar, 1987). The observed data indicates the extent of secondary structure changes which can be induced by the stationary phase, and the importance of the immobilized hydrocarbon ligand on the interactive process. It appears that the increase in chromatographic contact area and the subsequent decrease in the affinity of the comparatively larger ß1-40 and ß8-40 peptides for the stationary phase surface are directly related to significant changes in conformation of these peptides. Based on the observed chromatographic parameters between the His → Arg and the L-Asp → D-Asp analogs, it would be safe to assume that the stationary phase surface has the potential to perceive changes in the amino acid side chains.

The rates of band broadening in ß1-40 and ß8-40 within the imposed parameters differed on the chromatographic time scale. Although it was not proven by the approach employed in this study, the role of the amino terminal

was evident due to the difference in the half-life of bandwidth increase for these two peptides. Within the chromatographic elution time, a change in orientation due to the interaction with the stationary phase surface ligands, or due to mobile phase polarity can destabilize the native conformation; the subsequent folding/unfolding of the peptide backbone can cause a change in the interactive behavior. The resolution of the mixture of ß1-40 and ß8-40 was, however, optimized by using the chromatographic bandwidth rates as a determinant to yield the pure peptides. The inherent tendency of ß1-40 to elute as a broad component on reversed-phase liquid chromatography observed in other laboratories is therefore understandable in light of the data observed here.

It is worth noting that the hydrophobic matrix was instrumental in dictating the elution behavior of co-incubated peptide mixtures. The chromatographic approach of determining the rate constant for the oligomerization of two fragments of the parent Alzheimer ß-protein, viz., ß1-40 and ß26-40, employed an approach which is unique for this field. The bell-shaped behavior indicated a barrier for the process of oligomerization. The presence of a small amount of peptide ß26-40 may lower this barrier and shift the equilibrium toward the oligomer concentration. At least 5 mole% of ß26-40 was needed to observe hetero-oligomers which were chromatographically resolvable. The rate constant for the association (oligomerization) of ß1-40 and ß26-40 indicated that at a low ß26-40:ß1-40 ratio, the association of monomers was a slow step. This point was seen clearly when the incubation times were

long (> 168 h); the oligomers were formed entirely at the expense of the respective monomers. The increased turbidity of ß26-40 solutions after 12 h has previously been reported (Jarrett et al., 1993). Although the turbidity measurements did not indicate hetero-oligomers, the importance of the carboxy terminal in amyloid formation was emphasized. Also, strong hydrophobic interactions between core helices coupled with weaker hydrogen-bonding interactions between ß-pleated sheets have been proposed to be responsible for the deposits in systemic amyloidosis (Turnell et al., 1986). From the elution profiles of co-incubated ß26-40 and ß1-40 and the subsequent amino acid and sequence analyses, it would therefore seem that these are meta-stable hetero-oligomers. The resolution of oligomers of ß26-40 with ß1-40 and ß8-40 using the chromatographic approach proves that it is possible that 5 mole% ß26-40 would be sufficient to obtain hetero-oligomers, which could act as nucleating sites for aggregation.

Although the approach used in this examination of chromatographic structure may not be identical to the biologically relevant "*receptor interacting structure*" of AßP, analogy with the hydrophobic membrane-interaction can be made. Based on examination of ß1-40 and derived analogs, reversed-phase high-performance liquid chromatography provides a potential probe for this structure of the peptides' interaction with membranes. It can be hypothesized that the hydrophobic interaction of these peptide solutes is maximized, primarily from (i) the hydrophobic carboxy segment ß26-40, and (ii)

due to secondary interaction from the cluster of hydrophobic residues –LVFFA– corresponding to residues Leu^{17}–Ala^{21}. The secondary equilibria established due to these interactions could then explain the observed chromatographic behavior of band broadening and retention. The correlation between these synthetic peptide analogs and their chromatographic performance thus provides yet another approach to understanding the relationships between peptide structure and function. The conformation of the individual peptides on the chromatographic surface might not be analogous to the "biologically relevant" structure interacting with the cell-receptor. Nonetheless, there is a potential to exploit their chromatographic behavior as an experimental approach to studying their structure-function relationships.

The gradient elution protocols used in evaluating the interactive behavior of ß1-40 and derived analogs have provided clues to the dynamic nature of these molecules in a denaturing environment. This study reiterates the necessity of examining the peptide in the presence of membrane-like matrices, so that a better direction to the underlying molecular phenomenon can be obtained. AßP is one of the amyloidogenic proteins, but if the interactions of the derived analogs with the reversed-phase surface are any indication, similar methodology could be employed to lock the meta-stable conformation(s) for therapeutic intervention before the curtain call of amyloid formation.

Chapter 4

Conformational Transitions of AßP - A Far UV/CD Spectroscopy Study

Introduction

The importance of knowing the structure of a protein or a peptide in relation to its function is central to understanding their biochemical mechanisms. The three-dimensional structure of a protein arises from its amino acid sequence, *i.e.*, its primary structure. In a general scheme of protein folding, the primary structure dictates the secondary structure(s), which leads to formation of tertiary, and eventually, quaternary structures. Secondary structures have a limited merit compared to the complete three-dimensional protein structure; nonetheless, their formation precede most events in protein folding (Kim et al., 1982; Ptitsyn, 1987; Kuwajima, 1989; Ptitsyn et al., 1990; Lustig and Fink, 1992).

High resolution techniques like solid state nuclear magnetic resonance (ss-NMR) spectroscopy and X-ray diffraction studies provide information on biomolecules in a solid state. Application of these techniques is however cumbersome and their relevance to the solution structure remains doubtful. In the case of AßP, moderately resolved X-ray diffraction and electron microscopy (Castano et al., 1986; Kirschner et al. 1986; Halverson et al., 1990; Kirschner et al., 1990; Fraser et al., 1991; Burdick et al., 1992) have provided crude information of its quaternary structure. Information on secondary structure of AßP is also gleaned from low resolution techniques, like Fourier transform infrared (FTIR) (Halverson et al., 1990, 1991; Fraser et al., 1992) and circular dichroism (CD) spectroscopy (Hollosi et al., 1989; Barrow and Zagorski, 1991; Hilbich et al., 1991; Barrow et al., 1992; Caputo et al., 1992; Fabian et al., 1993; Otvos et al., 1993). These techniques are sensitive to backbone conformation and of great practical use. ß1-40 is a dynamic molecule with an inherent propensity for reorientation of its backbone which is further enhanced by its environment. The studies on synthetic AßP peptides have provided information about the conditions favoring aggregation, like pH, salts, and membrane-mimicking environments (Barrow and Zagorski, 1991; Hilbich et al., 1991; Barrow et al., 1992; Jarrett and Lansbury, 1993; Come et al., 1993; Otvos et al., 1993). A mathematical model based on kinetic evidence from light scattering measurements indicates that an end-to-end association of ß1-40 molecules could result in gel formation (Tomski and Murphy, 1992). This phenomenon is

not in keeping with the process of oligomerization via intermolecular attraction to form antiparallel ß-pleated sheets. However, this model does not characterize the changes in the structural subdomains of β1-40 along the pathway to its final folded form.

The studies outlined in this chapter provide qualitative and quantitative data of the conformational changes of ß1-40 and its derived ß6-25 analog in aqueous solutions. The peptide backbone conformation was studied spectroscopically over time by its absorption in the far UV region using CD spectroscopy. Spectroscopically distinct transitions were detected and characterized in terms of relative transformations of the secondary structural components. This knowledge is of interest in structure-function studies, and is discussed in terms of the *in vitro* aggregation of ß1-40 and its derived analogs.

4.1. Secondary Structure via Far UV Amide Circular Dichroism

It is critical to know how tertiary or quaternary structure formation takes place; thus a comprehensive understanding of the folding of the peptide backbone necessitates obtaining information on its secondary structure organization. It is generally believed that small peptides (≈ 30 residues) are capable of adopting a variety of interconverting conformations in solution

(Blundell and Wood, 1982). This phenomenon however depends on a number of extrinsic determinants which include, but is not limited to, time, concentration, pH, solvent, and presence of other molecules in solution. It is now understood that the environment of the protein molecule is a significant determinant of secondary structure (Zhong and Johnson, 1992). AßP seems to possess smaller regions (subdomains) and exhibits different secondary structures that are dependent on the amino acid sequence (Hollosi et al., 1989) and pH (Fraser et al., 1991b). Although the CD spectra of AßP can be used to detect secondary structure transitions, deconvolution of the spectrum does not allow unambiguous assignment to specific residues in the peptides. CD studies on ß1-40 have demonstrated that conformational changes occur in solution as a function of concentration (Burdick et al., 1992; Tomski and Murphy, 1992; Otvos et al., 1993). The preferred conformation of ß1-40 in aqueous solutions is a ß-pleated sheet and depends on the degree of self-association (Hilbich et al., 1991). At higher concentrations, oligomerization has been suggested to lead to gel formation in synthetic peptides (Tomski and Murphy, 1992; Jarret and Lansbury, 1993; Zhang et al., 1993), a process for which the kinetics of backbone folding are not fully established. In this study, the use of ß1-40 and its derived analog, ß6-25, provide excellent models to elucidate the transformations of secondary structure during folding.

4.1.1. Secondary Structure Studies of ß1-40 and Derived Analogs in Aqueous Solutions

The peptide backbone, with its amide -CONH- chromophore, rotates the plane of polarized light. Circular dichroism is the measurement of the difference between absorption for left- and right-circularly polarized light; CD bands are generated at wavelengths where absorption takes place. These bands will be either positive or negative depending on the strength of absorbed light. The difference is generally reported in terms of molar ellipticity at a given wavelength, $[\theta]_{\lambda,}$ and is given as:

$$[\theta]_{\lambda} = 3298\ (\epsilon_L - \epsilon_R) = 3298\ \theta_{\lambda} / C \cdot l \cdot (M / 100) \qquad (1)$$

where

θ_{λ} is the raw ellipticity,

ϵ is the molar extinction coefficient, for left (L) and right (R) polarized light,

C is the concentration of peptide in g/mL,

l is the path length in cm,

M is the mean residue weight of peptide in daltons.

Circular dichroism spectroscopy in the far ultraviolet region (far UV/CD) is very sensitive to the secondary structure of the polypeptide backbone. For ß1-40, this sensitivity is highlighted in Fig. 4.1. The occurrence of various CD bands has been explained by Tinoco (1962) as functions of oscillating electro-

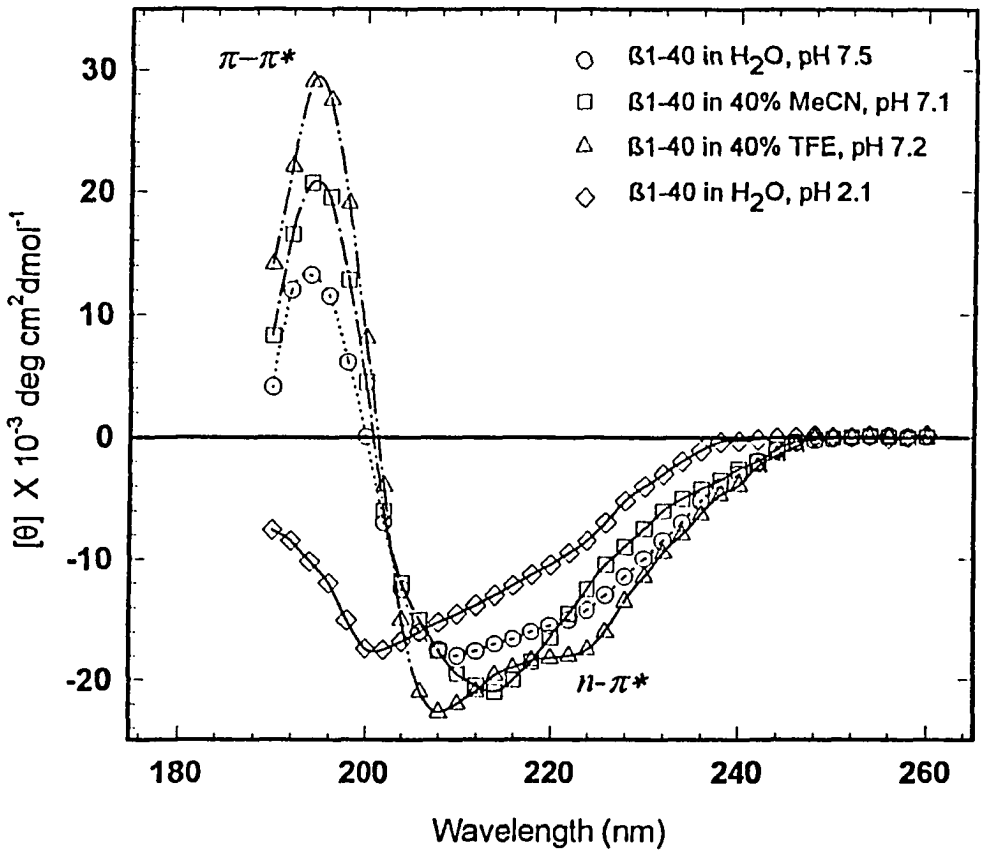

Fig. 4.1 Circular dichroism spectra of 250 μM synthetic ß1-40 in H_2O at pH 7.5, in 40% MeCN at pH 7.1 and 40% TFE at pH 7.2. A 50 mM HEPES buffer was used for preparing the solutions. The raw ellipticity was measured on a Jasco spectropolarimeter, J-720 at a scan rate of 1 nm/sec with an analog time constant of 1 sec and the data converted to molar ellipticity. The data are an average of four scans; no smoothing functions were applied. The ellipticities were calculated using a mean residue weight of 108.3 daltons. A cubic-spline algorithm was used to plot the CD curve. The occurrence of the excitation resonance transitions, n-π^* and π-π^*, are explained in the text.

magnetic vectors, electric transitions, and the dipole and rotational strengths characteristic of the peptide moiety. Additionally, polarity changes in the chromophore environment due to intrinsic and/or extrinsic factors cause shifts in intensities (Urry, 1985; Nicot and Waks, 1989). The CD study done on ß1-40 and its derived analogs is the core of this chapter and a brief review of the positions and intensities of the various CD bands in terms of its secondary structural components is in order.

For the amide chromophore containing only the *pure* optical properties of an α-helix, an n-π^* transition gives rise to a weak but broad band near 220 nm. This electronic absorption is assigned on the basis of transition energy, low absorbance and high rotational strength. There is another negative band near 208 nm, crossover to positive ellipticity takes place near 200 nm and a positive band near 190 nm (202 and 195 nm respectively in the case of ß1-40) which are due to excitation resonance interactions. The 220 nm band is polarized parallel to and the positive band near 190 nm is polarized perpendicular to the helical axis. A predominantly α-helical CD spectrum of ß1-40 is denoted by the hollow triangles in Fig. 4.1. For a mostly ß-pleated sheet structure, the band near 215 nm is assigned to the n-π^* transition, and the positive band near 195 nm due to the splitting of the π-π^* band which is due to excitation resonance interactions. In the case of ß-pleated sheets, a crossover to positive ellipticity usually takes place around 205 nm; in this study for aqueous ß1-40 solutions, the crossover was at 202 nm. There is also an occurrence of unordered or random structure

(type C-D, according to contemporary nomenclature) for ß1-40 solutions below pH 3. The prominent feature of this structural class is the negative band near 200 nm and no positive CD signal.

The positions of the respective positive and negative bands in the three different classes of secondary structures given in Fig. 4.1 are only valid for polypeptides that do not possess any interfering electronic transitions in the side chains. For most amino acids side chains, these transitions are below 190 nm, except for the aromatic functionalities of tryptophan, tyrosine and phenylalanine, and histidine and cysteine which appear around 280 nm. When CD is measured between 260 and 175 nm, this contribution is minimized. No CD signal was detected above 240 nm for ß1-40, indicating that the single tyrosine did not contribute to the ellipticity of ß1-40. ß1-40 exhibited mixed α-helical and ß-pleated sheet character in aqueous solution as depicted in Fig. 4.1. CD spectroscopy therefore, makes it easier to monitor changes in conformation of ß1-40 that result from changes in environmental parameters. The spectra also contrast well with the X-ray diffraction data on oriented fibrils of ß1-40 (Inouye et al., 1993), and with spectra from other laboratories (Barrow and Zagorski, 1991; Hilbich et al.,1991; Barrow et al., 1992; Exley et al., 1993; Otvos et al., 1993).

Analyses of secondary structural components from CD spectra

Mathematical deconvolution of the experimental CD spectra is undertaken to determine the secondary structural content in terms of α-helical (*H*), antiparallel (*A*) and parallel (*P*) ß-pleated sheets, ß-turns (*T*) and any other unordered (*O*) structures. The spectrum is then fit with a reference set of CD spectra of known secondary structures. The pioneering work by Greenfield and Fasman (1969) has set a trend for secondary structure estimation methods, and was later extended by Argos et al. (1978). The methods currently in vogue are (i) the variable selection method (Varselec) of Johnson and colleagues (1987), and (ii) those advocated by Fasman and coworkers (1991) *viz.*, the convex constraint analysis (CCA). The structural information provided by these methods, at least for the α-helical and ß-pleated sheets agrees with that obtained from the ellipticities at 220, 215 and 195 nm for the helices (Greenfield and Fasman, 1969), and at 215, 190 nm for the sheets (Sarkar and Doty, 1966).

The CD spectra were measured between 260 and 175 nm and were digitized every 2 nm for analyses using Varselec, and mathematically reduced to a wavelength interval of 1 nm between 240 and 195 nm for CCA. In cases where background absorbance was high, CD spectra were truncated when absorption exceeded 1.2 AU. The constraint placed on Varselec analyses was that the total secondary structure equals 100%. If *f* denotes the weighted fraction of each secondary structure *i*, then

$$\Sigma f_i = 1.0 \qquad (2)$$

Although both these mathematical analyses provide similar information for the five classes of secondary structures, the uncertainty in data varies with the structural classes. Data for α-helices and ß-pleated sheets are usually more reliable within experimental limits than the other classes. Equation 2 can be written in terms of five individual components

$$[\theta]_\lambda = f_H\theta_H(\lambda) + f_A\theta_A(\lambda) + f_P\theta_P(\lambda) + f_T\theta_T(\lambda) + f_O\theta_O(\lambda) \quad (3)$$

where

$[\theta]_\lambda$ is the molar ellipticity in $deg \cdot cm^2 \cdot dmol^{-1}$,

f is weighted fraction of the secondary structural component,

θ is the reference ellipticity, and

the subscripts *H*, *A*, *P*, *T*, and *O* denote the α-helical, antiparallel β-pleated sheet, parallel β-pleated sheet, β-turns, and unordered secondary strucutres respectively. This equation can be simplified to a three component analysis:

$$[\theta]_\lambda = f_\alpha r_\alpha(\lambda) + f_\beta r_\beta(\lambda) + f_o r_o(\lambda) \quad (4)$$

where f_α denotes the α-helical content, f_β denotes the fractional antiparallel and parallel ß-pleated sheet content, and f_o is the fraction of all other structures that are not α-helical or ß-pleated sheet. For simplicity of data treatment, the ß-turns (*T*) and other unordered structures (*O*) were grouped together as "other," (f_o), to perform a three component analysis. It is rational to include all the other

structural components into one spectral class since they are not defined as a ß-pleated sheet unfolds. Linear least-square fittings were then performed on data obtained from equation 4 using the criteria given in equation 2.

Assignments of secondary structural elements gleaned from a CD spectrum are based on empirical correlations with pure component spectra and/or theoretical calculations (Johnson, 1980; Provencher and Glöckner, 1981) using model and synthetic peptides (Chou and Fasman, 1977; Yang et al. 1986), globular proteins (Hennessey and Johnson, 1981), and pattern-recognizing algorithms (Kabsch and Sander, 1983). Contemporary methods using statistical procedures give high correlation coefficients compared to the X-ray structure of proteins. Varselec is one such method based on a sixteen protein database and gives correlation coefficients of 0.97, 0.76, 0.49 and 0.86 respectively for α-helix, ß-pleated sheet, ß-turn and other secondary structural elements (Manavalan and Johnson, 1987). Most often, reliable results are obtained using Varselec when the CD data are extended to 184 nm as the lower wavelength (Johnson, 1990). Obtaining such statistically significant secondary structural information is however, not always feasible due to practical limitations in achieving the low wavelength limit in a protein solution.

The decision of using reference proteins remains one of the uncertainties in analyzing CD spectra (Venyaminov et al., 1991). Besides, the low probability of finding proteins in which one or the other secondary structure

predominates precludes the study of biomolecules having an abundance of one secondary structure (van Stokkum et al., 1990; Perczel et al., 1992).

Deconvolution of CD spectra of polypeptides to extract the pure components having very high α-helix content is satisfactory but at best questionable when the ß-pleated sheet content is low (Perczel et al., 1992). Deduction of spectral contribution of secondary structures by Convex Constraint Analysis (CCA) algorithm is done directly from the deconvolution information of experimental CD spectra using a larger spectral data base (Perczel et al., 1991). This method improvises the standard data set of Yang et al. (1986) by including a "beta set proteins" from Kabsch and Sander (1983) to contain the CD curves of 23 proteins in the wavelength range between 190 and 240 nm (Perczel et al., 1992). The CD spectra of α-helices generally vary with the length of the helix (Yang et al., 1986), whereas the ß-pleated sheet, which exists in fundamentally different forms (*i.e.*, parallel-ß-sheets, antiparallel-ß-sheets, twisted and extended, and ß-barrels) exhibits significant fluctuations in band intensity (Manning and Woody, 1987). Deconvolution of the measured spectra by CCA therefore allows a better estimation of secondary structures in proteins with ß-pleated sheet structure. Perczel et al. (1992) demonstrated improved success by extracting unambiguous information of antiparallel ß-pleated sheet for the membrane bound CheY protein using CCA than with other deconvolution methods.

Varselec and CCA methods were used in this study to deconvolute kinetic information from the CD spectra of ß1-40 and ß6-25. When background absorbance of solvent or buffer forced truncation of spectra due to poor signal/noise ratio below 195 nm, the kinetics were emulated from the variation of molar ellipticity. In either case, the secondary structure content was correlated by fitting the observed CD spectrum to reference spectra of pure components. In cases where the observed CD spectra could not be satisfactorily fit by the reference spectra, an alternate reference set was generated using the information given in Fig.4.1 as per Appendix C. The interest in the conformational studies presented here is to delineate the local conformational changes for ß1-40 which guide folding of its tertiary structure. Analyses of the changes in apparent structural composition then permits one to detect the stabilizing components of secondary structure. This information provides an avenue for deciphering the pathways leading to organization of the ß1-40 backbone as oligomers from solution.

Concentration-dependent conformational changes for ß1-40

The CD spectra of ß1-40 solutions at 25 pM, 175 µM, 500 µM and 2.5 mM are given in Fig. 4.2. The concentration dependence of the CD spectra on ß1-40 conformation is seen from the change in ellipticity as the minima near 215 nm red-shifts to 207 nm when the concentration was increased from 25 µM to 2.5 mM. The CD spectrum at high concentration is typical of high antiparallel

ß-pleated sheet content. At low concentration (25 µM), there was considerable decrease in the intensity of the minima at 210 nm and, the maxima at 190 nm disappeared with a concomitant appearance of a shoulder near 200 nm. At concentrations higher than 0.5 mM, the positive band was very prominent and the minima near 215 nm was intensified. The presence of a shoulder near 220 nm at intermediate concentrations indicated a mixture of α-helical and ß-pleated sheet conformations. The CD spectra of ß1-40 between 25 µM and 2.5 mM shown in Fig. 4.2 are nearly isodichroic at 207 nm.

The variation in ellipticity at five wavelength intervals as a function of concentration is graphically depicted in Fig. 4.3. There was an overall increase in the positive band at 195 nm with an increase in concentration from 25 µM to 2.5 mM which was followed closely by an increase at 200 nm (bottom panel). This correlation is also seen by a simultaneous increase in the minimum ellipticity at 210 nm. The intensities of CD at 210 and 215 nm both increased as concentration was increased to 250 µM with a greater increase beyond 2 mM ß1-40 (top panel, Fig. 4.3). The changes in θ_{210} were coincident with that of θ_{215}, indicating the sensitivity of CD at these wavelengths in terms of concentration.

The spectral changes of ß1-40 are reminiscent of interconversion of secondary structural components to enhance the antiparallel ß-pleated sheet content observed by other laboratories using AßP derived analogs in aqueous cosolvents (Hollosi et al., 1989; Barrow and Zagorski, 1991). The changes in ellipticity and the spectral features indicate conformational adaptability of ß1-40

in aqueous solution with respect to changes in peptide concentration to self-associate to give oligomeric ß-pleated sheets (Kirschner et al., 1987; Fraser et al., 1991; Inouye et al., 1993). The propensity of ß1-40 to oligomerize in aqueous milieu therefore prohibits the exact determination of its secondary structural components in its *monomeric* state.

Deconvolution of CD spectra using Varselec and CCA analyses indicated an increase in the ß-pleated sheet content as concentration was increased (Fig.4.4). The positive correlation of molar ellipticity at either 210 or 215 nm with the $f_{ß}$ content seen from Fig. 4.4 suggested that these wavelengths were suitable indicators of ß-pleated sheet content (Sarkar and Doty, 1966). The f_{α} content also showed similar correlation with the ellipticity at 220 nm; however the variation was minimal compared to the changes at 210 and 215 nm. The poor correlation between molar ellipticity at 220 nm for higher concentrations of ß1-40 and f_{α} could probably be due to the lack of substantial α-helical structure at these concentrations. The molar ellipticity at 215 nm was therefore used as a measure of the ß-pleated sheet character for ß1-40 and derived analogs.

pH dependence of CD for ß1-40 and [Arg]ß1-40 analogs

The CD spectra of pH titrations for a 325 µM aqueous solution of ß1-40 are given in Fig. 4.5 (panel A). ß1-40 exhibited a preference for antiparallel ß-pleated sheets at pH values between 4 and 6. The following percentages were derived for the secondary structural components:

Varselec: 13.0 (*H*), 25.3 (*A*), 5.7 (*P*), 56.1 (*O*);

CCA: 14.8 (*H*), 32.3 (*A*), 6.2 (*P*), 46.7 (*O*).

The spectrum at pH 2 resembled unordered structure with considerably less α-helical and ß-pleated sheet content:

Varselec: 13.3 (*H*), 13.7 (*A*), 1.9 (*P*), 71.1 (*O*);

CCA: 12.8 (*H*), 14.5 (*A*), 2.4 (*P*), 70.3 (*O*).

At pH 9.1, the CD spectrum resembled an unordered structure although the intensities and positions were not coincident with those at acidic pH. In the intermediate pH range (6-8.5), the CD spectra suggested that the conformation of ß1-40 was predominantly ß-pleated sheets.

The peptide concentrations used for this study were rigorously controlled and therefore, conformational assignments can be compared in this pH range. The isodichroic point was blue shifted as pH was increased from 2.2 to 7.4, but red shifted as pH was increased to 9.1. This suggested that significant rearrangement of the peptide backbone took place to form ß-pleated sheets as the intermediate pH range was approached. This observation was in keeping with secondary structure prediction methods which identify that residues 9 - 19 are responsible for ß-pleated sheet formation (Argos et al., 1978). The acidic Asp^{23} and the basic His^{13} are ideally suited to favor self-association in ß1-40 (Fig. 1.4) by forming ion-pairs; other possible associations include glutamates and lysines. The observed pH dependence implies the importance the residues at these positions which are predominantly ionized in the

intermediate pH range. The ion-pair interactions between amino acids on neighboring peptide strands must lead to oligomerization in ß1-40. Self-association was also concentration dependent as demonstrated earlier, and now the importance of the polar amino terminal region is noted. From these data it was deduced that the solution conformation of ß1-40 was also effectively controlled by pH.

The propensity of ß1-40 to stabilize into oligomeric ß-pleated sheets at intermediate pH by salt-bridge formation was further explored by using the [Arg^{13}]ß1-40, [Arg^{14}]ß1-40, and [$Arg^{13,14}$]ß1-40 derived analogs. Significant decreases in the CD intensity was observed at 210 and 215 nm for [Arg^{13}], [Arg^{14}] and [$Arg^{13,14}$] analogs (panel B, Fig. 4.5). The molar ellipticity at 215 nm for the [$Arg^{13,14}$]ß1–40 analog was significantly lower as compared to ß1-40 at pH 7.4 (panel A). The CD spectra of the [Arg^{13}]ß1-40, [Arg^{14}]ß1-40 and [$Arg^{13,14}$]ß1-40 derived analogs have their minima near 215 nm and a slight inflection near 220 nm. The crossover to positive ellipticity is near 200 nm and the maxima is at 195 nm. This is consistent with a presence of substantial ß-pleated sheet structure (Sarkar and Doty, 1966). It is however noteworthy that the isodichroic point of these derived analogs is at 205 nm, the same as that of unsubstituted ß1-40 (panel B, Fig. 4.5; also Fig. 4.2). Although unambiguous assignments of secondary structure based on amino acids is difficult, since the CD were recorded under identical conditions, the substitution of His → Arg at these positions becomes relatively important in oligomer formation.

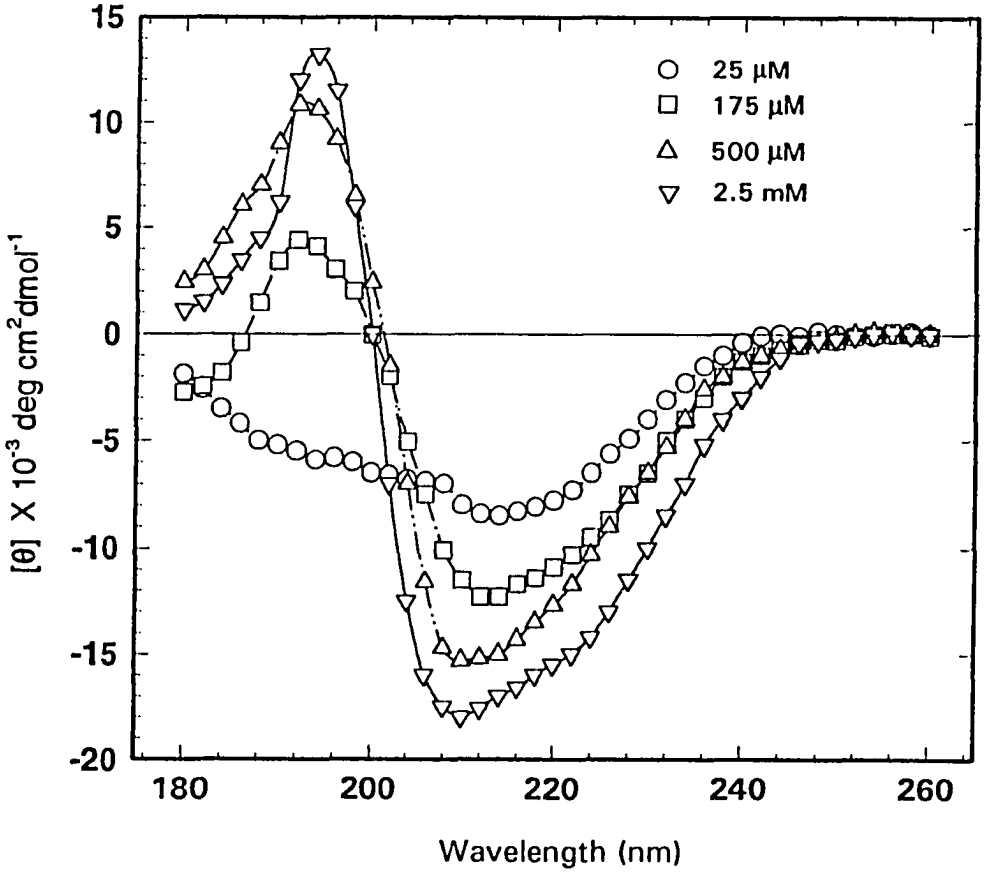

Fig. 4.2 CD spectra of ß1-40 as a function of concentration. The CD spectra of ß1-40 at concentrations of 25 µM, 175 pM 500 µM, and 2.5 mM were recorded at ambient temperature on freshly prepared solutions in a 50 mM HEPES buffer at pH 7.2. All concentrations were determined by quantitative amino acid analyses. The data points represent an average of six scans taken on the home built vacuum far UV/CD spectrophotometer at NSLS, and were plotted according to criteria given in Fig. 4.1. The spectrum for intermediate concentrations resemble a mixture of α-helical and ß-pleated sheet structures, while the spectrum for 2.5 mM is predominantly antiparallel ß-pleated sheet.

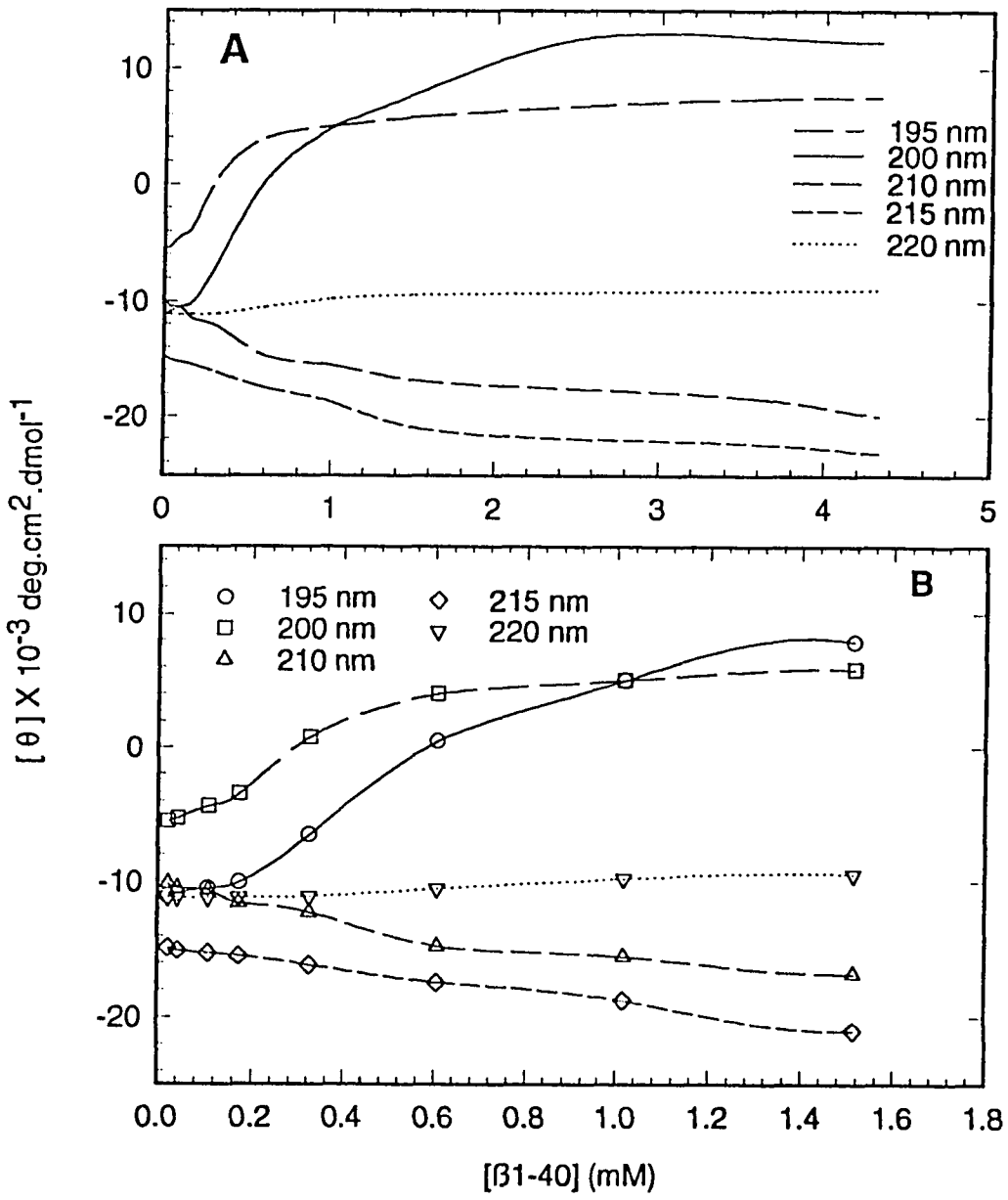

Fig. 4.3 Variation in ellipticity for ß1-40 as a function of concentration. The two panels represent the data at two scales, betwen 0-5 mM (panel A) and between 0-1.8 mM (panel; B). All solutions were freshly prepared and their CD measured at ambient temperature on the J-720.

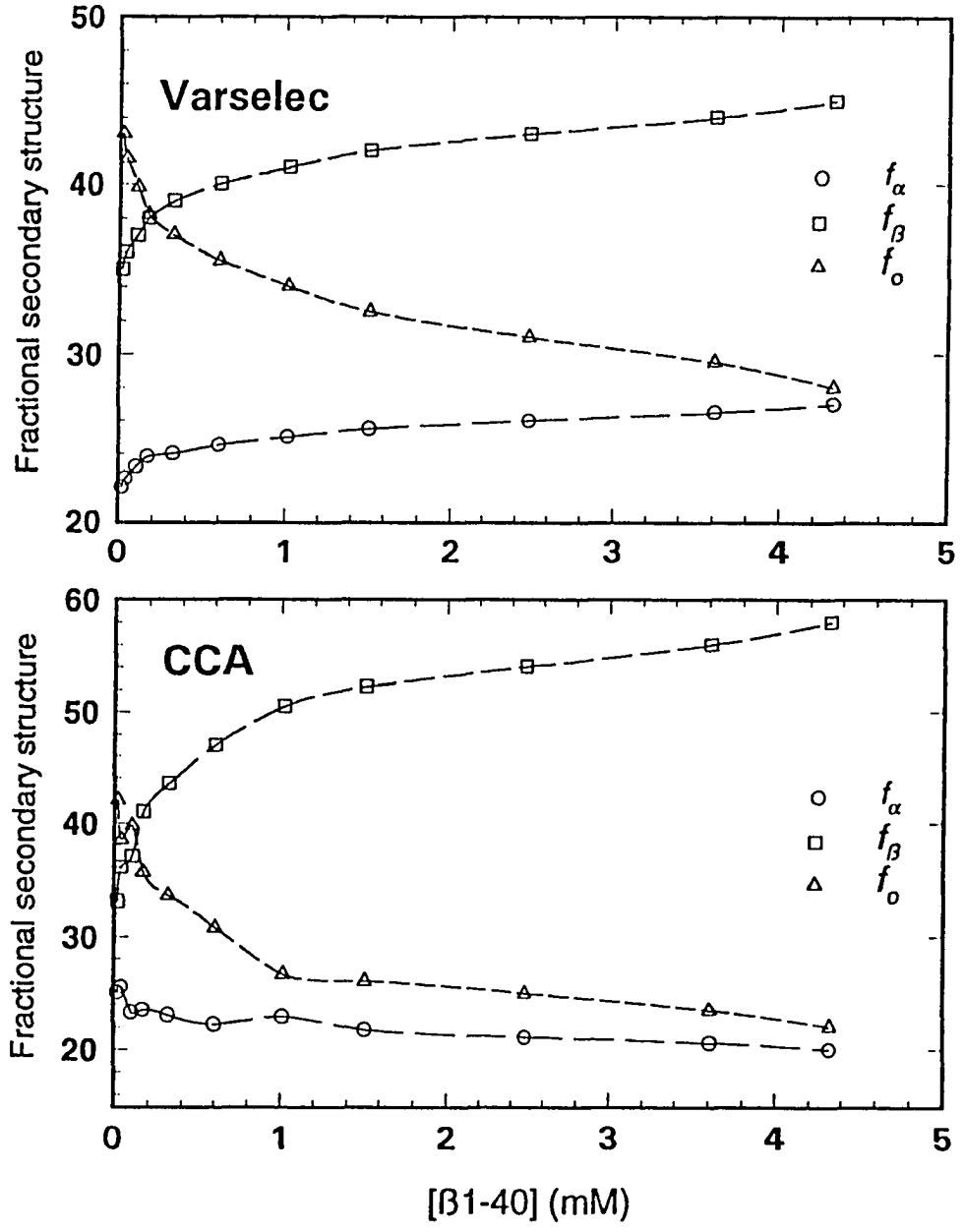

Fig. 4.4 Spectral decompositions for concentration dependence of CD for ß1-40 - Analyses using Varselec (top panel) and CCA (bottom panel).

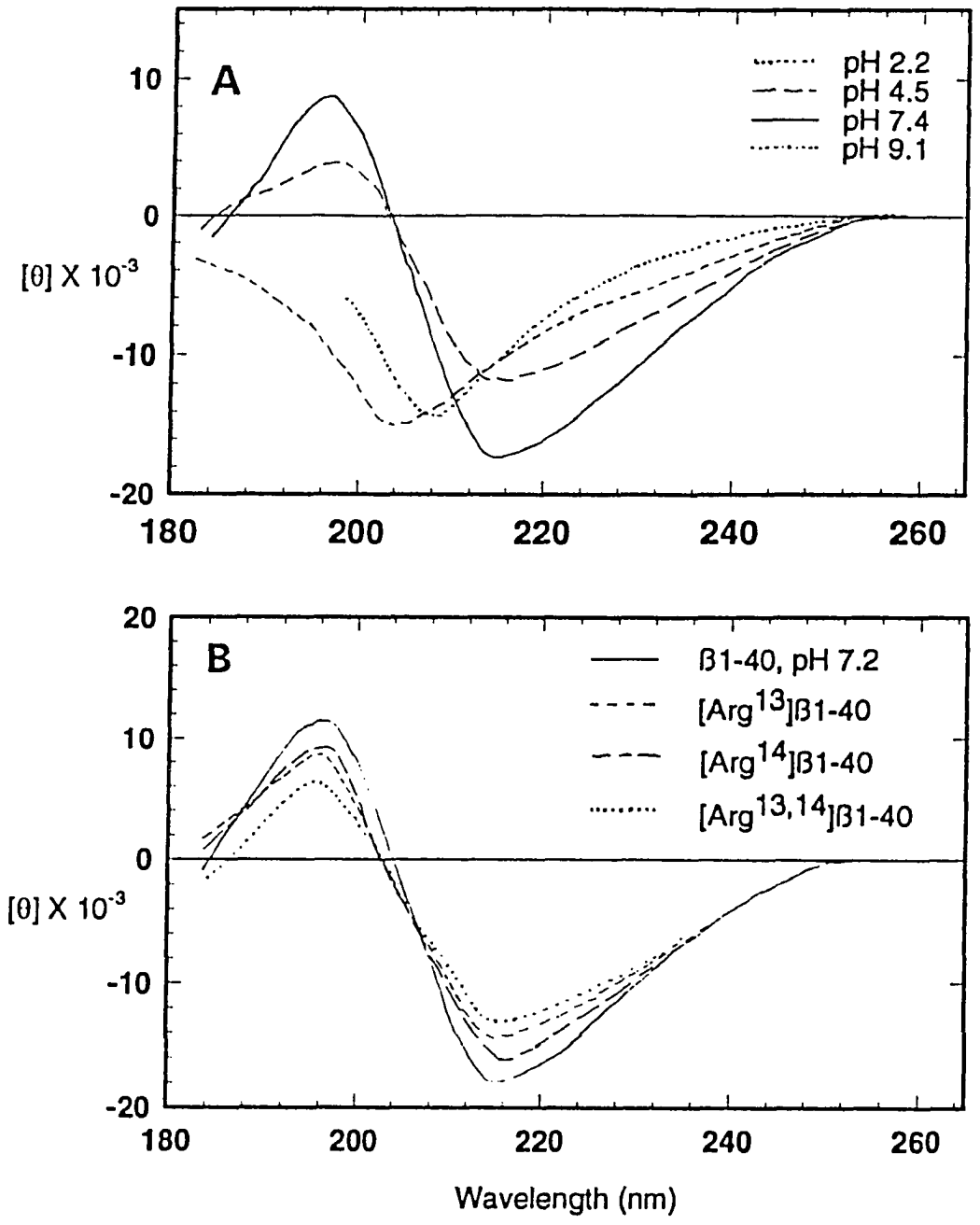

Fig. 4.5 Circular dichroism spectra of 325 μM ß1-40 as a function of pH. Data are averages of eight scans collected on J-720 with an analog time constant of 4 sec at a scan rate 1 nm/sec; the spectrum at pH 9 was truncated at 195 nm due to absorption by buffer. Panel B compares the CD for the [Arg^{13}]ß1–40, [Arg^{14}]ß1–40 and [Arg^{13,14}]ß1–40 analogs at pH 7.2. Ellipticities were calculated using a mean residue weight of 109 daltons.

The CD spectra of the His → Arg substituted sequence analogs further emphasized the role of His^{13} to ion-pair with Asp^{23} (*cf.* Fig. 1.4), and the importance of these residues at intermediate pH in stabilizing the intermolecular ß–pleated sheet structure. Additional ion-pairing could also take place between the Lys and/or Glu residues which are partly ionized at intermediate pH, although their positions would impede oligomerization to ß-pleated sheets. The estimated secondary structure and the changes in CD of the [Arg] derived analogs of ß1-40 are consistent with conformational transitions due to the central 11–25 region (Argos et al., 1978; Hollosi et al., 1989; Fabian et al., 1993; Otvos et al., 1993).

4.1.2. Variation in Ellipticity: Secondary Structure Transformational Analysis

The following protocol was employed to aid the investigation of conformational transitions occurring in peptide solutions over time:

Stock solution of peptide was prepared in 40% MeCN. Quantitative amino acid analysis was performed to determine the amount of peptide. Aliquots were withdrawn to get desirable amounts in 0.5 mL centrifuge tubes and the peptide concentrated *in vacuo* and lyophilized. The resulting solids were redissolved in 100 mM NaF in 50 mM HEPES buffer at pH 7.5 and the solutions were rigorously vortexed or sonicated. After standing for 10 min, the solutions were centrifuged

at 12000 rpm using an Eppendorf 421C microcentrifuge. The supernatant was assayed for peptide content using control ß1-40 peptides which were calibrated by quantitative amino acid analyses. CD spectra were recorded at ambient temperatures using the light source at Port U9B of the NSLS.

The CD spectra for an aqueous 320 µM ß1-40 solution at pH 7.5 and room temperature exhibited reductions in ellipticity as a function of time (Fig. 4.6). The positions of the CD bands for antiparallel ß-pleated sheets near 195 and 215 nm showed a slight red-shift with a simultaneous decrease in ellipticity over a period of 168 hours. The change in ellipticity at 215 nm was used to provide a qualitative basis for ß-pleated sheet content of ß1-40 in a single conformation (Fig. 4.7). The decrease in ellipticity was minimal in the first 3 h (lag period), slow during the first 24 hours, and then changed monotonously as time progressed to 168 hours. The overall trend in the change of ellipticity represented a multiphasic process. Analyses of secondary structure content were done using Varselec over the time frame of 168 h and is given in Table 4.1. It is obvious that the fractional α-helix content decreased within 24 h with a concomitant increase in the other structures, although the ß-pleated sheet content was not affected significantly. However, at the end of 168 h, the α-helix content increased at the expense of other structures. The fractional ß-pleated sheet content showed a varying trend with a subsequent decrease at the end of 168 h.

To determine the sensitivity of wavelength-dependence on observed CD, the molar ellipticity was also plotted at 210 (Fig. 4.8) and 220 nm (Fig. 4.9). At 210 nm, the observed kinetics were also illustrated by multiphasic processes. The change in ellipticity was minimal at 220 for 36 hours after which there was a slight decrease. The overall decrease in ellipticity at 220 nm was small (1.6 $deg \cdot cm^2 \cdot dmol^{-1}$) as compared with the decrease observed at 210 (17.2 $deg \cdot cm^2 \cdot dmol^{-1}$) and 215 nm (17 $deg \cdot cm^2 \cdot dmol^{-1}$).

The kinetics of observed multiphasic variation in ellipticity can be given by the nonlinear fit to the equation

$$\theta(t) = \theta(\infty) - \Sigma_{\Delta}\theta_i^{-t/\tau i} \qquad (5)$$

where $\theta(t)$ and $\theta(\infty)$ are the observed ellipticities at any time t and infinite time respectively, $_{\Delta}\theta_i$ is the amplitude of the i th phase, and the apparent relaxation time associated with this phase is τ_i. The ellipticity of the 320 μM ß1-40 solution did not change significantly after 216 h and was considered as $\theta(\infty)$.

Using a nonlinear least-squares calculation, the kinetics of ellipticity change over a period of 168 h were fit to data in Figs. 4.7 ($[\theta]_{215}$), 4.8 ($[\theta]_{210}$) and 4.9 ($[\theta]_{220}$) by a two- and three-exponential function of equation 5. This kinetic data could be conservatively fit with a two-term equation given by the parameters in Table 4.2. The curves for each of these wavelengths provided satisfactory fits with the two-term exponential. However, the apparent relaxation times observed

at 210 and 215 nm for the two-exponential fit are between 2.2 to 8.1 times as large as those at 220 nm (Table 4.2). It was therefore likely that such deviations could arise due to presence of more than two phases for the variation of ellipticity observed at these wavelengths.

To provide a better fit of the kinetic data, three- and four-exponential fits were tried for each wavelengths. The calculations for the kinetic curves obtained at 210 and 215 nm converged when used with three-exponentials (Table 4.2) and did not improve significantly with four-exponentials. The observed ellipticities at 210 and 215 nm at the end of the test period matched closely with the theoretical values using three-exponentials, better than the equivalent values at 220 nm. This is also indicated in Table 4.2 by the higher RMS values for 210 and 215 nm compared to 220 nm, and in Fig. 4.10 by the residual plots. The lower RMS deviations at 220 nm indicated that there might be amplitudes other than those observed. The apparent relaxation times for the three phases of each exponential fit at 210 and 215 nm were now only 3.4- to 4.9-fold than those at 220 nm.

From Table 4.2, it is seen that the θ(0) values from the three-exponential fit at 215 nm agree with the observed ellipticity (Fig. 4.6). This would suggest that all the phases of relaxation are accounted for. It is possible that the variation at 220 nm could be due to minor inconsequential amplitudes of some phases involving a helical segment of ß1-40. The transition to a structure with helical content is consistent with the deconvolution methods which predicted

more f_α content than f_β. There was also a lag time, a minimum of 3 hours for 210 and 215 nm, longer for 220 nm, before decreases in ellipticity occurred as demonstrated by the plots of variation in ellipticity (Figs. 4.7 and 4.8).

Correlating elution behavior of ß1-40 solutions as a function of time

To ascertain the cause of the loss in CD intensity, it was necessary to verify if there was a physical loss of the peptide. ß1-40 solutions studied for change in ellipticity over time were therefore characterized by studying their chromatographic behavior. These solutions were chromatographed under *normal* gradient conditions (chapter 2) on a Vydac C_{18} reversed-phase column using a linear gradient, with 0.1% TFA as solvent A, and 0.1% TFA in 100% MeCN as solvent B at a flow rate of 1 mL/min. Fig. 4.11 shows the elution profiles of a 215 µM ß1-40 solution which was chromatographed at 0, 24, 96 and 168 hours. The retention times and peak areas were nearly identical within the chromatographic parameters, with a slightly later elution after 168 hours (R_t increased by approximately 2 min). This was a clear demonstration that ß1-40 maintained its chromatographic integrity as a function of time. There were obviously no loss of peptide from these solutions. This illustrated that the cause of loss in CD signal was invariably endogenous.

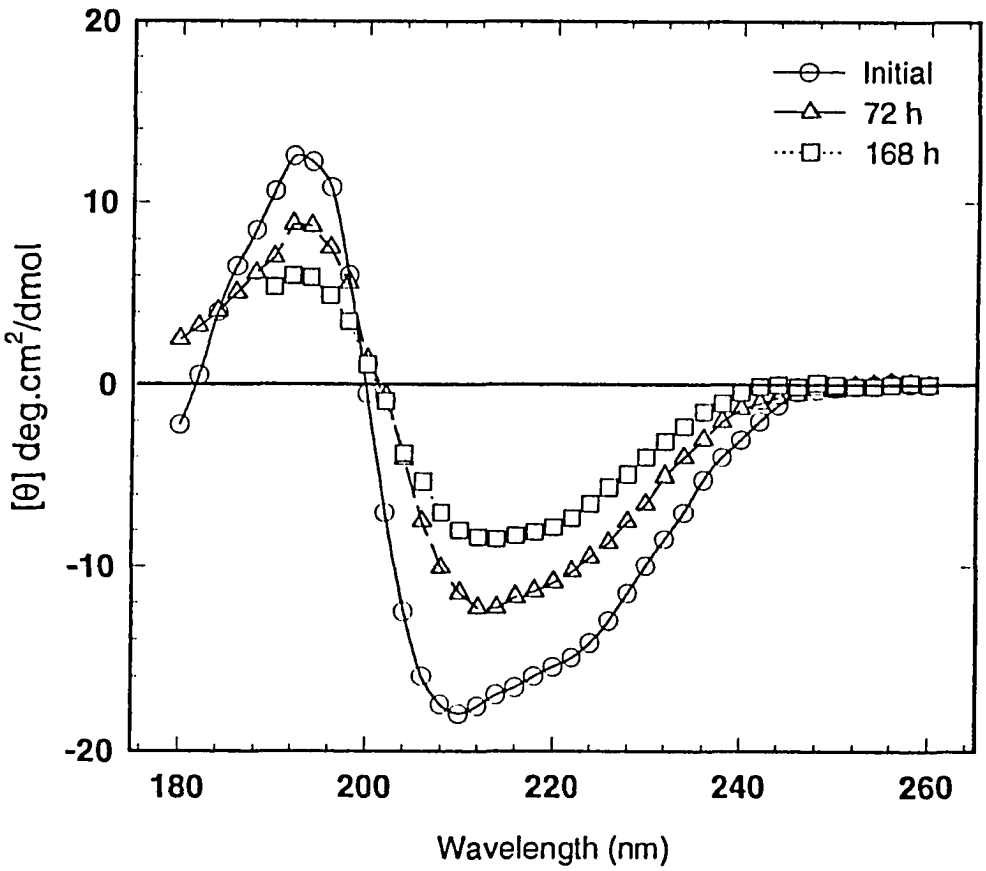

Fig. 4.6 Circular dichroism spectra of a 320 μM ß1-40 solution, pH 7.5, taken over a period of 168 hours. The raw data were collected at ambient temperatures using the vacuum spectrometer at NSLS with an analog time constant of 4 sec at a scan rate of 0.5 nm/sec. The data points represent the molar ellipticity calculated using mean residue weight of 108.3, and are an average of four measurements. Spectra were recorded every hour for the first 24 hours, and every 4 hours thereafter and were truncated at 195 nm after 100 h; only the CD measurements at time, t = 0, 72 and 168 hours are given for clarity.

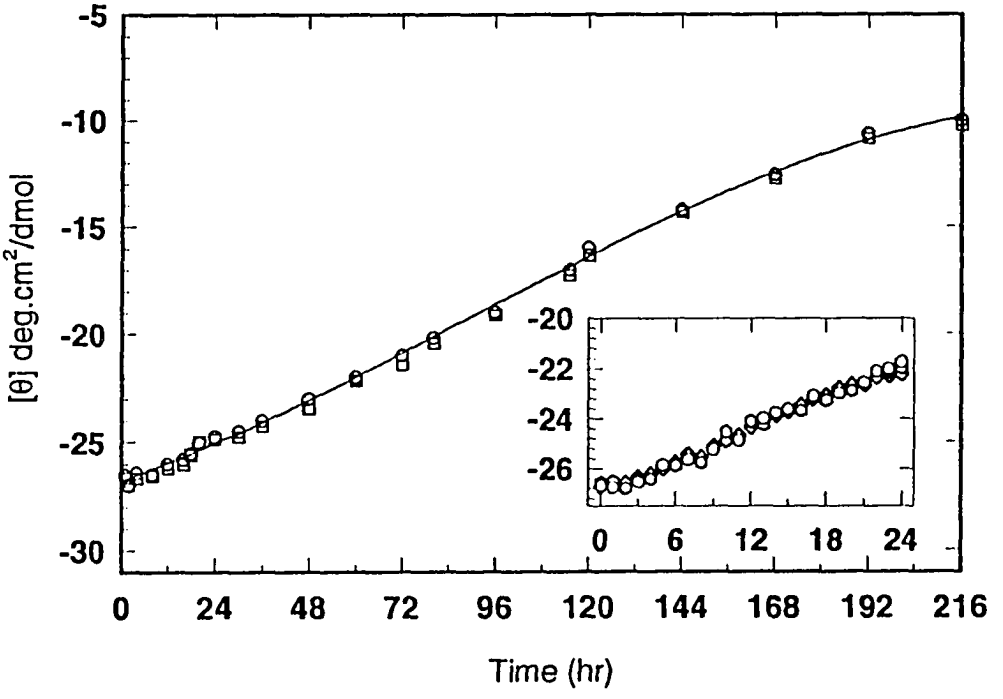

Fig. 4.7 Variation in ellipticity for a 320 μM ß1-40 solution at 215 nm as a function of time. The open symbols indicate the observed data from the CD spectra shown in Fig. 4.6. The solid line is the theoretical fit to the kinetic data as per equation 5. The kinetic data are plotted to show the changes occurring during the first 24 hr (inset) and for 216 hr.

Table 4.1

Secondary Structure Content of ß1-40 as a Function of Time [a]

Varselec Analysis			
time	f_α (%)	$f_ß$ (%)	f_o (%)
0 h	13 ± 2	28 ± 4	59 ± 3
12 h	15 ± 3	29 ± 5	56 ± 5
24 h	6 ± 5	27 ± 6	67 ± 6
48 h	18 ± 3	16 ± 7	66 ± 5
72 h	17 ± 4	17 ± 8	66 ± 4
96 h	21 ± 5	25 ± 6	54 ± 9
144 h	26 ± 4	18 ± 7	56 ± 7
168 h	37 ± 5	22 ± 8	41 ± 8

[a] CD data was truncated at 195 nm for spectra taken after 100 h.

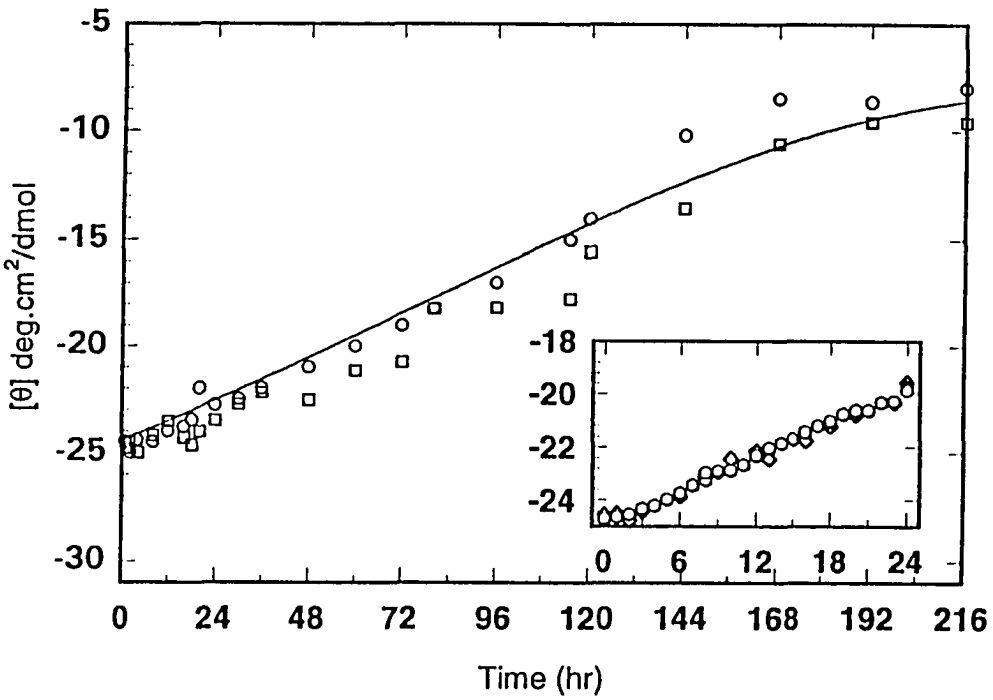

Fig. 4.8 Variation in ellipticity monitored at 210 nm for 320 μM ß1-40 as a function of time. The open symbols indicate the mean of the observed kinetic data; the inset shows the changes in ellipticity during the first 24 hours. The solid line indicates the theoretical fit to the observed CD as per equation 5.

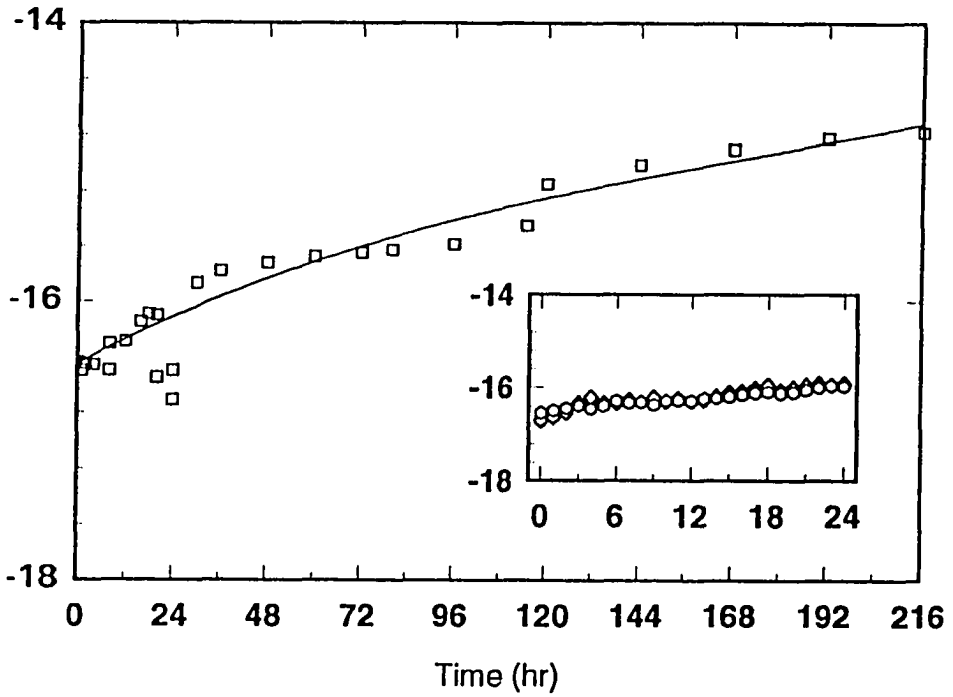

Fig. 4.9 Variation in ellipticity monitored at 220 nm for 320 μM ß1-40 as a function of time. The open symbols show the observed kinetic data which is plotted to show the differences in variations during the first 24 hours (inset). The solid line is the theoretical fit to the observed data as per equation 5.

Table 4.2.

Kinetic Parameters of Variation in Ellipticity of ß1-40 at pH 7.5

CD at	τ_1	τ_2	τ_3	$\Delta\theta_1$	$\Delta\theta_2$	$\Delta\theta_3$	θ_0	θ_∞	RMS
	(h)			(X 10^{-3} deg · cm^2 · $dmol^{-1}$)					
210 nm									
n [a] = 2	65.5	9.2		- 2.56	- 4.44		- 17.57	- 10.57	165
n = 3	100.3	42.5	1.21	- 1.18	- 8.19	- 0.93	- 16.62	- 6.32	182
215 nm									
n = 2	68.9	9.7		- 3.33	- 5.87		- 22.34	- 10.28	236
n = 3	154.2	57.3	2.23	- 1.12	- 14.65	- 1.63	- 26.64	- 10.24	327
220 nm									
n = 2	31.2	1.2		- 1.12	- 2.39		- 8.47	- 4.96	49
n = 3	45.5	11.7	0.81	- 1.89	- 7.98	- 0.60	- 12.12	- 1.68	72

[a] The number of exponentials required to fit the observed data according to equation 5.

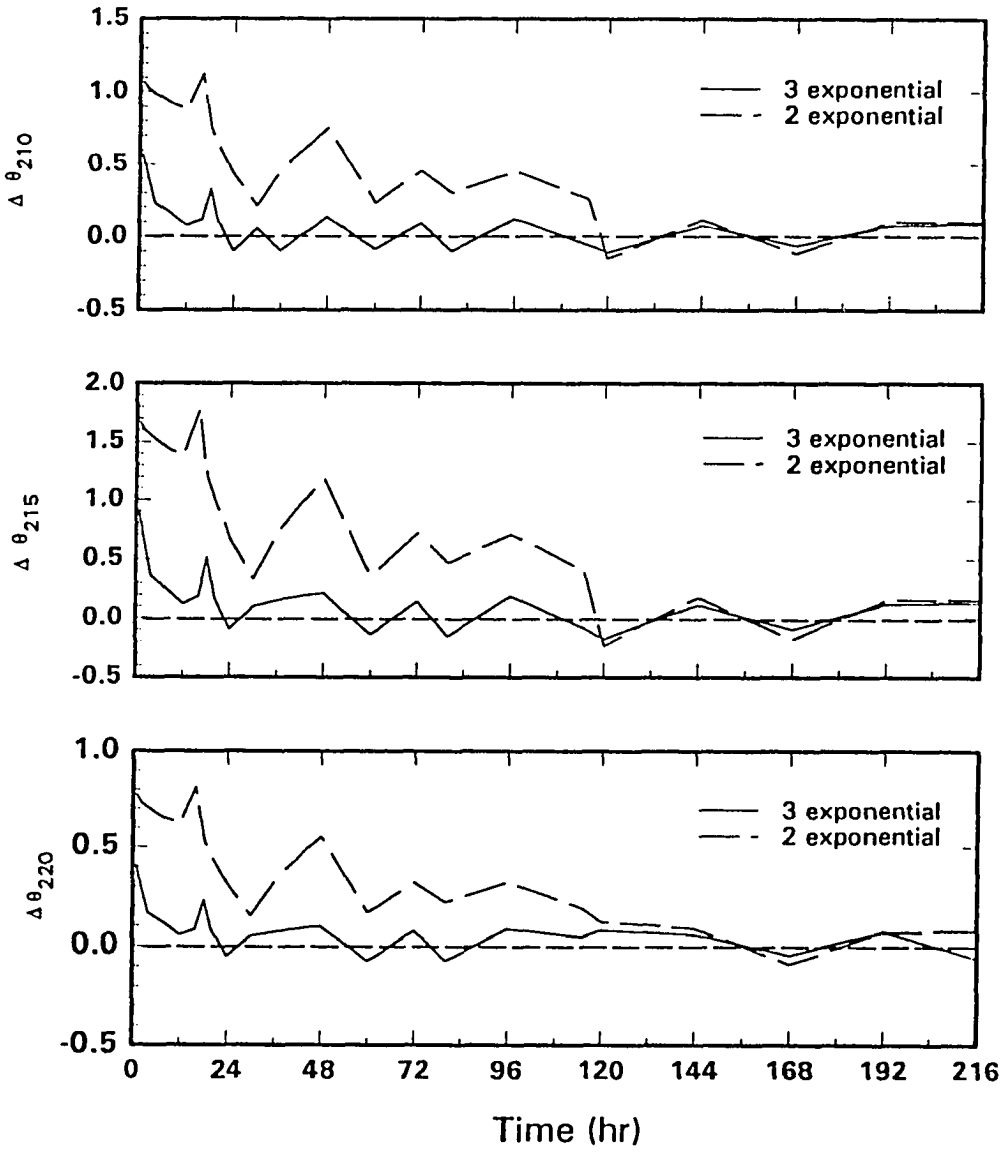

Fig. 4.10 Residual plots for a two- and three-exponential fit of kinetic data for 320 μM ß1-40 at 210, 215 and 220 nm.

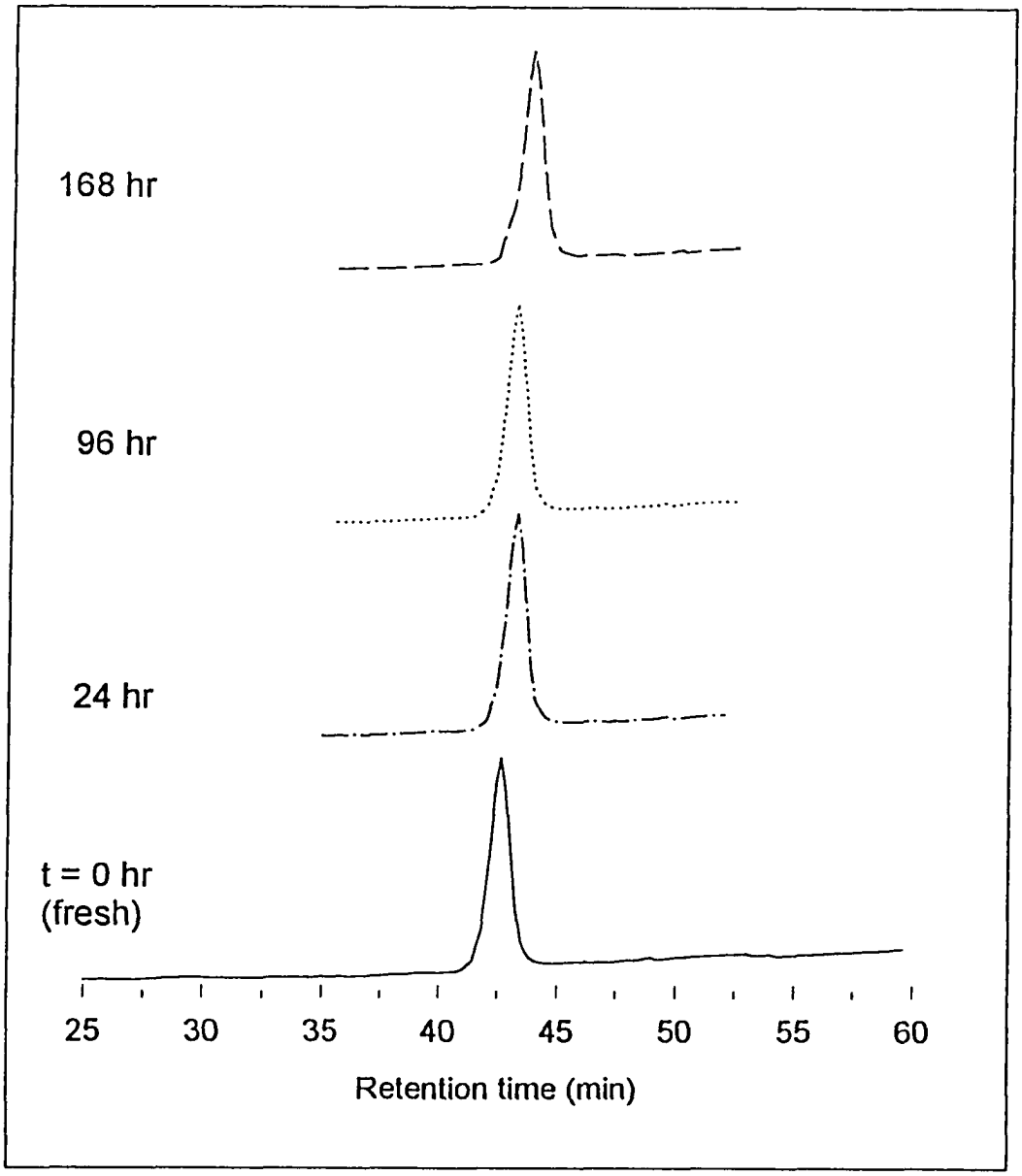

Fig. 4.11 Characterizing ß1-40 solution as a function of time by RP-HPLC. Chromatography was performed on a 4.6 X 300 mm Beckman Ultrasphere ODS column at room temperature using solvent A as 0.1% TFA and solvent B as 0.1% TFA in MeCN with a flow rate of 1.0 mL/min and the gradient from 0-100%B was in 60 min. Aliquots (10-20 µL) were drawn periodically from the time-dependent CD study for a 215 mM ß1-40 solution and loaded on the column without any treatment. The retention times increased by approximately 2 min as time progressed; the band broadening was insignificant.

Kinetic difference CD analysis for ß1-40: time effects

The good fit observed with three-exponential functions at 210 and 215 nm provides a basis for evaluating difference CD spectra for the individual kinetic phases. From equation 5, the difference spectrum of the *i* th phase is given by the wavelength dependence of the amplitude, $\Delta\theta_i$. Moreover, the observed ellipticity, according to equations 3 and 4, is the sum of the ellipticities of the individual secondary structural elements. Therefore the difference spectra are related to the fractional changes occurring during the respective kinetic phases for the secondary structural elements.

The fractional changes in ellipticity for the three phases obtained from equations 3 and 4 are graphically represented in Fig. 4.12. The fractional changes of the secondary structural elements for the three kinetic phases after deconvolution treatment are summarized in Table 4.3. These parameters were used to generate the theoretical fits for the experimentally observed kinetic CD depicted in Fig. 4.12.

It can be observed from Fig. 4.12 that the τ_1 phase had the smallest amplitude of the difference spectra ($\Delta\theta_1$ = -1.15 10^{-3} deg · cm^2 · $dmol^{-1}$) with a minimum near 215 nm. Although it is difficult to appraise the secondary structure changes taking place in this phase due to the small amplitude, the presence of a minimum at 215 nm would suggest changes in the ß-pleated sheet content. Overall, the decrease in ellipticity signifies a decrease in the ß-pleated sheet content. τ_2 has a more prominent difference CD centered around 215 nm. This

suggested that the change in ellipticity was significant change in the ß-pleated sheet content. The presence of a positive difference CD during this phase can be interpreted in terms of decrease in the α-helical content. Of the three phases, τ_3 phase has the worst calculated fits of the difference spectrum. However, with a stronger minimum around 220 nm and a positive difference around 235 nm, this could be interpreted as a significant change in the antiparallel ß-pleated sheet content with a simultaneous change in all other secondary structural elements, *viz.*, α–helical and other structures. This would mean that significant rearrangement between the secondary structural elements was involved in τ_3 phase, mostly indicated by α-helical → ß-pleated sheet transformation. Since these spectral changes are manifested over time without any change in the characterisitic chromatographic behavior (Fig. 4.11), contributions other than changes in secondary structure could be significant for this phase; possibly, tertiary or quaternary structure interactions.

Kinetic difference CD of ß1-40 - concentration effects

Fig. 4.13 illustrates the ellipticity variation at 210, 215, and 220 nm as a function of concentration of ß1-40 over time. The variations were affected differently as concentrations were increased from 25 µM to 4.3 mM. The ellipticity at 210 nm was most susceptible to variations in concentrations greater than 325 µM. Over a period of 216 h, no such lag in ellipticity was observed at 220 nm for concentrations below 325 µM ß1-40 (Fig. 4.13). Similar behavior was

also observed over the concentration range studied and the data in Fig. 4.13 demonstrate the monotonous decrease in the variation in ellipticity at 220 nm. This indicates that ellipticity changes at 220 nm were not as sensitive a measure of variation as those at 210 and 215 nm for change in secondary structure of ß1-40. It would therefore seem that the variation in ellipticity follows multiphasic kinetics which is strongly dependent on concentration. The relaxation times for the slow phase of the decrease in ellipticity with respect to concentrations are summarized in Table 4.4. It is clear that the change in the relaxation for the slow phase was directly dependent on concentration.

4.2. Kinetic Variation in CD for ß6-25 and [D-Asp] Derived Analogs

Conformational changes in a 0.4 mM solution of ß6-25 at pH 7.0 were studied for 225 h. The CD spectra are summarized in Fig. 4.14. The prominent feature of the spectra is the decrease in intensity of the 215 nm minima, and a simultaneous increase in the 195 nm maxima. This indicates that the major structural change occurs in the ß-pleated sheet content. There was no appreciable change in the CD spectrum after 250 h. The kinetics of the variation in ellipticity at 215 nm were described by two exponential terms (Fig. 4.15). The slow phase in the ellipticity decrease was similar to the slow phase detected for

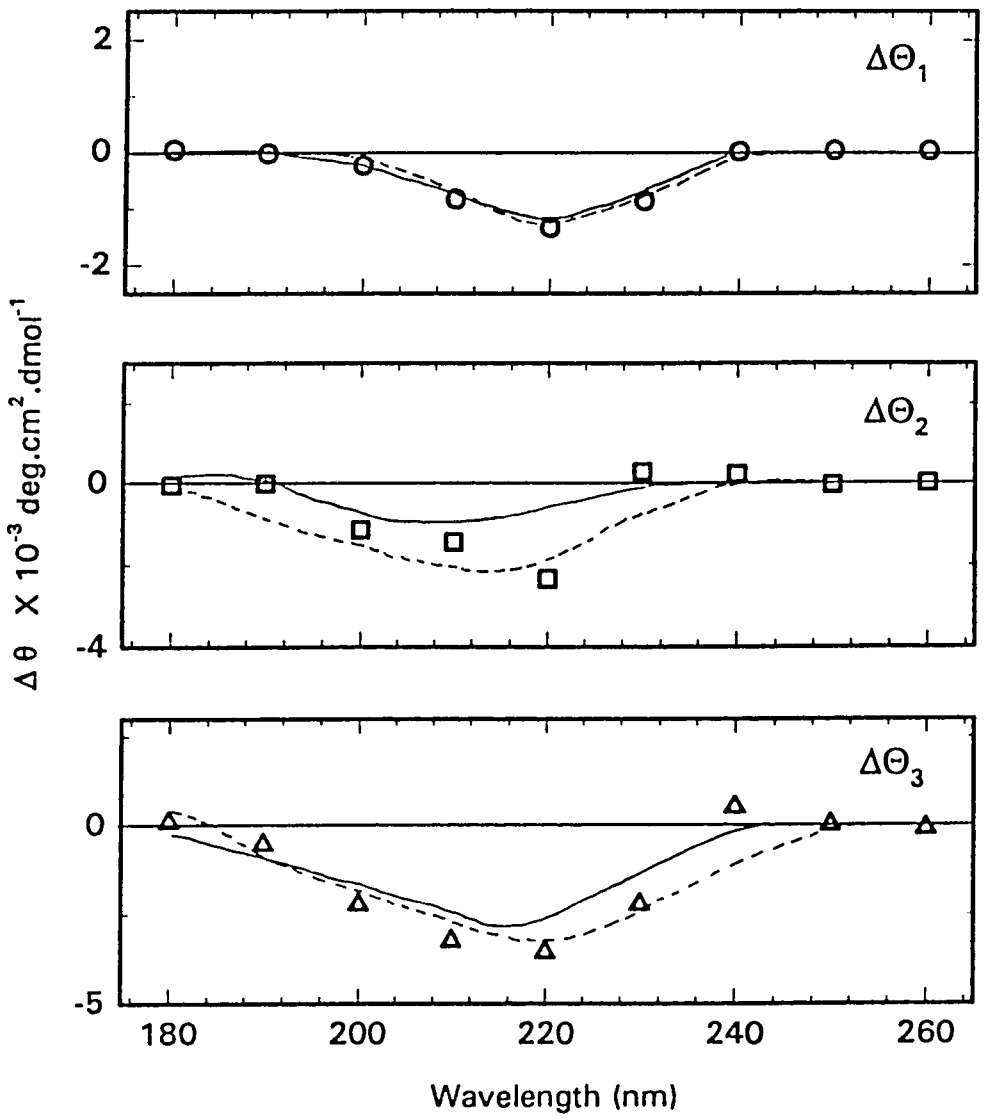

Fig. 4.12 Kinetic difference CD spectra for the three phases of ellipticity change for 320 μM ß1-40 solution at pH 7.5. The open circles represent the observed difference CD. The theoretical best-fit curves are shown for the Varselec (solid line) and CCA (dashed line) analyses.

Table 4.3

Fractional Changes in Secondary Structure Composition of ß1-40 Calculated from Kinetic Difference CD Spectra for the Three Phases of Variation in Ellipticity

	Varselec [a]				CCA [a]			
	Δf_α	$\Delta f_ß$	Δf_o	*RMS* [b]	Δf_α	$\Delta f_ß$	Δf_o	*RMS* [b]
τ_1	- 0.2	1.1	1.1	115	0.2	1.3	0.8	198
τ_2	- 1.6	- 15.8	- 12.3	227	0.8	- 11.8	1.1	329
τ_3	5.5	- 10.2	- 18.8	596	2.5	- 5.4	3.3	625

[a] CD data was truncated at 195 nm.
[b] Values in deg·cm^2 · dmol^{-1}

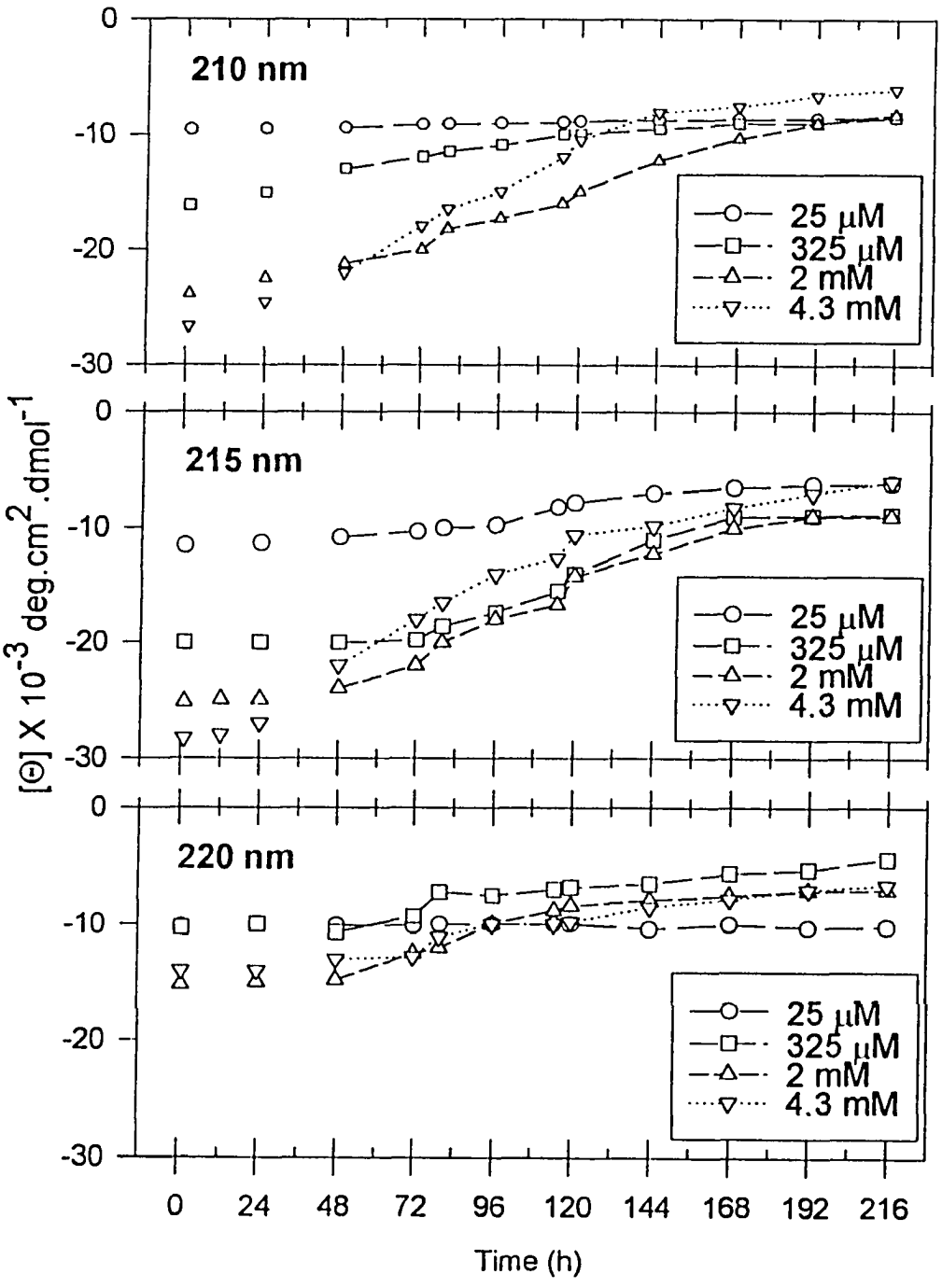

Fig. 4.13 Kinetics of ellipticity variation at 210, 215 and 220 nm as a function of ß1-40 concentration. All solutions were maintained between pH 7.2 and 7.7 in 50 mM HEPES buffer at room temperature.

Table 4.4

Relaxation Times and Amplitudes of ß1-40 as a Function of Concentration and Time

[ß1-40] (mM)	τ_1 (h)	τ_2 (h)	τ_3 (h)	$\Delta\theta_1$	$\Delta\theta_2$	$\Delta\theta_3$	θ_0	θ_∞
				(X 10^{-1} deg · cm^2 · $dmol^{-1}$)				
0.025	497.8	89.1	8.90	- 0.88	- 4.74	- 1.95	- 12.22	- 4.62
0.215	302.5	75.6	8.21	- 0.93	- 6.78	- 1.35	- 18.55	- 9.47
0.320	154.2	57.3	7.57	- 1.12	- 8.24	- 1.74	- 23.11	- 12.01
0.520	108.8	39.1	5.67	- 1.33	- 3.25	- 9.57	- 24.45	- 10.23
1.115	75.7	7.9	0.95	- 1.87	-7.68	- 17.51	- 27.20	- 0.12
2.315	57.1	5.5	0.79	- 2.23	- 9.77	- 15.82	- 28.56	- 0.75

ß1-40, with comparable time constants and relative amplitudes (Table 4.5).

A two-exponential fit for the variation of ellipticity furnished difference CD spectra of the two kinetic phases for ß6-25. These difference spectra are shown in Fig. 4.16. The goodness of fit with the two exponential term equation converged for 195 and 215 nm. The kinetic parameters of the ellipticity change for ß6-25 are summarized in Table 4.5. Both phases show the difference spectra centered between 210 and 215 nm. This was interpreted as an exclusive change in the $f_{ß}$ content. The lack of any other maxima or minima for ß6-25 strongly suggested that any α-helical and other structures remained unaltered.

Elution behavior of ß6-25 as a function of time

ß6-25 solutions studied for change in ellipticity over time were also studied for changes in chromatographic behavior. These solutions were chromatographed under conditions identical with studies done on ß1-40 solutions. Fig. 4.17 shows the difference in retention times and elution volume of ß6-25 solutions as a function of time on reversed-phase chromatography at 0, 16, 72 and 120 hours. There are insignificant increases in the retention times after long periods of incubation in solution. However, the change in elution volume was minimal and clearly demonstrated that there was no loss of peptide in these solutions and that ß6-25 maintains its chromatographic behavior as a function of time.

Equilibrium CD spectra of [D-Asp]ß6-25 analogs

Secondary structural analyses of the CD spectra of ß6–25 and its derived analogs [D-Asp^7]ß6–25, [D-Asp^{23}]ß6-25, and [D-Asp^{7,23}]ß6-25 at pH 7.2 were performed as a function of time. From the CD spectra recorded immediately after preparing the solutions, given in panel A of Fig. 4.18, a distinct red-shift in both the maximum near 195 nm and the minimum at 210 nm is evident for [D-Asp^7]ß6–25, [D-Asp^{23}]ß6-25 and [D-Asp^{7,23}]ß6-25. The overall CD intensity range did not change significantly, and it appears that the spectra seems to have been displaced with respect to the ellipticity coordinate. Spectral decompositions using Varselec gave the following results for percentage secondary structures for the ß6-25 analogs:

(a) ß6-25: $f_\alpha = 27\pm3$; $f_A = 22\pm2$; $f_P = 21\pm3$; $f_o = 30\pm5$;

(b) [D-Asp^7]ß6-25: $f_\alpha = 20\pm5$; $f_A = 20\pm3$; $f_P = 35\pm4$; $f_o = 25\pm6$;

(c) [D-Asp^{23}]ß6-25: $f_\alpha = 18\pm4$; $f_A = 19\pm2$; $f_P = 37\pm3$; $f_o = 26\pm4$;

(d) [D-Asp^{7,23}]ß6-25: $f_\alpha = 13\pm3$; $f_A = 12\pm3$; $f_P = 45\pm4$; $f_o = 30\pm5$.

The total fractional ß-pleated sheet content was between 43±3 and 57±4. The substitution of L-Asp → D-Asp at position 23 increased the parallel ß-pleated sheet content more than substitution at position 7, while a simultaneous substitution at positions 7 and 23 had the maximum parallel ß-pleated sheet content. From deconvolution of the respective CD spectra, it follows that the increase in the parallel ß-pleated sheet content of the [D-Asp] derived ß6-25 analogs takes place at the expense of their antiparallel ß-pleated sheet content.

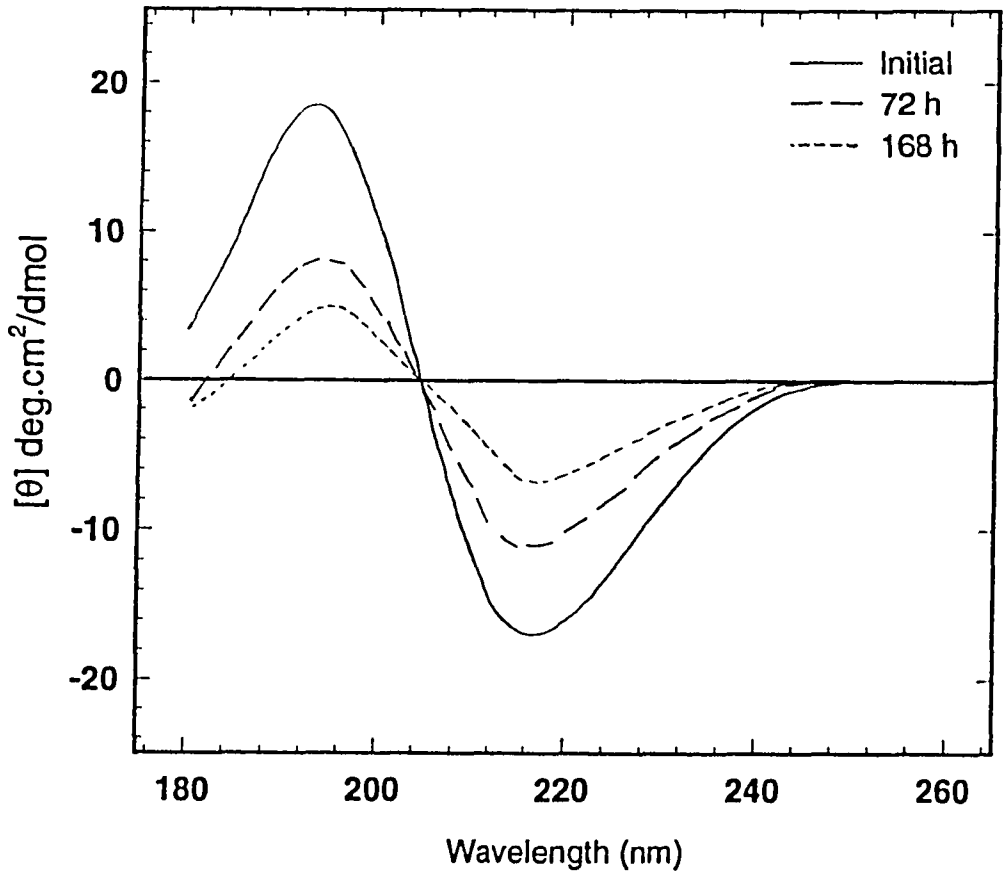

Fig. 4.14 CD spectra of 0.4 mM ß6-25 as a function of time. The spectra were recorded at room temperature every hour for eight hours and then every 4 hours using the vacuum UV/CD spectrometer at NSLS according to conditions given in Fig. 4.6. The ellipticity was calculated using a mean residue weight of 116 daltons.

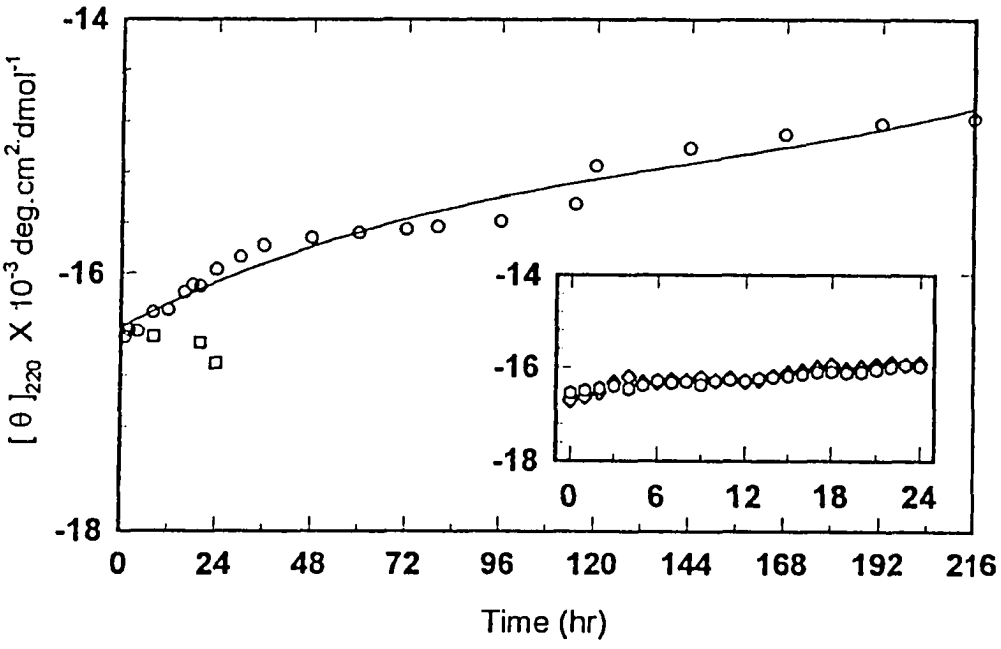

Fig. 4.15 Variation in ellipticity at 215 nm for ß6-25 as a function of time. The symbols represent the average of four scans for two independent samples. The inset shows the CD for the first 24 hours of the kinetic study illustrated in Fig. 4.14.

Table 4.5

Relaxation Times and Amplitudes of the Two Phases of Variation of Ellipticity for 0.4 mM ß6-25

τ_1 (h)	τ_2 (h)	$\Delta\theta_1$ ($\times 10^{-3}$ deg · cm^2 · dmol^{-1})	$\Delta\theta_2$ ($\times 10^{-3}$ deg · cm^2 · dmol^{-1})	θ_0 ($\times 10^{-3}$ deg · cm^2 · dmol^{-1})	θ_∞ ($\times 10^{-3}$ deg · cm^2 · dmol^{-1})
CD at 215 nm *n* [a] = 2					
264	55	- 1.85	- 10.84	- 20.27	- 7.54
CD at 195 nm *n* = 2					
237	49	2.43	14.84	19.74	2.47

[a] The number of exponentials in equation 5 necessary to fit the observed kinetic parameters.

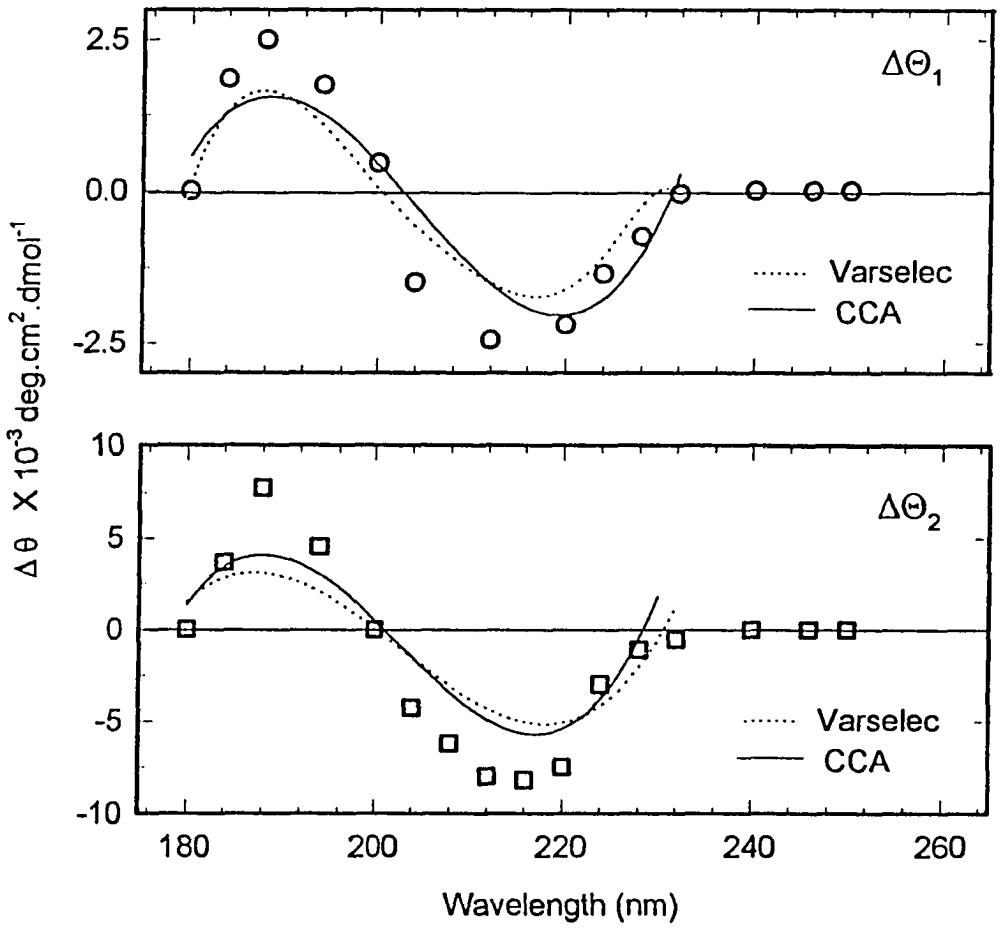

Fig. 4.16 Kinetic difference CD spectra for the two phases of ellipticity variation for ß6-25.

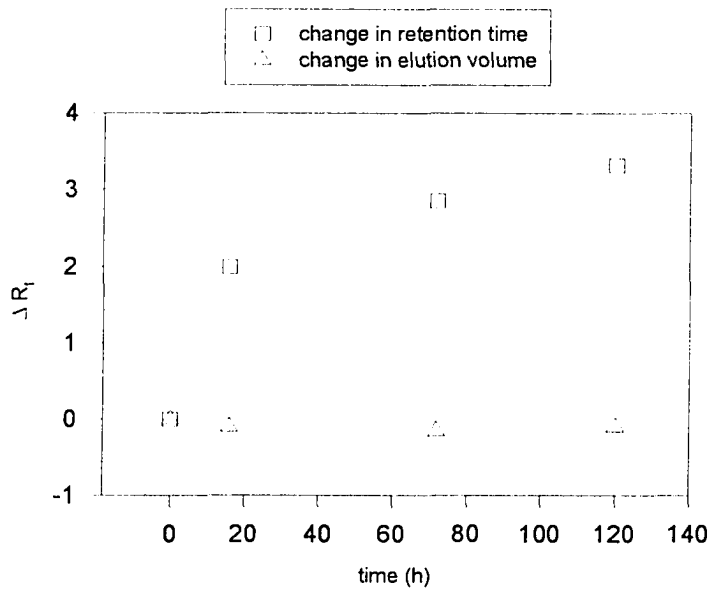

Fig. 4.17 Change in chromatographic parameters of ß6-25 solutions as a function of time. The chromatographic data were generated for 10 - 50 pL peptide solutions as per conditions given in Fig. 4.11 using samples for which CD were recorded in Fig. 4.14.

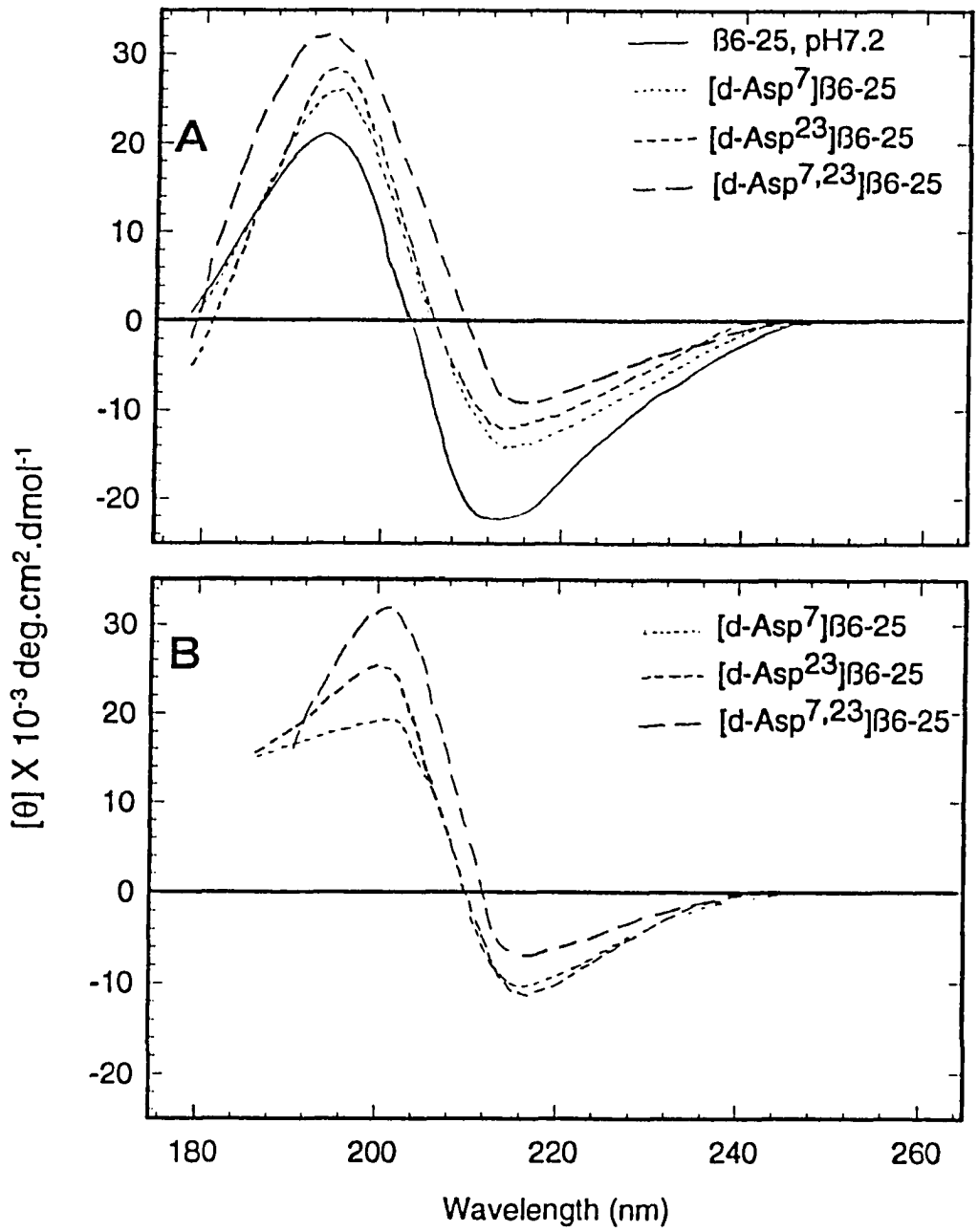

Fig. 4.18 Circular dichroism spectra for ß6-25 and its [D-Asp] derived analogs. Panel A shows CD data of 0.4 mM solutions of [D-Asp^{7}]ß6-25, [D-Asp^{23}]ß6-25, and [D-Asp^{7,23}]ß6-25 which was measured at time, t = 0 h. Panel **B** shows the corresponding CD data of [D-Asp^{7}]ß6-25, [D-Asp^{23}]ß6-25, and [D-Asp^{7,23}]ß6-25 derived analogs after 168 h.

The CD spectrum of [D-Asp^{7,23}]ß6-25 showed a slight decrease in the overall intensity after 168 h as illustrated by its spectrum given in panel B of Fig. 4.18. However, a red-shift in the positive band was more remarkable. Similar behavior was noted for the mono-substituted analogs [D-Asp^{7}]ß6-25 and [D-Asp^{23}]ß6-25. Comparison of the spectral features from CD spectra in Figs. 4.14 and 4.18 illustrates that the lack of significant variation in ellipticity for the [D-Asp] derived ß6-25 analogs was remarkable compared to the native L-Asp analog.

4.3. Effect of Alternative Reference Spectra

In order to fit the observed kinetic data better, an alternate reference spectrum set was generated using the procedures outlined in Appendix B. Deconvolution results for ß1-40 using the alternate reference spectra set are summarized by the kinetic difference CD spectra in Fig. 4.19. It is clearly seen that a better fit was obtained for all the phases of ellipticity change in ß1-40, including τ_3. The minimum near 220 nm with a corresponding maximum near 235 nm is very characteristic of transformation of α-helical→ß-pleated sheet content. Fig. 4.20 shows the corresponding kinetic plots for the two-exponential fits for ß6-25. The residual plots using the alternate spectra as the reference

spectra for fitting the kinetic difference spectra fits better than those provided by using parameters provided by the deconvolution methods.

It is noteworthy that the secondary structure decomposition using CCA provided results similar to those obtained from Varselec analyses when CD spectra were obtained in the 260 to 178 nm range (Fig. 4.4). However, when data were truncated due to experimental limitations of samples, and when the experimental kinetic difference data were analyzed, there were disagreements between these methods, and these did not agree with the observations (Table 4.3). Reliable estimation of fractional secondary structure is dependent on the wavelength region, and also on the spectral shape and intensity (Kuwajima et al. 1985; Johnson, 1990). The unequivocal determination of secondary structure in a monomeric state is hampered by the inherent propensity of ß1-40 to self-associate (Fig. 4.5). Thus, these deconvolution analyses are at best qualitative, and quantitative accuracy cannot be stressed without apprehension. There is no known spectrum available which bears any resemblance to the kinetic difference CD spectra obtained using these methods. The unsatisfactory calculated fits based on the kinetic parameters obtained from the deconvolution methods are therefore understandable. The possibility that spectral contributions other than those arising from the secondary structure also exists. Nonetheless, it was necessary to consider the accuracy of the estimated secondary structure fractions obtained on Varselec and CCA analyses.

Small distortions in the lower wavelength region results in lower fractional secondary structure components (Toumadge and Johnson, 1993). The most pronounced effect is for the negative bands; this was also indicated by the moderate RMS values for 215 nm (Table 4.3). The Varselec method always gives the total secondary structure content near 100% indicating a successful analysis rather than the goodness of fit to observed data. In the case of a predominantly antiparallel ß-pleated sheet protein, CheY, CCA provided unambiguous assignment of fractional secondary structure from the CD spectrum (Perczel et al., 1992). However, the changes in the antiparallel ß-pleated sheet content with change in intensity of the negative bands does not consistently show any definite trend (Venyaminov et al., 1991; Perczel et al., 1992) and therefore, more uncertainty exists. In any case, both these deconvolution methods gave unsatisfactory fits to the kinetic difference spectra for τ_2 and τ_3 phases of ß1-40.

The deconvolution approach, using equations 1 to 5, implies that:

(i) the fraction $(1 - f_\alpha - f_ß)$ derived from equations 2 and 4, remains as an "other" secondary structural component;

(ii) contribution from changes in the vicinity of aromatic amino acids are negligible;

(iii) application of the reference spectra used assumes that any secondary structural component will exhibit the same CD irrespective of the partial shielding of peptide backbone by the solvent.

In this study, there was no CD signal observed beyond 240 nm which indicated the contribution of the aromatic residues was negligible. However, assumptions *(i)* and *(iii)* were violated, since the CD spectra changed with time even when there was no loss of peptides from solution. The CD contribution of a flexible random-coil peptide chain may be different from that of an unordered structure; also, intermolecular oligomerization could exclude the solvent and consequently affect the CD contribution due to this phenomenon. The reference spectra for the "pure" secondary structure components used by Varselec and CCA methods were therefore abandoned and replaced by the measured spectra of ß1-40 and ß6-25. Equilibrium difference CD spectra generated by the three secondary structural components used in this study were verified according to treatment given in Appendix B to satisfy assumption *(i)*. To distinguish the fractional secondary structural components obtained using the measured CD spectra, these are now expressed as *apparent* fractional secondary structural components.

If the modulation of the backbone conformation of ß1-40 depends on the environment then the apparent fractional secondary structural components of these peptides will result in the following:

(a) spectral fits will be better than those using reference spectra,

(b) the apparent fractional f_{β} content will not be significantly affected by the choice of alternative spectra,

(c) the apparent fractional f_α content will have a greater effect on the difference spectra of ß1-40.

Deconvolution results for ß1-40 using the alternate reference spectra set are summarized by the kinetic difference CD spectra in Fig. 4.19. It is clearly seen that a better fit was obtained for all the phases of ellipticity change in ß1-40, including τ_3. The minimum near 220 nm with a corresponding maximum near 235 nm is very characteristic of transformation of α-helical→ß-pleated sheet content. Fig. 4.20 shows the corresponding kinetic plots for the two-exponential fits for ß6-25. The residual plots using the alternate spectra as the reference spectra for fitting the kinetic difference spectra fits better than those provided by using parameters provided by the deconvolution methods. It follows therefore, that the deconvolution treatments had overestimated the α-helix content of these peptides, and as a result assessed a lower ß-pleated sheet content.

4.4. Discussion

The CD spectroscopy in the far UV region for ß1-40 and ß6-25 undertaken here provided information about the conformational changes for the polypeptide backbone in aqueous solutions. The methods used here furnished new evidence about the kinetic variations in ellipticity which occurred as a

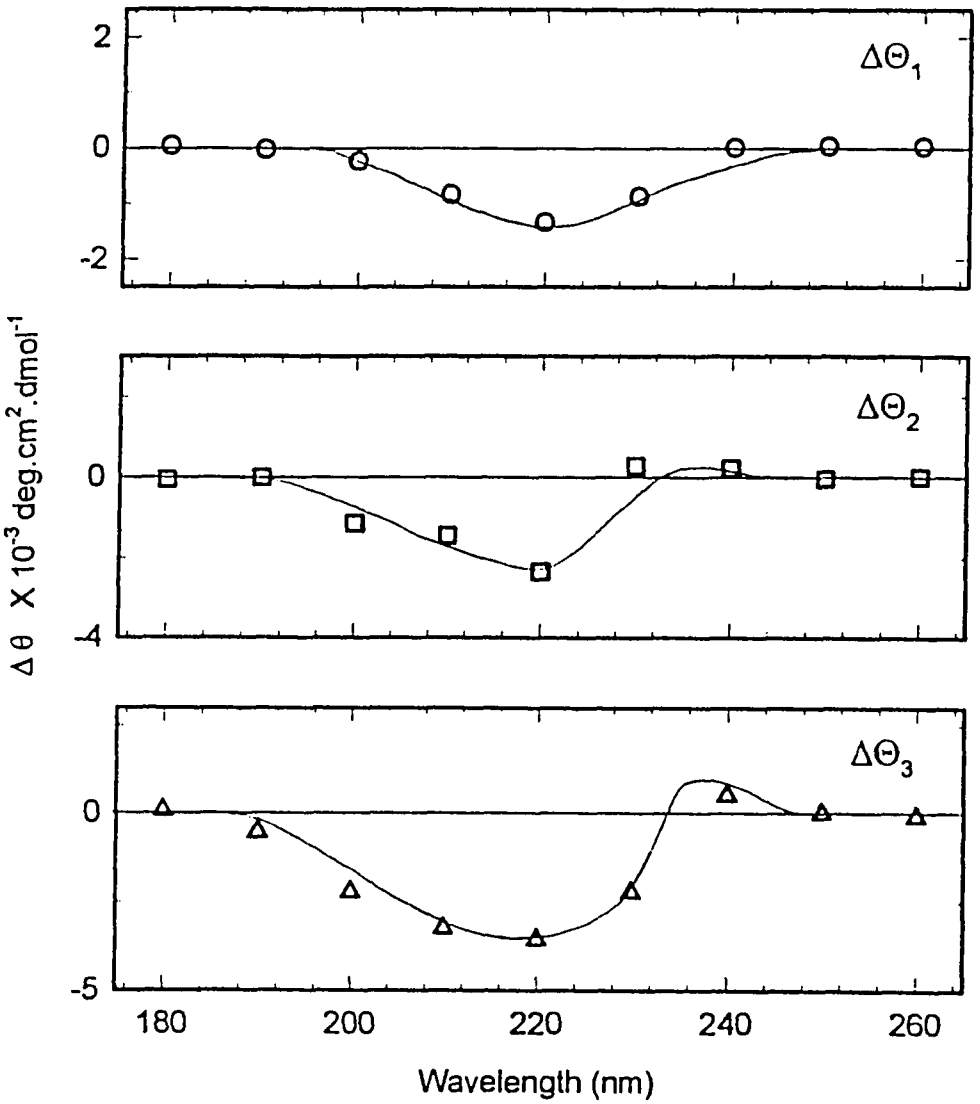

Fig. 4.19 Kinetic difference CD spectra for the three phases of ellipticity variation of ß1-40 based on alternate reference CD spectra. The alternate reference spectra were generated according to Appendix B and the spectral fits to the observed CD data are shown by the solid line.

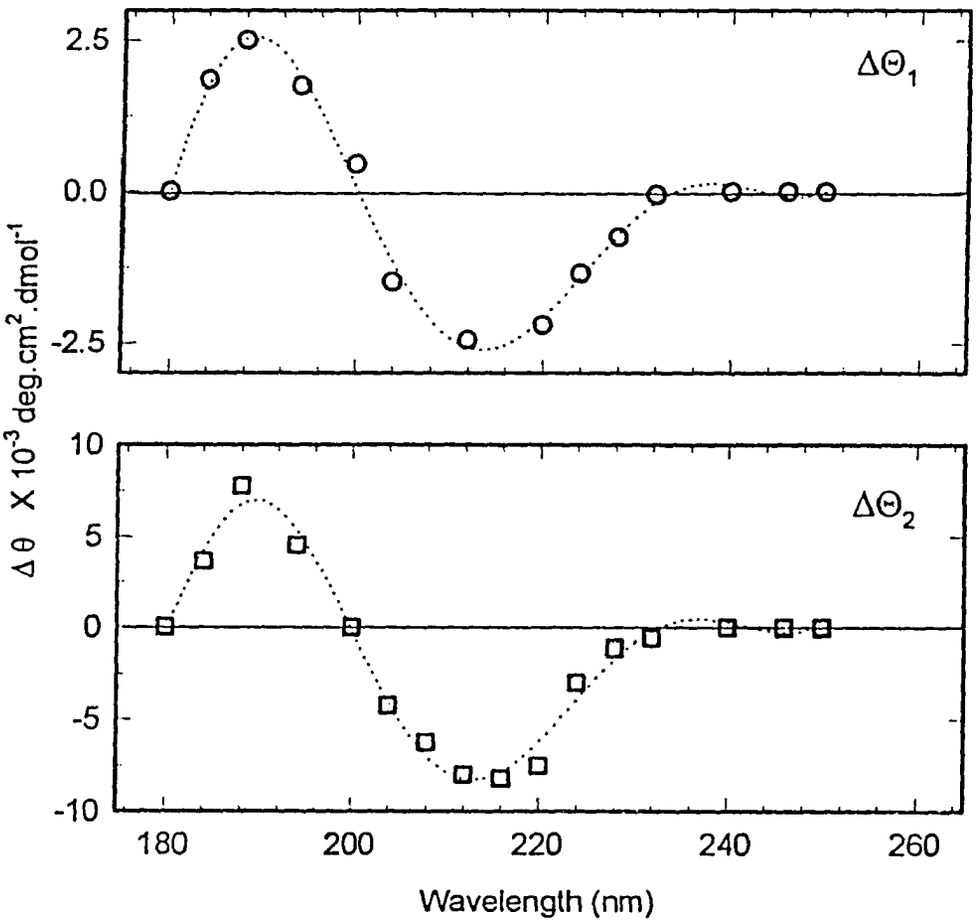

Fig. 4.20 Kinetic difference CD spectra for the two phases of ellipticity variation for ß6-25 based on alternate reference CD spectra. The dotted lines are the spectral fits to the observed kinetic CD data obtained from the alternate spectra generated according to Appendix B.

function of concentration, pH, time, and amino acid substitutions. The main purpose of this study was to garner knowledge about the kinetics of stable structure formation of ß1-40 in terms of its constituent secondary structural components. On the basis of the spectral data presented above, three distinct secondary structural components can be defined. These components will be *qualitatively* labeled α_1, $ß_1$, and $ß_2$ for the sake of discussion. The entire ß1-40 peptide can now be denoted by $\alpha_1 ß_1 ß_2$, and the observed kinetic behavior explained in terms of the apparent relaxation times. Comparison of the observed changes for ß1-40 and ß6-25 permits the specification of these spectroscopically and kinetically distinct moieties (or domains) within the peptide molecule.

The characterization of pH dependence of ß1-40 and its derived analogs illustrated that acidification disrupted the ß-pleated sheet structure which was predominant in the intermediate pH range. At basic pH values, the most dominant secondary structure represented that of random-coil. Disruption of ion-pairs at pH extremes causes a pronounced rearrangement of the peptide backbone. Inspection of the ion-pairing residues suggest that the ionizable amino acids are located within the first 28 residues of the peptide chain. Ion-pairing is however not an absolute requirement for stable antiparallel ß-pleated sheet formation in ß1-40, other contributions include van der Waals forces and, interstrand and intersheet side-chain packing. The sensitivity of [Arg^{13}]ß1-40, [Arg^{14}]ß1-40 and [$Arg^{13,14}$]ß1-40 derived analogs at intermediate pH suggest that the ion-pairing residues involve positions 13 and/or 14 with Asp/Glu;

this finding also supports the contention that oligomeric ß-sheet in fibrils took place at intermediate pH (Fraser et al., 1991a; Fraser et al., 1992; Inouye et al., 1993), and the popular observation of increased viscosity in aqueous peptide solutions leading to irreversible gellation and aggregation (Jarret and Lansbury, 1992; Tomski and Murphy, 1992; Sorimachi and Craik, 1994). The His → Arg substitutions at positions 13 and 14 therefore weaken the possible ionic interactions. These residues are located in the central portion of the peptide and based on empirical secondary structural parameters given in Fig. 1.5, it could be postulated this region bestows the observed ß-pleated sheet component. This component is *qualitatively* represented as $ß_1$.

The assignment of $ß_1$ is further affirmed by the CD spectra of ß6-25. From Fig. 4.14 it is clear that ß6-25 does not exhibit any CD band near 220 nm, a characterisitic which is seen in α-helical structures and is a prominent feature in the ß1-40 spectra taken in aqueous and 40% TFE solutions (Fig. 4.1). The CD spectra for ß6-25, however, always resemble that of ß-pleated sheets. The fibrils formed by ß6-25 were observed as "well-oriented" (Fraser et al., 1991; Inouye et al., 1993), which also recommends the suitability of this central region as the $ß_1$ component. The $ß_1$ therefore *qualitatively* resides within ß6-25. This element is mandatory for ß-pleated sheet formation and possesses the maximum amplitude change of the three structural elements. The kinetic difference CD for ß6-25 had minima centered around 215 nm which suggests the conformational change is limited to the antiparallel ß-pleated sheet content.

The component which gives rise to the α-helical characteristics in the CD spectrum can be labeled α_1. The α_1 component must reside in that region of ß1-40 exclusive of the central ß6-25 region. The kinetic difference spectra for these resemble helix → sheet transitions, both of which have faster relaxation times (Table 4.2). The amplitude of the third phase is approximately 10% of the total change in ellipticity, but is necessary for a good fit to the experimental CD (Fig. 4.10 and Table 4.2). This faster phase involves the α_1 component resulting in the minimum near 220 nm and the maximum at 235 nm. The lack of helix → sheet transitions in the kinetic difference spectra of ß6-25 suggest the absence of an α_1 component in this peptide. In organic cosolvents, the helical structure appears to be stabilized only for peptides which include the first 11 residues of the amino terminus (Hollosi et al., 1989; Hilbich et al., 1991; Barrow et al., 1992). It is therefore possible that α_1 is located within the first seven residues of the amino terminus of ß1-40.

The carboxyl terminal of ß1-40, exclusive of the central 6-25 region, is the qualitative $ß_2$ component. The location of $ß_2$ component is indirect and relies on spectroscopic data from other laboratories. The ß-pleated sheet forming sequence in the full-length AßP was attributed to residues 34-42 using FTIR (Halverson et al., 1990). Peptides having residues 10-43 (Hilbich et al., 1991), and residues 29-42 (Barrow and Zagorski, 1992) show substantial ß-pleated sheet structure in organic cosolvents. Thus, the $ß_2$ component can be expected

to reside at the carboxyl terminal of ß1-40. This would also suggest that only ß-pleated sheets are involved during the observed decrease in ellipticity.

The α_1 and $ß_2$ components in the complete ß1-40 sequence needs all three amplitudes of relaxation $_{\Delta}\theta_1$, $_{\Delta}\theta_2$, and $_{\Delta}\theta_3$. The kinetic difference spectra fit the observed data better when the third phase was included. The $ß_1$ component needs only two amplitudes of relaxation. The apparent relaxation time constant for the fastest phase, τ_3, for ß1-40 was 2.23 hours. The kinetic difference spectra demonstrate that changes occurring during τ_1, τ_2, and τ_3 for ß1-40 are fundamentally different. Although the amplitude for τ_1 is small, rendering assessment difficult, the presence of minimum around 220 nm indicates that antiparallel ß-pleated sheet structure increases at the expense of other structures. The minima near 220 in the τ_2 and τ_3 phases is enhanced also supports this fact. The appearance of positive differences in the kinetic spectrum highlights the decrease of α-helical structure with a concomitant increase in the antiparallel ß-pleated sheet structure. This suggests that a mutual rearrangement of the α_1 and $ß_2$ components takes place entirely due to intrinsic factors, which consequentially increases the process of oligomerization due to intermolecular attraction. Alternately, this phenomenon can be enhanced due to external factors which include inoculation of preformed oligomers which could act as nucleation sites (Jarret et al., 1993).

These results demonstrate that the CD spectra for ß1-40 and ß6-25 involve a significant rearrangement in the three structural components over a

period of 168 hours. While it can be postulated that the presence of the $ß_2$ component is mandatory to impart antiparallel ß-pleated sheet structure to the peptide backbone, it is seen from the above studies that a substantial change in the α_1 component is needed. In the case of ß6-25 the only changes are in the antiparallel ß-pleated sheet structure indicated by the substantial amplitude near 220 nm for *both* phases. It can be recalled that the unfolding kinetics for ß1-40 seen on a reversed-phase support had a half-life of approximately 25 min. This would suggest that in the presence of a hydrophobic matrix, the peptide backbone "relaxes" faster than in a solution environment. These observations are in keeping with Otvos et al. (1993) who noted the increase in the ß-pleated sheet nature for ß1-40 in the presence of membrane-mimicking agents. The chromatographic behavior did not change, even though considerable rearrangement of the secondary structural components took place in solution. This suggests very strongly that the process of oligomerization is reversed by the presence of a reversed-phase matrix.

The presence of D-Asp in the $ß_1$ element causes an antiparallel → parallel ß-pleated sheet conversion. The increase in the parallel ß-pleated sheet content with an increase in D-Asp substitution in ß6-25 is striking. The shifts in the CD bands can be accounted for by considering the change in polarization experienced by the peptide backbone (Tinoco, 1962). The observation of ion-channel formation by ß1-40 has been made by Arispe et al., (1993). The CD of these analogs resemble spectra exhibited by the ionophore, gramicidin A, a

D-, L- alternating cyclic pentadecapetpide, in a micellar environment (Salom et al., 1992). The conformation exhibited by the [D-Asp]ß6-25 analogs would indicate that the 6-25 region could form ion-channels in ß1-40. The current understanding among CD spectroscopists is that there is no unique CD spectrum for any peptide having structures like ß1-40. The CD data presented above provide further verification that a proper reference is mandatory for quantitative accuracy of structural changes, especially with comparatively flexible peptides which are capable of interconverting between a gamut of available conformations. The theoretical curves generated by parameters provided by Varselec and CCA did not account for the observed difference CD spectra. In contrast, alternate reference spectra generated using ß1-40 and its derived analogs provided a better fit. The three *qualitative* components, derived from the kinetic data, mutually exert a stabilizing influence on the secondary structure, and therefore lead to tertiary structure formation.

This chapter presented evidence for the conformational change in the peptide backbone which was entirely due to intrinsic factors. The demonstration that the ellipticity change of ß1-40 over time was a dynamic process, affected by concentration and minor modifications in the chemical structure was significant in comprehending how the peptide backbone rearranges in solution. The kinetic observations made here provide critical information concerning the soluble ß1-40 which forms gels in solution. This information is necessary to understand the molecular mechanisms of stable aggregates formed by AßP in AD brains.

Chapter 5

Interaction of Aluminum(III) with AßP and Derived Analogs in Aqueous Solutions

Introduction

The exact function of aqueous aluminum in physiological systems has been the subject of intense investigation, and is still an open question. Aluminum accumulates in brain and in soft and skeletal tissues in such pathological disorders as Parkinsonism with dementia (Hirano et al., 1961), amyotrophic lateral sclerosis (Stanhope et al., 1972), Alzheimer's disease (Crapper et al., 1973; Perl and Brody, 1980), dialysis encephalopathy (Mahurkar et al., 1973), osteodystrophy (Ott et al., 1982), and microcytic anemia (Prior et al., 1982). Aluminum levels in the normal brain are also found to increase with age (Katzman et al., 1978). The bioavailability of aluminum increases with acid

leaching (Tam and Williams, 1986) and therefore, its toxic potential in the environment has increased. The association of aluminum with AD was independently observed in the mid sixties, by Klatzo and colleagues (1965) and Terry and Peña (1965). The increased interest in the role of aluminum, however, has led some AD researchers to design experiments which overlook the bioinorganic chemistry of this ubiquitous ion, and thus propose mechanisms for its action which are inconsistent with its physical properties. There is yet no known biological function of this third most abundant element in the earth's crust.

The preferred coordination number for aluminum is six and exists *in vivo* as trivalent ions which form octahedral complexes. As a hard Lewis acid, Al(III) is very electropositive and therefore not easily polarized (Huheey, 1983). Coordination takes place with ligands which donate electrons to the vacant orbitals of Al(III) such as OH^-, F^-, PO_4^{3-}, SO_4^{2-}, $CH_3CO_2^-$, ROH, RO^-, and RNH_2. Most negatively charged oxygen donor groups are effective Al(III) chelators, but coordination via nitrogen also occurs. In general, most chelators form very stable, water-soluble octahedral complexes with Al(III) which do not hydrolyze at physiological pH. Ligand exchange in solution is usually slow, either due to the covalent distribution of the Al–O and Al–N bonds, or due to the dissociative mechanism of ligand exchange (Burgess, 1978). The slowness of such an exchange exemplifies the caveat in underestimating the effects of Al(III) in short-term experiments. These effects however cannot be accelerated or

augmented by increasing Al(III); such actions usually result in formation of polynuclear species of Al(III) (Bottero et al., 1980).

A review of available literature on aluminum action indicates that the mechanism of aluminum action in its neurotoxicity is not clear; however, it is widely recognized that it depends on the chemical forms in which aluminum is transported and stored in tissues. The presence of aluminum silicate was reported in the senile plaques where amyloid deposits are found (Candy et al., 1986), and in neurofibrillary tangles (Perl and Brody, 1980). In post-mortem human AD brains, appearance of elevated levels of aluminum is at best, uncertain. This could arise due to the sensitivity of different analytical techniques employed for aluminum detection, and the mode of preparation of samples. McDermott et al. (1979) used atomic absorption spectrometry and reported no significant differences in aluminum content of Alzheimer brains and controls. Stern et al. (1986) used laser microprobe mass analysis to investigate silicon and aluminum and did not find any pronounced levels in brain tissue. Using the more sensitive ion and electron microprobe, Chafi and coworkers (1991) found absence of aluminum from the frontal cortex and lysosomes of AD brains. However, intracellular localization of aluminum was traced to lysosomes by Schuurmans Stekhoven et al. (1990). Masters et al. (1985) have reported detection of aluminum in neuritic plaques from AD patients, a finding which is in agreement with the increased aluminosilicate levels in the senile plaque cores found by Candy et al. (1986). Many patients with Creutzfeld-Jakob's disease, a

neurological disorder, on the other hand, do not have elevated brain aluminum (Traub et al., 1981).

It must be noted here that the amyloid core protein from AD brains has racemic aspartic acid and serine contents higher than other short-lived proteins (Shapira et al., 1988; Roher et al., 1993). An increased racemization of D-Asp in the brain protein(s) of rats fed with aluminum-rich diet was found by Anderson et al. (1990). Using dynamic secondary ion mass spectrometry, Candy et al. (1992) showed co-localization of aluminum with the amyloid in cortical pyramidal neurons, while on the other hand, Landsberg et al. (1992) failed to demonstrate the presence of aluminum in untreated amyloid plaque cores from brain tissue.

As highlighted above, there are many indications which point to Al(III) as a culpable etiologic agent in many neurological disorders, including AD. However, the skepticism of most researchers on its accumulation in the afflicted neuronal tissue arises in part due to the wide variations in the modes of preparation of brain tissue. Even though the exact mode of accumulation and transport of Al(III) in the brain is not known, complexation seems to be the most favored. Also, Al(III) uptake by the brain is slow compared to other organs and therefore not amenable for short term studies (Ganrot, 1986). Most age-related diseases and disorders lack definite etiology but show features which favor putative Al(III) related diseases, and these changes are manifested over a lifetime of the tissue or organ.

Having gained notoriety as an etiologic agent, aluminum salts are used by many researchers without full appreciation of its solution chemistry. In acidic solutions (pH < 5), Al(III) exists as an octahedral hexahydrate complex, $[Al(H_2O)_6]^{3+}$. Successive deprotonations occur as pH is increased, and $Al(OH)_3$ precipitates in neutral solutions. The precipitate is redissolved at basic pHs, forming a tetrahedral complex, $[Al(OH)_4]^-$. At physiological pH the highest allowed hexahydrate concentration derived from the solubility product of $Al(OH)_3$ is given by $[Al(III)]/[H^+]^3 = 10^{10.7}$ ($[Al(III)] \approx 10^{-18}$M) (Martin, 1986b). The ensuing *total* Al(III) concentration is 8 μM. It is necessary to reflect on the implication of this result. Even though the total Al(III) is as high as 8 μM, approximately 10^{-12} M is *available*, the rest appears as $[Al(OH)_4]^-$ (Martin, 1986b). Speciation due to ion-solvation further reduces the available Al(III) (Martin, 1988; Harris, 1992). It therefore follows that at physiological pH, obtaining available Al(III) higher than nanomolar concentrations is only possible in solutions supersaturated with $Al(OH)_3$, and it is the available Al(III) concentration that is consequential for biomolecules. These ideas have been summarized in Appendix C. Disregard to the aqueous chemistry of Al(III) has therefore lead to debatable conclusions in the literature on the toxic levels of Al(III).

The knowledge of chemical properties of Al(III) facilitates the prediction of the effective functional groups for chelation. Plasma Al(III) is usually associated with citrate, phosphate and transferrin (Martin, 1986a). Citrate (cit),

a tridentate carboxylic acid ligand, forms a soluble neutral Al(III)-cit complex between pH 2 and 5 which could increase its gastrointestinal absorption. Transferrin (Tf) in blood plasma is another effective complexation agent for Al(III) and prevents its precipitation from physiological fluids (Martin, 1986a; Harris and Sheldon, 1990). Tf binds Al(III) in a non-specific manner at its end terminals and given sufficient time, extracts more than 80% Al(III) from the Al(III)-cit complex (Martin et al., 1986b; Harris, 1992). Oxygen and nitrogen are good donor ligands, and the Al(III)-complexes once formed are metastable under nonequilibrium conditions (Karlik et al., 1983). The most effective Al(III) ion complexing amino acids in peptides and proteins are aspartic and glutamic acids, histidine, and cysteine (Charlet et al., 1984). The importance of Asp/Glu and His residues in the secondary structural stability of ß1-40 oligomerization was demonstrated in chapter 4. these amino acids to form ion-pairs in ß1-40 oligomers was demonstrated in chapter 4. The presence of L-glutamate has been shown to increase the ability of Al(III) to enter erythrocytes *in vitro* and rat brain (Deloncle et al., 1990). It has also been proposed that Al(III) could form stable complexes with two adjacent glutamates or aspartates which might be found in proteins (Anghileri, 1992). In phosphorylated proteins, Al(III) has been proposed to form intrachain and interchain complexes (Hollosi et al., 1994).

In spite of technological advances in analyses, the presence of aluminum in the Alzheimer brain is ascertained only by post-mortem examination, often assayed by destructive digestion of the tissue. Many powerful

techniques are available to spectroscopists for investigating isolated biochemical species. By virtue of 100% natural abundance of the ^{27}Al nucleus and good sensitivity (20% relative to ^{1}H), ^{27}Al nuclear magnetic resonance (NMR) spectroscopy is valuable in the study of Al(III) complexation. The quadrupole moment of the ^{27}Al nucleus (I = 5/2, Q = 0.149 X 10^{-28} m^2) gives rise to efficient quadrupolar relaxation which in severe instances result in resonances having large linewidths, sometimes up to kilohertz. Moreover, the relatively large shielding range (≈ 200 ppm) offers scope for simultaneous determination of chemical shifts for octahedral and tetrahedral complexes. The chemical shifts and linewidths of Al(III) complexes also depend on its chemical character, *viz.*, coordination geometry, symmetry of the complex, and exchange rates of Al(III) with its environment. In aqueous solutions at acidic pH, Al(III) exists as hexa-coordinated species, $[Al(H_2O)_6]^{3+}$, and at pH > 7 the tetrahedral complex predominates, $[Al(OH)_4]^-$ (Haraguchi and Fujiwara, 1969; Hinton and Briggs, 1978; Bottero et al., 1980; Martin, 1986b; Martin, 1988). In a general sense, in complexes of type AlL_4, ^{27}Al resonates downfield of octahedral Al(III) complexes of the type AlL_6 by 80 ppm (Haraguchi and Fujiwara, 1969; Akitt and Farthing, 1978; Bottero et al., 1980; Wehrli and Wehrli, 1981; Akitt, 1987). The exceptions are the tetrahedral iodo-complexes which resonate in the octahedral region of ^{27}Al NMR spectrum (Haraguchi and Fujiwara, 1969; Hinton and Briggs, 1978; Akitt, 1987). Nonetheless, each type of complex exhibits slightly different chemical shift which is dependent upon the coordinating ligand (Haraguchi and

Fujiwara, 1969). The linewidths of the resonances on the other hand, provide information on the symmetry of the complex and reflects the quadrupole interactions. Taken together, these two parameters furnish reliable data on the contribution of various chelating ligands to the environment of Al(III).

^{27}Al NMR spectroscopy has been used by Canet et al. (1973), and other spectroscopists (Wehrli and Wehrli, 1981; Akitt et al., 1981, 1984, 1985; Mazurguil et al., 1982; Karlik et al., 1983) to determine the complexation of Al(III) in solutions. ^{27}Al NMR spectroscopic investigation of aluminum binding with [Leu^5]-enkephalin (Mazurguil et al., 1982), with serum proteins, albumin (Fatemi et al., 1992) and transferrin (Aramini et al., 1993) has shed light on the nature of the metal-binding sites in biomolecules. ^{27}Al NMR spectroscopy was used in this study to elaborate the role of Al(III) binding to ß1-40 and its derived analog, ß6-25. The experiments were designed to study Al(III) association to ß1-40, the site(s) of complexation, and its influence on the peptide backbone. Chromatographic and spectroscopic strategies were employed to outline the possible role of Al(III) in the aggregation of ß1-40 and derived analogs. RP-HPLC was used to "purify" Al(III)-bound peptides, which were subsequently characterized by sequence and amino acid analyses, and by ^{27}Al NMR spectroscopy. The influence of trivalent metal ions on the secondary structure of ß1-40 and ß6-25 derived analogs was evaluated by far UV/CD spectroscopy. The spectroscopic investigations of the Al(III) association reveal mutually supporting data for metal-binding sites in ß1-40 and ß6-25. These data, when

considered collectively, provide unequivocal evidence for the mutual effect of Al(III) and ß1-40 in solution with respect to the stability of its secondary structure.

5.1. Al(III) and ß1-40 Derived Analogs: Chromatographic Analysis

The reversed-phase matrix was shown to influence the retention characteristics of ß1-40 and its derived analogs based on the studies given in chapter 3. It was also pointed out that the behavior of the peptides was primarily governed by hydrophobicity. The peptide backbone studies in chapter 4 showed the role of charged residues and the solution environment in secondary structure stability. This section outlines an experimental design to selectively isolate Al(III)-associated peptide fragments using RP-HPLC and the characterization of the modified amino acid residues by Edman degradation. The kinetics of the formation of Al(III)-associated ß1-40 and derived analogs is also highlighted.

5.1.1. Incubation of Al(III) and Fe(III) with ß1-40: Time-dependency

Exposure of 100 µM solution of ß1-40 to 200 µM $AlCl_3$ at pH 6.2 and 37°C initiated HPLC-detectable microheterogeneity after 24 h. Fig. 5.1 shows the generation of Al(III)-induced effect on the elution of ß1-40 over a course of 168 h when the metal:peptide mole ratio was 2:1 . This study was carried out at

pH < 6.5, where free Al(III) ions exists in solution as $[Al(H_2O)_6]^{3+}$ and the precipitation of $Al(OH)_3$ is prevented. When the incubated mixture was applied to the reversed-phase surface, the microheterogeneity seen during the first 24 h increased as time of incubation increased.

Verification of chromatographically pure Al(III)-ß1-40 peptide fractions

Determination of the compositions of Al(III)-ß1-40 incubation were performed by quantitative amino acid analyses on lyophilized pooled fractions. Typical results for a mean of three such analyses are shown in Table 5.1. Except for serine, histidine and methionine residues, there was no significant difference in the amino acid content with respect to control.

In order to identify the nature of the eluting components, the chromatographically-pure fractions (A, B, and C, Fig. 5.1) were collected and attached to a Sequelon-AA membrane for amino acid sequencing. The sequencing data for these fractions is given in Table 5.2. Edman degradation did not proceed beyond *(i)* the sixth cycle for fraction A, corresponding to blocking at Asp^7, *(ii)* the thirteenth cycle for fraction B, indicating blocking at His^{14}, and *(iii)* the 22nd cycle for fraction C, which would signify a block at Asp^{23}. The method of using Edman degradation to identify sites of blocking for chemically modified ß1-40 has been reported before (Vyas and Duffy, 1989) and was therefore considered significant. In order to obtain the complete internal sequence, peptide mapping was performed. The chromatographically-pure

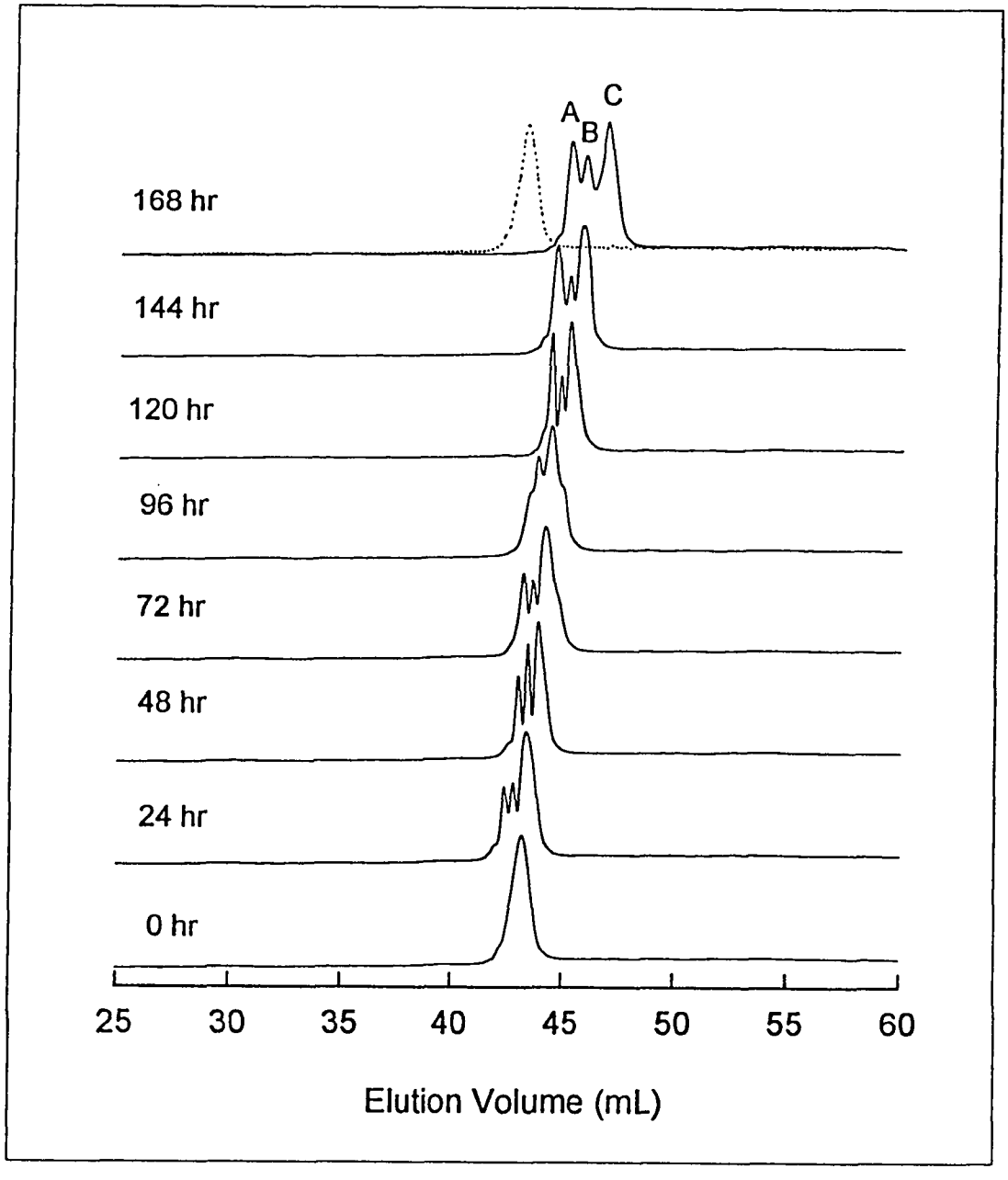

Fig. 5.1 RP-HPLC of ß1-40 incubation with Al(III), as a function of time. The metal:peptide mole ratio was 2:1, and the solutions were maintained at 37°C, in 50 mM Tris buffer at pH 6.2. Chromatography was performed on a 4.6 X 150 mm Vydac C_{18}, operated at room temperature using an AB gradient; solvent A was 0.1%TFA and solvent B was 0.1% TFA in 80% MeCN; flow rate was 1.0 ml/min, with a gradient time of 60 min. The volume of solution loaded varied between 10 and 50 µL. The dotted chromatogram in the top panel shows the ß1-40 control.

Table 5.1

Quantitative Amino Acid Analysis on Microheterogeneous Products of Al(III)–Incubation with ß1-40 [a]

Expected Composition	Fraction A[b]	Fraction B[b]	Fraction C[b]	Control[1]
D (4)[2]	2.62	2.54	2.73	3.76
E (4)	3.44	3.59	3.65	3.64
S (2)	0.19	0.15	0.21	0.29
G (6)	5.57	5.75	5.81	5.73
H (3)	1.89	1.92	1.99	2.12
R (1)	1.01	0.94	0.89	0.95
A (3)	2.75	2.63	2.73	2.89
Y (1)	0.79	0.85	0.81	0.89
V (6)	5.88	5.88	5.74	5.92
M (1)	0.33	0.39	0.24	0.41
I (2)	1.72	1.69	1.65	1.69
L (2)	1.79	1.72	1.75	1.82
F (3)	2.65	2.56	2.59	2.73
K (2)	1.67	1.72	1.61	1.74

a Mean of three analyses each from two independent incubations.
b Pooled fractions as per Fig. 5.1.
1 Control ß1-40 incubated for 168 hours.
2 Values in parentheses represent the expected amino acid content.

Table 5.2

Summary of Sequence Analyses of Chromatographically-pure Al(III)-Incubated ß1-40 Fractions

Preparation		Sequence Assignments
Fraction A		DAEFR*H***X***
Tryptic Digest	(i)	*D*AEFR
	(ii)	*L*VFFAE**X***
	(iii)	XAII*G*LXV*GG*VV
CNBr Digest	(i)	*D*AEFR**X***
	(ii)	*VGG***VV**
Fraction B		*D*AEFR*HDS*GYEV*H***X***
Tryptic Digest	(i	*D*AEFX
	(ii)	X*DSG*YEV*H***X***
	(iii	LVFFAE**X***
	(iv)	XAII*G*LXV*GG*VV
CNBr Digest	(i)	*D*AEFRHXXXXEV*H***X***
	(ii)	*VG*GVV
Fraction C		DAEFR*HDS***G**YEV*HH*QKLVFFAE**X***
Tryptic Digest	(i)	*DA*EFR
	(ii)	XDXXYEVXXQX
	(iii	LVFFAE**X***
	(iv)	XAII*G*LXV*GGVV*
CNBr Digest	(i)	*D*AEFRXD*S*XYEVXXQKLVF*F*A*E***X***

X Denotes that the PTH-amino acid was not identified.
X* Denotes that sequencing cycles did not proceed beyond that cycle.
The *underlined italics* denote that the yield of the PTH-amino acid was less than 0.25 relative to PTH-Phe[4] or PTH-Leu[17] during the sequencing cycle.

fractions A, B and C were pooled individually and subjected to CNBr and trypsin digests as described in methods (section 2.6). The tryptic digests of these pooled fractions were concentrated on Immobilon membranes and subjected to automated sequencing. The results obtained for the internal amino acid sequence of these fractions are summarized in Table 5.2. The digestion maps of these analyses indicated the desired sequence for each fraction. The CNBr digests of all the chromatographically-pure peptides indicated the –VGGVV– sequence which was expected for cleavage at Met^{35}.

Fe^{3+} is an effective competitor of Al^{3+} in plasma due to similar ionic sizes (Crumbliss et al., 1988). Ca^{2+} has a much larger ionic radius than Al^{3+} and the binding pocket in Ca^{2+}-binding proteins is large enough to accommodate Al^{3+}. Mg^{2+} is easily displaced by Al^{3+} in physiological systems since Al^{3+} binds 10^7 times more strongly to ATP^{4-}, and nanomolar quantities of Al^{3+}therefore effectively compete for phosphate (Martin, 1986b). Subsequently, metal ions Fe^{3+}, Ca^{2+}, Mn^{2+} and Mg^{2+} were individually incubated with ß1-40 to study the specificity of their association to the peptide. When these incubations were chromatographed on a reversed-phase column, only Fe(III) showed any significant generation of microheterogeneity. The elution profiles for the Fe(III) incubations are shown in Fig. 5.2. The observed chromatographic behavior of Fe(III) ions in generating microheterogenous products with ß1-40 is comparable to that of Al(III). The elution profiles for Mg^{2+}, Zn^{2+} and Ca^{2+} incubations with

ß1-40 on RP-HPLC and the subsequent characterization of eluting fractions by sequence and amino acid analyses are given in Appendix D for comparison.

5.1.2. Effect of pH on Microheterogeneity Production

The aqueous chemistry of Al(III) is controlled by pH. The predominant soluble form of Al(III) at pH 7.5 is $[Al(OH)_4]^-$ and the concentration of available Al(III), *i.e.*, $[Al(H_2O)_6]^{3+}$ is $10^{-11.5}$ M (Martin, 1986b). The caveat of overestimating the available Al(III), and therefore its complex formation at any given pH was highlighted earlier. It is important to use conditions which mimic a physiological milieu like phosphate buffered saline, however, the formation of polynuclear complexes makes it very difficult to study the Al-PO_4 system. The use of phosphate buffers was therefore avoided in this pH based examination of Al(III) and ß1-40 and derived analogs. It has been demonstrated that in phosphate buffers, Al(III) forms its insoluble phosphate salt above pH 5 (Harris, 1992).

With the Al(III):ß1-40 mole ratio fixed at 10:1, the pH of incubating mixture was varied between 2 and 10. All incubations were allowed to stand with occasional vortexing for 4 days. After incubating for 100 hours at room temperature, these solutions were chromatographed. The elution profiles of these solutions are given in Fig. 5.3. There was increase in microheterogeneity between pH 3 and 5, while incubations above pH > 7 did not have any significant increase of the Al(III)-ß1-40 fraction (compare pH 7 and 9).

To test if the observed chromatographic behavior was due to influence by interfering polyatomic aluminum species which are usually generated at pH > 5, incubations were performed in citrate buffer. The chromatographic profiles of these incubations are shown in Fig. 5.4. More microheterogeneity was observed over longer times in citrate than in tris buffer.

The corresponding incubations using pure peptide preparations of ß1-28, ß6-25, and ß8-40 were also studied chromatographically for Al(III) and Fe(III) association. The elution profiles after 120 hours incubation are shown in Fig. 5.5. A distinct effect of Al(III) and Fe(III) in generating microheterogeneity was observed for ß1-28, ß6-25 and ß8-40.

5.1.3. Temperature Effects

Metal and peptide solutions were incubated in varying mole ratios at several different temperatures for 24 h and the mixtures applied individually without any treatment to the Vydac C_{18} reverse phase under normal gradient conditions. The chromatograms for a 10:1 Al(III):ß1-40 mole ratio for the solution incubation temperatures between 22° and 65°C are shown in Fig. 5.6. In general, all the solution incubations of ß1-40 and its fragments followed similar trends, *i.e.*, as temperature was increased, the microheterogeneity increased.

The results obtained with ß1-40 were exciting and inspired similar studies with its derived analogs, ß8-40, ß6-25, and ß1-28. Subsequently, these derived peptide analogs were incubated under optimal conditions and their elution from reversed-phase surface monitored. Fig. 5.7 depicts the chromatographic profiles of a 10:1 mole ratio incubation between Al(III) and ß8-40, ß6-25, and ß1-28 at 45°C after 24 h. Characterization of these eluting components were done by (a) sequence analyses using Edman degradation, and (b) quantitative amino acid analyses. The sequence data for pooled fractions from Fig. 5.7, and after their tryptic treatment are summarized in Table 5.3. The quantitative amino acid analyses results of chromatographically-pure components are given in Table 5.4.

Fraction 8A indicated a block at position 14, and after tryptic mapping revealed modifications at positions 14, and 23. This suggests that Al(III) association in ß8-40 was at His^{14} and Asp^{23}. Fraction 8B was blocked at position 22, and subsequent tryptic digest revealed the modified residue position as Asp^{23}. Mapping of this fraction indicated only one modification. Similar treatment for the 1A and 1B fractions demonstrated that modifications had taken place at positions 7 and 23 which corresponds to Asp residues. The ß6-25 fraction, 6A initially yielded no sequence information, but its tryptic digest indicated a blocked residue at position 23. This was interpreted as blocking at Asp^{7} and Asp^{23}, which is in keeping with the observations with ß1-40. Fraction 6B was not amenable to sequencing beyond position 13, which indicated

modification at His^{14}. Its tryptic digest however revealed a block at Asp^{23}. All fractions indicated blocking at which was due to association of Al(III) and sequence analyses of the tryptic digests confirmed that termination of Edman degradation was due to irreversible blocking of the amino acid. It was interesting to note that only aspartic acid and histidine residues at Asp^{7}, His^{14} and Asp^{23} were modified in all these peptides, even though other candidates for modification exist. Modifications at Asp^{1}, Glu^{3}, His^{6}, Glu^{11}, His^{13}, Glu^{22}, and the adjacent pair of Glu^{22}-Asp^{23} in any of these peptides were not observed by the methods employed in this study.

Quantitative amino acid analyses of pooled fractions 8B, 6B and 1B are given in Table 5.4. The calculated serine content was lower than expected for all the peptides. The calculated methionine content for ß8-40 was also low, while the histidine content was poorly detected for these fractions.

5.1.4. Kinetics of Microheterogeneity of Al(III) incubations with ß1-40 and Derived Analogs

The time-course of microheterogenous products' generation was also followed at room temperature for varying ratios of Al(III) with ß1-40, ß6-25, ß1-28, and ß8-40. The Al(III):peptide ratios were based on quantitative amino acid analysis. The kinetic profiles of mass increase in microheterogenous

products are depicted in Fig. 5.8. Since the generation of microheterogeneity was slow compared to the elution time, the increase was considered to be an accurate assessment of its proportion in the incubation medium which was resolved on the reversed-phase surface. To verify that such a behavior actually corresponded to a process of association of Al(III) with ß1-40, control runs for ß1-40 solutions were also performed (dotted chromatogram, Fig. 5.1). The difference in the areas for the control and Al(III)-incubations were normalized to fit an irreversible associative kinetic model, which can be schematically given as $M \rightarrow (k)\ M_h$:

$$\ln [M_h] = \ln [M_h]_0 + k \cdot t \qquad (1)$$

where

$[M_h]_0$ is the initial mass of peptide based on amount injected, (*i.e.*) at zero time this is corresponds to area for pure ß1-40 (control),

$[M_h]$ denotes the normalized mass of the microheterogenous product at time t,

k is the rate constant of the association of Al(III) with ß1-40 in solution.

When the kinetic profiles for varying Al(III):peptide ratios shown in Fig. 5.8 were fitted to equation 1, good mathematical fits were obtained (shown by the lines) for the metal:peptide ratios of 10:1 to 1:10 studied.

It is seen from the kinetic profiles for Al(III):peptides that at least 25 mole percent microheterogenous product can be generated after 72 h for ß1-40 incubation, when the metal:peptide ratio was greater than 4:1. However, greater mole percentages were achieved with ß6-25 at the same metal:peptide ratio.

The plot quantifying production of the Al(III)-associated peptides under optimum conditions is given by the histogram in Fig. 5.9. This histogram demonstrates that the mole percent yield for the Al(III)-associated product was maximum for ß6-25 followed by ß1-28, then ß8-40 and finally ß1-40.

5.1.5. Discussion

The RP-HPLC strategy was employed to obtain chromatographically-pure fractions of metal ion-associated ß1-40 and derived analogs. Incubations of ß1-40 and derived analogs with Al(III) and Fe(III) showed considerable microheterogeneity which was resolved on reverse-phase chromatography. The microheterogeneity on Mg^{2+}, Zn^{2+} and Ca^{2+} was comparable to that observed with Al(III) and Fe(III) ions, however, none of the chromatographically-pure fractions indicated any amino acid block on sequence analyses (Appendix D). The generation of microheterogenous components increased with temperature and time. Optimum incubation conditions included increase in incubation temperature to 45°C, for 24 hours. The chromatographic behavior of these

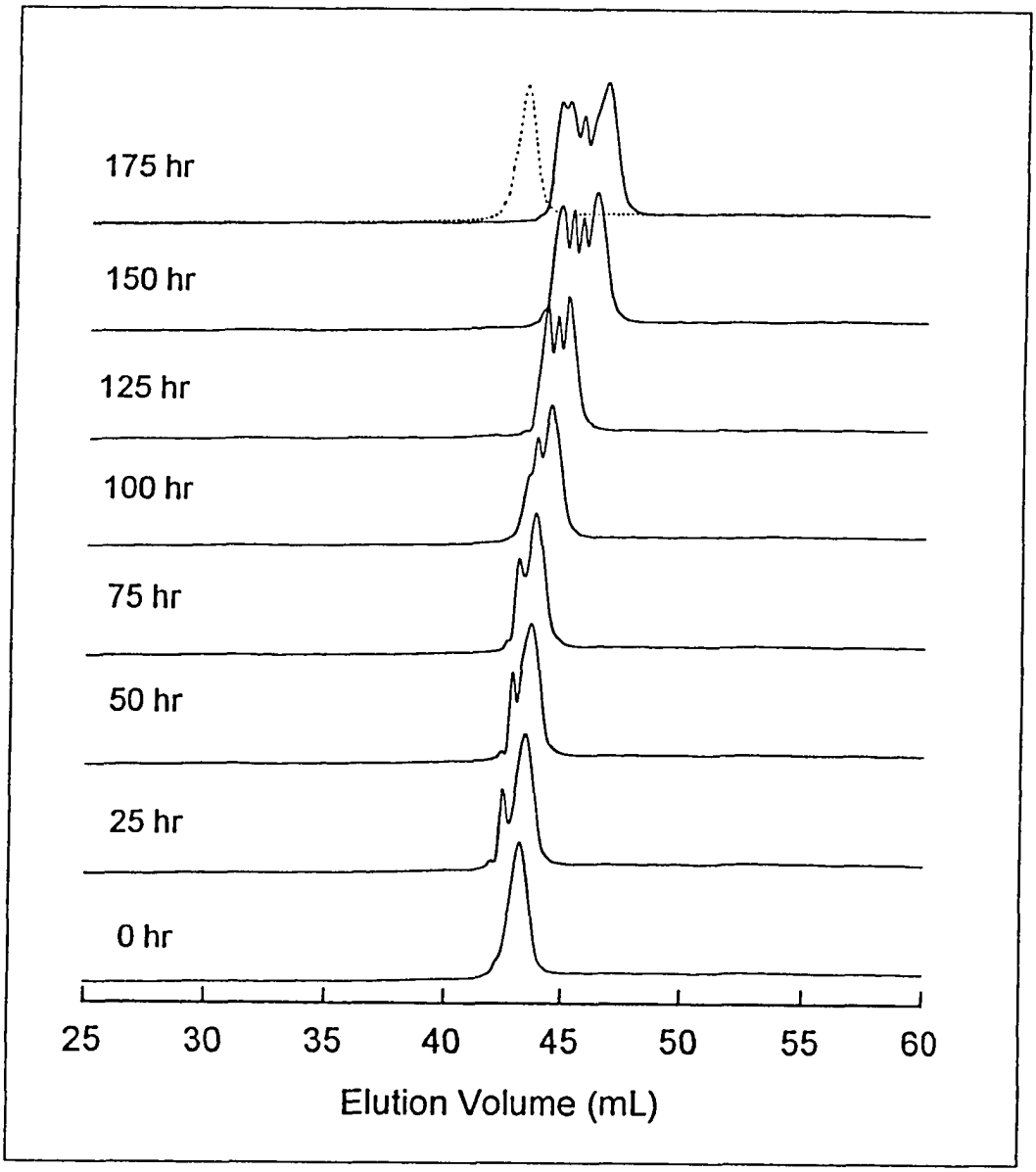

Fig. 5.2 RP-HPLC elution profiles of Fe(III) incubation with ß1-40 as a function of time. The incubation conditions were identical to the Al(III) incubations given in Fig. 5.1. The control incubation of metal:peptide at the end of 175 h incubation is indicated by the elution profile in the top panel by dots.

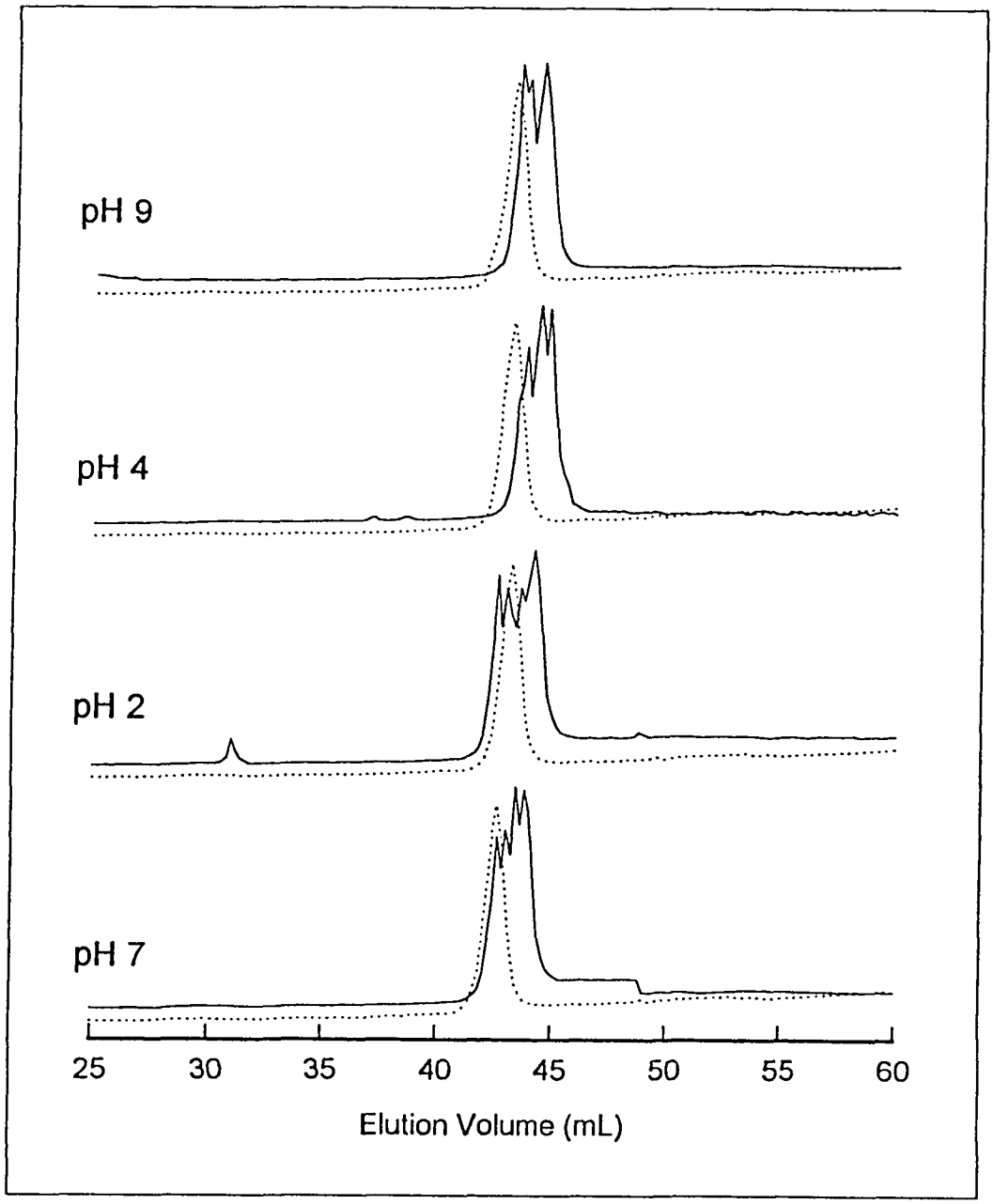

Fig. 5.3 RP-HPLC elution profiles of Al(III) and ß1-40: effect of incubation-pH. The incubations done at 25°C for 100 h, the solution s were introduced without any treatment on Vydac C_{18} as per conditions given in Fig. 5.1. The elution profiles for control runs are given for comparison (dots). The peak eluting around 32 min for the pH 2 incubation arose from an external impurity.

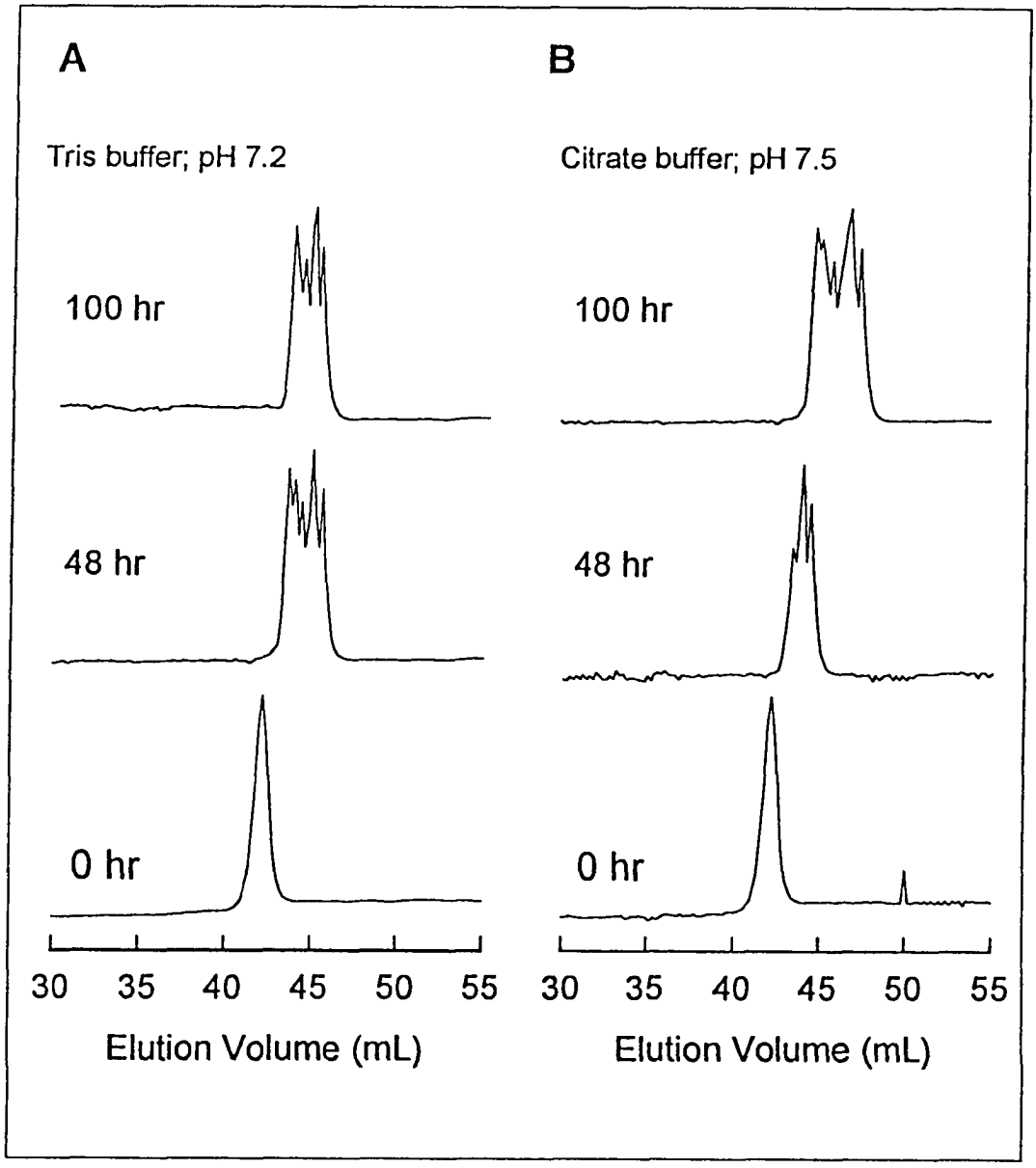

Fig. 5.4 RP-HPLC elution profiles for ß1-40 and Al(III) incubation as a function of buffer. Incubations were done at room temperature in 100 mM Tris buffer at pH 7.2 (panel A) and in 100 mM citrate buffer at pH 7.5 (panel B). The Al(III):ß1-40 mole ratio was 10:1. The samples were periodically drawn and chromatographed without any treatment according to conditions given in Fig. 5.1.

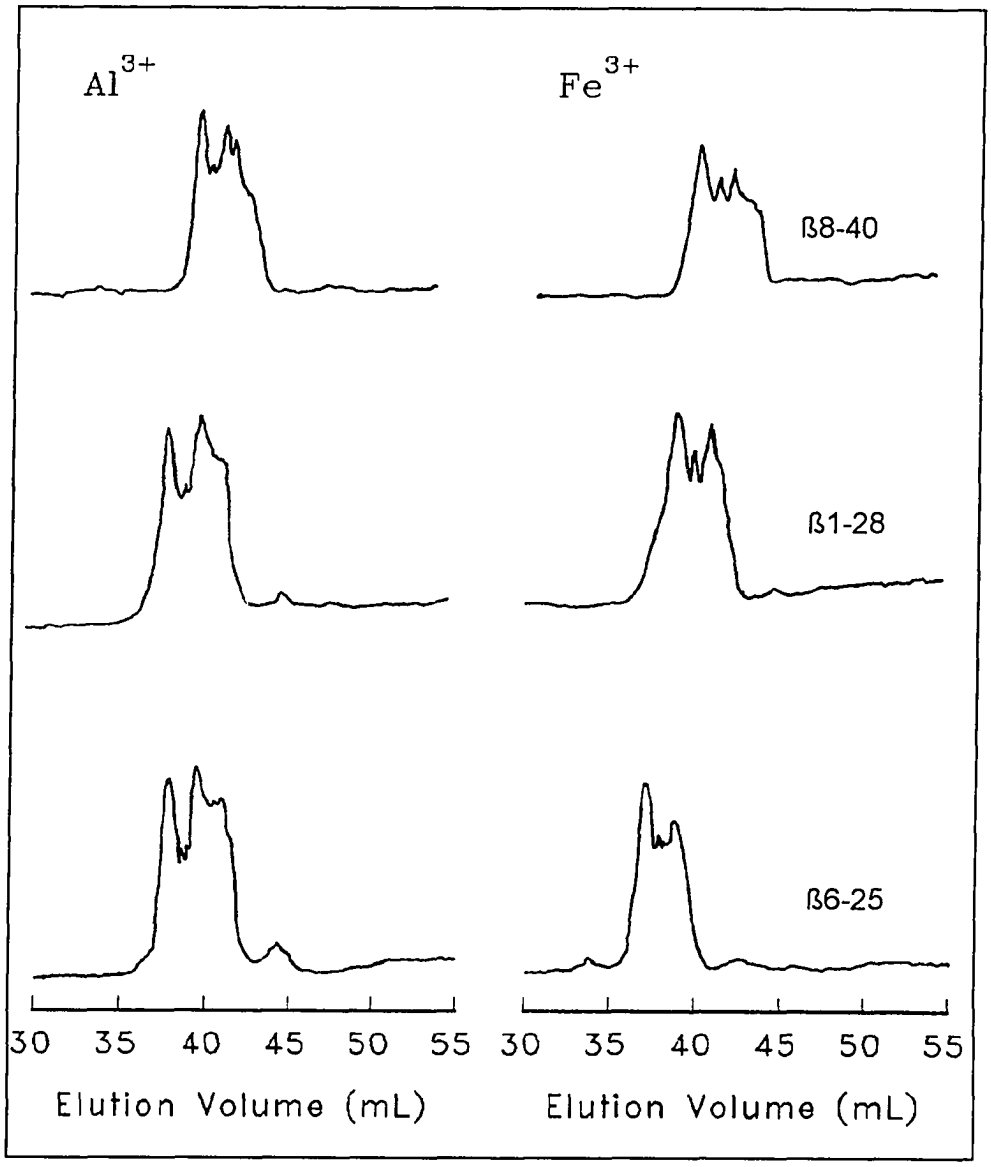

Fig. 5.5 RP-HPLC elution profiles for Al(III) and Fe(III) incubations with ß6-25, ß1-28, and ß8-40 after 120 hours. The metal:peptide mole ratios were 10:1; Incubations were pH 5.8 and ambient temperature at 28°C.

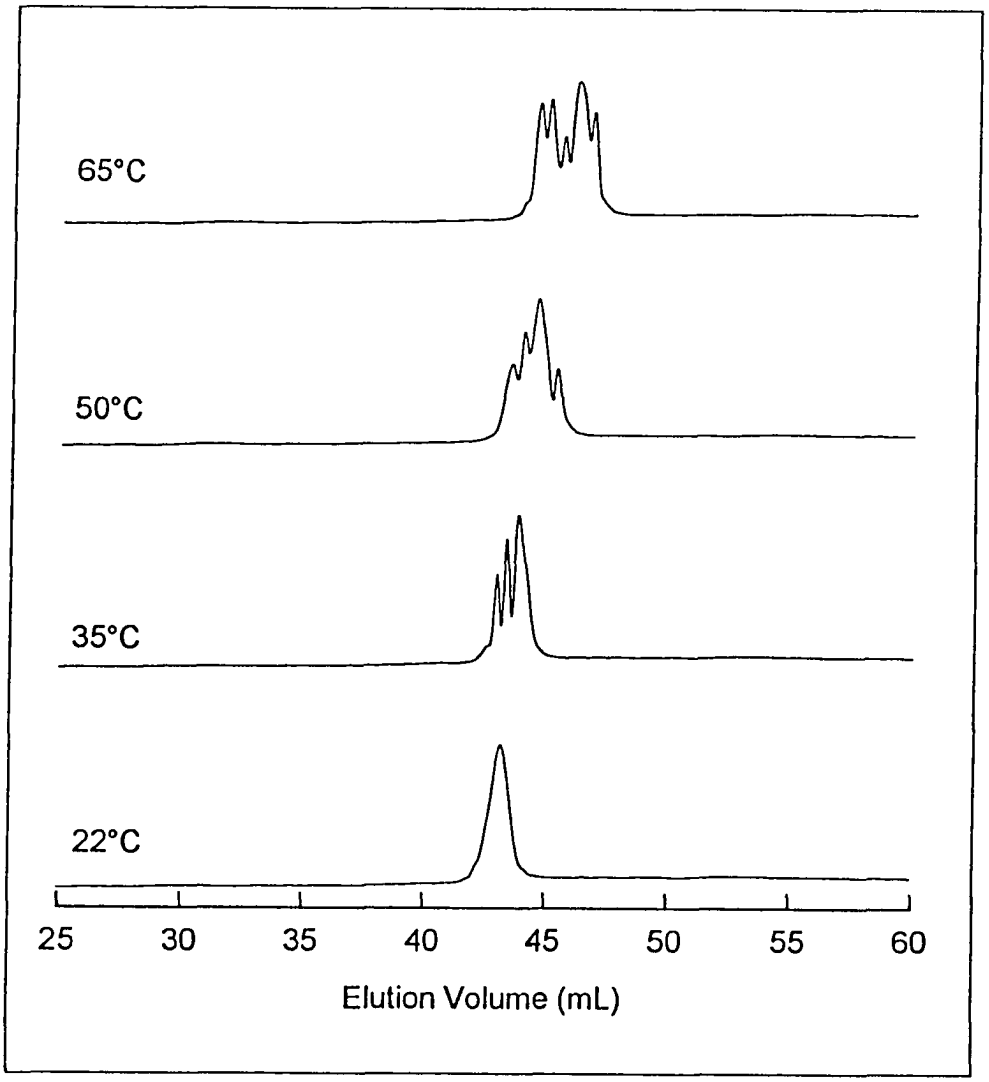

Fig. 5.6 RP-HPLC of Al(III):ß1-40 as a function of incubation-temperature at a mole ratio 10:1. All solutions were incubated for 24 hours between 22° and 65°C and were loaded without any treatment.

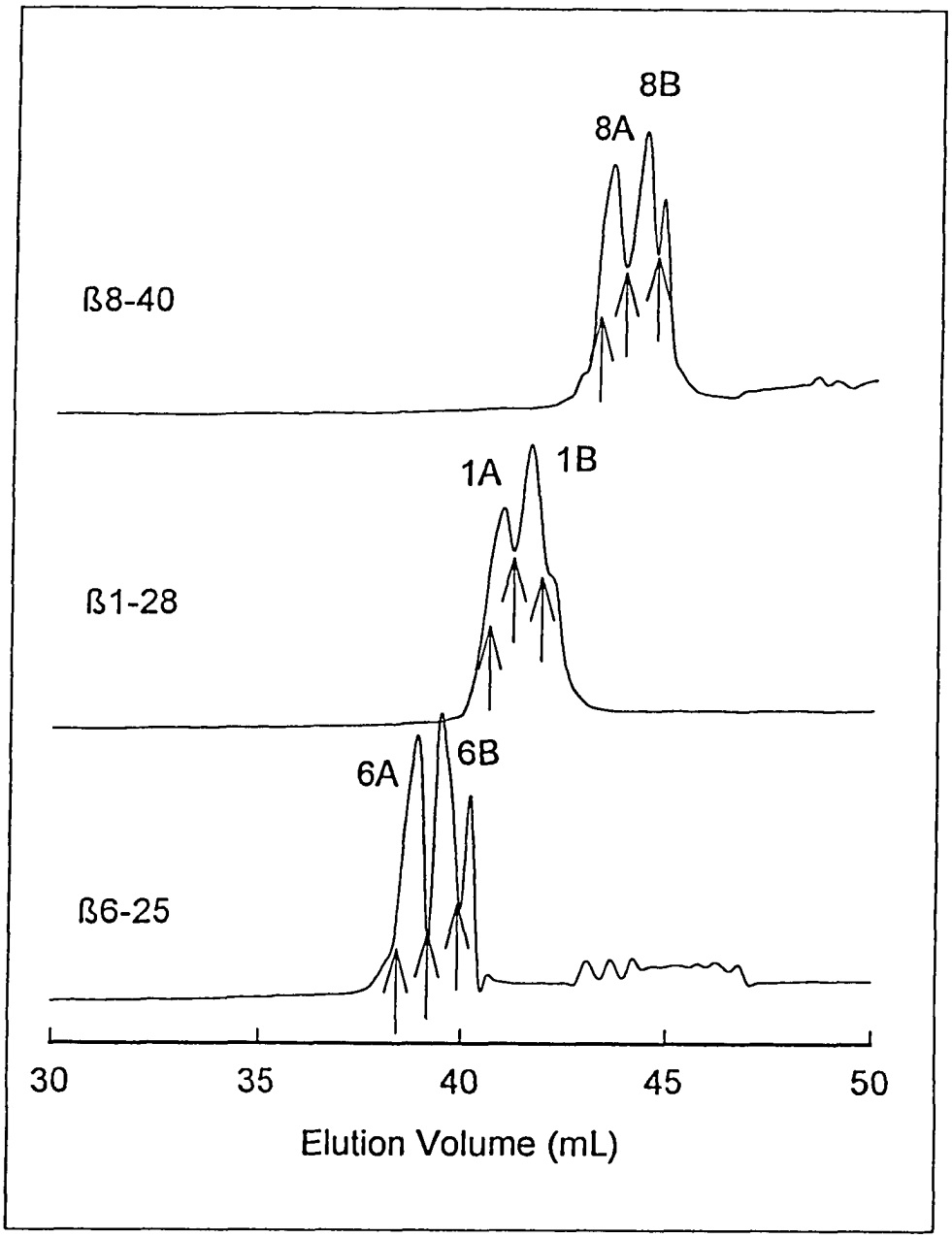

Fig. 5.7 RP-HPLC of Al(III) incubations with ß8-40, ß1-28 and ß6-25 after 24 hours at 45°C and mole ratio 10:1. All solutions were loaded without any treatment. The labels indicate the fractions which were collected at times marked by arrow. These fractions were characterized by sequence and quantitative amino acid analysis.

Table 5.3

Summary of Sequence Analyses for Al(III) Incubations with ß1-28, ß6-25 and ß8-40

Fraction	Sequence Assignment
8A	XGYEX*H*X*
On tryptic treatment	(i) XGYEX*H*X* (ii) XGYEV*HH*QX (iii) XVFFAEX* (iv) XAIXXLXV*GGV*V
8B	XGVXXQKLVFFAEX*
On tryptic treatment	(i) XGYEV*H*XQ (ii) *L*VF*FA*EX* (iii) XAIIGLM*VGGV*V
1A	*D*AEFRHX*
On tryptic treatment	(i) *D*AEF (ii) *L*VFFAEX*
1B	*D*AEFR*HD*SGYEVHX*
On tryptic treatment	(i) *D*AEF (ii) XXXGYEVHX* (iii) XVFFAEX*
6A	XX*
On tryptic treatment	(i) XVFFAEX*
6B	X*D*SGYEVHX*
On tryptic treatment	(i) XVFFAEX*

X Denotes that the PTH-amino acid was not identified.
X* Denotes that sequencing cycles did not proceed beyond that cycle.
The *underlined italics* denote that the yield of the PTH-amino acid was less than 0.25 relative to PTH-Phe[4] or PTH-Leu[17] during the sequencing cycle.

Table 5.4

Quantitative Amino Acid Analyses on Chromatographically-pure Al(III) Incubated Fractions of ß8-40, ß1-28 and ß6-25 [a]

Residue	Preparation		
	Fraction 8B [b]	Fraction 1B [b]	Fraction 6B [b]
D	1.62(2)[1]	3.47(4)[1]	1.42(2)[1]
E	2.64(3)	3.49(4)	1.55(2)
S	0.39(2)	0.19(1)	0.18(1)
G	5.77(6)	1.74(2)	1.70(2)
H	1.49(2)	1.74(3)	1.35(3)
R	0.09(0)	0.93(1)	0.19(0)
A	1.85(2)	1.77(2)	0.83(1)
Y	0.91(1)	0.82(1)	0.93(1)
V	5.89(6)	2.79(3)	2.67(3)
M	0.39(1)	0.17(0)	0.14(0)
I	1.77(2)	0.09(0)	0.05(0)
L	1.69(2)	0.89(1)	0.85(1)
F	1.75(2)	2.54(3)	1.53(2)
K	1.69(2)	1.77(2)	0.72(1)

[a] Mean of three analyses each from two independent incubations.
[b] Pooled fractions as per Fig. 5.8.
[1] Values in parentheses represent expected amino acid contents.

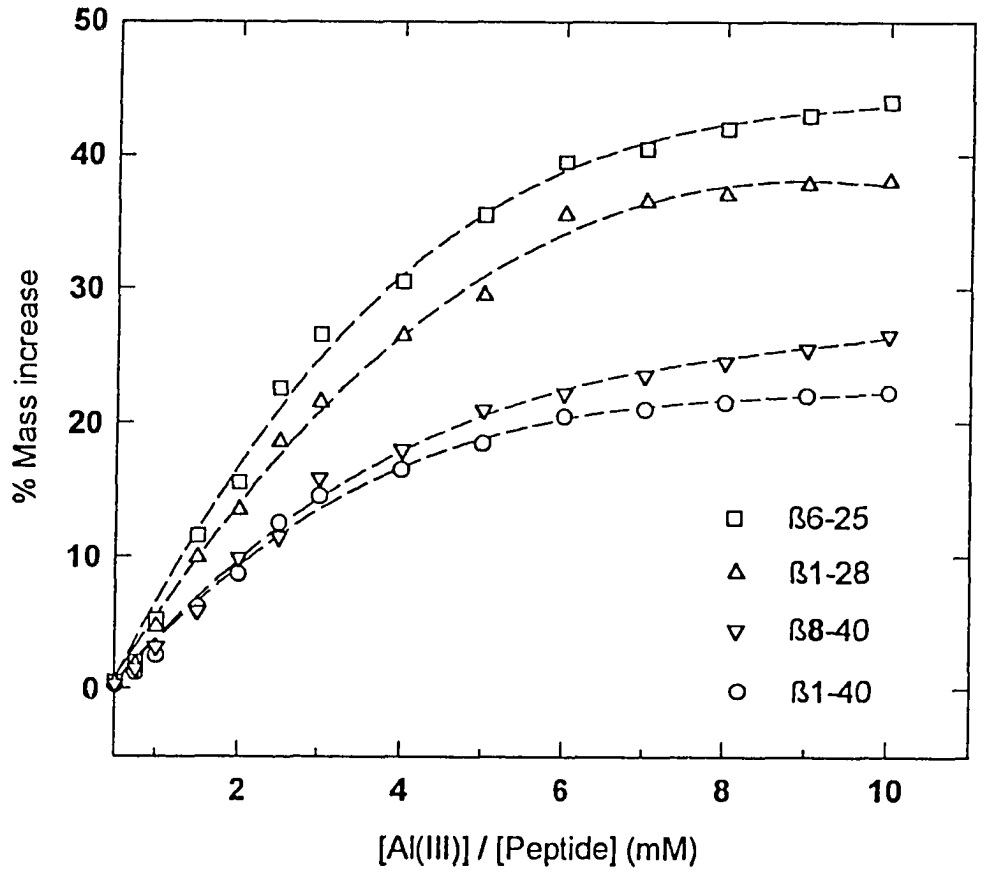

Fig. 5.8 Kinetic profiles for microheterogeneity production on incubation of Al(III) with ß1-40, 8-40, ß1-28 and ß6-25 by varying metal:peptide mole ratio. The mass increase (symbols) was normalized on the relative areas of the eluting components with respect to control runs. The broken lines are mathematical fits to the observed data according to equation 1. The fractions labeled A, B, and C were analyzed individually for their quantitatively amino acid analyses.

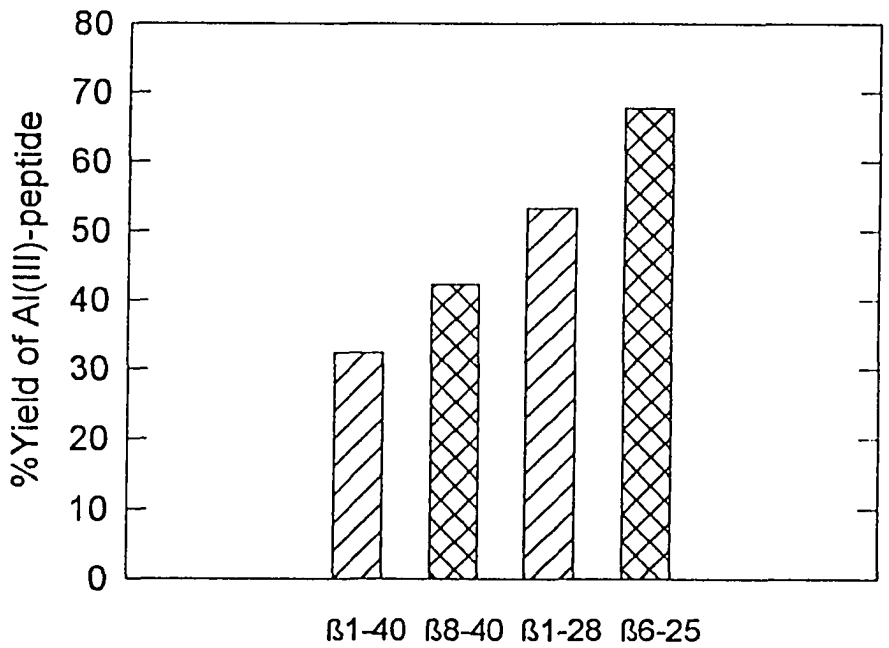

Fig. 5.9 Summary of yields for chromatographically-pure Al(III) associated pooled peptide fractions. A metal:peptide ratio of 10:1 was used for incubations which were performed at 45°C and pH 6.5-7.0. The solutions were chromatographed after 24 hours, the eluting fractions were pooled as per Fig. 5.8 and the resulting mass characterized by sequence and amino acid analyses. The yields represent the mean mass of each peptide from two incubations and three chromatographic runs, and were determined by normalizing elution volumes and quantitative amino acid analyses on the corresponding controls.

peptides in the presence of these trivalent metal ions demonstrate that microheterogeneity can be induced in peptide solutions by association. The verification of the nature of fractions which were resolved indicate modifications of amino acids only at positions 7, 14 and 23 which correspond to association of Al(III) with Asp^{7}, His^{14} and Asp^{23}. The kinetic profiles suggest that modification of the amino acids took place at a higher rate for the shorter than the longer peptides. One explanation of this observation could be that the ß6-25 fragment possesses the maximum number of Al(III)-chelating residues for its length. The similarities observed in elution profiles and sequence analyses suggest that these peptides must associate with Al(III) in a similar fashion.

Aspartic acid residues in proteins have been known to undergo nonenzymatic structural modifications spontaneously with age giving rise to unusual residues (Robinson and Rudd, 1974). This modification usually results from hydrolysis of the labile cyclized succinimide which is formed due to the intramolecular attack by the backbone nitrogen on the side chain carbonyl carbon (Stephenson and Clarke, 1989). The racemization of L-Asp residues in protein to form D-Asp, L-iso-Asp D-iso-Asp is enhanced by presence of the Asp-Gly and Asp-Ser sequence (Stephenson and Clarke, 1989). This modification however does not alter the mass of the resulting protein. External factors which accelerate amino acid racemizations include chelation, temperature, and to a lesser extent, higher pH levels (Buckingham et al., 1967; Bada, 1985). The intractable nature of amino acid sequencing observed in this

study, before aspartic acid residues at positions 7 and 23, and histidine at position 13 would imply that these residues had undergone structural alterations, which was facilitated by chelation with Al(III) and Fe(III). Interestingly, the amyloid core proteins from brain parenchyma were also resistant to Edman degradation and constituted a mixture of D- and L-stereoconfigurations of aspartates and iso-aspartates at positions 1 and 7 (Roher et al., 1993).

Shapira et al. (1988) had earlier observed 5% D-Asp and 2% D-Ser in their amyloid preparations. The modification of serine hydroxyl groups in ß1-28 has been documented (Orlando et al., 1992). The significantly low serine content found on quantitative amino acid analyses of all chromatographically-pure fractions from the Al(III) incubations with ß1-40 and its derived analogs is therefore understandable. The propensity for aspartate isomerization is also dependent on the adjoining carboxyl terminal amino acid (Stephenson and Clarke, 1989). This confirms the observations of altered amino acids observed by Roher et al. (1993) and Shapira et al. (1988), however, it does not explain the resistance to Edman degradation at His^{14} and Asp^{23} seen in this study. Neither does it explain the Edman reaction at position 1 of ß1-40. Perhaps, there are other local factors which take place in solution. It was therefore necessary to elucidate the effect of metal ion and peptide in solution by other means in order to characterize the nature of their interactions.

Anderson et al. (1990) used Al(III) salts to demonstrate *in vivo* racemization of aspartic acids within ten weeks in rat brain proteins. They

reported a significant increase in the D-Asp content which correlated with increase in brain aluminum levels. With higher brain aluminum levels however, there was saturation of aspartate racemization. An excess of [Al(III)] in the brain environment may act as a metal-ion buffer which effectively removes OH^-, and this apparent decrease in pH checks the racemization. This present study employed high pH (> 6), higher temperatures, and comparatively long incubation times. *In vitro* Al(III)-induced catalysis of D-Asp from L-Asp usually takes place within two weeks (Anderson et al., 1990). It is possible that with factors favorable for structural modification, the presence of Al(III) and Fe(III) provided the necessary impetus for racemization of amino acids in ß1-40 and its derived analogs.

5.2. Al(III) and ß1-40 Analogs: ^{27}Al NMR Examination

The ^{27}Al nucleus occurs at 100% natural abundance with good sensitivity versus ^{1}H, although its quadrupole moment confers broadened resonances with respect to other spin-½ systems. The quadrupolar broadening however amounts to a few hertz in most cases, which has made ^{27}Al one of the popular metal nuclei in NMR spectroscopy (Akitt, 1987). The width factor ($=Q^2(2I+3)/I^2(2I-1)$), which is the nuclear contribution to quadrupolar relaxation,

provides ^{27}Al with good relative sensitivity (0.207), demonstrating the offsetting influence of high spin on quadrupolar broadening (Akitt, 1987). Of the four magnetically active quadrupolar nuclei of group III, ^{27}Al is easily observed with respect to ^{69}Ga, ^{71}Ga and ^{113}In or ^{115}In. At room temperature, linewidths of 10 to 14 Hz for $[Al(H_2O)_6]^{3+}$ were routinely obtained on the JEOL FX90Q NMR Spectrometer used in this study.

The large charge-to-radius ratio of Al(III) enhances its interaction with ligands, especially oxygen and nitrogen, which is exceptionally strong; and, therefore, ligand exchange is rather slow on the NMR time scale. For instance, the H_2O exchange from hexaaquo Al(III), $[Al(H_2O)_6]^{3+}$, is 0.6 s^{-1} at 298 K even though the protons exchange independently at a rate of 10^5 s^{-1} which is also the rate at which Al^{3+} changes environment during hydrolysis (Akitt and Elders, 1985). The most prominent species in solution, *viz.*, $[Al(H_2O)_6]^{3+}$, however undergoes hydrolysis which is dependent on (i) its concentration, and (ii) pH of solution. The linewidths for $[Al(H_2O)_6]^{3+}$ are known to range from a couple of hertz to several kilohertz, depending on the experimental conditions (Akitt, 1987). Line broadening is observed if concentrated solutions are heated, but narrowing takes place on addition of acid (Akitt and Milic, 1984). Bottero et al. (1980) studied very dilute solutions of pure aluminum salts and determined a broad ^{27}Al resonance of 150 Hz for 1 mM $AlCl_3$. The linewidth increase was also attributed to the presence of polymeric cation which takes place at higher temperatures.

Additionally, the chemical shift of the ^{27}Al nucleus also varies with the ligand. It is generally assumed that the hexahydrate, $[Al(H_2O)_6]^{3+}$, resonates at 0 ppm irrespective of its method of preparation, a condition which has never been tested (Akitt, 1987). While this cation is very visible in all aqueous solutions and therefore used as a reference, the broader resonance of $[Al(OH)_4]^-$ at 80 ppm is also used by some NMR spectroscopists as reference although solutions need to be prepared carefully. Karlik and colleagues (1983) determined that with citrate as a ligand, ^{27}Al resonates at 8 ppm at pH 2, 10 ppm at pH 3, and at 12 ppm between pH 5 and 8. They also observed that EDTA in Al(III) solutions gave a complex with a broad signal near 32 ppm, while in the presence of lactate the chemical shifts were dependent on the way the solutions were prepared, and the pH. The source of line broadening seen with these ligands can also simply be due to the likelihood that the solution contains a "NMR visible" Al(III) species which is exchanging with a broader nonvisible species. The phenomenon of changes in linewidths of a quadrupolar nucleus as a function of chemical exchange rate is however common to all NMR active nuclei. ^{27}Al NMR spectroscopy therefore offers a unique perspective on Al(III) solutions in the presence of competing ligands, especially with complexes whose stability can be modulated by solution conditions.

It was clear that the changes in linewidths and chemical shifts were a good source of information of the ligand geometry of Al(III) in solution, the caveat being knowledge of the involved species. The complexation geometry of

aluminum can be divided into two regions depending on the chemical shifts: (i) the octahedral complexes, with coordination number 6, generally resonate upfield at 0 ppm, (ii) the tetrahedral complexes, with coordination number 4, are found downfield, at 80 ppm for $Al(OH)_4^-$ (Hinton and Briggs, 1978). The few exceptions to this general behavior are iodo-complexes (Haraguchi and Fujiwara, 1969), and solution-complexes of Al(III) in mixed solvents (Wehrli and Wehrli, 1981). In a nonaqueous solvent like MeCN, there is a upfield shift to -34 ppm for the octahedral $[Al(MeCN)_6]^{3+}$ species. The tetrahedral $[AlI_4]^{1-}$ also resonates much upfield at -27 ppm, while $[AlCl_4]^-$ resonates downfield at 104 ppm. Even though there are regions for the two types of complexes in a given solvent system, there is considerable overlap of chemical shifts and an exact interpretation of the coordination geometry of Al(III) then becomes slightly speculative.

5.2.1. ^{27}Al Interaction with ß1-40 in Aqueous Media

All Al(III) solutions were prepared in keeping with the ideas highlighted in the earlier sections and compiled in Appendix C. The association of Al(III) with ß1-40 was measured at ambient temperature, varying the metal:peptide mole ratio. For each NMR sample, the external reference was prepared simultaneously and at the same Al(III) concentration for Al(III):ß1-40. All

solutions of Al(III) were freshly prepared, allowed to equilibrate for 4 hours then centrifuged before introducing the peptide. Spectra were usually taken 6 hours after treating Al(III) solutions with ß1-40 and centrifugation. Typical spectra obtained for 1024 transients of various Al(III) concentrations on treatment with 10 mM ß1-40 at pH 4.5 are given in Fig. 5.10.

The NMR spectrum corresponding to Al(III) in aqueous buffer solution, *i.e.*, no ß1-40, is given at the bottom of Fig. 5.10, exhibits the major *NMR-visible* species of ^{27}Al at pH 4.5. The strong signal at 0 ppm corresponds to $[Al(H_2O)_6]^{3+}$, had a linewidth of 14 Hz, and was fixed as the reference. The sharp small signal just downfield of $[Al(H_2O)_6]^{3+}$ resonance was assigned to a spinning side band. The resonance of the tetrahedral species $[Al(OH)_4]^-$ was located nearly 80 ppm upfield of the $[Al(H_2O)_6]^{3+}$ signal. A weak signal was seen at 63.1 ppm and was assigned to a tetrahedrally coordinated polymeric Al_{13} complex, according to Bottero et al. (1980).

On adding 10 mM ß1-40, two significant changes were obvious from the NMR spectra: (i) there was a new, relatively broad, downfield signal having a linewidth of 850 Hz, near 15 ppm as ß1-40 was introduced, and, (ii) significant broadening of this downfield signal to 1250 Hz took place as the Al(III):ß1-40 ratio was increased. The signal near 15 ppm occurred only on introduction of ß1-40 in the samples, and was therefore attributed to Al(III) bound to ß1-40, i.e. the Al(III)-ß1-40 species. The position of the Al(III)-ß1-40 signal did not change but was considerably broadened with increase in [Al(III)]. Chemical shift and

linewidth data for small ligands, *e.g.*, citrate, oxalate, lactate and EDTA, which form octahedral complexes with Al(III) are given in Table 5.5. The chemical shift of the Al(III)-ß1-40 resonance was in the octahedral region of the spectrum.

Relative Intensity of the Al(III)-ß1-40 Resonance

The spectra in Fig. 5.10 illustrate that as the concentration of Al(III) was increased relative to ß1-40, there was an increase in intensity for the Al(III)-ß1-40 resonance. The presence of relatively broad resonances precluded interpreting peak integration data to detect the amount of aluminum bound in each observed species (Bottero et al., 1980; Fatemi et al., 1992). To quantitate the concentration of the species giving rise to the various resonances observed in the spectra, their intensities were measured relative to the reference. The ratio of intensities of Al(III)-ß1-40 and $[Al(H_2O)_6]^{3+}$ resonances against the respective mole content of metal:peptide is plotted in Fig. 5.11. The intersection of the titration curves from the plot of relative intensities suggests the stoichiometry of the observed species. If it is assumed that all the detectable ^{27}Al species were observed, then within these limits there are between 4 to 6 Al(III) bound to each ß1-40. The pH of these samples was verified both, before and after the NMR spectra were recorded to insure maintenance of the $[Al(H_2O)_6]^{3+}$ species.

EDTA titration of Al(III)-ß1-40

EDTA, a mixed oxygen and nitrogen ligand system, is a very effective chelator of metal ions and is routinely employed in Al(III) studies. The interest in choosing an Al(III)-EDTA system in the NMR study arose out of curiosity to verify the effectiveness of EDTA in chelating Al(III) in presence of ß1-40. The following conditions were of interest: *(a)* introduction of ß1-40 solution in an equilibrated solution of Al(III)-EDTA; *(b)* addition of EDTA to a solution containing the Al(III)-ß1-40 species; and finally, *(c)* adding an Al(III) to solution containing both ß1-40 and EDTA. It was necessary to generate the Al(III)-bound species, and the pH of the solutions were rigorously controlled.

Fig. 5.12 depicts the NMR spectra recorded for the verifying conditions stated above. A 10 mM equimolar mixture of $AlCl_3$ and EDTA was maintained at pH 4.5 for 4 h to satisfy conditions given in *(a)* according to Appendix C. After centrifugation, NMR spectrum was recorded as illustrated by the dotted line in the bottom panel. There are two prominent signals, a sharp signal at 0 ppm, and a very broad signal downfield resonating near 38 ppm having, $\Delta\nu \approx 900$ Hz. The resonances were assigned to the reference hexahydrate and Al(III)-EDTA respectively. Equimolar ß1-40 was added to the equilibrated mixture of Al(III)-EDTA, and after 24 h another spectrum recorded. This is illustrated by the solid line in the bottom panel of the ^{27}Al NMR spectrum in Fig. 5.12. On addition of ß1-40, there was a small reduction in intensity of the hexahydrate signal at 0 ppm. This decrease occurred with a simultaneous increase in linewidth

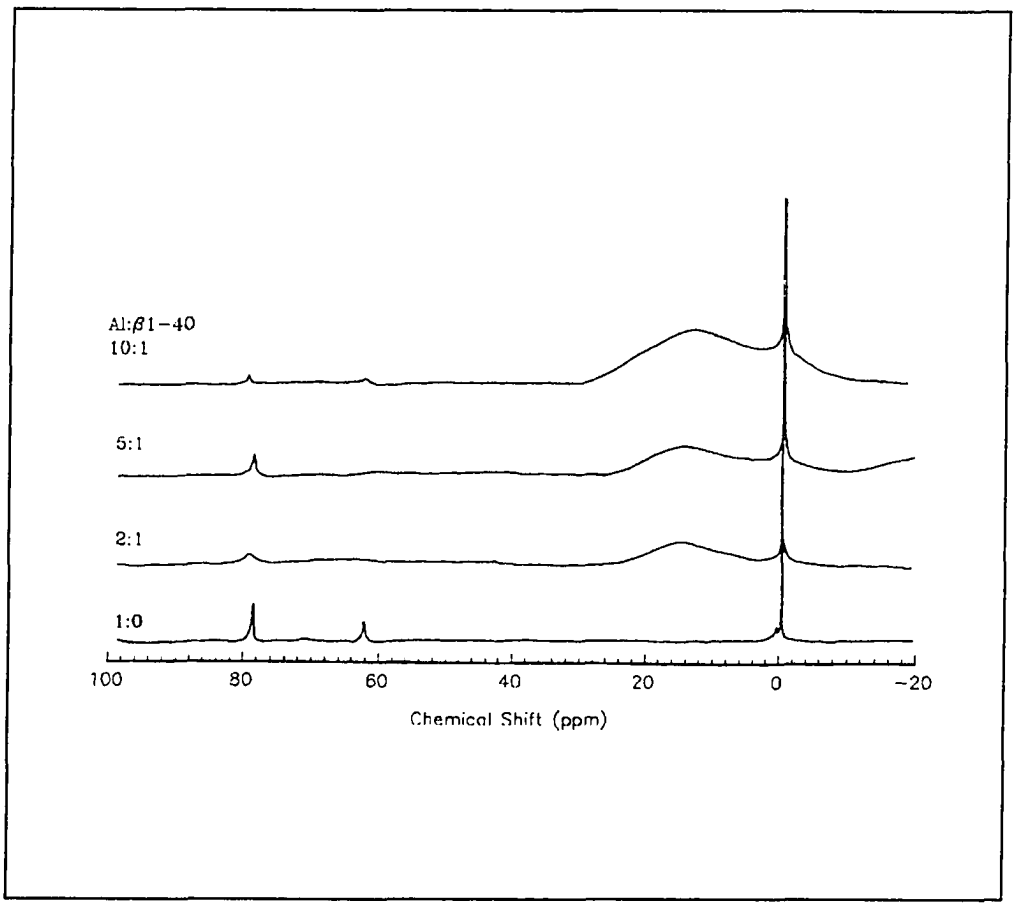

Fig. 5.10 ^{27}Al NMR spectra of Al(III) binding to synthetic ß1-40. The spectra were recorded on JEOL FX90Q operating at 23.30 MHz. All Al(III) solutions were aged for 4 hours before addition of 10 mM ß1-40 solutions at pH 4.5. Measurements were taken at room temperature 6 hours after introducing 10 mM ß1-40. The metal:peptide mole ratios are indicated. The sharp signal at 0 ppm is the reference signal for the hexahydrate, $[Al(H_2O)_6]^{3+}$ and the signal corresponding to the hydroxide is seen near 80 ppm. The weak resonance near 63 ppm corresponds to polymeric Al_{13} in the neat solution. The broad resonance near 15 ppm arises on introducing ß1-40 in the sample.

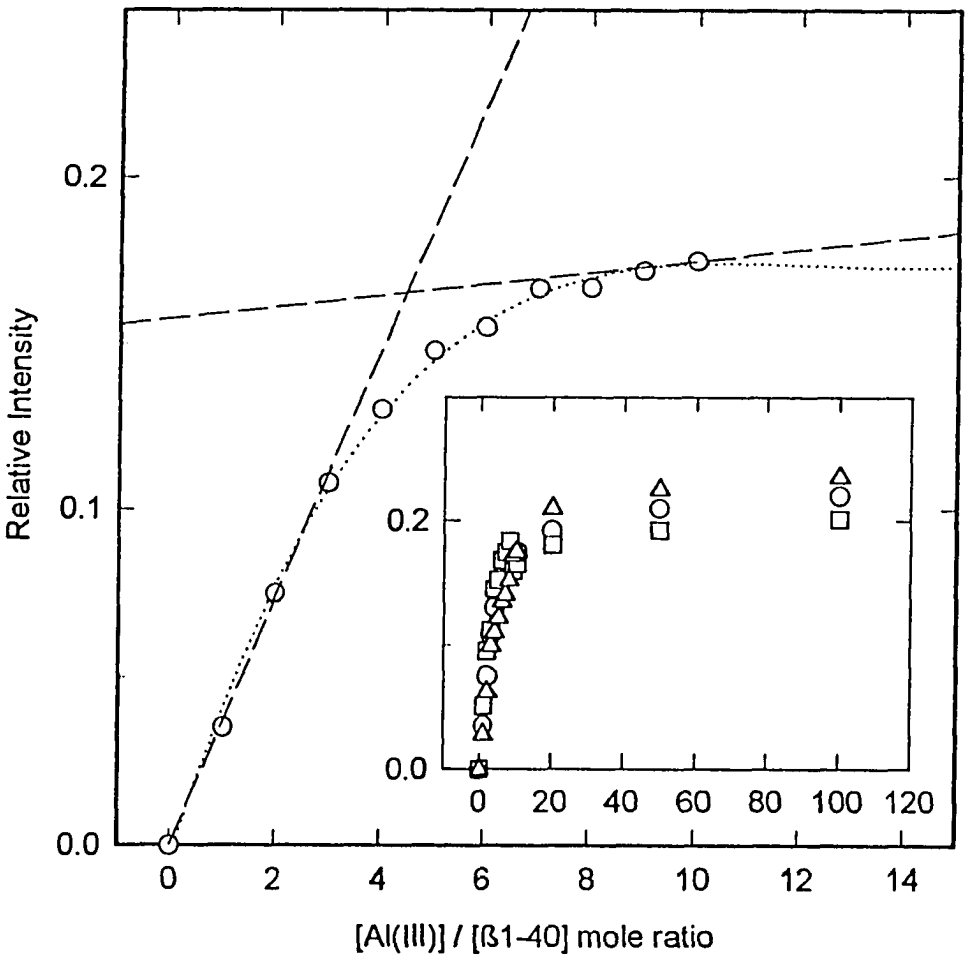

Fig. 5.11 Relative intensity of the ^{27}Al NMR resonance for Al(III)-ß1-40 as a function of Al(III):ß1-40 mole ratio. The intensity of the signal near 15 ppm was measured with respect to the external $[Al(H_2O)_6]^{3+}$ reference signal at 0 ppm. The data points are from spectra recorded at room temperature, pH 4.5. The inset shows titration curves for three separate measurements of relative intensities over a 100-fold excess of metal:peptide.

Table 5.5

^{27}Al NMR Chemical Shifts and Linewidths for Ligands at 23.30 Mhz [1]

Ligand	Chemical Shift (ppm[a])	Linewidth (Hz)	Coordination via[b]
Citrate (1:3)			OH^-, CO_2^-
pH 2.5	0 9	18 ≈ 1000	
pH 6.0	18	≈ 1200	
EDTA (1:1)			NH_2, CO_2^-
pH 2.5	0 38	14 ≈ 900	
pH 6.0	38	≈ 1200	
Oxalate (1:3)	18	N.D.	CO_2^-
Lactate (1:3)			OH^-, CO_2^-
pH 2.5	12	≈ 1100	N.D.
pH 7.1	25	v.broad	N.D.

[1]Spectral data obtained on JEOL FX90Q.
The numbers in parentheses signify the Al(III):Ligand ratios found in the octahedral complexes.
[a]The chemical shifts for resonances with large linewidths ($\Delta\nu \geq$ 100 Hz) are approximate.
[b] Information reviewed by Kragten (1978), and Akitt (1987).
N.D. not determined.

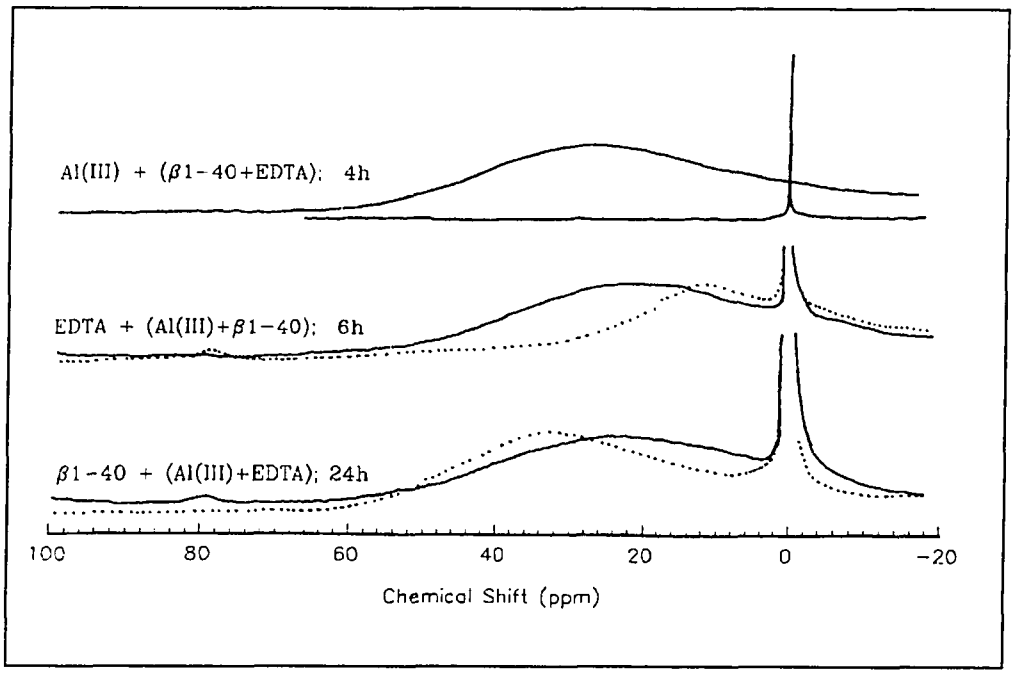

Fig. 5.12 Evolution of ^{27}Al NMR spectra for a 10 mM solution of Al(III)-ß1-40 on addition of equimolar EDTA. Bottom spectrum was taken 24 h after addition of ß1-40 to (Al(III)+EDTA); spectrum in the middle was taken 6 h after addition of EDTA to (Al(III)+ß1-40); spectrum at the top is for Al(III) addition to a mixture of (ß1-40+EDTA). EDTA and Al(III) were equimolar, with a mole ratio of 10:1 with ß1-40.

($\Delta\nu \approx 1600$ Hz) for the broader resonance. An Al(III)-EDTA solution without addition of ß1-40 maintained the chemical shifts and linewidths of its two Al(III) species. A slight upfield shift of the broad resonance ($\delta \approx 24$ ppm) is also evident from these two spectra. The Al(III)-ß1-40 species resonates near 15 ppm, and the increase in linewidth for the Al(III)-EDTA resonance on introducing ß1-40 indicated that these two Al(III) species were in a fast exchange situation.

The middle panel in Fig. 5.12 shows the ^{27}Al NMR spectrum which evolved 6 h after equimolar EDTA was added (solid line) to an equilibrated Al(III)-ß1-40 (dotted line). It is clearly seen that this spectrum reverted to that observed when ß1-40 was added to Al(III)-EDTA (compare the solid line spectra in the middle and bottom panels) with a prominent broad signal. The linewidth of the broad resonance near 24 ppm was found to be $\Delta\nu \approx 1200$ Hz, which was comparable to the observed linewidth on adding ß1-40 to Al(III)-EDTA. The disappearance of the resonance at 15 ppm with the simultaneous increase in linewidth for the broad signal indicated that the Al(III)-ß1-40 species must be in a fast exchange situation with the Al(III)-EDTA species.

To study the situation given by conditions in *(c)*, an equimolar solution of Al(III) was added to a solution of ß1-40 and EDTA which was allowed to equilibrate for 4 h. These ^{27}Al NMR spectra are given in the top panel of Fig. 5.12. The spectrum taken 4 h after addition of Al(III) is denoted by the dotted line. It is evident from the spectrum that there were no resonances other than that for the hexahydrate at 0 ppm. After 24 h, the ^{27}Al NMR spectrum

resulted in a broad resonance centered near 25 ppm and a complete disappearance of the reference signal (solid line). Although the chemical shift for this broad resonance could not be accurately determined, the linewidth was in excess of 1500 Hz which was comparable to those observed for the other two experiments. The eventual disappearance of the reference signal could be accounted by assuming, either *(a)* that all Al(III) was bound to the two ligands, or *(b)* Al(III) formed a nonvisible species in the presence of ß1-40 and EDTA. When the pH of this solution was decreased to 2, the spectrum reverted to the one observed before Al(III) addition to equilibrated solution of ß1-40 and EDTA (dashed line). This suggested that all Al(III) was bound to ß1-40 and EDTA, and was released as $[Al(H_2O)_6]^{3+}$ at low pH.

5.2.2. Al(III) Interaction with ß6-25 in Aqueous Media

ß6-25 was investigated primarily for the following reasons: (i) it is more hydrophilic than ß1-40 and has greater solubility, (ii) the coordinating ligands are potentially the same as ß1-40, viz., two histidine, two glutamate, and two aspartate residues, (iii) ß6-25 has a longer lag time of conformational change in solution.

The ^{27}Al NMR spectra of Al(III) and ß6-25 with incremental amounts of Al(III) are shown in Fig. 5.13. Solutions of Al(III) were equilibrated for 4 h and

then centrifuged. Spectra were taken on centrifuged samples which were equilibrated for 8 h at room temperature after adding ß6-25 in the desired ratio. The pH was diligently maintained at 6.0 and was again verified after accumulating the FIDs. A weak but broad resonance near 15 ppm ($\Delta\nu$ = 770 Hz) appeared for samples containing ß6-25. The intensity of this resonance increased as the Al(III):ß6-25 ratio was increased. This advent of this resonance, which was distinct from the reference signal, matched in position and intensity to that observed for Al(III)-ß1-40, and was therefore assigned to the generation of Al(III)-ß6-25 species. The intensities of the Al(III)-ß6-25 signal relative to $[Al(H_2O)_6]^{3+}$ are plotted in Fig. 5.14. The intersection of the titration curves of relative intensity versus the metal:peptide mole ratio indicates that there are approximately 6 Al(III) bound to each ß6-25 molecule. The chemical shift of this resonance indicates that Al(III) must be in an octahedral environment with ß6-25.

pH Titration of Al(III)-ß6-25 Species

The ^{27}Al NMR spectra of Al(III) containing ß6-25 were immensely affected by changes in pH of the solutions (Fig. 5.15). As the pH was increased from 6.1 to 7.5, there was an immediate reduction in the intensity of the signal near 15 ppm which disappeared within 2 h of change in the pH. There was a simultaneous appearance of a fairly sharp resonance ($\Delta\nu \approx$ 120 Hz) in the tetrahedral region of the spectrum at 80 ppm, which corresponds to the

generation of the aluminate. This result implied that all ß6-25 which was bound to Al(III) was exchanged by OH^- as the ligand. The maximal exchange in ligands occurred at pH 4.8 for ß6-25, while the equivalent change for ß1-40 indicated pH 4.2 to be more effective in the ligand change.

When the pH was decreased 6.1 to 1.5 by adding small increments of HCl, the intensity of the reference signal increased sharply (Fig. 5.15, panel B). There was a simultaneous reduction in linewidth which approached that of Al(III) salts in acidic environment ($\Delta\nu \approx 20$ Hz). The signal near 15 ppm gradually disappeared as the pH was lowered and below pH 3.5, was not detectable. These results imply that the hexaaquo species dominated in the acidic range. The presence of two separate resonances in the spectra between pH 4 and 6 indicates that the hexaaquo Al(III) was in slow exchange with ß6-25 in the ligand sphere.

The spectra also reveal a non-Lorentzian shape for the resonance near 15 ppm when the pH was between 4 and 6. The linewidth changes for the reference and the Al(III)-ß6-25 signals as a function of pH are shown in Fig. 5.16. These observations suggest that Al(III) was in slow equilibrium between the hexaaquo ion and the ß6-25-bound species. The maximal linewidth occurred near pH 6 indicating slow exchange occurring with the hexaaquo Al(III) below this pH and with the aluminate at higher pH. An upper limit for this slow exchange was calculated to be $\approx 10^4$ Hz. The change in linewidths was asymmetric as a function of pH, which meant that in the presence of ß6-25, the

hydroxide was a more effective ligand in exchanging the coordination sphere of Al(III) than water as a ligand. However, both these ligands displace ß6-25 from ligating Al(III) when $3.5 \leq pH \geq 6$.

When the pH was further increased, slight turbidity was observed beyond pH 7.5, and eventually a precipitate was formed. The solution was centrifuged and it was found that the precipitate dissolved only in acidic medium. The ^{27}Al NMR of this solution showed the exclusive presence of the hydrated ion resonating at 0 ppm. The spectrum did not change even after overnight equilibration. The dissolution characteristic of the precipitate strongly suggested that aluminate was formed.

5.2.3. ^{27}Al NMR of Chromatographically-pure Al(III)-bound Peptides

The microheterogeneous peptides observed on chromatographic analyses were studied for the presence of Al(III)-bound species. All observations were taken immediately after the peptides were prepared by RP-HPLC (section 5.1.3.). The ^{27}Al NMR spectrum of the chromatographically-pure fraction A (*cf.* Fig. 5.1) from the incubation of Al(III) and ß1-40 is shown in Fig. 5.17 (spectrum A). A moderately strong but broad resonance was located near 20 ppm was the most prominent feature in the NMR spectrum. This was assigned

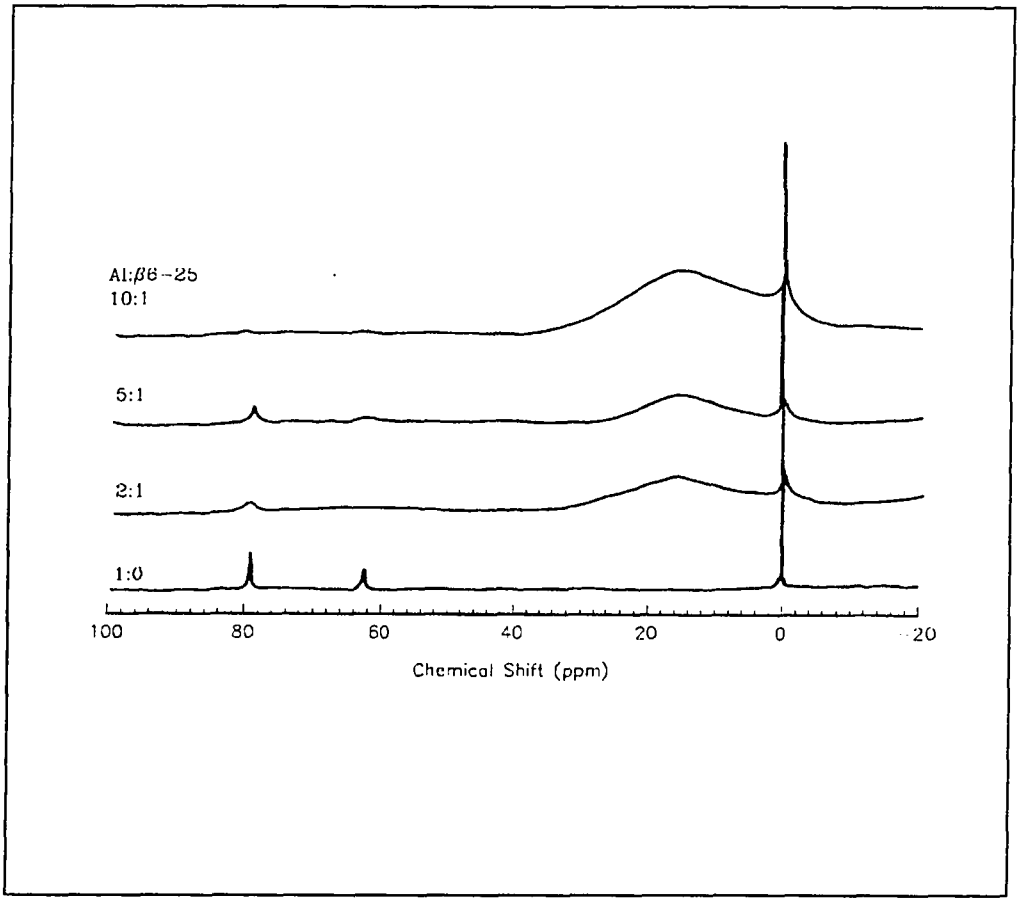

Fig. 5.13 ^{27}Al NMR spectra for Al(III) binding to 10 mM ß6-25 solution at pH 6.0. The solutions were equilibrated for 8 hours at room temperature before recording the spectra.

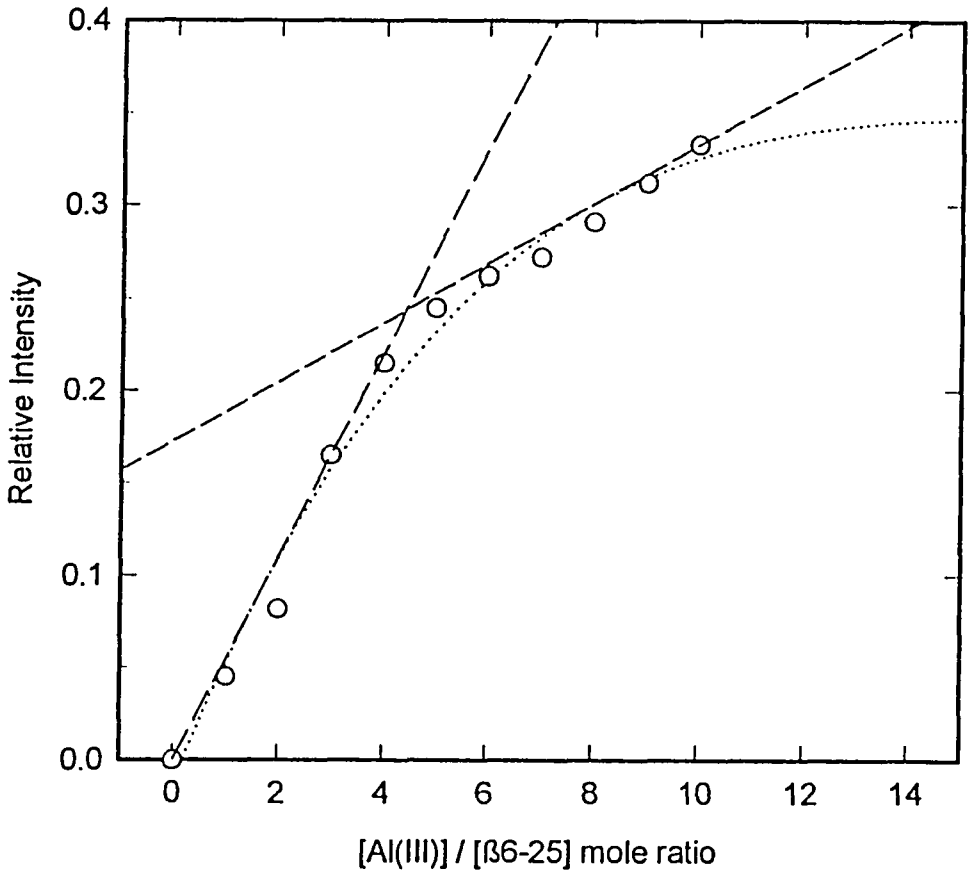

Fig. 5.14 Relative intensity of the Al(III)-ß6-25 resonance as a function of [Al(III)]. The intensity of the ^{27}Al NMR signal was measured against equivalent concentration of Al(III) resonating at 0 ppm. The relative intensity for the resonance near 15 ppm was at least 50% higher for ß6-25 than the equivalent mole ratio with ß1-40. The intersection of the straight lines gives the amount of Al(III) bound to each peptide molecule.

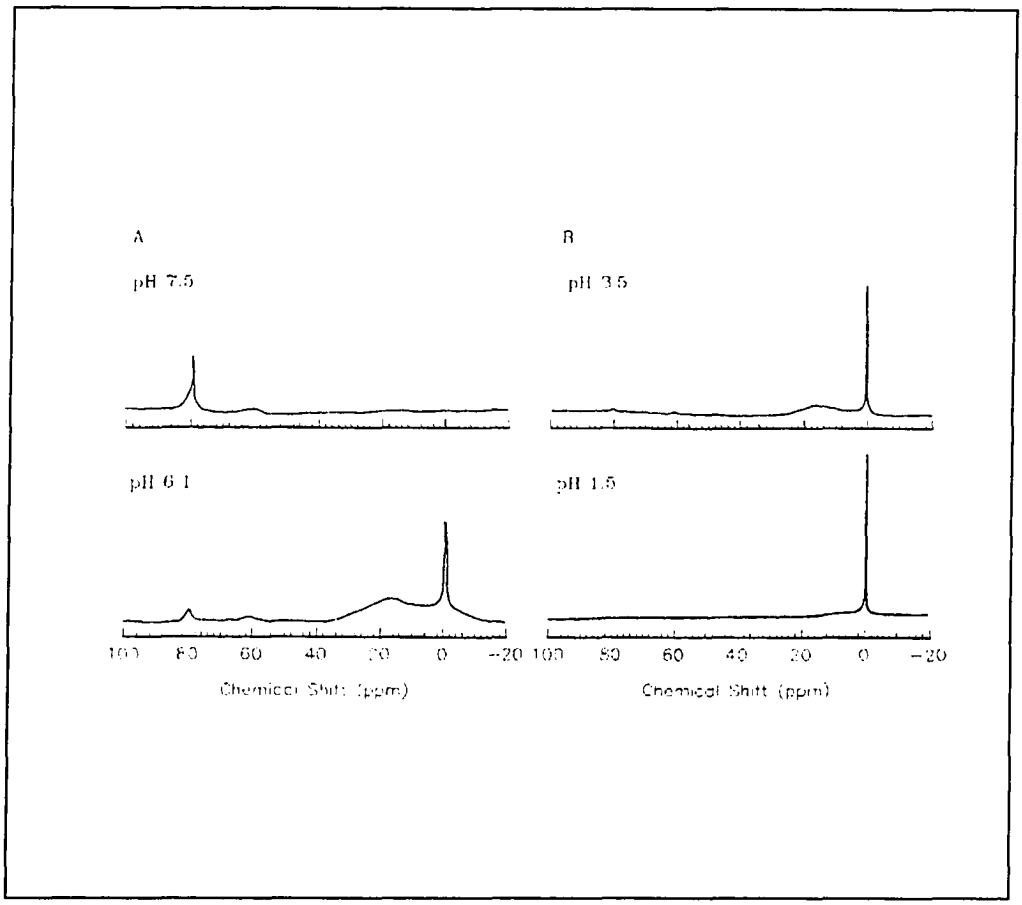

Fig. 5.15 ^{27}Al NMR spectra of Al(III) binding to 10 mM ß6-25 solution as a function of pH. Panel A denotes change in spectrum from pH 6.1 → 7.5; panel B denotes the change in spectrum from pH 3.5 → 1.5. The predominant Al(III) species at higher pH (≥ 6) is the tetrahedral hydroxide, $[Al(OH)_4]^-$ as seen from the resonance near 80 ppm, and at pH lower than 3.5, only the hexahydrate, $[Al(H_2O)_6]^{3+}$ is observed from the reference signal at 0 ppm. At slightly acidic pH (3.5 - 6), the resonance for the Al(III)-ß6-25 species can be observed near 15 ppm besides the hexahydrate signal.

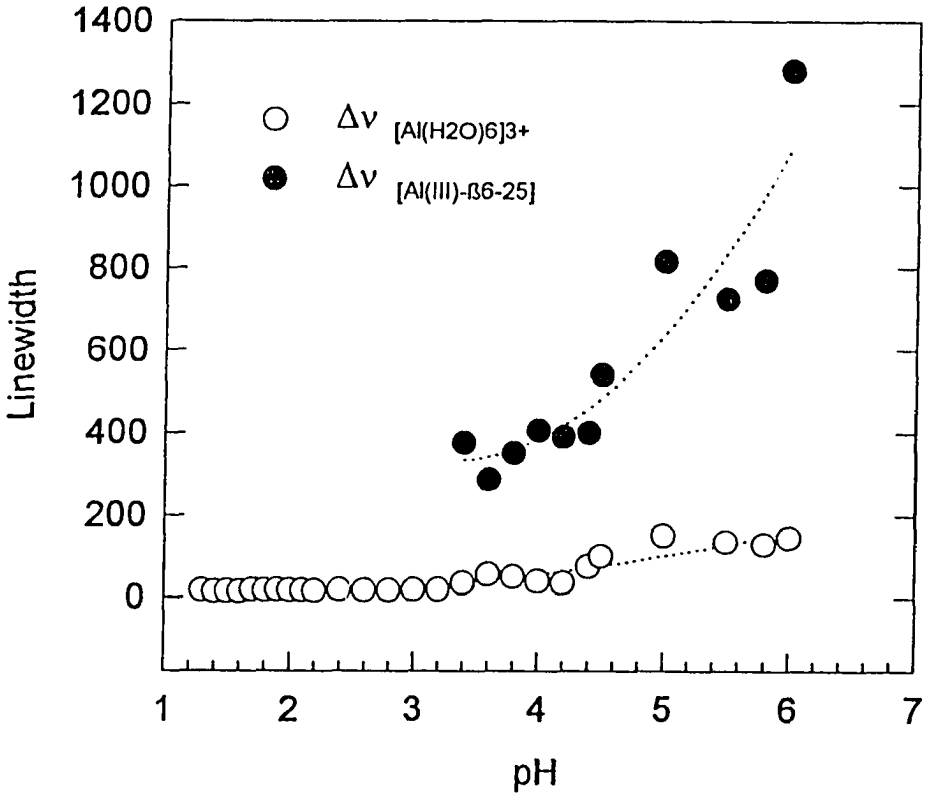

Fig. 5.16 Plot of linewidth change for $[Al(H_2O)_6]^{3+}$ and Al(III)-ß6-25 as a function of pH. The linewidths of the hexaaquo ion were measured according to spectral methods specified in chapter 2. The linewidth of the Al(III)-ß6-25 resonance was measured within 100 Hz.

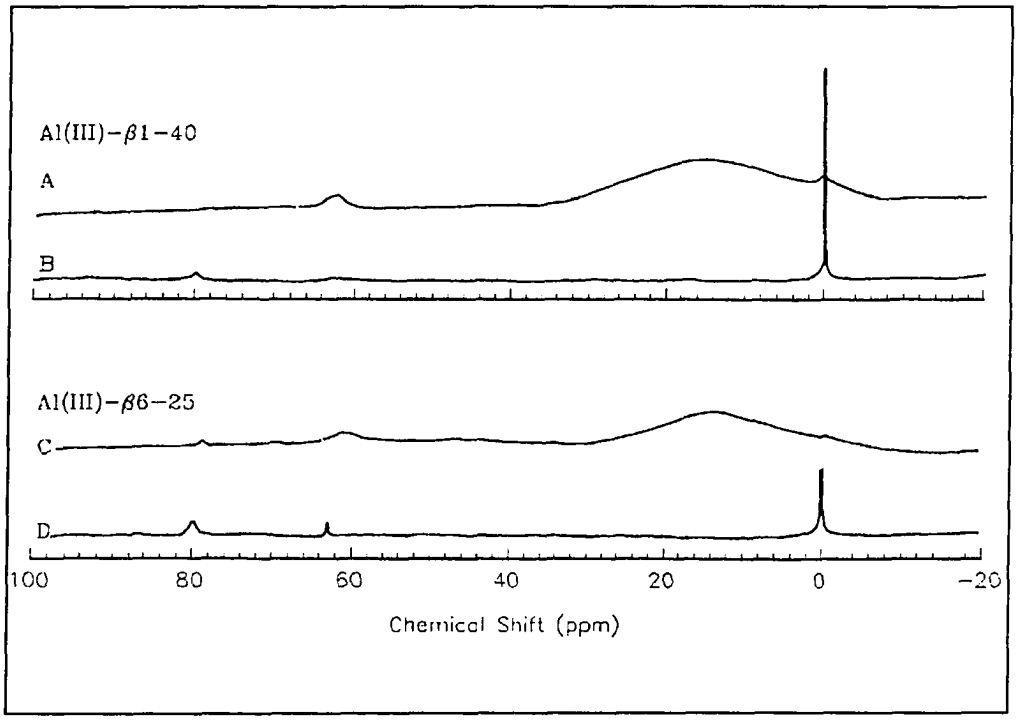

Fig. 5.17 ^{27}Al NMR of chromatographically-pure Al(III)-bound peptides. The top spectrum (**A**) is for Al(III)-ß1-40 corresponding to Fraction **A** from **Fig.** 5.1. The spectrum (**B**) shows the change after heating the peptide *in vacuo* with 100 µL of constant boiling HCl. (**C**) and (**D**) give the corresponding study with Fraction **6B** from **Fig.** 5.7 corresponding to Al(III)-ß6-25.

to the Al(III)-ß1-40 species present in fraction A. The relatively low concentration of the peptide fractions mandated longer accumulation times. At least 20 h were required to get satisfactory signal-to-noise ratio for a 0.5 mM solution. The signal/noise ratio did not improve after 20000 FIDs accumulations, and the linewidth was determined to be at least 1000 Hz. On addition of 100 µL of constant boiling HCl to the sample and heating *in vacuo* for 2 hours in an inert atmosphere, the resonance near 20 ppm disappeared and a sharp signal ($\Delta\nu \approx 24$ Hz) appeared at 0 ppm (spectrum B). This demonstrated that the Al(III) coordinated to ß1-40 in the chromatographically-pure product was completely displaced to give the hexahydrate species on acid treatment. The bottom panel in Fig. 5.17 shows the corresponding ^{27}Al NMR spectrum for fraction 6A (*cf.* Fig. 5.7) before (spectrum C) and after heating (spectrum D) with HCl and results similar to Al(III)-ß1-40 treatment were obtained.

5.2.4. Discussion

^{27}Al NMR spectroscopy provides an alternative avenue to explore the association of Al(III) with ß1-40 and ß6-25. The range of chemical shifts observed in these solutions is of interest since these variations provide clues to the geometry of the Al(III) associated species. The linewidths observed for the various Al(III) species are also of interest since these, along with information in

literature, indicate the ligand exchange taking place, a phenomenon which is popular among all NMR active nuclei. However, the finding of the ^{27}Al NMR resonance for chromatographicaily-pure peptide preparations very clearly demonstrated that Al(III) was complexed to ß1-40, very likely in 6:1 stoichiometry. The Edman reactions observed during sequence analyses must therefore be due to complexation of Al(III).

Oxygen and nitrogen are the principal donor groups involved during Al(III) complexation. It is seen that with oxygen as the principal donor ligand, the chemical shifts are usually upfield, whereas with nitrogen as the coordinating ligand, resonances are shifted to higher frequency (Wehrli and Wehrli, 1981; Akitt, 1987; Table 5.5). Of the ligands studied here, EDTA, with four carboxyls and two nitrogens, has the capacity to simultaneously occupy the coordination sphere of an octahedral metal ion (Kragten, 1978), giving rise to an inner-sphere complex. When coordination involves all six positions in an octahedral metal ion, the complex is usually very stable and exhibit resonance for one bound species. The signal located near 15 ppm on addition of ß1-40 and ß6-25 to Al(III) solutions presumably has all six ligand sites on Al(III) complexed by the peptides in a similar fashion.

It is therefore conceivable that complex formation in the Al(III)-peptides must be via the carboxylate groups of aspartates and/or via the imidazole side chain of histidine. The determination of at least four Al(III) binding per peptide molecule affirms the blocked sequencing sites at Asp^{7}, Asp^{23} and His^{14} in the

ß1-40 and its derived analogs on incubations with Al(III). Furthermore, the Al(III):peptide species is most possibly a symmetric octahedral complex. These Al(III)-peptide complexes were metastable within the experimental conditions but were affected by changes in pH. Moreover, these complexes existed only at pH between 3.5 and 6.1, *i.e.*, in the acidic range. At pH greater than 6.5, a strong presence of polymeric aluminum ion and the aluminate was detected. The lack of observation of any other resonance in the upfield region would suggest that any intermediate species did not exist.

A possible scenario for the complexation of Al(III) with ß1-40 and ß6-25 can now be visualized as taking place by simultaneous displacement of the ligands in the first coordination sphere of Al(III). Another possibility is that these are outer-sphere complexes. The line broadening observed as a function of pH suggests that the previous condition is more likely. There is a prominent broad resonance near 15 ppm between pH 3.5 and 6.1, which is not detectable beyond this pH range. Evidently, coordination by ß1-40 and ß6-25 results in displacing the water ligands from the hexahydrate, $[Al(H_2O)_6]^{3+}$. In the same token, at higher pH, the peptide ligand is displaced by the hydroxide. The structure of these complexes, however, needs to be verified by other techniques. It is also possible that due to the quadrupolar ^{27}Al nucleus giving rise to exceptionally broad resonances in an asymmetric ligand field, and the low field employed in this study, some Al(III)-peptide species were not detected, in which case other methodology needs to be developed. A similar observation was made by Fatemi

et al. (1992) after their study of aluminum complexes with albumin and transferrin using high frequency ^{27}Al NMR. Among processes besides quadrupolar nuclei which contribute to broadening, comprehending such data for Al(III) is marred with viscosity effects which are still not fully understood (Akitt and Milic, 1984). The linewidth data were therefore not exclusively interpreted here.

The study presented here also brings into question the validity of studies done by some researchers about the significance of trivalent metal interactions, especially Al(III) and Fe(III) with biomolecules. It was noted by Mantyh et al. (1993) that 1 mM Al(III) enhanced the aggregation of radioiodinated synthetic ß1-40 within 2 h at pH 7.4 by at least 100 fold. More recently, Kawahara et al., (1994) have demonstrated a direct effect of aluminum in aggregation of ß1-40 at pH 7. Their conclusions are particularly important to the study presented here in an attempt to discover the action of Al(III) in etiology of neurological disorders. However, the predominant Al(III) species above pH 6.5 are either the polymeric Al_{13} or the tetrahedral aluminate, neither of which are capable of providing Al(III) for complexation with ß1-40 and its derived analogs.

The discrepancy between observations made here and those currently available in the literature is however not mystifying in light of the following plausible explanations: (i) $[Al(OH)_4]^-$ is the predominant species in solution at pH $\rangle$ 6, even in the presence of buffer, (ii) the binding of Al(III) is maximum between pH 4 and 6 where free $[Al(H_2O)_6]^{3+}$ exchanges with ß1-40- and ß6-25-bound Al(III), (iii) given sufficient time, Al(III) is eventually released by the

Al(III)-EDTA complex when ß1-40 is present. In keeping with the bioinorganic chemistry exhibited by aluminum salts in solution, the Al(III) interaction studied here calls for reassessment of Al-induced aggregation experiments performed near physiological pH.

In spite of high quadrupole moment, the unique NMR properties of the ^{27}Al nucleus provided unequivocal evidence for its association with ß1-40. The low field ^{27}Al NMR investigation of ß1-40 and ß6-25 demonstrated that quadrupolar NMR spectroscopy can provide unique information about metal binding sites when used in conjunction with other studies. However, high frequency NMR can provide better determination of linewidth and chemical shift, which could be correlated to the nature of Al(III) bound in the complex. The observation of distinct Al(III)-peptide complexes provide protocols for non-invasive techniques in studying Al(III) interaction with peptides and proteins of biological importance.

5.3. Al(III), ß1-40 and ß6-25: Circular Dichroic Spectroscopy

The effect of aluminum at physiological concentrations (micromolar) on the conformation of ß1-40 was to decrease the α-helical and ß-pleated sheet content, (Exley et al., 1993). The importance of *available* aluminum has already

been emphasized in the interpretation of its solution effects (Martin, 1986b). The chromatographic evidence presented earlier demonstrate that the aluminum effects were manifested over time. It was also shown spectroscopically that between 4 and 6 Al(III) were bound with ß1-40 and ß6-25 only in the acidic region. Aluminum salts irreversibly block the calcium ion-channels formed by ß1-40 (Arispe et al., 1993). High molecular weight aggregation of ß1-40 was shown to be promoted *in vitro* at physiological pH by aluminum salts (Mantyh et al., 1993; Kawahara et al., 1994). These data indicate that the presence of aluminum greatly influences ß1-40 in solution.

Recently, substitution of D-Asp at positions 7 and 23 in the ß1-35 derived analogs was shown to hasten precipitation of these peptides from solution (Tomiyama et al., 1994). An increase in the aspartate racemization of brain proteins by aluminum was demonstrated (Anderson et al., 1990). In this section, the effects of Al(III) on the solution conformation of ß1-40 and ß6-25 derived analogs is presented. Titration curves of the ellipticity data were used to determine the number and nature of Al(III) binding sites. The importance of D-Asp at positions 1, 7 and 23 in ß1-40 and in 7 and 23 in ß6-25 was studied with respect to Al(III)-induced conformational change.

5.3.1. Effect of Al(III) on CD of ß1-40

The CD spectrum of a freshly prepared 250 µM solution of ß1-40 at pH 7.2 exhibited a predominant minimum at 210 nm and a shoulder at 224 nm (Fig. 5.18). This spectrum corresponded to the presence of 26% α-helix, 38% ß-pleated sheet, and 36% of other (as defined in section 4.1) structures on Varselec analyses (Table 5.6). Analyses using CCA yielded 23% α-helix, 42% ß-pleated sheet, and 35% of other structures. On addition of 0.5 mM Al(III) solution which was allowed to equilibrate for 4 h, another CD spectrum was recorded 4 h after addition and centrifugation of solution. The minimum at 210 nm was intensified while the shoulder at 224 nm disappeared. Deconvolution of this spectrum indicated that there was an increase in the $f_{ß}$ content with a concomitant decrease in the f_{α} content (Table 5.6). On addition of equimolar, in terms of Al(III), EDTA solution and recording another spectrum, it was evident that the effect of EDTA itself was minimal between 200 and 260 nm.

It was the purpose of this study to ascertain the effect of Al(III) on the secondary structure of the ß1-40 and derived analogs, but poor signal-to-noise ratio were usually obtained on addition of Al(III) and EDTA for all wavelengths below 240 nm. Most spectra were subsequently truncated at 195 nm, below which the noise level was not conducive for any meaningful CD determination. The changes in ellipticities at 210 and 224 nm with increase in Al(III) concentration are illustrated in Fig. 5.19. The plot shows a sigmoidal behavior

for the effect of Al(III) on ellipticities measured at 210 and 215 nm. Since the CD at 210 nm was more sensitive to change with Al(III) concentration and had good signal-to-noise ratios than that observed at any other wavelengths, ellipticities at this wavelength were titrated with Al(III).

The differences in observed mean residue ellipticities after addition of 0.5 mM $AlCl_3$ solution, and after addition of equimolar EDTA were calculated. When the fractional change in the mean residue ellipticity was plotted against the Al(III) concentration, a pseudo-sigmoidal dependence was noted as shown in Fig. 5.20. The fractional change is the ratio of the change in the mean residue ellipticity at any given Al(III) concentration to the ellipticity measured after equilibration with equimolar EDTA. The observed pseudo-sigmoidal behavior suggested that there was a cooperative effect of Al(III) on ß1-40. This titration curve can be considered to represent binding data in the same phenomenological sense as given by the Hill equation. The Hill equation for the change in ellipticity on Al(III) addition was thus defined as

$$\log K + n \log C = \log (R / 1 - R) \qquad (13)$$

where

K is a constant,

n is the Hill coefficient,

C is [Al(III)] concentration, and

R is the change in $[\theta]_\lambda$ at any given concentration of [Al(III)] divided by value of $[\theta]_\lambda$ on addition of equimolar EDTA after which no further change is observed.

A linear regression of the data near the midpoint of transition for the plot of fractional change versus Al(III) gave a straight line for the mean residue ellipticity at 210 nm (Fig. 5.21). When deducing the effect of concentration of [Al(III)] on the observed CD at 210 nm, a straight line (r = 0.881) was obtained with a slope of 1.67. The titration of CD of ß1-40 thus calculated the binding of at least 2 Al(III) with an apparent association constant of 150 µM. Additional Al(III) could be complexed to ß1-40, as derived from the NMR observations. However, the change in secondary structure due to this binding was not detectable by the CD method applied here. The aluminum-induced change in ß-pleated sheet character suggests that the complexation of aluminum is associated with conformational change.

Effect of Al(III) on CD for [D-Asp] Analogs of ß1-40

The primary evidence from sequence data from Al(III) incubations with ß1-40 and derived analogs was modifications at Asp^7, His^{14}, and Asp^{23}. When these were studied by NMR, the presence of aluminum was observed in the chromatographically-pure fractions. Also noted was the complexation of between 4 and 6 Al(III) per ß1-40 molecule in solution. Since it has been shown that D-Asp residues impart structural stability to the amyloid peptides, it was

imperative to verify the role of Al(III) for this modification on the peptide backbone. Subsequently, [D-Asp^{7}]ß1-40, [D-Asp^{7,23}]ß1-40, and [D-Asp^{1,7,23}]ß1-40 were synthesized and studied for conformational effects induced by Al(III).

Fig. 5. 22 depicts the spectral changes in CD of [D-Asp^{7}]ß1-40, [D-Asp^{7,23}]ß1-40, and [D-Asp ^{1,7,23}]ß1-40 solutions at pH 7.1 associated with addition of 0.5 mM Al(III) solution after 4 h. The following interesting features are seen from these spectra: there is a distinct minimum intensity between 210 and 215 nm, and no shoulder near 224 nm for any of these three derived analogs, compared to native ß1-40. The overall CD intensity varied with the number of D-Asp substitutions, being maximum for the triply substituted [D-Asp^{1,7,23}]ß1-40. On the introduction of Al(III), all these D-Asp analogs showed a distinct blue-shifting of the minima. The influence of Al(III) was maximum on the triply substituted analog which showed a significant reduction in the minimum near 210 nm and a simultaneous increase in the maxima near 200 nm. Exact quantification of overall CD intensity on addition of Al(III) was limited due to solvent absorbance. The influence of Al(III) on the spectral features shown by [D-Asp^{7}]ß1-40, [D-Asp ^{7,23}]ß1-40, and [D-Asp ^{1,7,23}]ß1-40 are consistent with the changes seen in native ß1-40, but opposite.

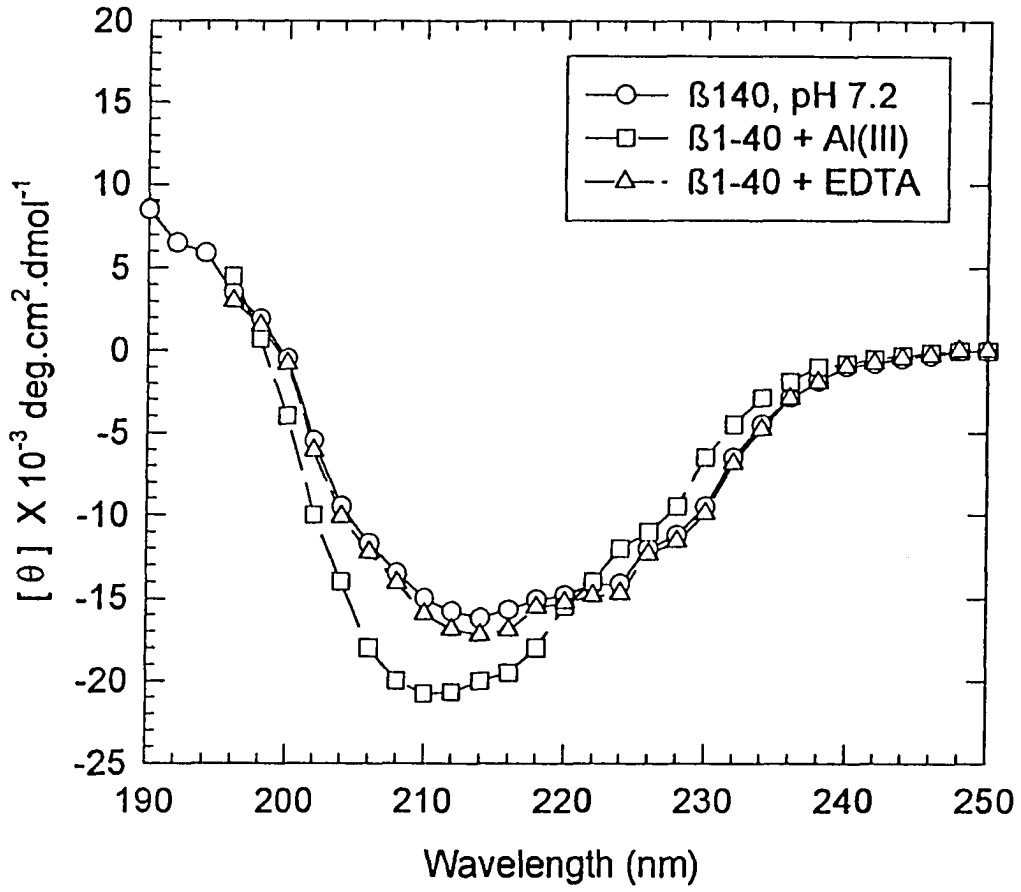

Fig. 5.18 Circular dichroism spectra of 250 µM ß1-40 at pH 7.2 with 0.5 mM Al(III) and EDTA. $AlCl_3$ was added to ß1-40 after equilibration for 4 hours at room temperature. The CD spectrum after 0.5 mM EDTA addition was taken 4 hours after addition of Al(III) to ß1-40. The concentrations are after dilution. Spectra for Al(III) and EDTA solutions were truncated at 197 nm due to excessive background absorbance. Each symbol represents the average of four individual CD measurements. The lines are generated on application of a cubic-spline algorithm to the observed data.

Table 5.6

Secondary Structure Content of ß1-40 in Presence of Al(III) and EDTA

	Varselec[1]				CCA			
	f_α	$f_ß$	f_o	*RMS*[2]	f_α	$f_ß$	f_o	*RMS*[2]
	(%)				(%)			
ß1-40, pH 7.2	26±3	38±4	36±3	654	23±3	42±3	35±3	975
+ 0.5 mM Al(III)	18±4	46±4	36±4	865	12±3	58±4	30±3	1119
+ EDTA	31±3	40±3	29±3	525	21±2	40±3	39±4	865
+ 0.25 mM Al(III)	23±4	35±4	42±4	645	21±3	48±4	30±3	819
+ EDTA	31±3	36±3	33±3	385	22±2	40±3	38±4	775
+ 0.10 mM Al(III)	18±4	46±4	36±4	854	12±3	58±4	30±3	1225
+ EDTA	24±3	35±3	41±3	475	18±2	39±3	43±4	965

1 All fractional percentages from Varselec analyses were normalized to 100.
2 RMS values are in deg · cm^2 · $dmol^{-1}$.

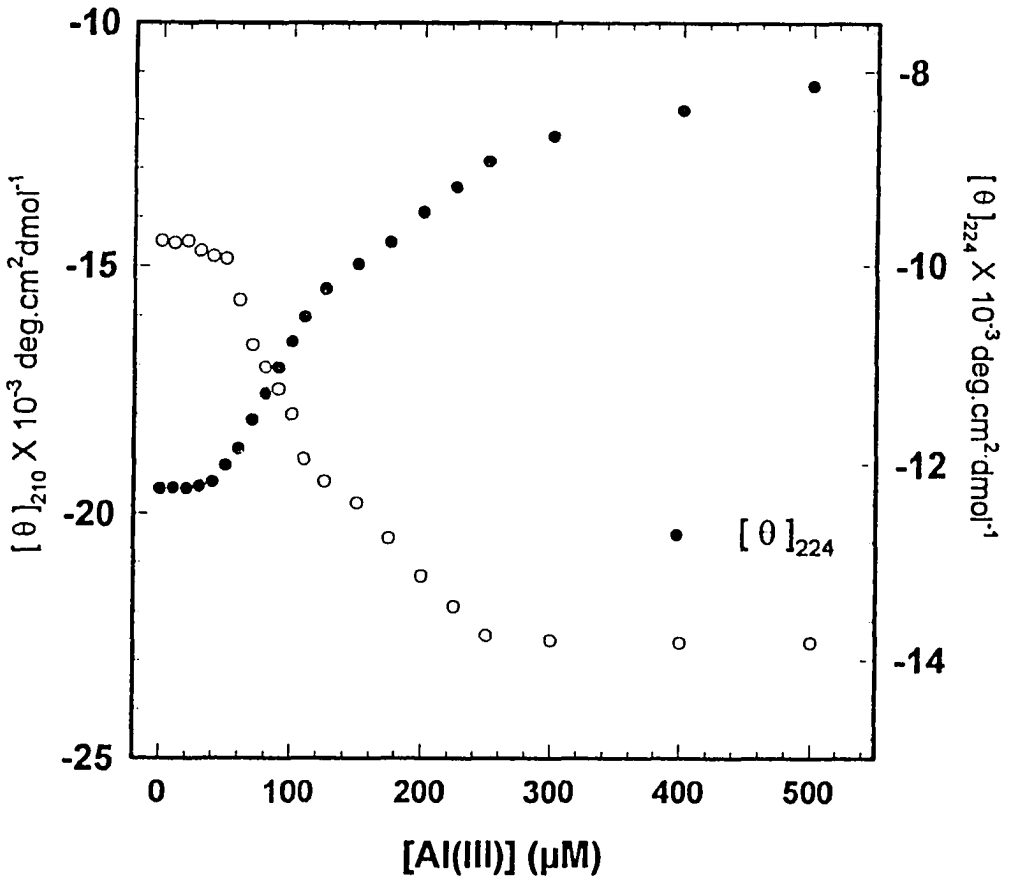

Fig. 5.19 Comparison of the mean residue ellipticity at 210 and 224 nm on addition of Al(III) to 250 μM solution of ß1-40. The observed ellipticity is given as an mean of four individual measurements, open symbols are for 210 nm and solid symbols for 224 nm. The molar ellipticities for the wavelengths are given at two different scales.

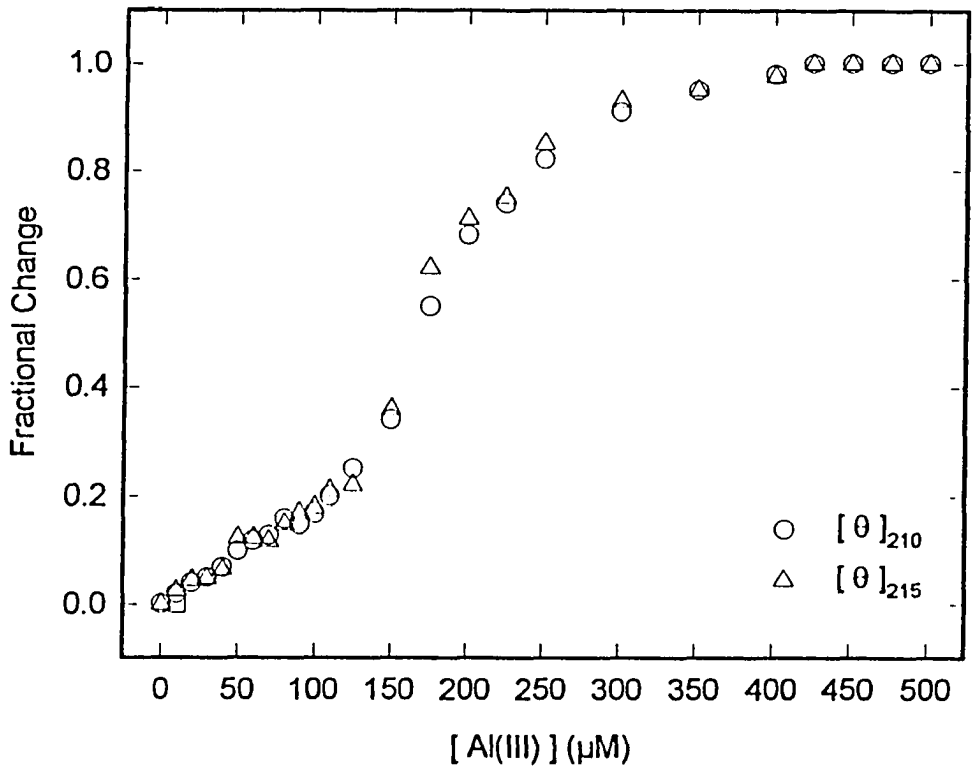

Fig. 5.20 Fractional change in mean residue ellipticity at 210 and 215 nm for Al(III) titration of CD of the CD spectra of ß1-40. Each data point represents the average of four spectra. The fractional change in mean residue ellipticity is the ratio of ellipticity at the given [Al(III)] and the observed ellipticity after addition of equimolar EDTA to the solution of Al(III) and ß1-40.

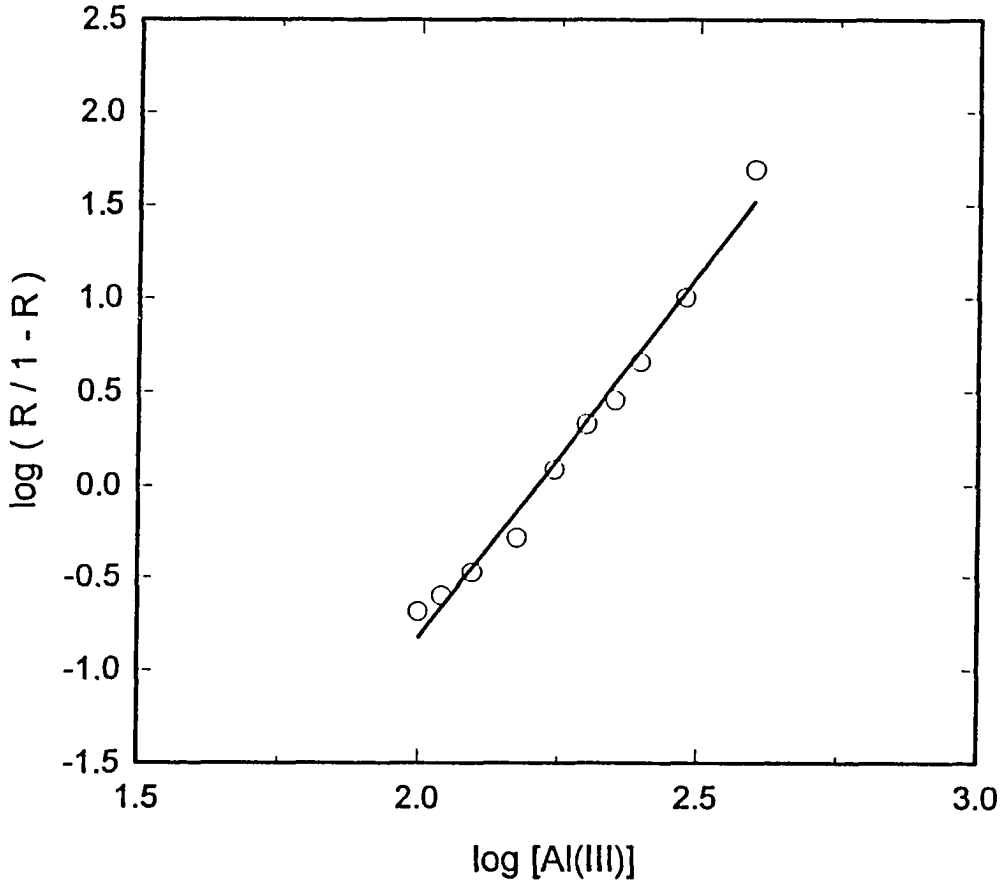

Fig. 5.21 Hill plot of CD data near midpoint of pseudo-sigmoidal transition of the fractional change in mean residue ellipticity titration of ß1-40 with Al(III).

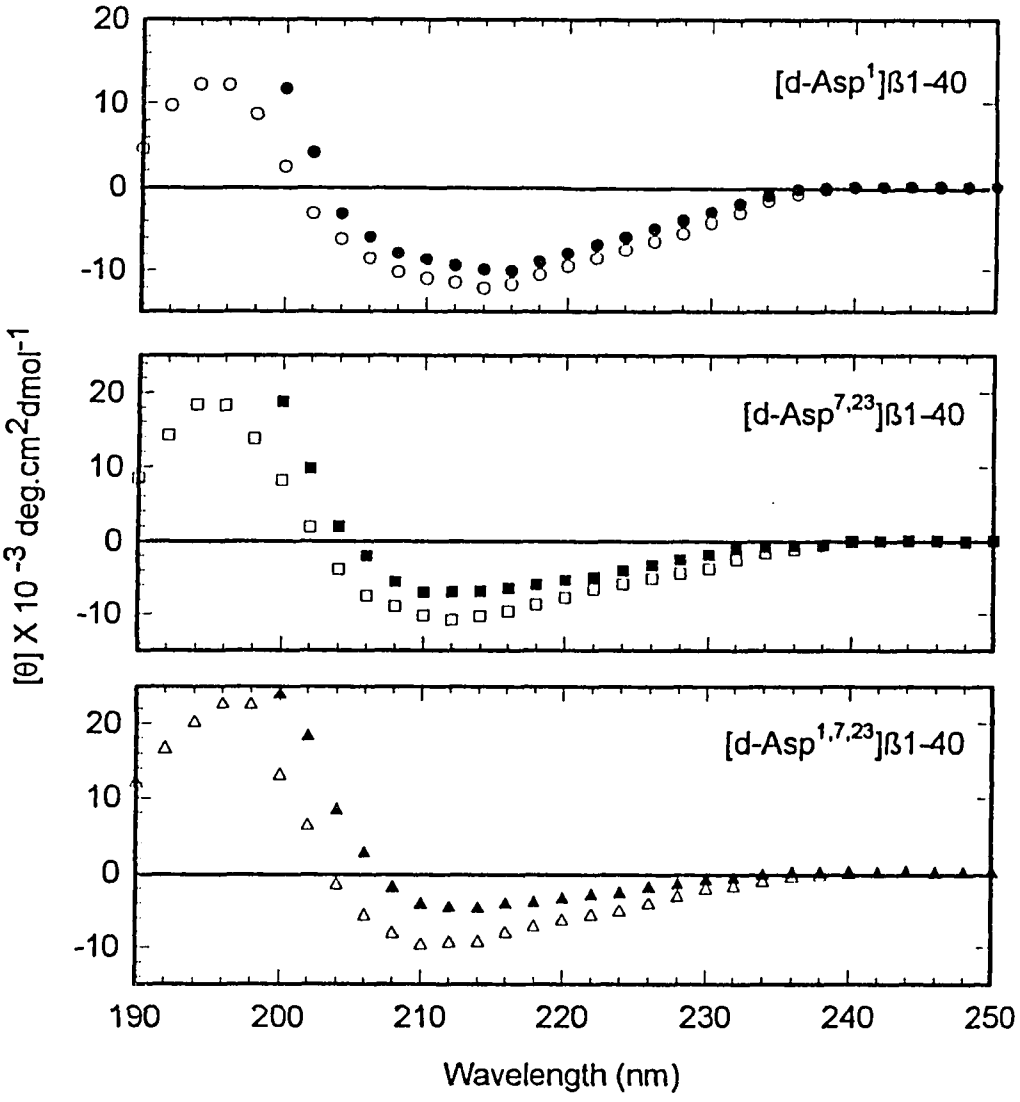

Fig. 5.22 CD spectra for [D-Asp^{7}]ß1-40, [D-Asp^{7,23}]ß1-40 and [D-Asp^{1,7,23}]ß1-40 on addition of 0.5 mM Al(III) after 4 hours. These measurements were taken on 130 µM solutions of the peptide analogs. The symbols represent the mean residue ellipticity for four scans: open symbols (no Al(III), + EDTA), solid symbols (after addition of Al(III)).

5.3.2. Effect of Al(III) on ß6-25 and Derived Analogs

The ß6-25 analog includes the ion-pair forming component of ß1-40 which forms the putative oligomeric ß-pleated sheet structure. The mole percent yield of the aluminum induced microheterogeneity was maximum in the case of ß6-25. It was also seen from the NMR spectra that there were between 4 and 6 Al(III) bound to ß6-25, which was similar to ß1-40, and which were released on treating the peptides with acid. The [D-Asp^{7}]ß6-25 and [D-Asp^{7,23}]ß6-25 derived analogs were synthesized to investigate the influence of aluminum induced conformational change on D-Asp substituted ß6-25 backbone.

For the Al(III)-induced conformation change study, initially the CD spectra for unsubstituted ß6-25 derived analog were recorded. Typical CD spectra for a 325 µM solution of ß6-25 at pH 7.1, and after addition of 0.5 mM Al(III) solution are given in Fig. 5.23. There is a prominent minimum near 215 nm which increases in intensity with Al(III) addition. This effect is removed when EDTA is added. Subsequently, the titration of ellipticity at 215 nm was plotted in terms of fractional change in ellipticity when no further change occurred on addition of EDTA against Al(III) concentration (Fig 5.24). The titration curve for Al(III) titration of fractional change in ellipticity was pseudo-sigmoidal for which the midpoint of transition was achieved at a free Al(III) concentration of 66 µM. When linear regression was performed in this region, in keeping with equation 13, a straight line having a correlation coefficient = 0.93 was obtained. The slope for this fit was 1.88 (Fig. 5.24). This would indicate

that ß6-25 has capability of binding more Al(III) than ß1-40, since the equivalent number for ß1-40 was 1.67.

Effect of Al(III) on [D-Asp] Analogs of ß6-25

The CD spectra of [D-Asp^{7}]ß6-25 and [D-Asp^{7,23}]ß6-25 derived analogs on addition of Al(III) are shown in Fig. 5.25. Distinct variations in ellipticity at all wavelengths are immediately evident for these analogs before addition of Al(III). There is an intense minimum at 216 nm for the mono-substituted analog and at 224 nm for the di-substituted analog. The overall CD intensity was however not significantly different. On introduction of Al(III), minima for both these derived analogs were blue-shifted to 212 nm and 218 nm for [D-Asp^{7}]ß6-25 and [D-Asp^{7,23}]ß6-25, respectively. A distinct reduction in intensity of the minimum was also noticeable in the presence of Al(III) for both peptides. The spectra for added Al(III) were truncated at 195 nm, however, the overall CD intensities were not significantly changed. The similarities in trend with an increase in the D-Asp content between ß1-40 and ß6-25 was striking.

5.3.3. Effect of Fe(III) on ß1-40 and ß6-25

The change in the mean residue ellipticity at 210 nm was measured with increasing amounts of Fe(III) with ß1-40 and ß6-25. This was then calculated

as fractional change in ellipticity and is given in Fig. 5.26. On performing a linear regression at the midpoint of transition on the Hill plots for Fe(III) (Fig. 5.27), a straight line with a fairly good correlation was obtained ($r = 0.82$) which yielded a slope of 1.28. A comparison of the effect of Fe(III) titration with Al(III) titration of the change in mean residue ellipticity at 210 nm indicate that these follow similar trends. Thus, Fe(III) and Al(III) both exert similar effects on the backbone conformation of ß1-40.

5.3.4. Discussion

In this section, characterization of the behavior of ß1-40 and ß6-25 backbone was carried out using their respective D-Asp substituted analogs in the presence of trivalent aluminum and iron salts. The CD methodology used here required that all freshly prepared salt solutions be equilibrated for at least 4 h to get the desired *available* Al(III) (Appendix C; Martin, 1986b), the implications of which will now be addressed.

The CD spectrum of ß1-40 in this study generally resemble the spectra obtained for aqueous solutions of ß1-42, ß1-40, and ß1-39 by other laboratories (Barrow and Zagorski, 1991; Hilbich et al., 1991; Barrow et al., 1992; Exley et al., 1993). Deconvolution of the CD spectrum using Varselec and CCA agree with the estimation of various secondary structural components, but did not exactly

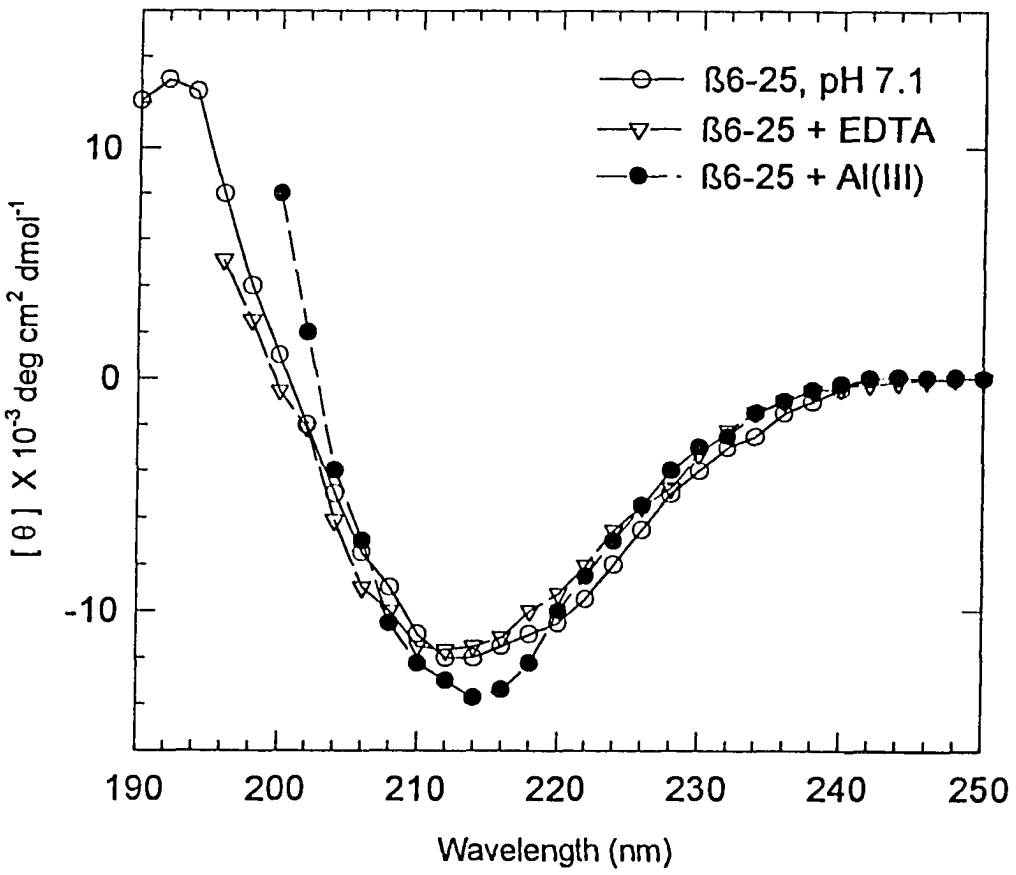

Fig. 5.23 Circular dichroism spectra of ß6-25 solution in the presence of Al(III). The concentration of ß6-25 was 325 µM and he pH was maintained at 7.1. The spectra were recorded under conditions given in Fig. 5.18. Each symbol represents the average mean residue ellipticity of three measurements; truncation at 195 and 200 nm respectively was necessary for EDTA and Al(III) additions because of high background absorbance.

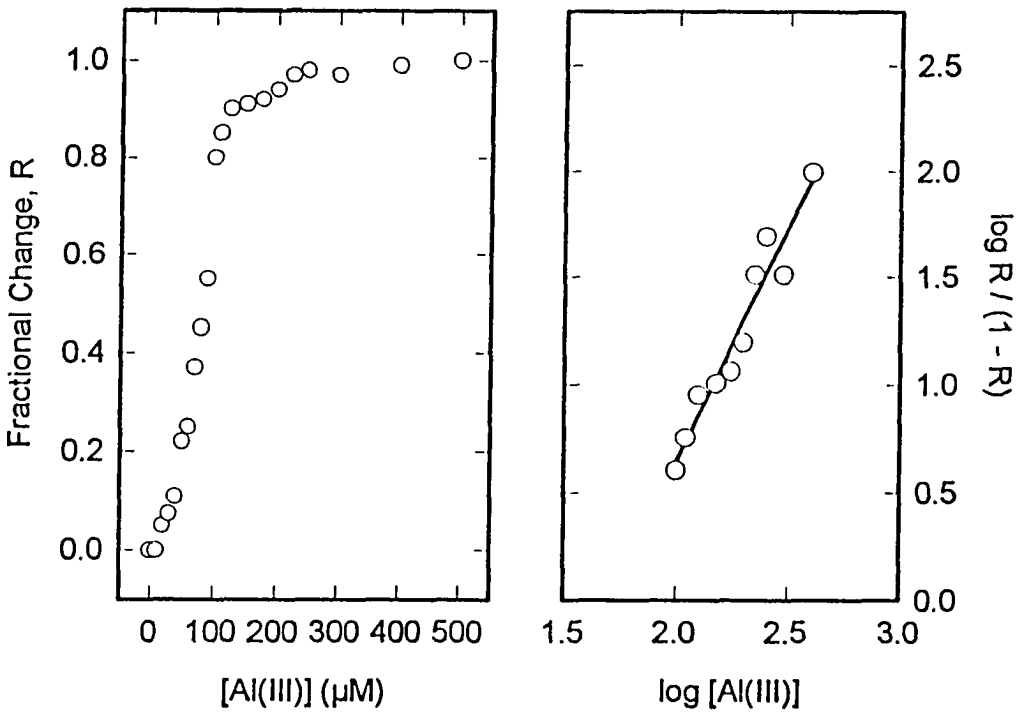

Fig. 5.24 Fractional change in mean residue ellipticity at 215 nm for Al(III) titration of CD spectra of ß6-25. The Hill plot of CD data near the transition midpoint of fractional change in mean residue ellipticity is given on the right-side panel. The fractional change is the ratio of mean residue ellipticity at a given [Al(III)] and the observed mean residue ellipticity after addition of EDTA.

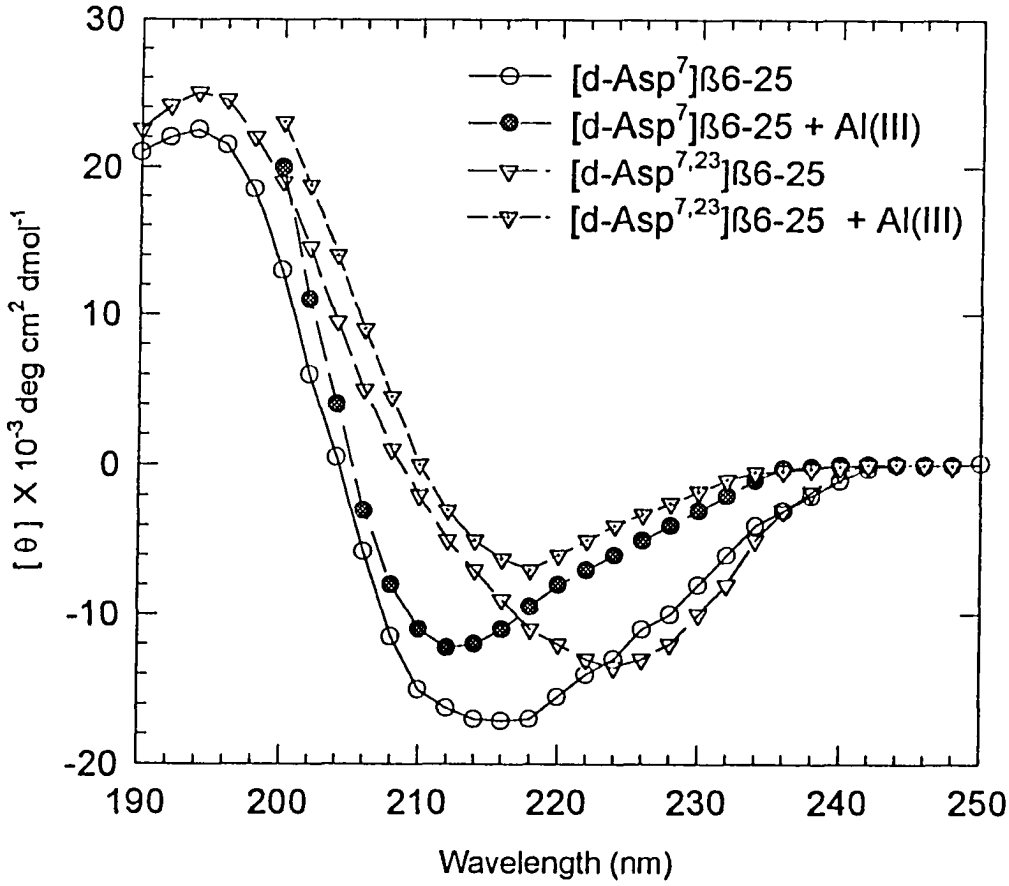

Fig. 5.25 Circular dichroism spectra for [D-Asp] analogs of ß6-25 in presence of Al(III). These are average spectra of four measurements. Only the effect with Al(III) are shown. The concentrations of [D-Asp^{7,23}]ß6-25 and [D-Asp^{7}]ß6-25 were 325 and 420 µM respectively.

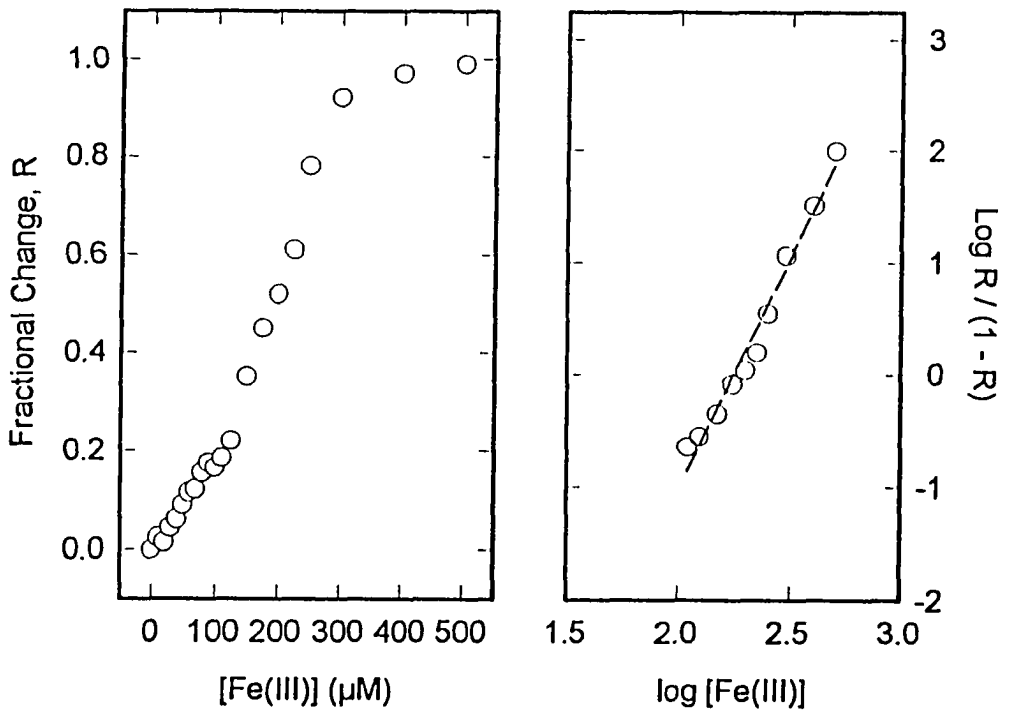

Fig. 5.26 Fractional change in mean residue ellipticity at 210 nm as a function of Fe(III) titration of CD spectra of ß1-40. Hill plot of Fe(III) of CD data near the transition midpoint of fractional change in ellipticity as a function of [Fe(III)]. The fractional change represents the ratio of change in mean residue ellipticity at any given [Fe(III)] and the ellipticity after addition of EDTA.

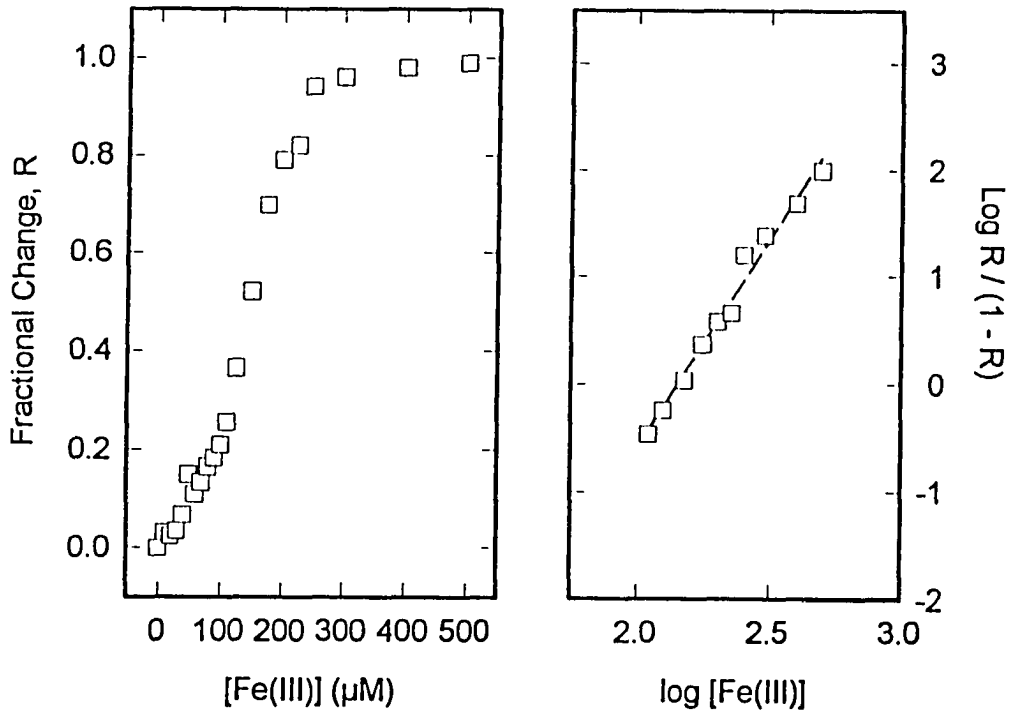

Fig. 5.27 Fractional change in mean residue ellipticity at 210 nm of Fe(III) titration of CD spectra ß6-25 (A). The fractional change denotes the ratio of change in ellipticity at the given concentration of Fe(III) and the ellipticity after addition of EDTA. (B) Hill plot at midpoint of transition of CD data.

match corresponding values obtained in other laboratories. This may partly be due to peptides obtained using different protocols, and also due to the concentrations studied. However, analyses of the spectra obtained on addition of aluminum estimate an increased $f_{ß}$ content with a concomitant decrease in f_{α}. This is in contradistinction to observations made by Exley et al. (1993) who reported a decrease in the α-helical and ß-sheet structure with an increase in the remainder secondary structures. While the f_{α} estimated here using Varselec and CCA was in keeping with their observation of reduction in α-helical content, changes in the ß-pleated sheet content did not agree. Application of the deconvolution methods thus reveal the caveat associated with secondary structure estimations: the reference protein data base *must* provide a good representation of the sample under investigation. Varselec and CCA use reference spectra of proteins which *do not* resemble the ß1-40. Therefore, deconvolution procedures were abandoned, in lieu, the aluminum-induced change in ellipticity was used as a good measure of aluminum binding in ß1-40 and ß6-25 in this study. The ellipticity at 215 nm provides a good estimate of antiparallel ß-pleated sheet content (Sarkar and Doty, 1966). Reliable deductions about the number of metal-binding sites were therefore done from the ellipticity change at 215 nm.

Aluminum titrations of the CD of ß1-40 and ß6-25 estimated that close to 2 Al(III) were bound with an average association constant of 150 μM and 66 μM, respectively. Additionally, the effect of Al(III) on the CD indicated

cooperative binding with ß1-40 and ß6-25 in solution. Using ^{27}Al NMR, these peptides were shown to bind between 4 and 6 Al(III) per peptide molecule. The poor signal to noise ratios from the solvent precluded accurate determination of CD which would account for the disagreement between the two spectroscopic determinations. The NMR evidence indicated that the peptide molecule competes with EDTA for complexation with Al(III); this was also observed in the CD study by the reversal of the Al(III)-induced effect with EDTA.

The contribution of peptide concentrations used in this study in affecting the available Al(III) concentration was considered to be minimal. However, if it is assumed that 4 Al(III) are complexed per molecule in the time frame of the CD experiment, an assumption based on the observed chromatographic and NMR data, then the transition midpoint for titration of CD for ß1-40 will be achieved at 200 µM. The equivalent value for ß6-25 will be 97 µM. These correspond to an underestimation of transition midpoint by 25% in the case of ß1-40 and 32% for ß6-25, which translate to 2.21 and 2.76 Al(III) per peptide molecule, respectively. When the upper limits of complexation are considered these values can be improved still further. It therefore follows that, in determining the nature of species which forms complex(es) with aluminum, the contribution from the peptide as a competing ligand cannot be ruled out.

The presence of aluminum in the peptide milieu significantly altered the CD spectra which suggested, but did not prove, that aluminum binding was associated with conformational changes. However, the addition of EDTA almost

completely abolished the conformational changes induced by aluminum, which was in agreement with the NMR observations. Therefore, when the data was used in conjunction with the *complex* aqueous nature of Al(III), supporting conformational evidence for the chromatographic and NMR data was obtained. The spectroscopic methodology used here provided an insight into the nature of aluminum-binding sites and the conformational effects of aluminum on ß1-40.

The CD spectra of the D-Asp analogs of ß1-40 and ß6-25 were distinctly different than those for the corresponding native peptide. These spectra are the first ones to show the importance of the amino acid side chain at positions 1, 7, and 23 in the peptide backbone. Secondary structure predictions based on primary sequence do not suggest any conformational differences; while analysis of CD spectra using CCA revealed "hidden" secondary structures (Perczel et al., 1992), reference spectra for peptides or proteins with D- configuration are not used by any of the deconvolution methods. Racemization leading to aspartic and iso-aspartic acids having L- and D-stereoconfigurations have been shown to occur spontaneously (Stephenson and Clarke, 1989), and these structurally modified aspartates were found in the amyloid protein (Roher et al., 1993). Kirschner et al. (1987) have proposed the putative ß-pleated sheet formation in ß1-28 due to ion-pairing between His^{13} and Asp^{23}. These side chains were partially charged under the conditions of the study, and therefore expected to form oligomeric ß-pleated sheets.

Although done in different laboratories, the spectral differences between [D-Asp^1]ß1-40 studied here and the commercially available synthetic ß1-40 used by other researchers are immediately evident. Substitution of a single amino acid, *e.g.*, L-Asp → D-Asp, or Arg → His, inflicts a very significant perturbation in the backbone, suggesting its key role in the folding of peptide. The presence of D-Asp^1 was reported in amyloid core protein preparations and was suggested as one of the factors for the structural stability of the AßP (Roher et al., 1993). The conformational change in D-Asp substitutions at position 23 in the ß1-40 derived analogs observed here, further emphasizes the role of Asp^{23} in the formation of ß-pleated sheets. Interestingly, as the number of D-Asp substitutions in ß1-40 was increased, the minimum intensity was blue-shifted as seen with the triply substituted [D-Asp^{1,7,23}]ß1-40. However, since the overall CD intensity was not changed, it was deemed safe to assume there was no loss in secondary structure. The current optical rotation theory limits the explanation of the shifts in CD bands based on D-amino acid substitution. However, since the polarization of the peptide backbone affects the electronic transitions (Urry, 1985), it would seem that the change in the orientation of the side-chain from a L- configuration to a D-configuration significantly affects the polarization of ß6-25 and ß1-40, and this effect is enhanced by the presence of Al(III) in the peptide environment.

The conformational changes in the D-Asp substituted ß6-25 were more impressive than those observed for the D-Asp analogs of ß1-40 due to the

red-shifting in the CD minima. The secondary structure in these amyloid peptides depends on the length of the peptide backbone (Barrow et al., 1992), and conclusions based on CD can only be drawn on peptides with same chain lengths. The behavior exhibited by [D-Asp^{7}]ß6-25 and [D-Asp^{7,23}]ß6-25 can be justified on the basis of their comparatively shorter length which provides more flexibility, and more hydrophilic nature compared to ß1-40. The well-defined fibrillar assembly of ß6-25 and extensive ß-pleated sheet formation has been emphasized in the EM and X-ray scattering studies (Fraser et al., 1991; Inouye et al., 1993). The red-shift of the CD minima in the D-Asp derived analogs of ß6-25 increased with the number of substitutions. This phenomenon is comparable to the blue-shifts observed for the D-Asp derived analogs of ß1-40. However, the very large red-shifting in the [D-Asp^{7,23}]ß6-25 analog solicits more comment. Among the CD spectra available in the literature, the spectrum exhibited by the [D-Asp^{7,23}]ß6-25 analog closely resembles gramicidin A in inverted micelles (Salom et al., 1992) with respect to the CD bands. Gramicidin A is an antibiotic with an alternating D- L- pentadecapeptide backbone which acts as a transbilayer monovalent cation channel. The substitution of L-Asp $\rightarrow$ D-Asp caused significant change in ß6-25 backbone which then conformationally resembled an ionophore. Work done by Arispe et al. (1993) has shown that ß1-40 forms calcium channels in bilayers which are blocked by aluminum. The CD spectrum for the [D-Asp^{7,23}]ß6-25 in this study suggests that the peptide

which is the sequence analog of the intermediate region is likely to form ion-channels in ß1-40.

The study of aluminum-induced effects on ß1-40 and ß6-25 demonstrated that: (i) the antiparallel ß-pleated sheet content increased at the expense of all other secondary structural components, (ii) this effect was almost completely reversible - by chelating aluminum, (ii) at least 2 aluminum ions each are bound to ß1-40 and ß6-25 in solution, (iii) it was necessary to ascertain *all* ligand species when dealing with aqueous aluminum solutions to obtain a credible estimate of aluminum ions with peptides, (iv) derivations based on observed ellipticity provide reliable evidence than those derived from deconvolution methods.

Summary

The current understanding of the role of AßP in the neuropathology of Alzheimer's disease has been like a roller coaster ride, making some researchers skeptics, while the others become *ßAPtists*. Since its discovery by Glenner and Wong (1984), this ride has been plagued with unresolved arguments about whether amyloid deposition is the cause, or an effect of the neuronal degeneration in AD. At the heart of the matter lingers the contradictory evidence of the neurotoxicity of AßP (Whitson et al., 1989; Yankner et al., 1990), and the apparent protection offered by exogenous factors (Wisniewski et al., 1993; Zhao et al., 1993), where the key issue is the aggregated state of the protein. Moreover, AßP disrupts calcium homeostasis (Hardy and Higgins, 1992) by forming ion channels in membranes which are inhibited by aluminum (Arispe

et al., 1993). Keeping these concepts in mind, answers to two questions pertinent to the pathway leading to amyloid deposition were sought: (i) how does soluble AßP form aggregates over time?, and (ii) what is the role of aluminum in the stability of AßP in solution?

The study presented in this thesis capitalized on the utilitarian approach of chemically obtaining ß1-40 and derived analogs toward understanding their behavior in solution. While not unique, the stepwise assembly of fmoc-amino acid esters required considerable manipulations of synthetic conditions before satisfactory yields of pure peptide analogs could be obtained. The growth of truncated peptides was avoided by using low resin substitutions, and by maintaining the growing resin-peptide solvated by a mixture of polar organic cosolvents; this approach allowed for a total synthesis of ß1-40. The Mtr protecting group for the guanidine of Arg proved to be the most unyielding during TFA cleavage and required optimized use of specific scavenging agents.

The chromatographic approach used in this study permitted the determination of the parameters related to the hydrophobic contact area of ß1-40 and derived analogs, the resolution of hetero-oligomers of ß26-40 with ß1-40 and ß8-40, and the manufacture of Al(III)-bound peptides. Interestingly, the RP-HPLC study demonstrated that the elution of ß1-40 as a broad band was due to secondary retention - a phenomenon which is also found in many other peptides. Except ß22-35, all sequence analogs of ß1-40 were bound in their monomeric form on the reversed-phase matrix. This is an important finding since the

monomeric form of ß1-40 is not neurotoxic (Yankner et al., 1990; Pike et al., 1993), nor does the constitutively produced and secreted ß1-40 generate neuritic plaques (Haass et al., 1992; Seubert et al., 1992).

It was fascinating to find that ß26-40 oligomerized with ß1-40 and ß8-40 if incubated in solution prior to introduction on the reversed-phase surface. This observation has implications on the nucleation hypothesis of amyloidogenesis (Jarrett and Lansbury, 1992; Jarrett et al., 1993). The subunit structure for the systemic amyloid combines strong hydrophobic interactions between core helices and weaker hydrogen-bonding interactions between ß-sheets (Turnell et al., 1986). A similar phenomenon with ß26-40 and ß-40 incubations could have resulted in the observed chromatographic behavior; however, it was surprising that these hetero-oligomers were stable in the denaturing conditions of RP-HPLC. The clustering of these hydrophobic moieties could form nucleation sites which are necessary for aggregation of ß1-40. The close association of apoE, phospholipids and proteoglycans with the CV deposits (Snow et al., 1987; Wisniewski and Frangione, 1992) suggests a high probability that these exogenous factors might also act as the seed which causes aggregation of soluble ß1-40. Nonetheless, it was of interest to find that oligopeptides of AßP containing complementary sequences spontaneously assembled to form macromolecules, independent of any external assembly or instruction code.

The conformational state of AßP has raised the thorniest issue in the pathway to understanding its neurotoxicity. Although many *in vitro* studies on

synthetic ß1-40 homologs have demonstrated the formation of amyloid-like fibrils under the influence of pH, metal ions, and tissue specific factors (Castano et al., 1986; Kirschner et al., 1987; Halverson et al., 1990; Kirschner et al., 1990; Fraser et al., 1991a, 1991b, 1993), none had demonstrated the gradual loss of secondary structure over time. The circular dichroism study done here demonstrated that in the absence of any external stimuli, the kinetic change in molar ellipticity of aqueous ß1-40 and ß6-25 solutions took place as a function of time, and concentration. The resultant conformational variations suggested a gradual loss in secondary structure by a rearrangement of secondary structural components. The data presented here provides proof necessary to support the conformational theory of amyloid deposition, and bridges the section from the relatively benign soluble ß1-40 to the pre-amyloid state, before the final toxic state of ß1-40 is attained. The proceedings on this route would explain the neurotoxicity found by some (Yankner et al., 1990; Pike et al., 1991; Zhao et al., 1993), but not others (Whitson et al., 1989, 1990). This study provided the first kinetic evidence of the secondary structural changes in any amyloidogenic proteins in aqueous solutions; since many proteins having little or no sequence homology form amyloid fibrils, these investigations fills up an important hole in the path toward comprehending the recalcitrancy of amyloid deposits.

The evidence presented here also implies that aluminum ions play an important role in the relative orientation of the ß1-40 peptide backbone in solution – a role which is intensified when D-Asp amino acids constitute the

peptide. The presence of aluminum all but abolishes the "ion-channel-like" conformation of the di-substituted D-Asp derived analog of ß6-25. Thus, it would seem that the ß6-25 segment could play a prominent role in the ion-channels formed by ß1-40 (Arispe et al., 1993). Also, since racemization takes a slow and arduous route within physiological parameters (Stephenson and Clarke, 1989), chelation with aluminum could accelerate the spontaneous catalysis (Buckingham et al., 1967) of AßP, eventually resulting in racemized Asp residues in core amyloid protein (Roher et al., 1993).

The implications of considering the aqueous chemistry of aluminum to gain insight on nature of interaction with the peptides proved to be advantageous in interpreting its association with the peptides. A better agreement between the CD and NMR spectroscopic data was achieved when the *available* aluminum was taken into consideration. Although, the nature of the Al(III)-peptide complexes formed was not determined, it was evident that Al(III) induced conformational changes in ß1-40 and ß6-25 which could be partially reversed by EDTA. The stabilizing effect of Al(III) on the secondary structure of ß1-40 and its fragments support the conformational change hypothesis that Al(III) could contribute to the structural stability of amyloid in AD. Al(III) can form both, intermolecular and intramolecular complexes with ß1-40 and derived analogs, the latter could be stabilized by potential salt-bridges (Kirshner et al., 1987; Hollósi et al., 1994). In spite of the evidence in favor of Al(III) ions in the conformational stability of ß1-40 and derived analogs, this study does not negate

the role of other factors, like paired helical filaments (Perl, 1988), neurofibrillary tangles (Perl and Brody, 1980; Candy et al., 1992), and phosphorylated *tau* protein (Lee et al., 1991), which play a prominent role in the etiology of Alzheimer's disease. Evidence on synthetic model peptides from neurofilament proteins suggest that phosphorylation of these proteins leads to their eventual deposition as paired helical filaments (Otvos et al., 1988; Lang et al., 1992; Hollósi et al., 1992; Fasman and Moore, 1994). It is possible that the Al(III) implicated in the makings of these tangles and filaments could have indeed been carried by the circulating ß1-40. Based on the observations made in this study, the following scenario could now be visualized: ß1-40 gradually procures a higher order in structure, and simultaneously provides an anchor for aqueous Al(III) to bind, from which Al(III) can orchestrate the chaotic events - disrupting chemical homeostasis, racemization of amino acids in the complexed peptide, and sabotaging the tau-machinery. Collectively, these events lead to a gradual deposition of amyloid and other factors in the neuronal milieu.

The findings from this study are provocative at best and raises more questions than provide answers. To rephrase Sherrard (1991) in light of the current data, "Is it time to throw away grandma's time-tested aluminum pot?" Not necessarily! Although inhaling aluminum is another matter (Beyreuther, 1993), especially if there is soluble ß1-40 which is available freely. Implications of the strategy employed in this study using the selectivity of aluminum toward bioactive ligand peptides, like ß1-40, to gain insight on how the conformational

nature can be modulated in aqueous solutions, however, deserve further consideration. The mechanism of prohibiting the conformational change of soluble AßP will also be necessary if therapeutic intervention is to be successful. The chromatographic studies which were used to characterise the ligand-peptide interactions with a reversed-phase surface could also be used to develop a model for stabilizing the conformation of ß1-40 and derived analogs. Other future directions in brain amyloid research will most probably include methods to prohibit the interaction of soluble ß1-40 with exogenous protein factors. In any case, unravelling the tangles, or conserving the solubility of ß1-40 will most likely also involve aluminum. Be as it may, this study provides one more brick *on* the wall of neuronal degeneration; yet another direction in navigating the labyrinthian pathways of structure-function relationships in proteins and peptides, leading to a better understanding of the conformational stability of soluble AßP, and other amyloidogenic proteins.

Appendix A

Evaluation of Interactive Chromatographic Parameters During Gradient Elution RP-HPLC

The chromatographic parameters related to the hydrophobic contact area of ß1-40 and derived analogs on the reversed-phase surfaces were determined by using the concepts outlined by Horvath et al. (1976), Hearn et al. (1985) and Hearn and Aguilar (1987). To determine the chromatographic parameters, mathematical transformations using SigmaPlot 4.1 were performed by adopting the Pek'N-ese protocol (Hearn et al., 1985). The retention coefficients of amino acids were obtained from Guo et al. (1986).

Retention relationships

The retention time, t_g, for a polypeptide chromatographed under ideal gradient elution conditions is related to the gradient steepness parameter, b, through the expression

$$t_g = (t_0 / b) [\log 2.3\ k'_0 b] + t_0 + t_c \quad (1)$$

where

$$b = t_0 \log ß / [t_{g1} - (t_{g2} / ß) + t_0(t_{G1} - t_{G2}) / t_{G2}] \quad (2)$$

Alternatively, when gradient times are maintained constant, using different flow rates F_1 and F_2, then b can be determined as follows:

$$b_1 = (\log (F_2 / F_1)) / [\, X_1 - X_2 (F_2 / F_1) \,] \quad (3)$$

where

$$X_1 = (t_{g1} - t_{0.1}) / t_{0.1} \quad (3a)$$

$$X_2 = (t_{g2} - t_{0.2}) / t_{0.2} \quad (3b)$$

Evaluation of b values from retention data obtained for various gradient times

Evaluation of b values from retention data obtained for various gradient times and solvent flow-rate conditions allows the calculation of the median capacity factors, k^*, and the corresponding organic mole fraction ψ^*.

Provided the retention of the polypeptide in question follows an ideal linear solvent strength behavior, k^* and ψ^* can be derived, to a first approximation from equations 4 and 5, namely

$$k^* = 1 / 1.15b \tag{4}$$

$$\psi^* = [t_{g1} - t_0 - (t_0 / b) \log 2] / (t_G / \Delta\psi) \tag{5}$$

The parameters k^* and ψ^* are equivalent to the isocratic parameters k' and ψ^* under regular reversed-phase elution conditions are empirically related through the expression

$$\log k' = \log k'_0 - S\psi \tag{6}$$

The tangent (or slope) S to the curve obtained in a plot of log k^* *versus* ψ^* is determined at any particular value of k^* and the value of log k^* at $\psi^* = 0$, (*i.e.*, log k'_0) are obtained by extrapolation using regression analysis.

The relations summarized in equations 1-6 give rise to a number of predictions related to the retention behavior of peptide solutes under linear solvent strength gradient conditions:

Firstly, the corresponding gradient form of equations 6 predicts linear dependencies of log k^* on ψ^*, provided the solutes are eluted under regular reversed-phase conditions and their retention behavior does not involve any significant participation of slow secondary equilibria associated with either ionization, surface-adsorption or conformational effects.

Secondly, as the b value is changed through alteration of t_G or F, selectivity changes should become evident for those peptides with different S values in which the processes of their adsorption-desorption result in different association constants or kinetic rate constants, either through participation of:
(i) different classes of binding sites on the heterogenous stationary-phase surface (*i.e.,* through different binding mechanisms), or
(ii) through the involvement of different topographic regions on the solute surface (*i.e,*. via the same mechanism but different effective hydrophobic contact areas), or
(iii) through hybrid combinations of both processes.

With solute analogs in which identical molecular regions are involved in the interaction with the stationary-phase surface, coincidental retention behavior with parallelism in the log k^* versus ψ^* plots should be observed. In the case of closely eluting peptides, with fundamentally different contact area dependencies, manipulation of secondary solution equilibria through, for instance, pH, ion-pairing or solvation effects, should result in selectivity changes due to alteration of the topographical dimensions of the interactive region of the solute.

Bandwidth relationships

The peak capacity, *PC*, for a chromatographic separation of gradient time t_G and average resolution, R_s, equal unity for all peptide pairs can be given by

$$PC = t_G \cdot F / 4\,\sigma_v \tag{7}$$

where σ_v is the bandwidth measured in volume units (1 S.D.). Furthermore, the relationship between σ_v and k^* for linear solvent systems can be expressed as

$$\sigma_{v,calc} = [(k^* / 2) + 1]\; G \cdot V_m \cdot N^{-0.5} \tag{8}$$

where *G* is the band compression factor which arises from the increase in solvent strength across the solute zone as the gradient develops along the column, and is given by the expression

$$G^2 = [1 + 2.3b + 1/3(2.3b)^2] / (1 + 2.3b)^2 \tag{9}$$

where V_m is the column void volume ($= t_0 \cdot F$). Under the typical flow-rate conditions used for separations of peptides in RP-HPLC, the plate number, *N*, can be approximated by

$$N = D_m \cdot t_0 / C \cdot d_p^2 \tag{10}$$

where d_p is the mean particle diameter, and *C* is the Knox equation parameter which accounts for resistance to mass transfer at the stationary-phase surface and can be estimated by

$$C = [\{(1 - x + k^*) / (1 + k^*)\}^2] / [15\rho a' + 15\rho b' k^* - 19.2\rho x] \tag{11}$$

where x is the interstitial column volume fraction, was taken as 0.67 for the Vydac C_{18} column, a' was taken as 1.1, b' is the surface diffusion parameter and ρ is the restricted diffusion parameter.

The diffusion coefficient of a solute in the mobile phase (D_m) can be expressed in terms of the solute molecular weight and evaluated from equation 12,

$$D_m = [\, 8.34 \times 10^{-10} \cdot T \,] / [\, \eta \cdot MW^{0.33} \,] \qquad (12)$$

where T is the temperature (K) and η is the eluent viscosity (poise).

The assumption in the derivation of the above bandwidth was that the solute migrated as an unique, conformationally rigid moiety. It is generally accepted that peptides and proteins can explore a variety of conformations in solutions. If it is assumed that these processes or any additional secondary equilibria are extremely rapid compared to the chromatographic separation time, then the ratio between the experimentally observed bandwidth $\sigma_{v,exp}$, and the bandwidth determined by equation 8, $\sigma_{v,calc}$, should approach unity over the normal operational range of retention values commonly used in optimization studies, i.e. $1 < k^* < 10$.

LIST OF SYMBOLS USED:

a'	Intercept of the B versus k^* plot, taken to be 1.1.
B	Knox equation constant, which arises from zone dispersion due to longitudinal diffusion.
b	Gradient steepness parameter, as defined by equation 2.
b'	Solute diffusion parameter, equal to the ratio at solute diffusion in the stationary and mobile phases (D_s/D_m).
C	Knox equation constant, which accounts for mass transfer contributions throughout the pore structure of the stationary phase.
D_m	Diffusion coefficient (cm^2/s) of the solute in the mobile phase.
D_s	Diffusion coefficient (cm^2/s) of the solute at the stationary-phase surface.
d	Intercept of the $[\log K_m]^{-1}$ versus τ plot.
d_p	Mean particle diameter (cm).
e	Slope of the $[\log K_m]^{-1}$ versus τ plot.
F_1, F_2...	Flow-rate of mobile phase at different values.
G	Band compression factor, as defined by equation 9.
K_m	Michaelis constant.

k'	Capacity factor for the solute determined from isocratic retention data.
k^*	Median capacity factor for the solute determined from gradient retention data as defined by equation 4.
k'_0	Capacity factor for the solute determined or extrapolated at $\psi = 0$.
L	Column length (cm).
MW	Molecular weight.
N	Column plate number.
PC_{exp}	Peak capacity as defined by equation 7 from experimental values of t_G and $\sigma_{v,exp}$.
PC_{calc}	Peak capacity as defined by equation 13.
R_s	Average resolution for gradient separation.
S	Slope of the plot log k' *versus* ψ as defined by equation 6.
T	Absolute temperature.
t_d	Chromatographic dwell time.
t_e	Gradient elapse time.
t_{G1}, t_{G2},	Gradient times.
t_{g1}, t_{g2},	Gradient elution times for the solute under two different gradient times.
$t_{0.1}$, $t_{0.2}$,	Column dead times for different conditions of flow.
V_m	Column void volume.
V_{max}	Maximum velocity of enzyme-substrate reaction.
x	Fraction of the column void volume in the interstitial spaces of the column bed.
α	Gradient separation factor, as defined by the ratio of k^* values for two adjacent solute zones.
ß	Ratio of the gradient times as defined by ß = t_{G2}/t_{G1}.
$\Delta\psi$	Change in the organic modifier mole fraction.
η	Mobile phase viscosity at a defined temperature (poise).
ρ	Restricted diffusion parameter.
$\sigma_{v,exp}$	Peak bandwidth in volume units (mL), determined experimentally.
$\sigma_{v,calc}$	Peak bandwidth in volume units (mL), calculated according to equation 8.
τ	Solute selectivity parameter (= ln α).
ψ	Organic solvent modifier mole fraction in isocratic system.
ψ^*	Median organic modifier mole fraction as defined by equation 5.
χ	Hydrophobic retention coefficient.

Appendix B

Decomposition Procedures for Secondary Structure Transitions from Amide Circular Dichroism Spectroscopy of ß1-40 and Derived Analogs

The deconvolution of observed CD spectra was performed using Varselec (Manavalan and Johnson, 1987) and CCA (Perczel et al., 1991) analyses and from the observed mean residue molar ellipticity. The decomposition of spectral data was done as per Labhardt (1982), Kuwajima et al. (1987) and Ptitsyn (1987).

Using the reference spectra for α-helix $r_h(\lambda)$, $r_a(\lambda)$ for antiparallel ß-sheet, r_p parallel ß-pleated sheets, r_t for ß-turns and r_o for all other structures, all observed CD spectra were approximated at an interval of 5 nm for 11 different wavelengths between 210 and 260 nm to least-squares by a superposition of the form:

$$[\theta] = f_h r_h(\lambda) + f_a r_a(\lambda) + f_p r_p(\lambda) + f_t r_t(\lambda) + f_o r_o(\lambda) \quad (6)$$

The only constraint imposed on this equation was that

$$\Sigma f_i = 1.0 \quad (7)$$

Therefore, this was equivalent to approximating the measured difference spectrum $\Delta[\theta]' = [\theta]_{measured} - r_o(\lambda)$ to least-squares by a 2-parameter expression:

$$\Delta[\theta] = f_\alpha(r_\alpha - r_o) + f_ß(r_ß - r_o) \quad (8)$$

where f_α is the fractional α-helical content, $f_ß$ is the sum of antiparallel and parallel ß-pleated sheets, r_o represents the basis spectra for all other structures which are neither α-helical nor ß-pleated sheets structures, which yields the individual f for the secondary structural elements, which are analytical solutions to the system of linear equations:

$$\partial I \partial f_\alpha \; \Sigma\{\Delta[\theta]' - \Delta[\theta]\} = 0 \quad (9a)$$

$$\partial I \partial f_ß \; \Sigma\{\Delta[\theta]' - \Delta[\theta]\} = 0 \quad (9b)$$

$$\partial I \partial f_o \, \Sigma\{\Delta[\theta]' - \Delta[\theta]\} = 0 \qquad (9c)$$

The difference spectra were orthogonal in the wavelength range from 260 to 195 nm, *i.e.*, $\int_\lambda \Delta\alpha \Delta\beta \cdot d\lambda = 0$.

The fractions of α-helical (f_α) and ß-pleated sheet (f_β) were calculated from the measured difference spectrum for conformational change, $\Delta[\theta]' = [\theta]_{measured} - r_o(\lambda)$, by using

$f_h = (\Sigma_\lambda \Delta[\theta]' \cdot \Delta\beta \cdot \Sigma_\lambda \Delta\alpha\Delta\beta - \Sigma_\lambda \Delta[\theta]' \cdot \Delta\alpha \cdot \Sigma_\lambda \Delta\beta^2)/D$, and

$f_\beta = (\Sigma_\lambda \Delta[\theta]' \cdot \Delta\alpha \cdot \Sigma_\lambda \Delta\alpha\Delta\beta - \Sigma_\lambda \Delta[\theta]' \cdot \Delta\beta \cdot \Sigma_\lambda \Delta\alpha^2)/D$,

where,
$D = (\Sigma \Delta\alpha \cdot \Delta\beta)^2 - \Sigma_\lambda \Delta\alpha^2 \cdot \Sigma_\lambda \Delta\beta^2$, and

$\Delta\alpha = r_h(\lambda) - r_o(\lambda)$; $\Delta\beta = r_\beta(\lambda) - r_o(\lambda)$; etc.

The success in fitting the measured CD spectra of the native conformational state with the correct f_h and f_β fractions given by equation 5 showed that in the range of wavelengths in the random-coil and the unordered structure (f_o) CD spectra were not sufficiently orthogonal for both to be incorporated at the same time as reference spectra. The reference spectra of α-helical and ß-pleated sheet structures were, however, well decoupled in the wavelength region of 260 to 195 nm; *i.e.* $r_\beta(\lambda)$ went through zero near 225 nm whereas $r_h(\lambda)$ reached the maximum (of its absolute value) nearby.

Verification of $f_h(r_h(\lambda) - r_o(\lambda))$ and $f_\beta(r_\beta(\lambda) - r_o(\lambda))$

To verify if the reference spectra which were used provided satisfactory estimates, all three `pure' spectra, *α*, *ß*, and *o*, were abandoned and replaced with the measured spectra, $J_j(\lambda)$, of mixed conformations of ß1-40 and derived analogs. Native spectra ($J_1(\lambda)$), and `denatured' spectra ($J_2(\lambda)$ and $J_3(\lambda)$) at pH 2 were included to expand the spectra [θ] of the peptide(s) to

$$[\theta] = \sum_1^3 g_j J_j(\lambda) \qquad (10)$$

Assuming that each of the $J_j(\lambda)$ was only defined by 3 different types of secondary structure, according to equations 6 and 7, this implied that the three g_j values add up to unity. Therefore, equation 10 can be reformulated in a way analogous to equation 8 as

$$[\theta] - J_3 = g_1(J_1 - J_3) + g_2(J_2 - J_3) \qquad (11)$$

The meaning of the g_j values can be discerned from equation 11: the deviation of the actual conformation, spectrum [θ], from the conformation of folded peptide (J_3) is measured by g_1 in terms of conformational transitions which are spectrally equivalent to the disappearance of the α-helix forming segment. This was presumed to dominate $J_1 - J_3$), and by g_2 in terms of the appearance of the conformation of completely denatured peptide (pH 2) given by ($J_2 - J_3$).

Appendix C

Concentration of Aqueous Aluminum(III): Metal-ion Buffers

The determination of available Al(III) in aqueous solutions were taken from the concepts presented by Martin (1986), Crumbliss and Garrison (1988) and Martin (1988).

The control of metal ion concentrations in solutions is analogous to pH buffers, except that it is the free metal-ion concentration which is controlled in the presence of excess ligand. Most effective buffering takes place when the complexed ligand to total ligand molar concentrations lie between 0.15 and 0.85. Normally the ligand concentration exceeds the metal concentration, and the total metal-ion to total ligand ratio, R, must be maintained to have any metal buffering action.

The conditional stability constants, K_c, permits the formulation of equation for metal-ion buffering. For a AlL^0 system at neutral pH, like Al-cit or Al-EDTA, the conditional stability $K_c = [HOAlL^-] / [Al(III)][HL^{2-}]$, refers to the overall reaction $Al^{3+} + HL^{2-} \rightleftharpoons HOAlL^- + H^+$, for which the total ligand concentration is given by:

$$C_L = [HOAlL^-] + [HL^{2-}] \quad (1)$$

Since the ligand is in excess, the total metal concentration is given by:

$$C_M = [HOAlL^-] \quad (2)$$

All Al^{3+} is assumed to be tightly bound so that free Al^{3+} is negligible. Substituting this equation for the conditional stability constant equation for a AlL^0 complex at neutral pH, the following general equation is arrived:

$$[Al^{3+}] = R / (1 - R)K_c \quad (3)$$

where $R = C_M / C_L$. This equation gives the free $[Al^{3+}]$ and is applicable at the pH at which the conditional stability constant applies.

In the case of EDTA, K_c was formally given by:

$$K_c = K_s(1 + K_b / [H^+])/(1 + [H^+] / K_a) \quad (4)$$

since most of the ligand appears as a species with a net charge of 2- at neutral pH. The $[H^+] / K_a$ term accounts for the protonated ligand, HL^{2-}, and the $K_b / [H^+]$ term for the deprotonated Al(III)-bound water, $[Al(H_2O)_5(OH)]^{2+}$, which are generated during complex formation.

The metal-ion buffer equations 3 and 4 gives the free metal ion as a function of the known equilibrium constants, pH, and the ratio of total metal ion to excess total ligand concentration, R, and not their absolute concentrations.

Varying R, affects the free metal ion concentrations at any given pH. At pH 7.4, for Al(III)-EDTA, pAl = 15.0, and at pH 7.0, pAl = 14.2. For an equivalent Al(III)-cit system, the corresponding values are 12.4 and 11.7 respectively. The [Al(III)] in both cases is low, but is controlled.

The situation where $R = 1$ or $C_M = C_L$ was avoided because of wide variations in pAl due to unbuffering of the solutions. Since these ligands are prone to time-dependent reactions, *i.e.*, the equilibrium with complexes was reached slowly, they were allowed to stand for at least 4 hours before any measurements were taken. When a wider range of R was required, the variation in pH was sufficient to achieve the desired free $[Al^{3+}]$; although $R = 1$, and $C_M = C_L$ situations were circumvented at all times during the spectroscopic investigations.

Appendix D

Characterization of Mg^{2+}, Zn^{2+} and Ca^{2+} Incubations with ß1-40 and Derived Analogs

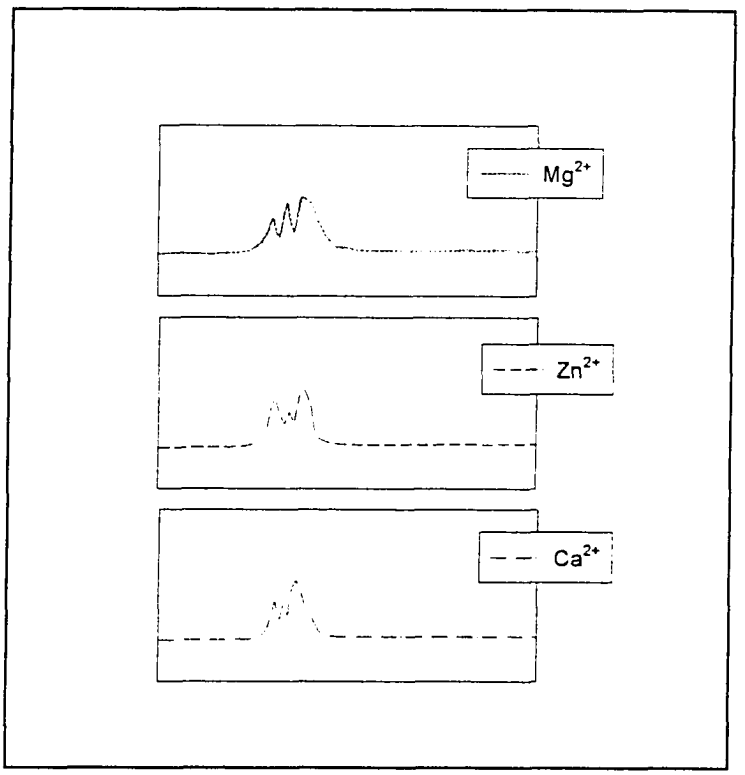

Fig. 1. RP-HPLC elution profiles for ß1-40 incubations with Mg^{2+}, Zn^{2+} and Ca^{2+}. The incubations were performed at 35°C for 24 h using the metal ion-peptide ratio as 10:1. The solutions were occassionally vortexed, and after 24 h, the samples were loaded directly on a 4.6 X 300 mm Beckman Ultrasphere ODS column. Chromatography was done using a AB gradient; solvent A was 0.1% TFA and solvent B was 0.1% TFA in 80% MeCN. The flow rate was 0.8 mL/min with a gradient time from 0-100%B in 60 min. The major hydrophobic fraction was collected, concentrated *in vacuo*, and characterized by automatic amino acid sequence analysis.

Sequence analysis:

The major fraction eluting after RP-HPLC of the incubations were attached on PVDF membranes and Edman degradation performed. The sequence analysis is given in Table 1.

Incubation with	Sequence assignment for the major fraction on RP-HPLC
Mg^{2+}	*DA*EFRXXXG*Y*EVHX*QK*LVFFAE*D*VGXNKGA...
Zn^{2+}	*D*AEFRHXXG*Y*EVHXX*K*LVFFAE*D*VGXNKGA...
Ca^{2+}	*DA*EFRHDXGYEVHHXKLVFFAXXVGXNKGA...

The *underlined italics* indicate the repetitive yield of the PTH-amino acid was less than 0.25 relative to PTH-Phe[4] or PTH-Leu[17].
The "..." indicate that sequence analysis was not performed beyond this amino acid because the repetititve yield was significantly less than 0.10 relative to PTH-Phe[4] or PTH-Leu[17].

Bibliography

Aguilar, M. I., S. Mougos, J. Boublik, J. Rivier and M. T. W. Hearn. **1993**. High-performance liquid chromatography of amino acids, peptides and proteins. cxxviii. effect of D-amino acid substitutions on the reversed-phase high-performance liquid chromatography retention behaviour of neuropeptide Y[18-36] analogues. *J. Chromatogr.* **646**:53–65.

Akitt, J. W. and A. Farthing. **1978**. New ^{27}Al NMR studies of the hydrolysis of the aluminum(III) cation. *J. Magn. Reson.* **32**:345–352.

Akitt, J. W. and B. E. Mann. **1981**. ^{27}Al NMR spectroscopy at 104.2 MHz. *J. Magn. Reson.* **44**:584–589.

Akitt, J. W. and N. B. Milic. **1984a**. Aluminium·27 nuclear magnetic resonance studies of the hydrolysis of aluminium(III). part 6. hydrolysis with sodium acetate. *J. Chem. Soc. Dalton Trans.* 981–984.

Akitt, J. W. and W. S. MacDonald. **1984b**. Arrangement of ligands giving low electric-field gradients. *J. Magn. Reson.* **58**:401–412.

Akitt, J. W. and J. M. Elders. **1985**. Aluminium·27 nuclear magnetic resonance studies of the hydrolysis of aluminium(III). part 7. spectroscopic evidence for the cation $[AlOH]^{2+}$ from line-broadening studies at high dilution. *J. Chem. Soc. Faraday Trans. 1* **81**:1923–1930.

Akitt, J. W. **1987**. Aluminum, Gallium, Indium and Thallium, in "Multinuclear NMR," (ed. Mason, J.), Plenum Press, New York, USA.

Anderson, K. K., G. L. Perez, G. H. Fisher and E. H. Man. **1990**. Effect of aluminum ingestion on aspartate racemization in the protein of rat brain. *Neurosci. Res. Commun.* **6**:45–50.

Anghileri, L. J. **1992**. Ehrlich tumour cells: Ca^{2+}–uptake modification by aluminium lactate. *Cell Calcium* **13**:277–279.

Aramini, J. M., M. W. Germann and H. J. Vogel. **1993.** Field-dependent aluminum-27 NMR studies of the transferrins: an approach for the study of metal ion binding sites in larger proteins. *J. Am. Chem. Soc.* **115**:9750–9753.

Argos, P., M. Hanei and R. M. Garavito. **1978**. The Chou-Fasman secondary structure prediction method with an extended data base. *FEBS Lett.* **93**:19-24.

Arispe, N., E. Rojas and H. B. Pollard. **1993**. Alzheimer disease amyloid ß protein forms calcium channels in bilayer membranes: blockade by tromethamine and aluminum. *Proc. Natl. Acad. Sci. USA* **90**:567–571.

Armstrong, R. A., D. Myers, C. U. Smith, N. Cairns and P. J. Luthert. **1991**. Alzheimer's disease: the relationship between the density of senile plaques, neurofibrillary tangles and A4 protein in human patients. *Neurosci. Lett.* **123**:141–143.

Atherton, E., E. Brown and R. C. Sheppard. **1981.** A physically supported gel polymer for low pressure, continous flow solid-phase reactions. applications for SPPS. *J. Chem. Soc. Chem. Commun.* 1151–1152.

Atherton, E., R. C. Sheppard and J. D. Wade. **1983**. Side-shain protected N^{α}-fluorenylmethoxycarbonyl amino acids for solid phase peptide synthesis. N^{α}-fluorenylmethoxycarbonyl-N^{G}-4-methoxy-2,3,6-trimethylbenzenesulfonyl-L-arginine. *J. Chem. Soc. Chem. Commun.* 1060–1062.

Atherton, E., L. E. Cammish, P. Goddard, J. D. Richards and R. C. Sheppard. **1984**. in "The Peptides 1984," (eds. Ragnarsson, A., B. Almquist and C. Wiksell) Stockholm, Sweden.

Atherton, E. and R. C. Sheppard. **1985**. Solid phase peptide synthesis using N^{α}-fluorenylmethoxycarbonyl amino acid pentafluorophenyl esters. *J. Chem. Soc. Chem. Commun.* **3**:165–166.

Atherton, E. and R. C. Sheppard. **1987**. in "The peptides, analysis, synthesis, biology," Vol. 9 (eds. Gross, E. and J. Meienhofer) Academic Press, New York, USA.

Atherton, E., J. Holder, M. Meldal, R. C. Sheppard and R. M. Valerio. **1988**. 3,4-dihydro-4-oxo-1,2,3-benzotriazin-3-yl esters of fluorenylmethoxycarbonyl amino acids as self-indicating reagents for SPPS. *J. Chem. Soc. 1, Perkin Trans.* **10**:2887–2894.

Bada, J. L. **1985**. *In vivo* racemization in mammalian proteins. *Met. Enzymol.* **106**:98–115.

Baes, C. F., Jr. and R. E. Mesmer. **1976**. in "The hydrolysis of cations," John Wiley, New York, USA.

Banin, E. and H. Meiri. **1990**. Toxic effects of alumino-silicates on nerve cells. *Neuroscience* **39**:171–178.

Barrow, C. J. and M. G. Zagorski. **1991**. Solution structures of ß peptide and its constituent fragments: relation to amyloid deposition. *Science* **253**:179–182.

Barrow, C. J., A. Yasuda, P. T. M. Kenny and M. G. Zagorski. **1992**. Solution conformations and aggregational properties of synthetic amyloid ß-peptides of Alzheimer's disease - analysis of circular dichroic spectra. *J. Mol. Biol.* **225**:1075–1093.

Benedek, K., S. Dong and B. L. Karger. **1984**. Kinetics of unfolding of proteins on hydrophobic surfaces in reversed-phase liquid chromatography. *J. Chromatogr.* **317**:227–243.

Beyreuther, K. **1993**. Inhalation of aluminium salts and Alzheimer's disease. *Hautarzt* **44**:810.

Blondelle, S. E. and R. A. Houghten. **1992**. Design of model amphipathic peptides having potent antimicrobial activities. *Biochemistry* **31**:12688–12694.

Blundell, T., and S. Wood. **1982**. The conformation, flexibility, and dynamics of polypeptide hormones. *Ann. Rev. Biochem.* **51**:123–154.

Bodanszky, M., and A. Bodanszky. **1984**. in "The practice of peptide synthesis," Springer-Verlag, Heidelburg, Germany.

Bottero, J. Y., J. M. Cases, F. Flessinger and J. E. Poirer. **980**. Studies of hydrolyzed aluminum chloride solutions. 1. nature of aluminum species and composition of aqueous solutions. *J. Phys. Chem.* **84**:2933–2939.

Bradford, M. M. **1976**. A rapid and sensitive method for the quantitation of microgram quantities of protein utilizing the principle of protein-dye binding. *Anal. Biochem.* **72**:248–254.

Buckingham, D. A., L. G. Marzilli and A. M. Sargeson. **1986**. Proton exchange and mutarotation of chelated amino acids *via* carbanion intermediate. *J. Am. Chem. Soc.* **89**:5133–5144.

Burdick, D. B. Soreghan, M. Kwon, J. Kosmoski, M. Knauer, A. Henschen, J. Yates, C. Cotman and C. Glabe. **1992**. Assembly and aggregation properties of synthetic Alzheimer's A4/ß amyloid peptide analogs. *J. Biol. Chem.* **267**:546–554.

Burgess, J. **1978**. in "Metal ions in solution," Ellis Horwood Ltd., Chichester, UK.

Busciglio, J., A. Lorenzo and B. A. Yankner. **1992**. Methodological variables in the assessment of beta amyloid neurotoxicity. *Neurobiol. Aging* **113**:609–612.

Cai, X.-D., T. E. Golde and S. G. Younkin. **1993**. Release of excess amyloid ß protein from a mutant amyloid ß protein precursor. *Science* **259**:514–516.

Candy, J. M., A. E. Oakley, J. Klinowski, T. A. Carpenter, R. H. Perry, J. R. Atack, E. K. Perry, G. Blessed, A. Fairbairn and J. A. Edwardson. **1986**. Aluminosilicate and senile plaque formation in Alzheimer's disease. *Lancet* **i**:354–357.

Candy, J. M., F. K. McArthur, A. E. Oakley, G. A. Taylor, C. P. L.-H. Chen and S. A. Mountfort. **1992**. Aluminium accumulation in relation to senile plaque and neurofibrillary tangle formation in the brains of patients with Alzheimer's disease. *J. Neurol. Sci.* **107**:210–218.

Canet, D., J. J. Delpeuch, M. R. Khaddar and P. Rubini. **1973**. Direct observation of solvated species by ^{27}Al NMR. *J. Magn. Reson.* **9**:329–330.

Castano, E. M., J. Ghiso, F. Prelli, P. D. Gorevic, A. Migheli and B. Frangione. **1986**. *In vitro* formation of amyloid fibrils from two synthetic peptides of different lengths homologous to Alzheimer's disease ß-protein. *Biochem. Biophys. Res. Commun.* **141**:782–789.

Chafi, A. H., J.-J. Hauw, G. Rancurel, J.-P. Berry and C. Galle. **1991**. Absence of aluminium in Alzheimer's disease brain tissue: electron microprobe and ion microprobe studies. *Neurosci. Lett.* **123**:61–64.

Charlet, Ph., J. P. Deloume, G. Duc and G. Thomas-David. **1984**. Chelation des ions Al^{3+} par les acides succinique, aspartique, glutamique et l'histidine etude potentiométrique. *Bull. Soc. Chim.* **7-8**:I222–I226.

Chen, G. C. and J. T. Yang. **1977**. Two-point calibration of circular dichrometer with d-10 amphorsulfonic acid. *Anal. Lett.* **10**:1195–1207.

Chen, M. and B. A. Yankner. **1991**. An antibody to ß-amyloid and amyloid precursor protein inhibits cell adhesion in many mammalian cell types. *Neurosci. Lett.* **125**:223–226.

Chou, P. Y. and G. D. Fasman. **1977**. ß-turns in proteins. *J. Mol. Biol.* **115**:135–175.

Chou, P. Y. and G. D. Fasman. **1978**. Prediction of the secondary structure of proteins from their amino acid sequence. *Adv. Enzymol.* **47**:45–148.

Chrastil, J. **1986**. Spectrophotometric determination of tryptophan and tyrosine in peptides and proteins based on new color reactions. *Anal. Biochem.* **158**:443–446.

Cohen, A. S. and E. Calkins. **1959**. Electron microscopic observations on a fibrous component in amyloid of diverse origins. *Nature* **183**:1202–1203.

Cohen, K. A., K. Schellenberg, K. Benedek, B. L. Karger, B. Grego and M. T. W. Hearn. **1984**. Mobile phase and temperature-effects in the reversed phase chromatographic separation of proteins. *Anal. Biochem.* **140**:223–235.

Connor, J. R., S. L. Menzies, S. M. St.-Martin, E. J. Mufson. **1992**. A histochemical study of iron, transferrin, and ferritin in Alzheimer diseased brains. *J. Neurosci. Res.* **31**:75–83.

Cooper, J. H. **1974**. Selective amyloid staining as a function of amyloid composition and structure. histochemical analysis of the alkaline Congo red standardized toluidine blue and iodine methodology. *Lab. Invest.* **31**:232–238.

Crapper, D. R., S. S. Krishnan and A. J. Dalton. **1973**. Brain aluminum distribution in Alzheimer's disease and especially neurofibrillary degeneration. *Science* **180**:511–513.

Crowther, R. A. **1991**. Straight and paired helical filaments in Alzheimer's disease have a common structural unit. *Proc. Natl. Acad. Sci. USA* **88**: 2288–2292.

Crumbliss, A. L. and J. M. Garrison. **1988**. A comparison of some aspects of the aqueous coordination chemistry of aluminum(III) and iron(III). *Comments Inorg. Chem.* **8**:1–26.

Davies, P. **1994**. Neuronal abnormalities, not amyloid, are cause of dementia in Alzheimer disease, in "Alzheimer's disease," (eds. Terry, R. D., R. Katzman and K. L. Bick), Raven Press Ltd., New York, USA.

Dawson, J. **1989.** Unravelling the Alzheimer tangle. *Brit. Med. J.* **297**:444.

Deloncle, R., O. Guillard, F. Clanet, P. Courtois and A. Piriou. **1990**. Aluminum transfer as glutamate complex through blood-brain barrier. *Biol. Trace Elem. Res.* **25**:39–45.

Divry, P. **1952**. La pathochimie generale et cellulaire des processus senile et preseniles. *Proc. 1st Int. Congr. Neuropathol. (Rome)* **2**:313 .

Esch, F. S., P. S. Keim, E. C. Beattie, R. W. Blacher, A. R. Culwell, T. Oltersdorf, D. McClure and P. J. Ward. **1990**. Cleavage of amyloid ß peptide during constitutive processing of its precursor. *Science* **248**:1122–1124.

Exley, C., N. C. Price, S. M. Kelly and J. D. Birchall. **1993**. An interaction of ß-amyloid with aluminium in vitro. *FEBS Lett.* **324**:293–295.

Fabian, H., G. I. Szendrei, H. H. Mantsch and L. Otvos, Jr. **1993**. Comparative analysis of human and Dutch-type Alzheimer ß-amyloid peptides by infrared spectroscopy and circular dichroism. *Biochem. Biophys. Res. Commun.* **191**:232-239.

Fankhauser, P., B. Schilling, P. Fries and M. Brenner. **1973**. in "Peptides 1971," (ed. Nesvadba, H.), North-Holland, Amsterdam.

Farnsworth, V., W. Carson and H. Krutzsch. **1991**. Reducing chemical background noise in automated protein sequencers. *Peptide Research* **4**:245–251.

Fasman, G. D. and C. D. Moore. **1994**. The solubilization of model Alzheimer tangles: reversing the ß-sheet conformation induced by aluminum with silicates. *Proc. Natl. Acad. Sci.* **91**:11232–11235.

Fatemi, S. J. A., D. J. Williamson and G. R. Moore. **1992**. A ^{27}Al NMR investigation of Al^{3+} binding to small carboxylic acids and the proteins albumin and transferrin. *J. Inorg. Biochem.* **46**:35–40.

Frangione, B., T. Wisniewski, F. Tagliavani, O. Bugiani and J. Ghiso. **1993**. Alzheimer's disease and Dutch variant: opposing faces of a single coin, in "Alzheimer's disease: advances in clinical and basic research," (eds. B. Corain, K. Iqbal, B. Nicolini, B. Winblad, H. Wisniewski and P. Zatta), Wiley, New York, USA.

Fraser, P. E., J. T. Nguyen, W. K. Surewicz and D. A. Kirschner. **1991a**. pH-dependent structural transitions of Alzheimer amyloid peptides. *Biophys. J.* **60**:1190–1201.

Fraser, P. E., L. K. Duffy, M. B. O'Malley, J. Nguyen, H. Inouye and D. A. Kirschner. **1991b**. Morphology and antibody recognition of synthetic ß-amyloid peptides. *J. Neurosci. Res.* **28**:474–485.

Fraser, P. E., J. T. Nguyen, H. Inouye, W. K. Surewicz, D. J. Selkoe, M. B. Podlisny and D. A. Kirschner. **1992**. Fibril formation by primate, rodent, and Dutch-hemorrhagic analogues of Alzheimer amyloid ß-protein. *Biochemistry* **31**:10716–10723.

Frederickson, C. J. **1989**. Neurobiology of zinc and zinc-containing neurons. *J. Int. Rev. Neurobiol.* **31**:145–238.

Gandy, S. E., R. Bhasin, T. V. Ramabhadran, E. H. Koo, D. Price, D. Goldgaber and P. Greengard. **1992**. Alzheimer ßA/4 amyloid precursor protein: evidence for putative amyloidogenic fragment. *J. Neurochem.* **58**:383–386.

Gandy, S., G. Caparaso, J. Buxbaum, B. Frangione and P. Greengard. **1994**. APP processing, Aß-amyloidogenesis, and the pathogenesis of Alzheimer's disease. *Neurobiol. Aging* **15**:253–256.

Ganrot, P. O. **1986**. Metabolism and possible health effects of aluminum. *Environ. Health. Perspect.* **65**:363–441.

Gardella, J. E., G. Gorgone, P. C. Munoz, J. Ghiso, B. Frangione and P. D. Gorevic. **1992**. Beta protein precursor expression in human platelets and a megakaryocyte cell line. *Lab. Invest.* **67**:303–313.

Gauss, J., U. Schneider, R. Ahlrichs, C. Dohmeier and H. Schnökel. **1993.** ^{27}Al NMR spectroscopic investigation of aluminum(I) compounds: *ab initio* calculations and experiment. *J. Am. Chem. Soc.* **115**:2402–2408.

Ghiso, J., A. Rostagno, J. E. Gardella, L. Liem, P. D. Gorevic and B. Frangione. **1992**. A 109-amino-acid C-terminal fragment of Alzheimer's disease amyloid precursor protein contains a sequence -RHDS-, that promotes cell adhesion. *Biochem. J.* **288**:1053–1059.

Glabe, C. G. **1990**. Semi-automatic synthesis of large peptides with a continuous flow instrument using fmoc-amino acids chemistry. *Technique* **2**:138–146.

Glajch, J. L., M. A. Quarry, J. F. Vasta and L. R. Snyder. **1986**. Separation of peptide mixtures by reversed-phase gradient elution. use of flow-rate changes for controlling band spacing and improving resolution. *Anal. Chem.* **58**:280–285.

Glenner, G. G., J. Harbaugh, J. E. Ohms, M. Harada and P. Cuatrecasas. **1970**. An amyloid protein: the amino-terminal variable fragment of an immunoglobin light chain. *Biochem. Biophys. Res. Commun.* **41**:1287–1289.

Glenner, G., W. Terry, M. Harada, C. Isersky and D. Page. **1971**. Amyloid fibril proteins: proof of homology with immunoglobin light chains by sequence analyses. *Science* **172**:1150–1151.

Glenner, G. G., E. D. Eanes, H. A. Bladen, R. P. Linke and J. D. Termine. **1974**. ß-pleated sheet fibrils: a comparison of native amyloid with synthetic protein fibrils. *J. Histochem. Cytochem.* **22**:1141–1158.

Glenner, G. G. **1980**. Amyloid deposits and amyloidosis. the ß-fibrilloses. *N. Engl. J. Med.* **302**:1283–1292.

Glenner, G. G. and C. W. Wong. **1984a**. Alzheimer's disease: initial report of the purification and characterization of a novel cerebrovascular amyloid protein. *Biochem. Biophys. Res. Commun.* **120**:885–890.

Glenner, G. G. and C. W. Wong. **1984b**. Alzheimer's disease and Down's syndrome: sharing of a unique cerebrovascular amyloid fibril protein. *Biochem. Biophys. Res. Commun.* **120**:1131–1135.

Glenner, G. G. and C. Wong. **1987**. Amyloidosis in Alzheimer's disease and Down's syndrome. *Mol. Neuropathol. of Aging: Banbury Report* **27**:253–265.

Glenner G. G. **1988**. Alzheimer's disease: its proteins and genes. *Cell* **52**:307–308.

Golde, T. E., S. Estus, L. Younkin, D. J. Selkoe and S. G. Younkin. **1992**. Processing of the amyloid protein precursor to potentially amyloidogenic derivatives. *Science* **255**:728–730.

Gotham, S. M., P. J. Fryer and W. R. Paterson. **1988**. The measurement of insoluble proteins using a modified Bradford assay. *Anal. Biochem.* **173**:353–358.

Gray, D. M., D. Lang, E. Kuner, M. Vaughn and J. Sutherland. **1984**. A thin quartz cell suitable for vacuum ultraviolet absorbance and CD measurements. *Anal. Biochem.* **136**:247–250.

Greenfield, N. and G. D. Fasman. **1969**. Computed circular dichroism spectra for the evaluation of protein conformation. *Biochemistry* **8**:4108–4116.

Gregor, J. E. and H. K. J. Powell. **1986**. Aluminium(III)-citrate complexes: a potentiometric and ^{13}C NMR study. *Aust. J. Chem.* **39**:1851–1864.

Guo, D., C. T. Mant, A. K. Taneja, J. M. R. Parker and R. S. Hodges. **1986**. Prediction of peptide retention times in reversed-phase high-performance liquid chromatography. (I) determination of retention coefficients of amino acid residues of model synthetic peptides. *J. Chromatogr.* **359**:499–517.

Haass, C., E. H. Koo, A. Mellon, A, Y. Hung and D. J. Selkoe. **1992**. Targeting of cell-surface ß-amyloid precursor protein to lysosomes: alternative processing into amyloid-bearing fragments. *Nature* **357**:500–503.

Halverson, K., P. E. Fraser, D. A. Kirschner and P. T. Lansbury, Jr. **1990**. Molecular determinants of amyloid deposition in Alzheimer's disease: conformational studies of synthetic ß-protein fragments. *Biochemistry* **29**:2639–2644.

Halverson, K. J., I. Sucholeiki, T. T. Ashburn and P. T. Lansbury, Jr. **1991**. Location of ß-sheet forming sequences in amyloid proteins by FTIR. *J. Am. Chem. Soc.* **113**:6701–6703.

Halverson, K. J. **1992**. The molecular determinants of amyloid deposition in Alzheimer's disease. Ph.D. Thesis, M.I.T., MA, USA.

Haraguchi, H. and S. Fujuwara. **1969**. Aluminum complexes in solution as studied by aluminum-27 nuclear magnetic resonance. *J. Phys. Chem.* **73**:3467–3473.

Hardy, J. A. and G. A. Higgins. **1992**. Alzheimer's disease: the amyloid cascade hypothesis. *Science* **256**:184–185.

Harris, W. R. and J. Sheldon. **1990**. Equilibrium constants for the binding of aluminum to human serum transferrin. *Inorg. Chem.* **29**:119–124.

Harris, W. R. **1992**. Equilibrium model for speciation of aluminum in serum. *Clin. Chem.* **38**:1809–1818.

Hearn, M. T. W. and B. Grego. **1984**. High-performance liquid chromatography of amino acids, peptides and proteins. Iv. studies on the origin of band broadening of polypeptides and proteins separated by reversed-phase high-performance liquid chromatography. *J. Chromatogr.* **296**:61–82.

Hearn, M. T. W., A. N. Hodder and M.-I. Aguilar. **1985**. High-performance liquid chromatography of amino acids, peptides and proteins. lxvi. investigations on the effects of chromatographic dwell times in the reversed-phase high-performance liquid chromatographic separtions of proteins. *J. Chromatogr.* **327**:47–66.

Hearn, M. T. W. **1983**. in "HPLC - Advances and Perspectives," Vol. 3, (ed. Horvath. Cs.), Academic Press, New York, USA.

Hearn, M. T. W. and M .I. Aguilar. **1986**. High-performance liquid chromatography of amino acids, peptides, and proteins. lxvii. evaluation of bandwidth relationships of peptides related to human beta-endorphin, separated by gradient elution reversed-phase high-performance liquid chromatography. *J. Chromatogr.* **352**:35–52.

Hearn, M. T. W. and M. I. Aguilar. **1987**. High-performance liquid chromatography of amino acids, peptides and proteins. lxix. evaluation of retention and bandwidth relationships of myosin-related peptides separated by

gradient elution reversed-phase high-performance liquid chromatography. *J. Chromatogr.* **392**:33–49.

Hendrix, J. C. and P. T. Lansbury, Jr. **1992**. Synthesis of a protected peptide corresponding to residues 1–25 of the ß–amyloid protein of Alzheimer's disease. *J. Org. Chem.* **57**:3421–3426.

Hennessey, J. P. and W. C. Johnson, Jr. **1981**. Information content in the circular dichroism of proteins. *Biochemistry* **20**:1085–1094.

Hilbich, C., B. Kisters-Woike, J. Reed, C. L. Masters and K. Beyreuther. **1991**. Aggregation and secondary structure of synthetic amyloid ßA4 peptides of Alzheimer's disease. *J. Mol. Biol.* **218**:149–163.

Hilbich, C., B. Kisters-Woike, J. Reed, C. L. Masters and K. Beyreuther. **1992**. Substitutions of hydrophobic amino acids reduce the amyloidogenicity of Alzheimer's disease ßA4 peptides. *J. Mol. Biol.* **228**:460–473.

Hind, C. **1986**. in "Amyloidosis and amyloid P component," Longman Scientific and Technical, Essex, England.

Hinton, J. F. and R. W. Briggs. **1978**. in "NMR and the Periodic Table," (eds. Harris, R. K. and B. E. Mann), Academic Press, New York, USA.

Hirano, A., N. Malamud and L. T. Kurland. **1961**. Parkinsonism dementia complex, an endemic disease on the island of Guam. II. Pathological features. *Brain* **84**:662–679.

Hollosi, M., L. Otvos, Jr., J. Kajtar, A. Perczel and V. M.-Y. Lee. **1989**. Is amyloid deposition in Alzheimer's disease preceded by an environment-induced double conformational transition? *Peptide Research* **2**:109–113.

Hollósi, M., L. Ürge, A. Perczel, J. Kajtár, I. Teplán, L. Ötvös, Jr. and G. D. Fasman. **1992**. Metal ion-induced conformational changes of phosphorylated fragments of human neurofilament (NF-M) protein. *J. Mol. Biol.* **223**:673–682.

Hollósi, M., Z. M. Shen, A. Perczel and G. D. Fasman. **1994**. Stable intrachain and interchain complexes of neurofilament peptides: a putative link between Al^{3+} and Alzheimer's disease. *Proc. Natl. Acad. Sci. USA* **91**:4902–4906.

Hopp, T. P. and K. R. Woods. **1981**. Prediction of protein antigenic determinants from amino acid sequences. *Proc. Natl. Acad. Sci. USA* **78**:3824–3828.

Horvath, Cs., W. Melander and I. Molnar. **1976**. Solvophobic interactins in liquid chromatography with non-polar stationary phases. *J. Chromatogr.* **125**:129–156.

Houghton, R. A. and C. H. Li. **1977.** Reduction of methionine sulfoxide to methionine in peptides and proteins. *Peptides; Proceedings of American Peptide Symposium (5th)*, 458–460.

Huang, Y. P. and E. E. Bittar. **1991**. Protection by GTP from the effects of aluminum on the sodium efflux in barnacle muscle fibers. *Biochim. Biophys. Acta* **1062**:255–263.

Huang, Y. P. and E. E. Bittar. **1992**. The ability and inability of ATP to stop aluminum from reducing the sodium efflux in unpoisoned barnacle muscle fibers. *Biochim. Biophys. Acta* **1103**:77–84.

Huheey, J. E. **1983**. in "Inorganic chemistry," Harper and Row, New York, USA.

Inouye, H., P. E. Fraser and D. A. Kirschner. **1993**. Structure of ß-crystallite assemblies formed by Alzheimer ß-amyloid protein analogues: analysis by x-ray diffraction. *Biophys. J.* **64**:502–519.

Jarrett, J. T. and P. T. Lansbury, Jr. **1993**. Amyloid fibril formation requires a chemically discriminating nucleation event: studies of an amyloidogenic sequence from the bacterial protein OsmB. *Biochemistry* 31:12345–12352.

Jarrett, J. T., E. P. Berger and P. T. Lansbury, Jr. **1993**. The carboxy terminus of the ß amyloid protein is critical for the seeding of amyloid formation: implications for the pathogenesis of Alzheimer's disease. *Biochemistry* **32**:4673–4697.

Johnson, W. C., Jr. **1990**. Protein secondary structure and circular dichroism: a practical guide. *Proteins* **7**:205–214.

Johnson, W. C., Jr. **1988**. Secondary structure of proteins through circular dichroism spectroscopy. *Ann. Rev. Biophys. Biophys. Chem.* **17**:145–166.

Kabsch, W. and C. Sander. **1983**. Dictionary of protein secondary structure: pattern recognition of hydrogen-bonded and geometrical features. *Biopolymers* **22**:2577–2637.

Kaiser, E., R. L. Colescott, C. D. Bossinger and P. I. Cook. **1970**. Color test for detection of free terminal amino groups in the solid-phase synthesis of peptides. *Anal. Biochem.* **34**:595–598.

Kang, J., H.-G. Lemaire, A. Unterbeck, J. M. Salbaum, C. L. Masters, K.-H. Grzeschik, G. Multhaup, K. Beyreuther and B. Muller-Hill. **1987**. The precursor of Alzheimer's disease amyloid A4 protein resembles a cell-surface receptor. *Nature* **325**:733–736.

Karlik, S. J., E. Tarien, G. A. Elgavish and G. L. Eichhorn. **1983**. Aluminum-27 nuclear magnetic resonance study of aluminum(III) interaction with carboxylate ligands. *Inorg. Chem.* **2**:525–529.

Karlik, S. J., G. L. Eichhorn, P. N. Lewis and D. R. Crapper. **1980**. Interaction of aluminum species with deoxyribonucleic acid. *Biochemistry* **19**:5991–5998.

Katzman, R. and T. Saitoh. **1991**. Advances in Alzheimer's disease. *FASEB J.* **5**:278–286.

Katzman, R., R. D. Terry and K. L. Bick. **1978**. in "Alzheimer's senile dementia and related disorders," Raven Press, New York, USA.

Kawahara, M., K. Muromato, K. Kobayashi, H. Mori and Y. Kuroda. **1994**. Aluminum promotes the aggregation of Alzheimer's amyloid ß-protein *in vitro*. *Biochem. Biophys. Res. Commun.* **198**:531–535.

Kent, S. B. H., A. R. Mitchell, M. Engelhard and R. B. Merrifield. **1979**. Mechanisms and prevention of trifluoroacetylation in solid-phase peptide synthesis. *Proc. Natl. Acad. Sci. USA* **76**:2180–2184.

Kent, S. B. H. **1985**. in "Peptides: structure and function," (eds. Deber, C. M., V. J. Hruby and K. D. Kopple), Pierce Chemical, Illinois, USA.

Kent, S. B. H. **1988**. Chemical synthesis of peptides and proteins. *Ann. Rev. Biochem.* **57**:957–989.

Kerlavage, A. R., C. J. Weitzman, T. Hasan and B. S. Cooperman. **1983**. Reversed-phase high-performance liquid chromatography of *Escherichia coli* ribosomal proteins. characteristics of the separation of a complex protein mixture. *J. Chromatogr.* **266**:225–237.

Kirschner, D. A., H. Inouye, L. K. Duffy, A. Sinclair, M. Lind and D. J. Selkoe. **1986**. X-ray diffraction from intraneuronal paired helical filaments and

extraneuronal amyloid fibers in Alzheimer disease indicates cross-ß conformation. *Proc. Natl. Acad. Sci. USA* **83**:503–507.

Kirschner, D. A., H. Inouye, L. K. Duffy, A. Sinclair, M. Lind, and D. J. Selkoe. **1987**. Synthetic peptide homologous to ß-protein from Alzheimer disease forms amyloid-like fibrils *in vitro*. *Proc. Natl. Acad. Sci. USA* **84**:6953–6957.

Kirschner, D. A., P. E. Fraser, J. Nyugen, H. Inouye, K. halverson, P. T. Lansbury, Jr. and L. K. Duffy. **1990**. Structure of Alzheimer amyloid peptide assemblies *in vitro*. *Trans. Am. Soc. Neurochem.* **21**:112.

Kisfaludy, L. and I. Schon. **1983**. Preparation and application of pentafluorophenyl esters of 9-fluorenylmethloxycarbonyl amino acids for peptide synthesis. *Synthesis* 325–327.

Klatzo, I., H. Wisniewski and E. Streicher. **1965**. Experimental production of neurofibrillary degeneration. I. light microscopic observations. *J. Neuropathol. Exp. Neurol.* **24**:187–199.

Klunk, W., J. Pettegrew and D. Abraham. **1989**. Quantitative evaluation of Congo red binding to amyloid-like proteins with a ß-pleated conformation. *J. Histochem. Cytochem.* **37**:1273–1281.

Knauer, M. F., B. Soreghan, D. Burdick, J. Kosmoski and C. G. Glabe. **1992**. Intracellular accumulation and resistance to degradation of the Alzheimer amyloid A4/ß protein. *Proc. Natl. Acad. Sci. USA* **89**:7437–7441.

Kosik, K. and P. Coleman. **1992**. Is ß-amyloid neurotoxic? *Neurobiol. Aging* **13**:535–627.

Kragten, J. **1978**. in "Atlas of metal-ligand equilibria in aqueous solution," Vol. 3, Halstead Press, New York, USA.

Kuwajima, K., H. Yamaya, S. Miwa, S. Sugai and T. Nagamura. **1987**. Rapid formation of secondary structure framework in protein folding studied by stopped-flow circular dichroism. *FEBS Lett.* **221**:115–118.

Kuwajima, K. **1989**. The molten globule state as a clue for understanding the folding and cooperativity of globular-protein structure. *Proteins* **6**:87–103.

Labhardt, A. M. **1982**. Secondary structure in ribonuclease. I. equilibrium folding transitions seen by amide circular dichroism. *J. Mol. Biol.* **157**:331–335.

Laczko-Hollosi, I., M. Hollosi, V. M.-Y. Lee and H. H. Mantsch. **1992**. Conformational change of a synthetic amyloid analogue des[Ala^{21,30}]A42 upon binding to octyl glucoside micelles. *Eur. Biophys. J.* **21**:345–348.

Landsberg, J. P., B. McDonald and F. Watt. **1992**. Absence of aluminium in neuritic plaque cores in Alzheimer's disease. *Nature* **360**:65–68.

Lang, E., G.I. Szendrei, I. Elekes, V. M.-Y. Lee and L. Otvos, Jr. **1992**. Reversible ß-pleated sheet formation of a phosphorylated synthetic τ peptide. *Biochem. Biophys. Res. Commun.* **182**:63–69.

Lansbury, P. T., Jr. **1992**. In pursuit of the molecular structure of amyloid plaque: new technology provides unexpected and critical information. *Biochemistry* **31**:6865–6870.

Lau, S. Y. M., A. K. Taneja and R. S. Hodges. **1984**. Effects of high-performance liquid chromatographic solvents and hydrophobic matrices on the secondary and quaternary structure of a model protein. reversed-phase and size-exclusion high-performance liquid chromatography. *J. Chromatogr.* **317**:129–140.

Lee, V. M.-Y., B. J. Balin, L. Otvos, Jr. and L. Trojanowski. **1991**. A68: a major subunit of paired helical filaments and derivatized forms of normal tau. *Science* **251**:675–678.

Lemaire, H. G., J. M. Salbaum, G. Multhaup, J. Kang, R. M. Bayney, A. Unterbeck, K. Beyreuther and B. Muller-Hill. **1989**. The preA4(695) precursor protein of Alzheimer's disease A4 amyloid is encoded by 16 exons. *Nucleic Acids Res.* **17**:517–522.

LeVine, H., III. **1993**. Thioflavine T interaction with synthetic Alzheimer's disease ß-amyloid peptides: detection of amyloid aggregation in solution. *Protein Science* **2**:404–410.

Levy, E., M. D. Carman, I. J. Fernandez-Madrid, M. D. Power, I. Lieberburg, S. G. van Duinen, G. T. A. M. Bots, W. Luyendijk and B. Frangione. **1990**. Mutation of the Alzheimer's disease amyloid gene in hereditary cerebral hemorrhage, Dutch type. *Science* **248**:1121–1126.

Lu, X. M., K. Benedek and B. L. Karger. **1986**. Conformational effects in the high-performance liquid chromatography of proteins. further studies of the reversed-phase chromatographic behaviour or ribonuclease A. *J. Chromatogr.* **359**:19–29.

Lukas, T., M. B. Prystowsky and B. W. Erickson. **1981**. Solid-phase peptide synthesis under continuous-flow conditions. *Proc. Natl. Acad. Sci. USA* **78**:2791–2795.

Lustig, B. and A. L. Fink. **1992**. Secondary structure precedes tertiary structure in the refolding of ribonuclease A. *Biochim. Biophys. Acta* **1121**:229–233.

Mahurkar, S. D., S. K. Dhar, S. Salta, L. Meyers, Jr., E. C. Smith and G. Dunea. **1973**. Dialysis dementia. *Lancet* **i**:1412–1415.

Man, E. H., G. H. Fisher, I. L. Payan, R. Cadilla-Perezrios, N. M. Garcia, R. Chemburkar, G. Arends and W. H. Frey, II. **1983**. Accumulation of D-aspartic acid with age in human brain. *Science* **220**:1407–1408.

Manavalan, P. and W. C. Johnson, Jr. **1987**. Variable selection method improves the prediction of protein secondary structure from circular dichroism spectra. *Anal. Biochem.* **167**:76–85.

Mann, D. M. A. **1989**. Cerebral amyloidosis, aging and Alzheimer's disease: a contribution from studies on Down's syndrome. *Neurobiol. Aging* **10**:397–399.

Manning, M. C. and R. W. Woody. **1987**. Theoretical determination of the cd of proteins containing closely packed antiparallel ß-sheets. *Biopolymers* **26**:1731–1732.

Manning, M. C. and R. W. Woody. **1989**. Theoretical study of the contribution of aromatic side chains to the circular dichroism of basic bovine pancreatic trypsin inhibitor. *Biochemistry* **28**:8609–8613.

Mant, C. T. and R. S. Hodges. **1987**. Monitoring free silanols on reversed-phase supports with peptide standards. *Chromatographia* **24**:805–814.

Mant, C. T., J. M. R. Parker and R. S. Hodges. **1987**. Size-exclusion high-performance liquid chromatography of peptides. requirement for peptide standards to monitor column performance and non-ideal behaviour. *J. Chromatogr.* **397**:99–112.

Mant, C. T., T. W. L. Burke, J. A. Black and R. S. Hodges. **1988**. Effect of peptide chain length on peptide retention behaviour in reversed-phase chromatography. *J. Chromatogr.* **458**:193–205.

Mant, C. T., N. E. Zhou and R. S. Hodges. **1989**. Correlation of protein retention times in reversed-phase chromatography with peptide chain length and hydrophobicity. *J. Chromatogr.* **476**:363–375.

Mantyh, P. W., J. R. Ghilardi, S. Rogers, E. DeMaster, C. J. Allen, E. R. Stimson and J. E. Maggio. **1993**. Aluminum, iron, and zinc ions promote aggregation of physiological concentrations of ß-amyloid peptide. *J. Neurochem.* **61**:1171–1174.

Markesbery, W. R., W. D. Ehmann, T. I. M. Hossain, M. Allaudin and D. T. Goodin. **1981**. Instrumental neutron activation analysis of brain aluminum in Alzheimer's disease and aging. *Ann. Neurol.* **10**:511–516.

Marsh, R. E., R. B. Corey and L. Pauling. **1955**. An investigation of the structure of silk fibroin. *Biochim. Biophys. Acta* **16**:1–34.

Martin, R. B. **1986a**. The chemistry of aluminum as related to biology and medicine. *Clin. Chem.* **32**:1797–1806.

Martin, R. B. **1986b**. Citrate binding of Al^{3+} and Fe^{3+}. *J. Inorg. Biochem.* **28**:181–187.

Martin, R. B., J. Savory, S. Brown, R. L. Berthoff and M. R. Wills. **1986**. Transferrin binding of Al^{3+} and Fe^{3+}. *Clin. Chem.* **33**:405–407.

Martin, R. B. **1988**. Bioinorganic chemistry of aluminum, in "Metal ions in biological systems, Vol. 24, (eds. Sigel. H. and A. Sigel), Marcel Dekker, New York, USA.

Masters, C. L., G. Simms, N. A. Weidemann, G. Multhaup, B. L. McDonald and K. Beyreuther. **1985**. Amyloid plaque core protein in Alzheimer disease and Down syndrome. *Proc. Natl. Acad. Sci. USA* **82**:4245–4249.

Matsoukas, J., J. Hondrelis, G. Agelis, R. Yamdughi, R. C. Gante and G. J. Moore. **1991**. in "Peptides, 1990," (eds. Girault, E. and D. Andrew), ESCOM, Leiden, Nederlands.

Matsudaira, P. **1987**. Sequence from picomole quantities of proteins electroblotted onto polyvinylidenedifluoride membranes. *J. Biol. Chem.* **262**:10035–10038.

Matsumoto, A. and Y. Fujiwara. **1991**. Abnormal and deficient processing of ß-amyloid precursor protein in familial Alzheimer's disease lymphoblastoid cells. *Biochem. Biophys. Res. Commun.* **175**:361–365.

Mazurguil, H., R. Haran and J.-P. Laussac. **1982**. The binding of aluminium to [leu^5]-enkephalin. an investigation using ^{1}H, ^{13}C and ^{27}Al NMR spectroscopy. *Biochim. Biophys. Acta* **717**:465–472.

McDermott, J. R., A. I. Smith, M. K. Ward, I. S. Parkinson and D. N. Kerr. **1978**. Brain aluminium concentration in dialysis encepalopathy. *Lancet* **1**:901–904.

McDermott, J. R., A. I. Smith, K. Iqbal and H. M. Wisniewski. **1979**. Brain aluminium in aging and Alzheimer disease. *Neurology* **29**:809–814.

McLachlan, D. R. C., W. J. Lukiw and T. P. A. Kruck. **1989**. New evidence for an active role of aluminum in Alzheimer's disease. *Can. J. Neurol. Sci.* **16**:490–497.

Meiri, H., E. Banin, M. Roll and A. Rousseau. **1993**. Toxic effects of aluminium on nerve cells and synaptic transmission. *Prog. Neurobiol.* **40**:89–121.

Merrifield, R. B. **1963**. Solid phase synthesis. I. the synthesis of a tetrapeptide. *J. Am. Chem. Soc.* **85**:2144–2154.

Mihalyi, E. **1969**. Spectrophotometric analysis of amino acids in proteins and peptides. *J. Chem. Engg. Data* **13**:179–182.

Miller, D. L., I. A. Papayannopoulous, J. Styles, S. A. Bobin, Y. Y, Lin, K. Biemann and K. Iqbal. **1993**. Peptide compositions of the cerebrovascular and senile plaque core amyloid deposits of Alzheimer's disease. *Arch. Biochem. Biophys.* **301**:41–52.

Molitoris, B. A., D. H. Froment, T. A. Mackenzie, W. H. Huffer and A. C. Alfrey. **1989**. Citrate: a major factor in the toxicity of orally administered aluminum compounds. *Kidney International* **36**:949–953.

Motte, J. and R. S. Williams. **1989**. Age-related changes in the density and morphology of plaques and neurofibrillary tangles in Down's syndrome brian. *Acta Neuropathol.* **77**:535–546.

Muga, A., W. K. Surewicz, P. T. T. Wong, H. H. Mantsch, V. K. Singh and T. Shinohara. **1990**. Structural studies with the uveopathogenic peptide M derived from retinal S-antigen. *Biochemistry* **29**:2925–2930.

Nicot, C. and M. Waks. **1989**. in "Structure and reactivity in reverse micelles," (ed. Pileni, M. P.), Elsevier, Amsterdam.

Nishi, M. T. Sanke, S. Nagamatsu, G. I. Bell. and D. F. Steiner. **1990**. Islet amyloid polypeptide . a new ß cell secretory product related to islet amyloid deposits. *J. Mol. Biol.* **265**:4173–4176.

Orlando, R., P. T. M. Kenny and M. G. Zagorski. **1992**. Covalent modification of Alzheimer's amyloid ß-peptide in formic acid solutions. *Biochem. Biophys. Res. Commun.* **184**:686–691.

Ott, S. M., N. A. Maloney, J. W. Coburn, A. C. Alfrey and D. J. Sherrard. **1982**. The prevalence of bone aluminum deposition in renal osteodystrophy and its relation to the response to calcitriol therapy. *N. Engl. J. Med.* **307**:709–713.

Otvos, L., Jr., M. Hollosi, A. Perczel, B. Dietzschold and G. D. Fasman. **1988**. Phosphorylation loops in synthetic peptides of the human neurofilament protein middle-sized subunit. *J. Protein Chem.* **7**:365–376.

Otvos, L., Jr., G. I. Szendrei, V. M.-Y. Lee and H. H. Mantsch. **1993**. Human and rodent Alzheimer ß-amyloid peptides acquire distinct conformations in membrane-mimicking solvents. *Eur. J. Biochem.* **211**:249–257.

Palmert, M. R., M. B. Podlisny, D. S. Witker, T. Oltersdorf, L. H. Younkin, D. J. Selkoe and S. G. Younkin. **1989**. The ß-amyloid protein precursor of Alzheimer disease has soluble derivatives found in human brain and cerebrospinal fluid. *Proc. Natl. Acad. Sci. USA* **86**:6338–6342.

Pauling, L. and R. B. Corey. **1951**. Configurations of polypeptide chains favored orientations around single bonds. *Proc. Natl. Acad. Sci. USA* **37**:729–740.

Pearson, R. C. A., M. M. Esiri, R. W. Hiorns, G. K. Wilcock and T. P. S. Powell. **1985**. Anatomical correlates of the distribution of the pathological changes in the neocortex in Alzheimer's disease. *Proc. Natl. Acad. Sci. USA* **82**:4531–4534.

Pena, M. C., M. Rico, M. A. Jimenez, J. Herranz, J. Santoro and J. L. Nieto. **1989**. Conformational properties of the isolated 1-23 fragment of human hemoglobin α-chain. *Biochim. Biophys. Acta* **957**:380–389.

Perczel, A., M. Hollósi, G. Tusnády and G. D. Fasman. **1991**. Convex constraint analysis: a natural deconvolution of circular dichroism curves in proteins. *Protein Engineering* **4**:669–679.

Perczel, A., K. Park and G. D. Fasman. **1992a**. Deconvolution of the circular dichroism spectra of proteins: the circular dichroism spectra of the antiparallel ß-sheet in proteins. *Proteins: Structure, Function, and Genetics* **13**:57–69.

Perczel, A., K. Park and G. D. Fasman. **1992b**. Analysis of the circular dichroism spectrum of proteins using convex constraint algorithm: a practical guide. *Anal. Biochem.* **203**:83–93.

Perl, D. and A. Brody. **1980**. X-ray spectrometric evidence of aluminum accumulation in neurofibrillary tangle-bearing neurons. *Science* **208**:297–299.

Perl, D. P. **1985**. Relationship of aluminum to Alzheimer's disease. *Environ. Health Perspect.* **63**:149–153.

Perl, D. P. **1988**. Aluminum and Alzheimer's disease: methodologic approaches, in "Metal ions in biological systems," Vol. 24, (eds. Sigel, H. and A. Sigel), Marcel-Dekker, New York, USA.

Pike, C. J., A. J. Walencewicz, C. G. Glabe and C. W. Cotman. **1991**. In vitro aging of ß-amyloid protein causes peptide aggregation and neurotoxicity. *Brain Research* **563**:311–314.

Pike, C. J., D. Burdick, A. J. Walencewicz, C. G. Glabe and C. W. Cotman. **1993**. Neurodegeneration induced by ß-amyloid peptides *in vitro*: the role of peptide assembly state. *J. Neurosci.* **13**:1676–1687.

Prelli, F., E. M. Castano, G. G. Glenner and B. Frangione. **1988**. Differences between vascular and plaque core amyloid in Alzheimer's disease. *J. Neurochem.* **51**:648–651.

Price, D. L. **1986**. New perspectives in Alzheimer's disease. *Ann. Rev. Neurosci.* **9**:489–512.

Prior, J. C., E. C. Cameron, W. J. Knickerbocker, V. P. Sweeney and O. Suchowersky. **1982**. Dialysis encephalopathy and osteomalacic bone disease. a case controlled study. *Am. J. Med.* **72**:33–42.

Provencher, S. W. and J. Glöckner. **1981**. Estimation of globular secondary structure from circular dichroism. *Biochemistry* **20**:33–37.

Prusiner, S. B., M. P. McKinley, K. A. Bowman, D. C. Bolton, P. E. Bendheim, D. F. Groth and G. G. Glenner. **1983**. Scrapie prions aggregate to form amyloid-like birefringent rods. *Cell* **35**:349.

Prusiner, S. B. **1991**. Molecular biology of prion diseases. *Science* **252**:1515–1522.

Ptitsyn, O. B. **1987**. Protein folding: hypotheses and experiments. *J. Prot. Chem.* **6**:273–293.

Ptitsyn, O. B., R. H. Pain, G. V. Semisotnov, E. Zerovnik and O. I. Razgulyaev. **1990**. Evidence for a molten globule state as a general intermediate in protein folding. *FEBS Lett.* **262**:20–24.

Ramabhadran, T. V., S. E. Gandy, J. Ghiso, A. Czernik, D. Ferris, R. Bhasin, D. Goldgaber, B. Frangione and P. Greengard. **1993**. Proteolytic processing of human amyloid ß protein precursor in insect cells. major carboxyl-termianl fragment is identical to its human counterpart. *J. Biol. Chem.* **268**:2009–2012.

Robinson, A. B. and C. J. Rudd. **1974**. Deamidation of glutaminyl and asparaginyl residues in peptides and proteins. *Curr. Top. Cell. Regul.* **8**:247–295.

Roher, A. E., J. D. Lowenson, S. Clarke, C. Wolkow, R. Wang, R. J. Cotter, I. M. Reardon, H. A. Zurcher-Neely, R. L. Heinrikson, M. J. Ball, and B. D. Greenburg. **1993**. Structural alterations in the peptide backbone of a ß-amyloid core protein may account for its deposition and stability in Alzheimer's disease. *J. Biol. Chem.* **268**:3072–3083.

Salom, D., C. Abad and L. Braco. **1992**. Characterization of gramicidin A in an inverted micellar environment. a combined high-performance liquid chromatography and spectroscopic study. *Biochemistry* **31**:8072–8079.

Sanan, D. A., K. Weisgraber, D. Y. Huang, A. Saunders, D. Schmechel, T. Wisniewski, B. Frangione, A. D. Roses and W. J. Strittmatter. **1994**. Apolipoprotein E associates with Aß amyloid peptide to form novel monofibrils: isoform apoE4 associates more efficiently than apoE3. *J. Clin. Invest.* **94**:860–869.

Sarin, V. K., S. B. H. Kent and R. B. Merrifield. **1980**. Properties of swollen polymer networks. solvation and swelling of peptide-containing resins in solid-phase peptide synthesis. *J. Am. Chem. Soc.* **102**:5463–5470.

Sarin, V. K., S. B. H. Kent, J. P. Tam and R. B. Merrifield. **1981**. Quantitative monitoring of solid-phase peptide synthesis by the ninhydrin reaction. *Anal. Biochem.* **117**:147–157.

Sarkar, P. K. and P. Doty. **1966**. Optical rotary properties of ß-configuration in polypeptides and proteins. *Proc. Natl. Acad. Sci. USA* **55**:981–989.

Schulz, G. E. **1988**. A critical evaluation of methods for prediction of protein secondary structures. *Ann. Rev. Biophys. Biophys. Chem.* **17**:1–21.

Schuurmans Stekhoven, J. H., K. Renkawek, I. Otte-Höller and A. Stols. **1990**. Exogenous aluminum accumulates in the lysosomes of cultured rat cortical neurons. *Neurosci. Lett.* **119**:71–74.

Scott, M. G., D. L. Crimmins, D. W. McCourt, J. J. Tarrand, M. C. Eyerman and M. H. Nahm. **1988**. A simple *in situ* cynogen bromide cleavage method to obtain internal amino acid sequence of proteins electroblotted to polyvinyldifluoride membranes. *Biochem. Biophys. Res. Commun.* **155**:1353–1359.

Selkoe, D. J. **1986**. Altered structural proteins in plaques and tangles: what do they tell us about the biology of Alzheimer's disease? *Neurobiol. Aging* **7**:425–432.

Selkoe, D. J., C. R. Abraham, M. B. Podlisny and L. K. Duffy. **1986**. Isolation of low-molecular weight proteins from amyloid plaque fibers in Alzheimer's disease. *J. Neurochem.* **146**:1820–1834.

Selkoe, D. J., L. K. Duffy, N. Nukina, C. L. Joachim, M. B. Podlisny and K. S. Kosik. **1987**. Biochemical analysis of amyloid filaments and paired helical filaments and their respective contributions to neuronal degeneration in Alzheimer's disease. *Mol. Neuropathol. of Aging: Banbury Report* **27**:235–252.

Selkoe, D. J. **1989**. Biochemistry of altered brain proteins in Alzheimer's disease. *Annu. Rev. Neurosci.* **12**:463–490.

Seubert, P., C. Vigo-Pelfrey, F. Esch, M. Lee, H. Dovey, D. Davis, S. Sinha, M. Schlossmacher, J. Whaley, C. Swindlehurst, R. McCormack, R. Wolfert, D. J. Selkoe, I. Lieberburg and D. Schenk. **1992**. Isolation and quantification of soluble Alzheimer ß-peptide from biological fluids. *Nature* **359**:325–327.

Seubert, P., T. Oltersdorf, M. G. Lee, R. Barbour, C. Blomquist, D. L. Davis, K. Bryant, L. C. Fritz, D. Galasko, L. J. Thal, I. Lieberburg and D. B. Schenk. **1993**. Secretion of ß-amyloid precursor protein cleaved at the amino terminus of the ß-amyloid peptide. *Nature* **361**:260–263.

Shapira, R., G. E. Austin and S. S. Mirra. **1988**. Neuritic plaque amyloid in Alzheimer's disease in highly racemized. *J. Neurochem.* **50**:69–74.

Sherrard, D. J. **1991**. Aluminium — much ado about something. *New. Engl. J. Med.* **324**:558-559.

Shigematsu, K. and P. L. McGeer. **1992**. Accumulation of amyloid precursor protein in damaged neuronal processes and microglia following intracerebral administration of aluminum salts. *Brain Research* **593**:117-123.

Shoji, M., T. E. Golde, J. Ghiso, T. T. Cheung, S. Estus, L. M. Shaffer, X.-D. Cai, D. M. McKay, R. Tintner, B. Frangione and S. G. Younkin. **1992**. Production of the Alzheimer amyloid ß-protein by normal proteolytic processing. *Science* **258**:126-129.

Sisodia, S. S., E. H. Koo, K. Beyreuther, A. Unterbeck and D. L. Price. **1990**. Evidence that ß-amyloid protein in Alzheimer's disease is not derived by normal processing. *Nature* **347**:194.

Smith, P. K., R. I. Krohn, G. T. Hermanson, A. K. Mallia, F. H. Gartner, M. D. Provenzano, E. K. Fujimoto, N. M. Goeke, B. J. Olson and D. C. Klenk. **1985**. Measurement of protein using bicinchoninic acid. *Anal. Biochem.* **150**:76–85.

Snow, A. D., J. Willner and R. Kisilevsky. **1987**. Sulphated glycosaminoglycans: a common constituent of all amyloids? *Lab. Invest.* **56**:120–124.

Snyder, L. R. **1980**. in "High-performance liquid chromatography," Vol. 1, (ed. Horvath, Cs.), Academic Press, New York, USA.

Sorimachi, K. and D. J. Craik. **1994**. Structure determination of extracellular fragments of amyloid proteins involved in Alzheimer's disease and Dutch-type hereditary cerebral haemorrhage with amyloidosis. *Eur. J. Biochem.* **219**:237–251.

Spencer, R. G. S., K. J. Halverson, M. Auger, A. E. McDermott, R. G. Griffin and P. T. Lansbury, Jr. **1991**. An unusual peptide conformation may precipitate amyloid formation in Alzheimer's disease: application of solid-state NMR to the determination of protein secondary structure. *Biochemistry* **30**:10382–10387.

Stadalius, M. A., H. S. Gold and L. R. Snyder. **1976**. Optimization model for the gradient elution separation of peptide mixtures by reversed-phase high-performance liquid chromatography. verification of retention relationships. *J. Chromatogr.* **296**:31–59.

Stanhope, J. M., J. A. Brody and C. E. Morris. **1972**. Epidemiologic features of amyotrophic lateral sclerosis and Parkinsonism-dementia in Guam, Mariana Islands. *Int. J. Epidemiol.* **1**:199–210.

Stephenson, R. L. and S. Clarke. **1989**. Succinimide formation from aspartyl and asparaginyl peptides as a model for the spontaneous degradation of proteins. *J. Biol. Chem.* **264**:6164–6170.

Stern, A., D. Perl, D. Munoz-Garcia, R. Good, C. Abraham and D. Selkoe. **1986**. Investigation of silicon and aluminium content in isolated senile plaque cores by laser microprobe mass analysis (LAMMA). *J. Neuropathol. Exp. Neurol.* **45**:361.

Stewart, S. M. and S. D. Young. **1984**. in "Solid Phase Peptide Synthesis," Pierce Chemical Company, Illinois, USA.

Strittmatter, W. J., A. M. Saunders, D. Schmechel, M. Pericak-Vance, J. Enghild, G. S. Salvesen and A. D. Roses. **1993**. Apolipoprotein E: high-avidity binding to ß-amyloid and increased frequency of type 4 allele in late-onset familial Alzheimer disease. *Proc. Natl. Acad. Sci. USA* **90**:1977–1981.

Sutherland, J. C., A. Emrick, L. L. France, D. C. Monteleone and J. Trunk. **1992**. Circular dichroism user facility at the National Synchrotron Light Source: estimation of protein secondary structure. *BioTechniques* **13**:588–590.

Tabaton, M., C. Caponnetto, G. Mancardi and C. Loeb. **1991**. Amyloid ß protein deposition in brains from elderly subjects with leukoariaosis. *J. Neurol. Sci.* **106**:123–127.

Tagliavani, F., G. Giaccone, B. Frangione and O. Bugiani. **1988**. Preamyloid deposits in the cerbral cortex of patients with Alzheimer's disease and nondemented individuals. *Neurosci. Lett.* **93**:191–196.

Tam, S. C. and R. J. P. Williams. **1986**. One problem with acid rain: aluminum. *J. Inorg. Chem.* **26**:35–44.

Terry, R. D. and C. Penã. **1965**. Experimental production of neurofibrillary degeneration. 2. electron microscopy, phosphatase histochemistry and electron probe analysis. *J. Neuropathol. Exp. Neurol.* **24**:200–210.

Thompson, C. M., W. R. Markesbury, W. D. Ehmann, Y.-X. Mao and D. E. Vance. **1988**. Regional brain trace-element studies in Alzheimer's disease. *Neurotoxicology* **9**:1–8.

Tinoco, Jr., I. **1962**. Absorption and rotation of light by helical polymers. *Adv. Chem. Phys.* **4**:113–160.

Tomski, S. J. and R. M. Murphy. **1992**. Kinetics of aggregation of synthetic ß-amyloid peptide. *Arch. Biochem. Biophys.* **294**:630–638.

Toumadje, A., S. W. Alcorn and W. C. Johnson, Jr. **1992**. Extending CD spectra of proteins to 168 nm improves the analysis for secondary structures. *Anal. Biochem.* **200**:321–331.

Toumadje, A. and W. C. Johnson, Jr. **1993**. Effects of relative band intensity on prediction of protein secondary structure from CD. *Anal. Biochem.* **211**:258–260.

Traub, R. D., T. C. Rains, R. M. Garruto, D. C. Gajdusek and C. J. Gibbs, Jr. **1981**. Brain destruction alone does not elevate brain aluminium. *Neurology* **31**:986–990.

Turnell, W., R. Sarra, I. D. Glover, J. O. Baum, D. Caspi, M. L. Baltz and M. B. Pepys. **1986**. Secondary structure prediction of human SAA_1: presumptive identification of calcium and lipid binding sites. *Mol. Biol. Med.* **3**:387–407.

Udenfriend, S. and J. Meienhofer. **1979-1985**. in "The peptides, analysis, synthesis, biology," Academic Press, New York, USA.

Urry, D. W. **1985**. Absorption, circular dichroism and optical rotatory dispersion of polypeptides, proteins, prosthetic groups and biomembranes, in "Modern physical methods in biochemistry, Part A," (eds. Neuberger, A. and L. L. M. van Deenan), Elsevier Science B.V., Holland.

Urry, D. V., L. Masotti and J. R. Krivacis. **1971**. Circular dichroism of biological membranes. 1. mitochondria and red blood cell ghost. *Biochim. Biophys. Acta* **241**:600–612.

van Broeckhoven, C., J. Haan, E. Bakker, J. A. Hardy, W. van Hul, A. Wehnert, M. Vegter-van der Vlis and R. A. C. Roos. **1990**. Amyloid ß protein precursor gene and hereditary cerebral hemorrhage with amyloidosis (Dutch). *Science* **248**:1120–1124.

Vassar, P. S. and C. F. A. Culling. **1959**. Fluoresence stains, with special reference to amyloid and connective tissue. *Arch. Pathol.* **68**:487–498.

Venyaminow, S. Y., I. A. Baikalov, C.-S. C. Wu and J. T. Yang. **1991**. Some problems of cd analyses of protein conformation. *Anal. Biochem.* **198**:250–255.

Vigo-Pelfrey, C., P. Keim, I. Lieberburg and D. B. Schenk. **1993**. Characterization of ß-amyloid peptide from human cerebrospinal fluid. *J. Neurochem.* **61**:1965–1968.

Villa, M. **1983.** Structure and ^{27}Al NMR spectra in ß-aluminas. *J. Magn. Reson.* **51**:349–360.

Virchow, R. **1855**. Zur cellulose-fruge. *Virchows Arch. Path. Anat.* **8**:140–144.

Vyas, S. B. and L. K. Duffy. **1989**. Chemical modification of histidines in Alzheimer amyloid, in Proceedings of the IVth Annual Protein Society Symposium, Seattle, Washington, July 1989.

Vyas, S., X. Zhao, T. J. Luick and L. K. Duffy. **1992**. ß-amyloid peptides, aluminum and albumin. *Adv. Behav. Biol.* **40**:503–513.

Wehr, C. T., L. Correia and S. R. Abbot. **1982**. Evaluation of stationary and mobile phases for reversed-phase high performance liquid chromatography of peptides. *J. Chromatogr. Sci.* **20**:114–119.

Wehrli, F. X. and S. Wehrli. **1981**. Solution complexes of the aluminum halides in acetonitrile and acetonitrile-water studied by high-field ^{27}Al NMR. *J. Magn. Reson.* **44**:197–207.

Whitehouse, P. J., D. L. Price, R. G. Struble, A. W. Clark, J. T. Coyle and M. R. DeLong. **1982**. Alzheimer's disease and senile dementia: loss of neurons in the basal forebrain. *Science* **215**:1237–1239.

Whitson, J. S., D. J. Selkoe and C. W. Cotman. **1989**. Amyloid beta protein enhances the survival of hippocampus neurons *in vitro*. *Science* **243**:1488–1490.

Whitson, J. S., C. G. Glabe, E. Shintani, A. Abcar and C. W. Cotman. **1990**. ß-amyloid protein promotes neuritic branching in hippocampal neurons. *Neurosci. Lett.* **110**:319–324.

Wieland, Th. **1978**. in "Versatility of proteins," (ed. Li, C. H.), Academic Press, New York, USA.

Wilson, K. J., A. Honegger, R. P. Stötzel and G. J. Hughes. **1981**. The behaviour of peptides on reversed-phase supports during high-pressure liquid chromatography. *Biochem. J.* **199**:31–41.

Wishart, D. S., B. D. Sykes and F. M. Richards. **1992**. Protein secondary structure through NMR spectroscopy. *Biochemistry* **31**:1647–1651.

Wisniewski, H. and R. D. Terry. **1973**. in "Progress in neuropathology," Vol. 2 (ed. Zimmerman, H. M.), Grune & Stratton, New York, USA.

Wisniewski, H. M., R. C. Moretz, J. A. Sturman, G. Y. Wen and J. W. Shek. **1990**. Aluminum neurotoxicity in mammals. *Environ. Geochem. Health* **12**:115–120.

Wisniewski, T. and B. Frangione. **1992**. Apolipoprotein E: a pathologic chaperone protein in patients with cerebral and systemic amyloid. *Neurosci. Lett.* **135**:235–238.

Wisniewski, T, J. Ghiso and B. Frangione. **1993**. CSF inhibits Alzheimer ß-amyloid fibril formation in vitro. *Ann. Neurol.* **34**:631–633.

Wisniewski, T., J. Ghiso and B. Frangione. **1994**. Alzheimer's disease and soluble Aß. *Neurobiol. Aging* **15**:143–152.

Woody, R. W. and I. Tinoco, Jr. **1967**. Optical rotation of oriented helices. 3. calculation of rotatory dispersion and circular dichroism of α- and 3_{10}-helix. *J. Chem. Phys.* **46**:4927–4975.

Woody, R. W. **1969**. Optical properties of polypeptides in the ß-conformation. *Biopolymers* **8**:669–683.

Woody, R. W. **1985**. Circular dichroism of peptides, in "The Peptides," (ed. Hruby, V. J.), Academic Press, Florida, USA.

Yamaguchi, H. S. Hirai, M. Morimatsu, M. Shoji and Y. Ihara. **1988**. A variety of cerebral deposits in the brains of the Alzheimer type dementia by a ß protein immunostaining. *Acta Neuropathologica* **76**:541–549.

Yang, J. T., C.-S. Wu and H. M. Martinez. **1986**. Calculation of protein conformation from circular dichroism. *Met. Enzymol.* **130**:208–269.

Yankner, B. A., L. K. Duffy and D. A. Kirschner. **1990**. Neurotrophic and neurotoxic effects of amyloid ß protein: reversal by tachykinin neuropeptides. *Science* **250**:279–282.

Yankner, B. A. and M.-M. Mesulam. **1991**. ß-amyloid and the pathogenesis of Alzheimer's disease. *New. Engl. J. Med.* **325**:1849–1857.

Yates, C. M., J. Butterworth, M. C. Tennant and A. Gordon. **1990**. Enzyme activities in relation to pH and lactate in postmortem brain in Alzheimer-type and other dementias. *J. Neurochem.* **55**:1624–1630.

Zagorski, M. G. and C. J. Barrow. **1992**. NMR studies of amyloid ß-peptides: proton assignments, secondary structure, and mechanism of an α-helix → ß-sheet conversion for a homologous, 28-residue, N-terminal fragment. *Biochemistry* **31**:5621–5631.

Zatta, P., R. Giordano, B. Corain and G. G. Bombi. **1988**. Alzheimer dementia and the aluminum hypothesis. *Medical Hypothesis* **26**:139–142.

Zhang, S., T. Holmes, C. Lockshin and A. Rich. **1993**. Spontaneous assembly of a self-complementary oligopeptide to form a stable macroscopic membrane. *Proc. Natl. Acad. Sci. USA* **90**:3334–3338.

Zhao, X., J. A. Valantas, S. Vyas and L. K. Duffy. **1993**. Comparative toxicity of amyloid ß-peptide in neuroblastoma cell lines: effects of albumin and physalaemin. *Comp. Biochem. Physiol.* **106C**:165–170.

Zhong, L. and W. C. Johnson, Jr. **1992**. Environment affects amino acid preference for secondary structure. *Proc. Natl. Acad. Sci. USA* **89**:4462–4465.

Zhou, N. E., C. T. Mant and R. S. Hodges. **1990**. Effect of preferred binding domains on peptide retention behavior in reversed-phase chromatography: amphipathic α-helices. *Peptide Research* **3**:8–20.